Die approbierte Originalversion dieser Dissertation ist in der Hauptbibliothek der Technischen Universität Wien aufgestellt und zugänglich.
http://www.ub.tuwien.ac.at

The approved original version of this thesis is available at the main library of the Vienna University of Technology.
http://www.ub.tuwien.ac.at/eng

TECHNISCHE UNIVERSITÄT WIEN

DISSERTATION

Surface-active ionic liquids in synthesis and catalysis

Ausgeführt zum Zwecke der Erlangung des akademischen Grades eines Doktors der technischen Wissenschaften unter der Leitung von

Ass. Prof. Dipl.-Ing. Dr. Katharina Schröder (née Bica)

E163 - Institut für Angewandte Synthesechemie

eingereicht an der Technischen Universität Wien

Chemische Fakultät

von

Alice Cognigni, M. Sc.

Matrikelnummer: 01329719

Johann-Strauß-Gasse 4/3/6, 1040 Wien

Wien, im September 2017

Acknowledgements

I would like to thank in the first place my supervisor Prof. Dr. Katharina Schröder, for offering me the opportunity to work in her group, for her valuable advice and support during my Ph.D.

My sincere gratitude goes to Prof. Dr. Milen Bogdanov and Prof. Dr. Erik Reimhult for the throughout reading and evaluation of my thesis.

I would like to give special thanks to all the former and current lab colleagues: Mahtab Hejazifar, Sebastian Kampichler, Ádám Márk Pálvölgyi, Olga Alina Lanaridi, Sonja Platzer, Jacqueline Bitai, Christian Hauzenberger, Stefan Weber, Winfried Nischkauer, Beñat Olave, Álvaro Silva Lima, Ana Filipa Cláudio, Rafal Kukawka, Anna Ressmann, Maria Vasiloiu, Meltem Taskin, Liene Anteina, Aitor Sainz Martinez and Diana Khlan for building a friendly and collaborative environment in the lab.

Thanks also to our neighbours from Prof. Dr. Peter Gärtner research group: Max Kaiser, Nicolas Kratena, David Schönbauer, Katharina Schragl, Sebastian Steiner and Dr. Valentin Enev.

Financial support from the Austrian Science Fund (FWF project P25504-N28) is gratefully acknowledged.

Many thanks to: Dr. Christian Hametner, Florian Untersteiner, Ing. Walter Dazinger and Laszlo Czollner, for NMR advice, computer fixing, autoclave assistance and HR-MS measurements, Prof. Matthias Weil for crystal structure measurements and Dr. Ronald Zirbs (BOKU) for help with DLS measurements. Special thanks go to all the non-scientific staff of the IAS institute.

I am also very thankful to my cooperation partners: Prof. Dr. Christian Schröder (Uni Wien) for having me in his lab and his fitting support, Prof. Dr. Herwig Peterlik for SAXS measurements (Uni Wien), Prof. Dr. Marija Bešter-Rogač from the University of Ljubljana for thermodynamic investigations and Prof. Dr. Richard Buchner from the University of Regensburg for dielectric spectroscopy studies.

Finally I would like to thank my family and friends from all around Europe.

Abstract

In order to reduce large volumes of volatile organic solvents that are often associated with human risk, safety issues and poor environmental sustainability, much effort has been spent on identifying more benign alternative solvents. In this regard water would be a prime candidate; however, the low solubility of organic compounds is a well known drawback for the implementation of water in organic reaction. It has been recently demonstrated that ionic liquids with long alkyl chain behave like surfactants and tend to aggregate in water forming micelles. This self-assembly and structural organization of ionic liquids in aqueous media enables their application in micellar catalysis, where the hydrophobic character of the micellar core is used to solubilize organic compounds and conduct reactions in water.

This thesis focuses on the design, synthesis and characterization of novel ionic liquids-water micellar systems and on their application in synthesis and catalysis. For this purpose a series of 1-dodecyl-3-methylimidazolium based ionic liquids with different anions such as halide and alkylsulfates, and variable core structures, including dicationic and zwitterionic ones, was synthesized. The aggregation behaviour of these ionic liquids in water was characterized by a number of techniques, including surface tension and conductivity measurements, in order to determine the critical micellar concentration (CMC). A clear influence of the structure on the CMC could be identified, suggesting that a more hydrophobic character favours aggregation. The obtained surface-active ionic liquids were further applied in micellar catalysis. Initially, the role of the anion in the ionic liquids was investigated in the degradation of organophosphorus compounds, which are analogous to pesticides, via nucleophilic substitution. After studying reaction kinetics in micellar media a correlation between the anion hydrophobicity and the reaction rate could be identified.

Further studies addressed the application of surface-active ionic liquids in catalysis with transition metal catalysts. For this purpose two important reactions in organic synthesis were selected: the challenging aerobic oxidation of 1-octanol to octanoic acid and a Heck cross-coupling reaction. Surface-active ionic liquids were able to stabilize catalytically active metal aggregates already when used in small amount and no further ligands were necessary. In both cases a strong dependence on the ionic liquid concentration and structure was identified, which is in accordance with the concepts of micellar catalysis. Optimum conditions for each reaction system could be identified, and in both applications the use of ionic liquids strongly improved the reaction performance compared to pure water.

The final part of the thesis addresses the application of surface-active ionic liquids for sustainable energy production. The oxidation of water to produce molecular oxygen using an Iridium based catalyst was investigated, using surface-active ionic liquids as ligands, but optionally also as surfactant. Excellent performance of the ionic liquid-derived catalyst was observed, and initial reaction rates could be further increased in the presence of micellar solutions as reaction media.

Kurzfassung

Nachdem flüchtige organische Lösungsmittel oft erhebliche Risiken und Umweltprobleme verursachen, wurde in den letzten Jahre intensiv an alternativen Lö sungsmitteln geforscht. In dieser Hinsicht erscheint Wasser als Alternative äußerst vielversprechend. Allerdings stellt die geringe Löslichkeit vieler organischen Verbindungen ein Problem für den Einsatz von Wasser in organischen Reaktionen dar. In den letzten Jahren wurde zunehmend das Verhalten von ionischen Flüssigkeiten in Wasser untersucht, wobei gezeigt wurde, dass bestimmte ionische Flüssigkeiten in Wasser Micellen bilden können. Diese Selbstorganisation von grenzflächenaktiven ionischen Flüssigkeiten in Wasser erlaubt deren Anwendung im Bereich der micellaren Katalyse, bei der die hydrophoben Bereiche einer Micelle genutzt werden können um organische Verbindungen zu lösen und somit Reaktionen im Wasser zu ermöglichen.

Die vorliegende Arbeit widmet sich der Synthese und der Charakterisierung von neuen grenzflächenaktiven ionischen Flüssigkeiten und deren Anwendung in der organischen Synthese und Katalyse.

In einem ersten Schritt wurde eine Reihe von ionischen Flüssigkeiten mit Imidazolium-Kationen und verschiedenen Anionen wie z. Beispiel Halogenid und Alkylsulfate synthetisiert. Die Charakterisierung der Aggregatbildung dieser Verbindungen in Wasser wurde mittels Oberflächenspannungs- und Leitfähigkeitsmessungen zur Bestimmung der kritischen micellaren Konzentration (CMC) durchgeführt. Es zeigte sich ein klarer Zusammenhang zwischen der chemischen Struktur der ionischen Flüssigkeiten und den erhaltenen CMC-Werten. Die Ergebnisse deuten darauf hin, dass ein hydrophober Charakter der ionischen Flüssigkeit das Aggregationsverhalten deutlich begünstigt. Die hergestellten grenzflächenaktiven ionischen Flüssigkeiten wurden daraufhin als Reaktionsmedium in der micellaren Katalyse eingesetzt. Der Einfluss des Anions wurde in der Abbaureaktion einer phosphororganische Verbindung durch nukleophile Substitution untersucht. Kinetische Messungen ergaben eine deutliche Korrelation zwischen der Reaktionsgeschwindigkeit und der Hydrophobie des verwendeten Anions.

In weiterer Folge wurde die Anwendung von grenzflächenaktiven ionische Flüssigkeiten in übergangsmetallkatalysierten Reaktion untersucht. Dafür wurden zwei in der organischen Synthese relevante Reaktionen ausgewählt: die aerobe Oxidation von 1-Oktanol zu Oktansäure, sowie eine Palladium-katalysierte Kupplungsreaktion. Die grenzflächenaktiven ionischen Flüssigkeiten konnten schon in geringer Menge die katalytisch aktiven Metallaggregate stabilisieren, wobei hier keine zusätzlichen Liganden notwendig waren. In beiden Fällen konnte eine starke Abhängigkeit des Reaktionsfortschrittes von der verwendeten Konzentration der ionischen Flüssigkeit und deren Struktur beobachtet werden. Dieser grundlegende Zusammenhang steht in Übereinstimmung mit den Prinzipien der micellaren Katalyse. Durch Optimierung der Reaktionsparameter konnte die Ausbeute in Gegenwart ionischer Flüssigkeiten im Vergleich zu reinem Wasser deutlich gesteigert werden.

Der letzte Teil dieser Dissertation beschäftigt sich mit der Anwendung von grenzflächenaktiven ionische Flüssigkeiten zur nachhaltigen Energieerzeugung. Hier wurde die Oxidation von Wasser mit einem Iridium-basiertem Katalysator untersucht, um molekularen Sauerstoff herzustellen. Grenzflächenaktive ionische Flüssigkeiten konnten hier entweder als Ligand aber auch als Tensid eingesetzt werden. Die hergestellten ionischen Katalysatoren zeigten ausgeze-

ichnete katalytische Aktivität, und die initiale Reaktionsgeschwindigkeit konnte durch weitere Zugabe von grenzflächenaktiver ionischer Flüssigkeit zusätzlich verbessert werden.

List of abbreviations

CMC	Critical Micellar Concentration
CTAB	Cetyl Trimethylammonium Bromide
DLS	Dynamic Light Scattering
IL	Ionic Liquid
ITC	Isothermal Titration Calorimetry
mM	Millimolar
nm	Nanometer
NMR	Nuclear Magnetic Resonance
PEG	Polyethylenglycole
pH	acidity
R	Long aliphatic chain
SAIL	Surface-Active Ionic Liquid
SANS	Small Angle Neutron Scattering
SAXS	Small Angle X-Ray Scattering
SDS	Sodium Dodecyl Sulfate
SEM	Scanning Electron Microscopy
T	Temperature
TEM	Transmission Electron Microscopy
UV-Vis	Ultraviolet-Visible Absorption Spectroscopy
ΔG_m°	Free energy of micellization
ΔH_m°	Enthalpy of micellization
ΔS_m°	Entropy of micellization

Ionic liquid cations

$[C_nTEA]^+$	Alkyltriethylammonium
$[(C_{12})_3N\text{-}C_n\text{-}N(C_{12})_3]^{2+}$	1,n-Bis(tridodecylammonium)alkane
$[C_nDEA\text{-}C_3\text{-}SO_3]$	3,*N*-Alkyl-*N*,*N*-(diethylammonio)-1-propanesulfonate
$[im]^+$	Imidazolium
$[C_nmim]^+$	1-Alkyl-3-methylimidazolium
$[C_nC_nim]^+$	1,3-Dialkylimidazolium
$[C_nim\text{-}C_m\text{-}C_nim]^{2+}$	1,m-Bis(3-alkylimidazolium-1-yl)alkane
$[C_nim\text{-}C_3\text{-}SO_3]$	3-(1-Alkyl-3-imidazolio)propanesulfonate
$[HO\text{-}C_nHEim]^+$	*N*-(2-Hydroxyalkyl)-*N*-(2-hydroxyethyl)imidazolium
$[C_{12}mim\text{-}PEG_{2000}\text{-}C_{12}mim]^{2+}$	Dicationic imidazolium SAILs with an ether spacer
$[C_nmim\text{-}(S\text{-}C_m\text{-}S)\text{-}C_nmim]^{2+}$	Dicationic imidazolium SAILs with a thioether spacer
$[C_nVim]^+$	1-Vinyl-3-alkylimidazolium
$[C_nEmim]^+$	1-Alkyloxycarbonyl-3-methylimidazolium
$[C_nAmim]^+$	1-Alkylcarbamyl-3-methylimidazolium
$[C_nCmim]^+$	1-Alkyloxycarbonyloxyethyl-3-methylimidazolium

$[C_{14}mimAzoPh]^+$	1-Tetradecyl-2-arylazo-3-methylimidazolium
$[C_{14}C_2imAzoPh]^+$	1-Tetradecyl-2-arylazo-3-ethylimidazolium
$[Si(3)C_3mim]^+$	Trisiloxane tailed methylimidazolium
$[C_nPyr]^+$	*N*-Alkylpyridinium
$[C_8ENic]Br$	Nicotine based cation
$[C_{12}Pyr(2)\text{-}C_n\text{-}(2)C_{12}Pyr]^{2+}$	2,2'-(α,ω -Alkanediyl)bis-(1-dodecylpyridinium)
$[C_nEPyr]^+$	*N*-Alkyloxycarbonylpyridinium
$[C_nAPyr]^+$	*N*-Alkylcarbamylpyridinium
$[Si(3)C_3Pyr]^+$	Trisiloxane tailed pyridinium
$[pyrr]^+$	Pyrrolidinium
$[C_nmpyrr]^+$	*N*-Alkyl-*N*-methylpyrrolidinium
$[C_nC_npyrr]^+$	*N*-*N*-Dialkylpyrrolidinium
$[C_nAmpyrr]^+$	1-Alkylcarbamylmethylpyrrolidinium
$[((Me)_3SiO)_3\text{-}C_3mpyrr]^+$	1-Methyl-1-[tri(trimethylsiloxy)]-silylpropylpyrrolidinium
$[C_nmpip]^+$	*N*-Alkyl-*N*-methylpiperidinium
$[C_nAmpip]^+$	1-Alkylcarbamylmethylpiperidinium
$[C_nEmorph]^+$	*N*-Alkyloxycarbonylmethylmorpholinium
$[C_nAmorph]^+$	*N*-Alkylcarbamylmethylmorpholinium
$[P_{14nnn}]^+$	Trialkyltetradecylphosphonium
$[Cho]^+$	Cholinium
$[Gua]^+$	Guanidinium

Ionic liquid anions

OAc^-	Acetate
$AcSal^-$	Acetylsalicylate
$[C_2H_{2n+1}CO_2]^-$	Alkylcarboxylate
$[C_nSO_3]^-$	Alkylsulfonate
$[C_nSO_4]^-$	Alkylsulphate
Br^-	Bromide
BS^-	Benzenesulfonate
[DEHP]	Bis(2-ethylhexyl) phosphate
Cl^-	Chloride
$[CA]^-$	Cinnamate
[AOT]	Dioctyl sulfosuccinate
$[C_{12}BzSO_3]^-$	*p*-Dodecylbenzylsulfonate
HSO_4^-	Hydrogensulphate
mHB^-	*m*-Hydroxybenzoate
pHB^-	*p*-Hydroxybenzoate
HBS^-	4-Hydroxybenzensulfonate
HNC^-	3-Hydroxy-2-naphthoate
I^-	Iodide
Ibu^-	Ibuprofenate
$[Lact]^-$	Lactate
OMs^-	Mesylate
$[C_nF_{2n+1}SO_3]^-$	Perfluoroalkylsulfonate
$[Prol]^-$	Prolinate
Sal^-	Salicylate
$[Tart]^-$	Tartrate
BF_4^-	Tetrafluoroborate
OTs^-	Tosylate

List of structures

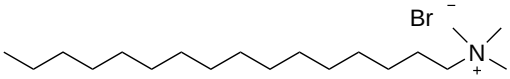

Cetyl Trimethylammonium Bromide
CTAB

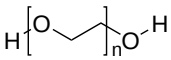

Polyethylene glycol
PEG

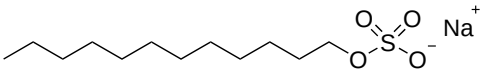

Sodium dodecyl sulfate
SDS

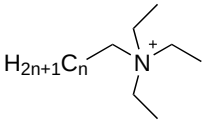

Alkyltriethylammonium
$[C_nTEA]^+$

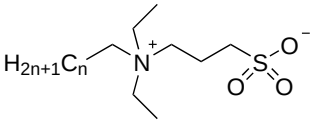

N-Alkyl-*N*,*N*-diethylammonio-1-propanesulfonate
$[C_nDEA\text{-}C_3\text{-}SO_3]$

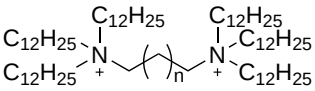

1,n-Bis(tridodecylammonium)alkane
$[(C_{12})_3N\text{-}C_n\text{-}N(C_{12})_3]^{2+}$

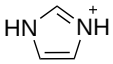

Imidazolium
$[Im]^+$

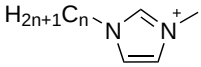

1-Alkyl-3-methylimidazolium
$[C_nmim]^+$

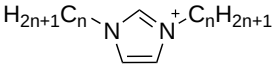

1,3-Dialkylimidazolium
$[C_nC_nim]^+$

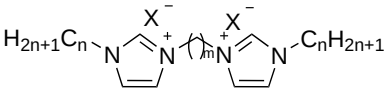

1,m-Bis(3-alkylimidazolium-1-yl)alkane
$[C_nim\text{-}C_m\text{-}C_nim]^{2+}$

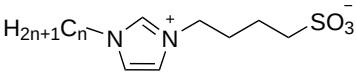

3-(1-Alkyl-3-imidazolio)propanesulfonate
$[C_nim\text{-}C_3\text{-}SO_3]$

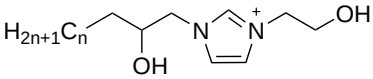

1-(2-Hydroxyalkyl)-3-(2-hydroxyethyl)imidazolium
$[HO\text{-}C_nHeim]^+$

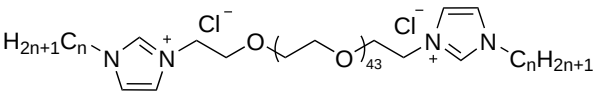

Dicationic imidazolium SAILs with an ether spacer
$[C_{12}im\text{-}PEG_{2000}\text{-}C_{12}im]^{2+}$

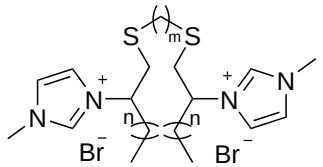

Thioether spacer
$[C_n mim\text{-}(S\text{-}C_m\text{-}S)\text{-}C_n mim]^{2+}$

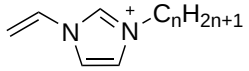

1-Vinyl-3-alkylimidazolium
$[C_n Vim]^+$

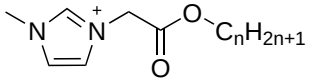

1-Alkyloxycarbonyl-3-methylimidazolium
$[C_n Emim]^+$

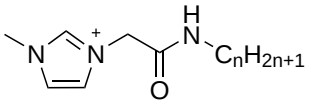

1-Alkylcarbamyl-3-methylimidazolium
$[C_n Amim]^+$

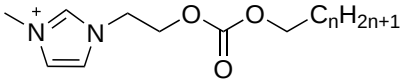

1-Alkyloxycarbonyloxyethyl-3-methylimidazolium
$[C_n Cmim]^+$

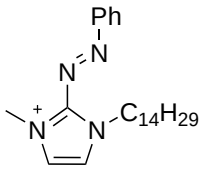

1-Tetradecyl-2-arylazo-3-methylimidazolium
$[C_{14} mimAzoPh]^+$

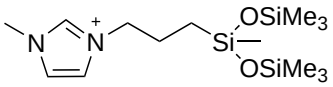

Trisiloxane tailed methylimidazolium
$[Si(3)C_3 mim]^+$

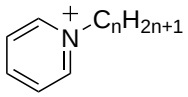

N-Alkylpyridinium
$[C_n Pyr]^+$

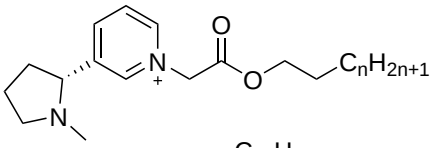

Nicotine-based cataions
$[C_n ENic]^+$

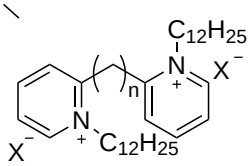

Ddicationic alkylpyridinium
$[C_{12} Pyr\text{-}C_n\text{-}C_{12} Pyr]^{2+}$

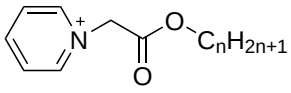

N-Alkyloxycarbonylpyridinium
$[C_n EPyr]^+$

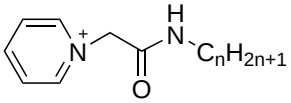

N-Alkylcarbamylpyridnium
$[C_n APyr]^+$

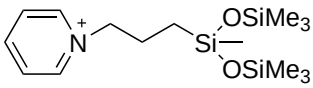

Trisiloxane tailed pyridinium
$[Si(3)C_3 Pyr]^+$

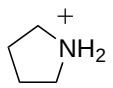

Pyrrolidinium
$[pyrr]^+$

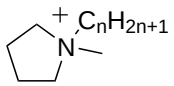

N-Alkyl-*N*-methyl pyrrolidinium
$[C_nmpyrr]^+$

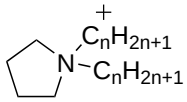

N,N-Dialkylpyrrolidinium
$[C_nC_npyrr]^+$

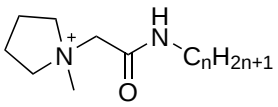

N-Alkyloxycarbamylmethylpyrrolidinium
$[C_nAmpyrr]^+$

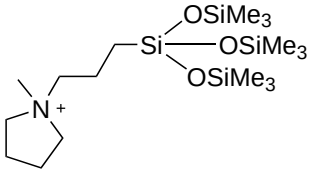

1-Methyl-1-[tri(trimethylsiloxy)]-silylpropylpyrrolidinium
$[((Me)_3SiO)_3\text{-}C_3mpyrr]^+$

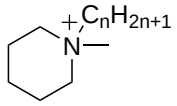

N-Alkyl-*N*-methyl piperidinium
$[C_nmpip]^+$

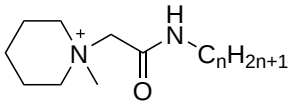

N-Alkylcarbamylmethylpiperidinium
$[C_nAmpip]^+$

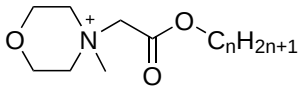

N-Alkyloxycarbonylmethylmorpholinium
$[C_nEmorph]^+$

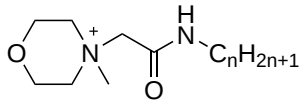

N-Alkylcarbamylmethylmorpholinium
$[C_nAmorph]^+$

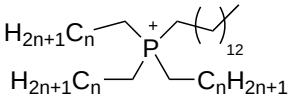

Trialkyltetradecylphosphonium
$[P_{14nnn}]^+$

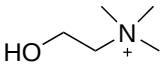

Cholinium
$[Cho]^+$

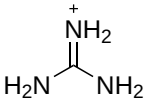

Guanidinium
$[Gua]^+$

Acetate
[OAc]$^-$

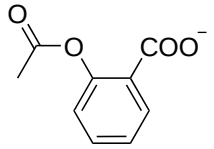

Acetylsalicylate
[AcSal]$^-$

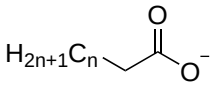

Alkylcarboxylate
[$C_nH_{2n+1}CO_2$]

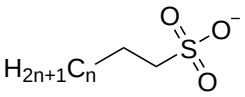

Alkylsulfonate
[C_nSO_3]

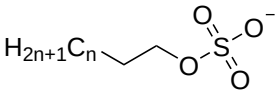

Alkylsulphate
[C_nSO_4]

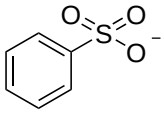

Benzenesulfonate
[BS]

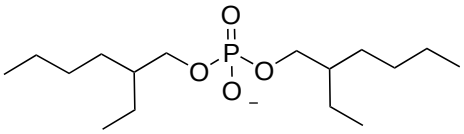

Bis(2-ethylhexyl) phosphate
[DEHP]

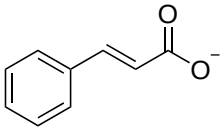

Cinnamate
[CA]

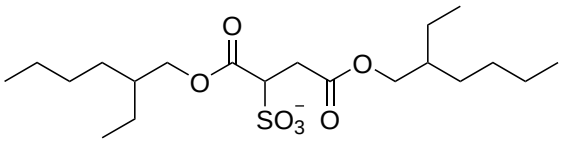

Dioctyl sulfosuccinate
[AOT]

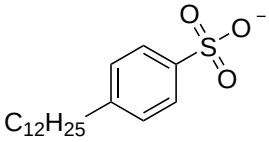

p-Dodecylbenzylsulfonate
[$C_{12}BzSO_3$]

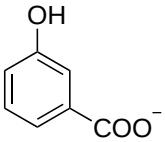

m-Hydroxybenzoate
[*m*HB]

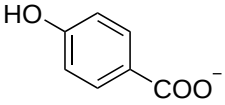

p-Hydroxybenzoate
[*p*HB]

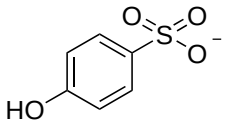

4-Hydroxybenzenesulfonate
[HBS]

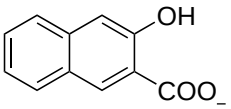

3-Hydroxy-2-naphthoate
[HNC]

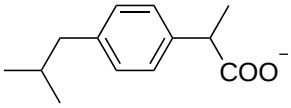

Ibuprofenate
[Ibu]

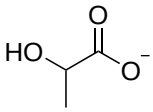

Lactate
[Lact]

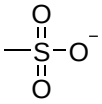

Mesylate
[OMs]

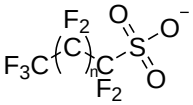

Perfluoroalkylsulfonate
[$C_nH_{2n+1}SO_3$]

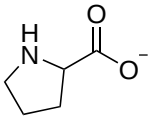

Prolinate
[Pro]

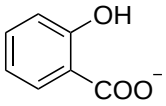

Salicylate
[Sal]

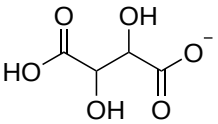

Tartrate
[Tart]

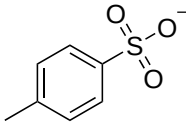

Tosylate
[OTs]

Contents

Acknowledgements **ii**

Abstract **iv**

Kurzfassung **vi**

List of abbreviations **ix**

List of structures **ix**

1 Introduction **1**
1.1 Solvent usage and sustainability 1
1.2 Ionic liquids and water: a powerful combination 3
1.3 Surface-active ionic liquids 5
1.3.1 Structures of surface-active ionic liquids 7
1.3.2 Further characterization and properties of surface-active ionic liquids 20
1.3.3 Applications of surface-active ionic liquids 22
1.4 Bibliography 30

2 Aim of the thesis **43**

3 Surface-active ionic liquids in micellar catalysis **45**
3.1 Surface-active ionic liquids in micellar catalysis: impact of anion selection on reaction rates in nucleophilic substitutions 47
3.2 Thermodynamic study for micellization of imidazolium based surface-active ionic liquids in water: Effect of alkyl chain length and anions 57
3.3 Hydration and Counterion Binding of (C_{12}MIM) Micelles 67

4 Application of surface-active ionic liquids in transition metal catalysis **113**
4.1 Surface-active ionic liquids in catalysis: Impact of structure and concentration on the aerobic oxidation of octanol in water 115
4.2 Surface-active ionic liquids for Palladium-catalysed cross coupling in water: Effect of ionic liquid concentration on the catalytically active species 125

5 Surface-active ionic liquids for sustainable energy production **133**
5.1 Surface-active ionic liquids in catalytic water splitting 135

6 Conclusions **143**

Appendix A **145**

Appendix B **203**

Appendix C **213**

Curriculum vitae **221**

Chapter 1

Introduction

1.1 Solvent usage and sustainability

Driven by an increasing awareness for safe, sustainable and environmentally benign chemistry, but also by increasing regulatory pressure, new solutions for greener chemical processes are required. Organic solvents usage is one of the main factors affecting the risk and the environmental impact of a chemical process. Their amount usually accounts for more than 50% of the materials used in the production of a drug or other fine chemicals (figure 1.1). In 2012 the global solvent consumption reached over 28 millions of metric tons.[1,2]

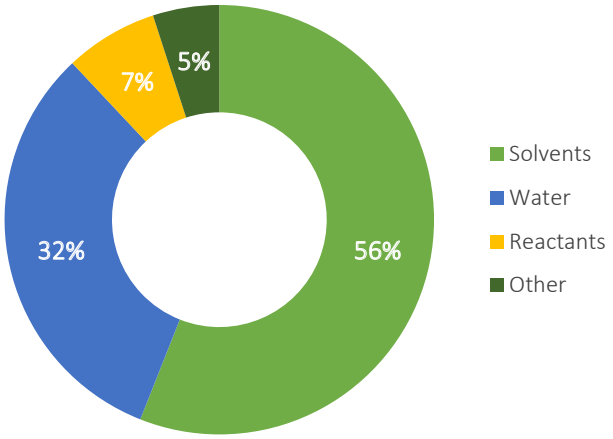

Figure 1.1: Composition of materials used to manufacture active pharmaceutical ingredients. Adapted from Gonzalez *at al.*[2]

As a consequence, limiting their used amount, increasing their recycling or replacing volatile organic solvents with more benign alternatives can strongly benefit the overall impact of a chemical process. There are many factors that influence the choice of a solvent: a balance between safety issues such as flammability or stability of the solvent, health conditions and exposure in the workplace, both areal and aqueous environmental impact, quality of the desired product, industrial constrains connected to the industrial process, waste treatment and costs needs to be obtained.[3,4] In order to simplify this choice an increasing number of companies are providing solvent selection guides, taking all these parameters in considerations.[2,4–7] These solvent selection guides provide a convenient tool to decide whether the use of a specific solvent is preferred, usable or undesired and should therefore be avoided. Even though differences can arise among companies due to their policy and culture, similarities can be identified such as considering solvents like ethanol or butyl acetate as preferred, while toxic hexane or solvents with high risk potential for the ozone layer such as carbon tetrachloride should be avoided.[6]

Although the best solvent would be no solvent, i.e. reactions performed in solvent-free manner, there are several alternatives to conventional organic solvents to improve a chemical process.[8] Among all the possible solvent options, water shows undoubtedly outstanding properties when it comes to safety and environmental concerns, and should therefore be a prime candidate for employment in the chemical industry. Water is in fact non-toxic, non-flammable, cheap and abundantly available.[9] Alternatively, a number of neoteric solvents such as ionic liquids, deep eutectic solvents, fluorous solvents, but also supercritical fluids such as supercritical carbon dioxide are available. Some ionic liquids can be considered as a sustainable solvent option, mainly due to their low flammability and vapour pressure. Moreover, with a careful adjustment of the cation and anion structure, low toxicity and high biodegradability can be achieved, while at the same time the price can be reduced.[10] A similar class of compounds with favourable economic properties are deep eutectic solvents, which consist mixture of ammonium or phosphonium salts with a hydrogen bond donor in a specific ratio so that the melting point of the mixture is decreased.[11]
As a result of this, renewed interest and intense research dedicated to the development of sustainable procedures, novel solvents, guides and solutions were implemented in the past years. In every case, advantages and disadvantages exist for all solvent options, requiring a careful evaluation of systems to identify the ideal solvent system for a particular reaction.

1.2 Ionic liquids and water: a powerful combination

Besides its safety and environmental superiority, water also shows excellent physical and chemical properties for organic synthesis. Due to its unique and strong hydrogen bond network, it can directly influence reaction mechanism and accelerate or decrease reaction rates.[12] Moreover, due to its polarity water also provides good solubility for inorganic additives such as bases, which are often required.[13] There are however two main drawbacks that have for a long time discouraged the broad implementation of water as reaction medium in organic reactions:

1. Some chemical functionalities are not stable in water and, even more importantly,
2. organic molecules usually show poor solubility in water, making it difficult to reach useful reactant concentrations.[14]

It is however possible to overcome this issue by the addition of additives that favour the solubility of organic molecules in water, such as amphiphilic molecules like surfactants that form aggregates in water with a liphopilic core.[15] A particularly interesting class of surface-active compounds for the application in synthesis and catalysis are ionic liquids with a long aliphatic rest that simultaneously act as surfactants. Ionic liquids have in fact shown in the past decades numerous successful applications in this field due to their unique reactivity. With the multiple possibilities obtained by combination and modification of the cation and anion structure, ionic liquids can fulfil the requirement for a variety of reaction types and set-ups, both from a chemical and technical point of view in laboratory as well as in industrial scale.[16] It is known that ionic liquids, and especially anions, can interact strongly with water and form clusters whose nature and size change with their structure and concentration. These clusters have also been shown to be able to influence and improve organic reactions, even though the mechanism is not always completely understood.[16–18]

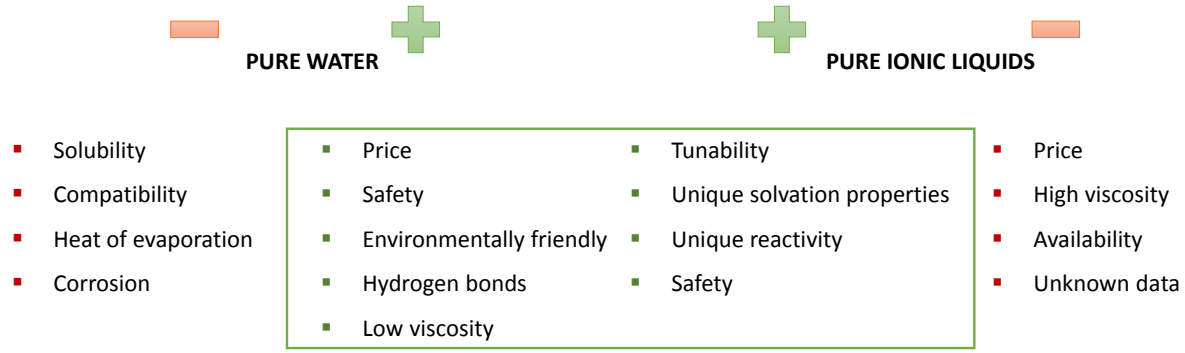

Figure 1.2: Advantages and drawbacks overcome by the combination of water with ionic liquids.[19]

From a practical point of view, the solvent systems water and ionic liquids can benefit from each other, forming a new media that manifests advantages from both, and, the same time, overcome the drawbacks of using them in a pure form, as it is summarized in figure 1.2. While ionic liquids are usually considered as expensive materials, in combination with water just a minor amount is required to benefit from their properties. Therefore cost issues that often exist when using ionic liquids as bulk solvent can be solved. Another problematic aspect that often exists when using pure ionic liquids is their high viscosity, which is drastically lowered by the addition of water.[20] Eventually, ionic liquids aggregates in water can provide a reaction environment different from bulk water, leading to a kinetic influence on a reaction

and hence can be able to catalyse or inhibit organic reactions, thereby providing a safer but yet cost-efficient reaction media for organic synthesis and catalysis.

1.3 Surface-active ionic liquids

In general surface-active ionic liquids (SAILs) can be classified as ionic liquids with a long alkyl chain substituent that is typically longer than eight carbon atoms.[21] As a result of the charged hydrophilic head group and the hydrophobic tail the ionic liquid has amphiphilic character and can behave like a surfactant, forming aggregates such as micelles when dissolved in water. The main parameter for the characterization of surface-active compounds is the critical micellar concentration (CMC), which corresponds to the threshold concentration at which the surfactant starts forming aggregates after saturation of the air-water interface. This process is depicted in figure 1.3.

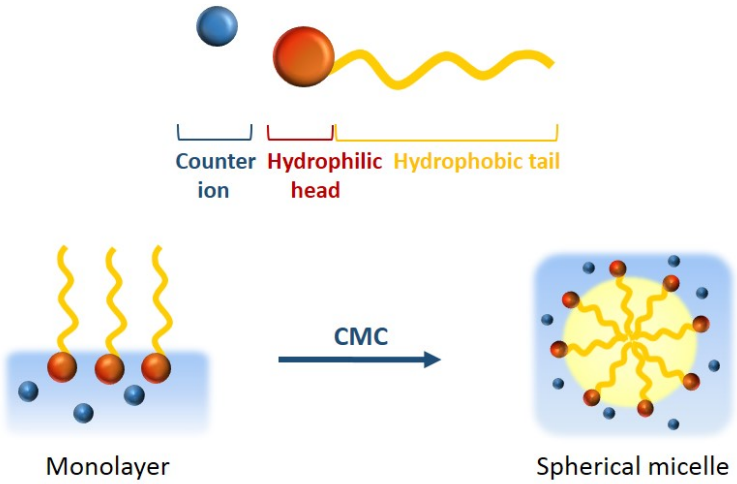

Figure 1.3: Amphiphile structure (top) and transition from monolayer formation at the air-water interface to micelles at the critical micellar concentration (bottom).

There are several experimental methods available to determine the CMC of surface-active ionic liquids, and results may vary considerable based on set-up and conditions of the measurement. For this reason, different values for the same surfactant can be reported in literature depending on the research group and the technique used, rendering the results not always reliable and consistent.[22] In general, the formation of micelles induces changes in several physical-chemical properties of the water solutions which can be used for the determination of the CMC with different strategies as briefly reported below.

- One of the most widespread technique for this purpose is surface tension measurement. As a consequence of surfactant absorption at the air-water interface, the surface tension of the solution decreases with increased concentration, until the surface is saturated and a stable value is obtained. The break point is defined as the CMC and the additional surfactant will contribute to the formation of micellar-like aggregates. This technique allows also for further characterization of surface-active compounds. Both efficiency (pC_{20}, usually given as -log of the concentration required to reduce the surface tension of the pure solvent by 20 mN/m) and effectiveness (Π_{CMC} defines how much the surface tension of the pure solvent is reduced) can be calculated as well. From surface tension curves the Gibbs adsorption isotherm equation can be used to estimate the average area per molecule residing at the surface (A_{min}) that gives information about the packing of the surfactant at the air-water interface.[23,24]

- Another simple and rather frequently applied technique for CMC determination is the measurement of conductivity. Curves of specific conductivity (k) versus surfactant concentration show two linear regimes with a breakpoint at the CMC. Micelles have lower

mobility than single ions and part of the anions are adsorbed on the surface of the aggregates, decreasing the total species contributing to the solution conductivity after the CMC is reached. Furthermore, the degree of counterion binding can be estimated from the ratio of the slopes of the two linear regimes, which indicates the ratio of counterions on the surface of the micelles.[25,26] Modifications to this conventional method have been reported including capillary electrophoresis and electromotive forces measurements.[27,28]

- When fluorescence spectroscopy is used to determine the CMC, a probe molecule such as pyrene is required. Both the solvent dipole moment and dielectric constant influence the vibrational band intensities in the fluorescence of pyrene. The ratio between the first and third vibrational peaks (I_I/I_{III}) decreases sharply when the pyrene passes from a polar water environment to a more apolar hydrocarbon-like solvent in the micelle core with increasing surfactant concentration. Typically, the curve has a sigmoidal shape, allowing to determine the CMC at the flex point.[26] When a quencher is added to the pyrene surfactant solution, aggregation numbers of the micelles can also be calculated.[29]

- Additionally, UV-Vis spectroscopy can be used for CMC determination, either by using the surfactant alone when it is UV-Vis active, or by implying the keto-enol tautomerism of probe molecule such as benzoylacetone, which is shifted toward the enol form in the micellar core.[26,30]

- ^{1}H NMR resonances undergo reasonable shifts as a function of the surfactant concentration because of the change in the solvation environment: protons from the charged head group get more exposure to water and are therefore less shielded, while terminal protons of the alkyl chain get shielded in the core.[31] The typical change in chemical shift can be used to calculate the CMC.

- Isothermal titration calorimetry measures the heat change due to the demicellization process when a diluted solution of the surfactant is titrated with a concentrated one. When the CMC is reached the only process taking place is micelles dilution. This technique can provide a broad thermodynamic characterization of the micellization process, enabling the determination of enthalpy and entropy as well as of the free energy of micellization.[32,33]

- Other methods that have been reported for the CMC determination of surface-active ionic liquids are scattering techniques such as Small Angle X-Ray Scattering (SAXS) and Small Angle Neutron Scattering (SANS). Both techniques are sensitive to electron-density differences and are therefore also powerful techniques for the determination of the structure of particle systems in terms of averaged aggregate size and shape.[34]

Several features of the molecular structure in surface-active ionic liquids have been modified and investigated, including different charged head groups, alkyl chain lengths, counter ions and also modification of the side chain. All these parameters influence the final aggregation behaviour. As a result of the intense research conducted in this area over the past years cationic, anionic, gemini, dicationic, zwitterionic, catanionic and otherwise functionalized surface-active ionic liquids have been reported. They have found application in different fields including analytical techniques, separations, inorganic material synthesis, organic synthesis, catalysis and biomolecules stabilization, as it will be summarized in the following chapters.

1.3.1 Structures of surface-active ionic liquids

Cationic surface-active ionic liquids

The most intensely investigated type of surface-active ionic liquids are cationic ones, which have a positively charged head group with a long alkyl chain and a variable counter anion. Various types based on imidazolium, pyridinium, pyrrolidinium, piperidinium and phosphonium head groups with different alkyl chain length have been reported and their structure is shown in figure 1.4.[31,35]

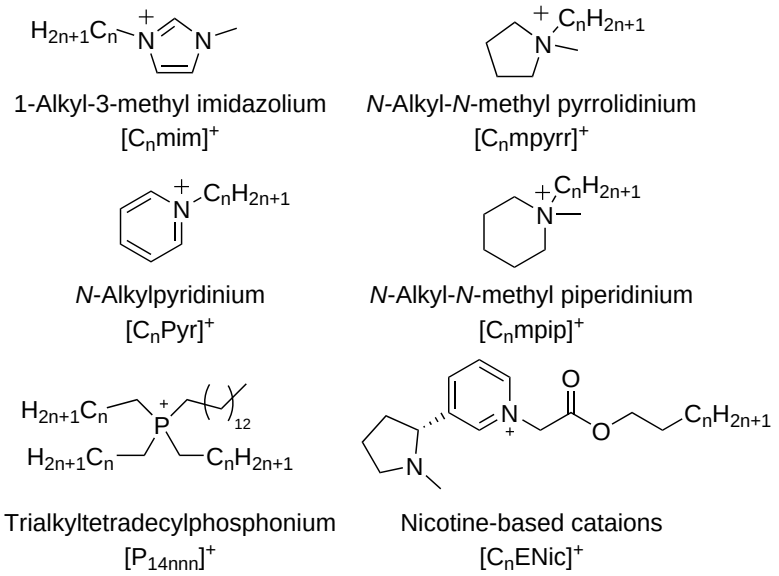

Figure 1.4: Typical head groups for cationic surface-active ionic liquids.

In the following table 1.1 the CMC values of different cationic surface-active ionic liquids with several head groups and hydrophobic chain length are given. The charged head group structure has a complex but minor influence on the CMC of the surfactants because it has two opposing effects: while electrostatic repulsion of the charged head within the micelles obstacles aggregation, the attempt to minimize interactions of hydrocarbons with water supports micelles formation. Due to the less polar head groups, surface-active ionic liquids usually show a higher surface-activity compared to conventional ammonium surfactants with similar alkyl chain length, showing both higher adsorption efficiency at the air-water interface and higher water surface tension decrease. This is particularly explicit for aromatic cations: the delocalization of the charge on the ionic liquid cation renders the electrostatic repulsion between the charged head groups less intense, thus favouring aggregation.[36] As a consequence several studies suggested that ionic liquids tend to aggregate into smaller micelles compared to the ammonium counterpart, also with lower aggregation number.[34,37,38] Moreover, pyridinium based ionic liquids have been found to be a fluorescence quenching agent.[31] Bio-inspired cations have also been reported, in fact through alkylation of the nitrogen on the pyridinium ring of nicotine with an ester-modified reactant a biodegradable surface-active ionic liquid with low toxicity could be obtained.[39]

As it can be seen from the data reported in the table 1.1 the CMC is decreasing with increasing length of the aliphatic chain and the effect is even stronger when a second medium/long chain, e.g. a butyl substituent is incorporated in the cation structure.[22] Also the addition of substituents on the ring of the head group increases the surface-activity as it was shown by a study on methylated pyridinium surface-active cations.[40]

Table 1.1: CMC of cationic surface-active ionic liquids measured with different techniques

IL	CMC [mM] method						Ref
	Surface tension	Conductivity	Fluorescence	NMR	Calorimetry	Other	
[C_{16}TEA]Cl			1.31				41, 42
[C_{12}TEA]Cl			24.4				41, 42
[C_{10}TEA]Cl	94.7, 68						41, 43
[C_{16}TEA]Br	0.93, 0.815	0.92, 0.92, 0.81	1				42, 44
[C_{14}TEA]Br	4.08,3.74	3.94, 3.94,3.78					44
[C_{12}TEA]Br	14.8	15.7, 15.3, 15.19	15.4				42, 44
[C_{10}TEA]Br	66.3	66.9, 65.6, 67.6					44
[C_{18}mim]Cl	0.45	0.40			0.2		41, 45
[C_{16}mim]Cl					0.753, 0.780, 0.892		46
	1.14	1.26					45
	0.87	0.86	1.30			0.92[a]	28
[C_{14}mim]Cl		3.4			4.6		41
	3.15	3.38					45
	2.98	3.68	3.65			3.52[a]	28
	4	3		4			47
		3.8			3.3		48
[C_{12}mim]Cl	16.8	15.1					25
					12.4, 12.9, 15.1		46
		14			13.8		48
	13.17	16.47	14			12.8[a]	28
	15		7	13			47
		14			13.8		48
[C_{10}mim]Cl		57.2			58.5		41
	53.8	59.9			58.5		45
		62			66		48
	39.9	40.47	40.52				28
	55		45	55			47
	45	78					49
[C_8mim]Cl	234	220					41, 45
	220			200			47
	100	90					50
	190	205					49
		200			263		48
[C_{16}mim]Br		0.653					51
		0.8					52
		0.61					37
[$C_{16}C_2$im]Br	0.26	0.27	0.29				53
[$C_{16}C_4$im]Br	0.1						52
[C_{14}mim]Br	1.9	2.5	1.8	1.4			35
		2.61					51
		2.5					37
[C_{12}mim]Br	10.6	10.6					25
	9	10	7	8			35
	10.9	8.5					36
		9.5					51
	4.3						52
		9.8					37
[$C_{12}C_4$im]Br	2.4						52
[$C_{12}C_{12}$im]Br	2.4						52
[C_{10}mim]Br	33	42	25	39			35
	40	30				39[b]	34
	20						52
	29.3	32.9					36
		40				40[a]	54
		41					37
[$C_{10}C_4$im]Br		74					52
[C_9mim]Br	6.3						37
[C_8mim]Br	170	160	130	177			35
	121						52
	150	150				160[a]	34
		160	190				55
[C_8C_4im]Br	41						52
[C_6C_4im]Br	271						52
[P_{14444}]Cl						1.0[c]	27
[C_{12}mpyrr]Cl	1.2						31
[C_{12}mpyrr]Br	15		15	10	15.3		22
[C_8mpyrr]Br		200	200				55

Continued on next page.

Table 1.1: CMC of cationic surface-active ionic liquids measured with different techniques

IL	CMC [mM] method						Ref
	Surface tension	Conductivity	Fluorescence	NMR	Calorimetry	Other	
[$C_{12}C_4$pyrr]Br	6			5	6.1		22
[$C_{12}C_8$pyrr]Br	150		150	120	144.7		22
[C_{16}Pyr]Cl	0.95 (30°C)	0.98 (30°C)	0.98				28
[C_{14}Pyr]Cl	3.5	4.18 (30°C)	3.88				28
[C_{12}Pyr]Cl	12.4 (30°C)	18	17.5				28
[C_{10}Pyr]Cl	63.3						28
[C_8Pyr]Cl	193						56
[C_{14}Pyr]Br	2.2	2.8	2.4	1.5			35
[C_{12}Pyr]Br	9.3	12	10	9.3			35
[C_{10}Pyr]Br	30	45		48			35
[C_8Pyr]Br	180	190		184			35
[C_8mPyr]Br		160	130				55
[C_{12}mPyr]Br	11						31
[C_{18}mPyr]Cl	0.3		0.23	0.25			31
[C_{16}mPyr]Cl	0.8		0.77	0.9			31
[C_{14}mPyr]Cl	3.1		3.1	3.2			31
[C_{12}mPyr]Cl	13		13.5	12.5			31
[C_{10}mPyr]Cl	45		44				31
[C_{12}mPyr]Br	10						31
[C_{12}mpip]Cl	19.79	19.93	19.50	17.5			57
[C_{12}mpip]Br	11						31
[C_{12}ENic]Br		8.7	8.7	10.3	6.1		39
[C_{10}ENic]Br		16.6	15.3	14.6			39
[C_8ENic]Br		55.1	54.3	62.0	54.7		39

[a] EMF (Electromotive Forces)
[b] SANS (Small Angle Neutron Scattering)
[c] Capillary electrophoresis

In analogy to conventional single chain surfactants, a correlation between the logarithms of the CMC and the number of carbon atoms in the hydrocarbon chain has been found to be valid for imidazolium based surface-active ionic liquids, as it can be seen in figure 1.5. This correlation is described by the empirical Stauff-Klevens rule:

$$logCMC = A - Bn$$

where the constants A and B are characteristics for a particular homologous series and temperatures. n is the number of carbon atoms in the side chain, A is a constant specific for the nature and the number of the hydrophilic groups, while B corresponds to the effect of each additional methylene group in the alkyl chain.

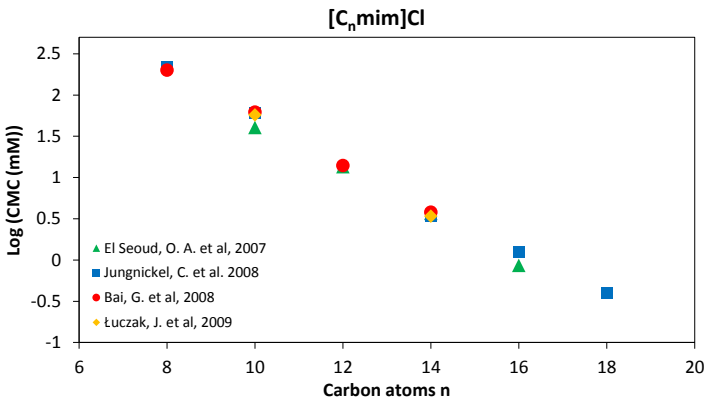

Figure 1.5: Linear correlation between the CMC and the alkyl chain length for a series of surface-active ionic liquids based on the 1-alkyl-3-methylimidazolium chloride structural motive.

Dicationic and zwitterionic surface-active ionic liquids

A special class of cationic surface-active ionic liquids are dicationc ionic liquids that contain two charged head group with two liphophilic hydrocarbon chains. When the spacer between the two heads is relatively short they can also be termed as gemini structures. Different structural designs have been reported and are depicted in figure 1.6.

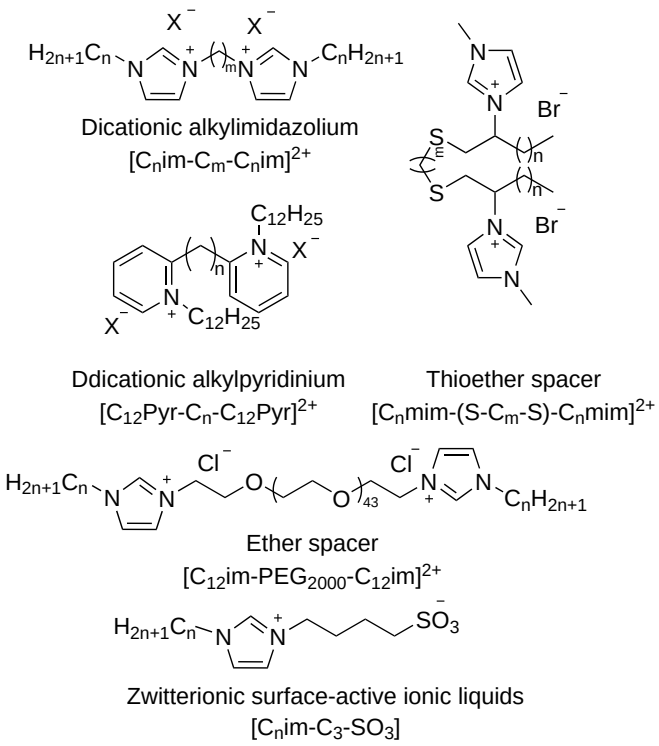

Figure 1.6: Reported head groups for dicationic surface-active ionic liquids.

A higher surface-activity has been found compared to the monocationic surface-active ionic liquids with an analogous hydrophilic and hydrophobic moieties, due to the additional head group and hydrophobic domain. In analogy to the monocationic surface-active ionic liquids a higher surface-activity is shown in comparison to the conventional ammonium surfactants and the strongest effect on CMC decrease is given by the length of the side chains, independently of their position on the ring. Moreover, the addition of aromatic groups in the side chain increases the overall hydrophobicity of the molecule and therefore further enhances surface-activity.[58,59] The spacer can be of different nature: a hydrocarbon chain, but also an ether or thioether chain can be present; moreover, the side chains can be modified as well with the addition of functional groups. The type of the spacer between the two charged head has an impact on the aggregation behaviour of the dicationic SAILs since it can manipulate the interactions of the charged head with each other and with water. An increase in the spacer length usually reduces the CMC, in fact, when flexible enough the spacer is able to fold inside the micelle. This is however a non-monotonic behaviour, as the CMC rather passes through a maximum or a minimum depending on the number of carbons in the spacer.[52,60,61] In the case of a series of $[C_{16}im\text{-}C_n\text{-}C_{16}im]Br_2$ a minimum in the CMC was observed when the spacer was formed by five methylene groups, while in the case of dicationic ammonium based surfactants a maximum is observed around n=6, clearly showing the different behaviour of this two types of surfactants. In table 1.2 the CMC values of different dicationic surface-active ionic liquids are reported. Nacham *et al.* reported even tricationic imidazolium surface-active ionic liquids with either a trimethylbenezene or a triethylamine bridging group and showed increased surface-activity compare to the dicationic ones.[62]

Table 1.2: CMC of dicationic surface-active ionic liquids measured with different techniques

IL	CMC [mM] method			
	Surface tension	Conductivity	Fluorescence	Ref
$[(C_{12})_3N\text{-}C_2\text{-}(C_{12})_3N]Br_2$	0.20			63
$[(C_{12})_3N\text{-}C_3\text{-}(C_{12})_3N]Br_2$	0.16			63
$[(C_{12})_3N\text{-}C_6\text{-}(C_{12})_3N]Br_2$	0.14			63
$[C_{16}im\text{-}C_{12}\text{-}C_{16}im]Br_2$		0.19	0.21	62
$[C_{12}im\text{-}C_4\text{-}C_{12}im]Br_2$	0.73			64
$[C_{12}mim\text{-}PEG_{2000}\text{-}C_{12}mim]Cl_2$	3.9	3.8		65
$[C_{12}im\text{-}C_3\text{-}C_{12}im]Br_2$	0.53	0.61	0.61	64
$[C_{10}im\text{-}C_{12}\text{-}C_{10}im]Br_2$	0.6			52
		0.66	1.04	62
$[C_{10}im\text{-}C_4\text{-}C_{10}im]Br_2$	2			52
	5.07			64
$[C_{10}im\text{-}C_3\text{-}C_{10}im]Br_2$	3.37	4.6	4.6	64
$[C_8im\text{-}C_3\text{-}C_8im]Br_2$	25	34.19	34.19	64
$[C_4im\text{-}C_{12}\text{-}C_4im]Br_2$	72			52
		58.6	58.5	62
$[C_4im\text{-}C_{10}\text{-}C_4im]Br_2$	117			52
$[C_4im\text{-}C_8\text{-}C_4im]Br_2$	323			52
$[C_1im\text{-}C_{10}\text{-}C_1im]Br_2$	149			52
$[C_{12}mim\text{-}(S\text{-}C_2\text{-}S)\text{-}C_{12}mim]Br_2$	0.32	0.40		66
$[C_{12}mim\text{-}(S\text{-}C_3\text{-}S)\text{-}C_{12}mim]Br_2$	0.26	0.35		66
$[C_{12}mim\text{-}(S\text{-}C_4\text{-}S)\text{-}C_{12}mim]Br_2$	0.22	0.31		66
$[C_{14}mim\text{-}(S\text{-}C_2\text{-}S)\text{-}C_{14}mim]Br_2$	0.072	0.10		66
$[C_{14}mim\text{-}(S\text{-}C_3\text{-}S)\text{-}C_{14}mim]Br_2$	0.063	0.085		66
$[C_{14}mim\text{-}(S\text{-}C_4\text{-}S)\text{-}C_{14}mim]Br_2$	0.058	0.071		66
$[C_{16}mim\text{-}(S\text{-}C_2\text{-}S)\text{-}C_{16}mim]Br_2$		0.022		66
$[C_{16}mim\text{-}(S\text{-}C_3\text{-}S)\text{-}C_{16}mim]Br_2$		0.021		66
$[C_{16}mim\text{-}(S\text{-}C_4\text{-}S)\text{-}C_{16}mim]Br_2$		0.020		66
$[C_{12}Pyr(2)\text{-}C_3\text{-}(2)C_{12}Pyr]Cl_2$		1.51		67
$[C_{12}Pyr(2)\text{-}C_4\text{-}(2)C_{12}Pyr]Cl_2$		1.28		67
$[C_{12}Pyr(2)\text{-}C_8\text{-}(2)C_{12}Pyr]Cl_2$		1.11		67
$[C_{12}Pyr(2)\text{-}C_{12}\text{-}(2)C_{12}Pyr]Cl_2$		0.22		67
$[C_{12}Pyr(2)\text{-}C_{12}\text{-}(2)C_{12}Pyr]Cl_2$		0.22		67

The concept was further developed by incorporating ester functionalities in the linker to the imidazolium or benzaimidazolium charged heads to afford a new class of biodegradable tricationic surface-active ionic liquids.[68]

The head group of the surface-active ionic liquid can be further modified to contain the counterion on the side chain producing zwitterionic surfactants. These have an overall neutral charge and therefore show an enhanced surface-activity. Different structures are possible in which the charged heads have different order. The anionic head is usually a sulphate group but also phosphate or carboxylates groups have been presented.[69] Souza *et al.* have reported a series of 3-(1-alky-3-imidazolium)propansulfonate based surface-active ionic liquids. Their solubility in pure water was however very poor due to strong interactions in the crystal lattice. Solubility was improved with the addition of electrolytes that interact with the micellar interface, and characterization of the aggregates could be performed, as shown by the CMC in table 1.3.[70]

Table 1.3: Comparison of the CMC of zwitterionic imidazolium based surface-active ionic liquids and corresponding sulfobetaines

n	CMC [mM]	
	$[C_n im\text{-}C_3\text{-}SO_3]$[a]	$[C_n TEA\text{-}C_3\text{-}SO_3]$[b]
16	0.0115	0.029
14	0.102	0.377
12	0.906	1.61
10	0.944	

[a] In electrolyte solution, Ref.[71]
[b] Ref.[72]

Side chain modification

Specific properties can be added to surface-active ionic liquids by modifying the side chains with targeted functional groups. Several modifications have been reported as depicted in figure 1.7 that strongly influence the properties and the surface-activity of the final compound (table 1.4).

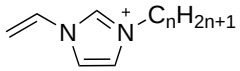

1-Vinyl-3-alkylimidazolium
$[C_nVim]^+$

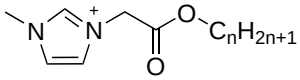

1-Alkyloxycarbonyl-3-methylimidazolium
$[C_nEmim]^+$

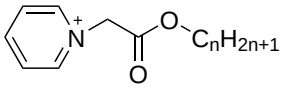

N-Alkyloxycarbonylpyridinium
$[C_nEPyr]^+$

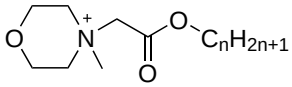

N-Alkyloxycarbonylmethylmorpholinium
$[C_nEmorph]^+$

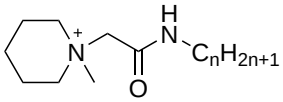

N-Alkylcarbamylmethylpiperidinium
$[C_nAmpip]^+$

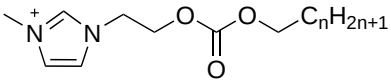

1-Alkyloxycarbonyloxyethyl-3-methylimidazolium
$[C_nCmim]^+$

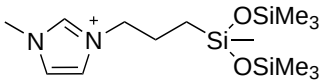

Trisiloxane tailed methylimidazolium
$[Si(3)C_3mim]^+$

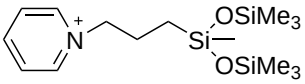

Trisiloxane tailed pyridinium
$[Si(3)C_3Pyr]^+$

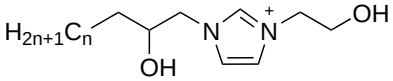

1-(2-Hydroxyalkyl)-3-(2-hydroxyethyl)imidazolium
$[HO\text{-}C_nHeim]^+$

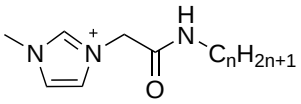

1-Alkylcarbamyl-3-methylimidazolium
$[C_nAmim]^+$

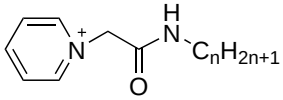

N-Alkylcarbamylpyridnium
$[C_nAPyr]^+$

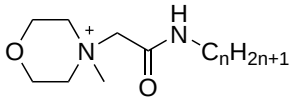

N-Alkylcarbamylmethylmorpholinium
$[C_nAmorph]^+$

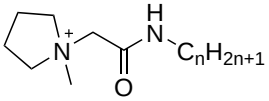

N-Alkyloxycarbamylmethylpyrrolidinium
$[C_nAmpyrr]^+$

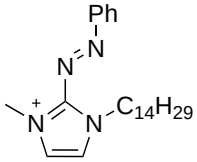

1-Tetradecyl-2-arylazo-3-methylimidazolium
$[C_{14}mimAzoPh]^+$

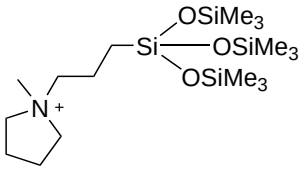

1-Methyl-1-[tri(trimethylsiloxy)]-silylpropylpyrrolidinium
$[((Me)_3SiO)_3\text{-}C_3mpyrr]^+$

Figure 1.7: Reported side chain modification for cationic surface-active ionic liquids.

The side chain modification can be a group with a chemical functionality such as a vinyl moiety, which showed a higher CMC value compared to the corresponding ethyl analogues because of the less hydrophobic character of the double bond.[53] Also a series of *N*-(2-hydroxyalkyl)-*N*-

(2-hydroxyethyl)imidazolium bromide surfactants was reported by Kamboj *et al.* and showed superior surface-activity in comparison to unfunctionalized ionic liquids.[38]
Since long alkyl chains in ionic liquids are typically associated with a higher (aqua-)toxicity, but also with poor biodegradability, increasing interest has been spent on the design of surface-active ionic liquids with improved properties in this regard.[73,74] In order to increase biodegradability of surface-active ionic liquids the addition of a cleavable bond such as an ester, an amide or a carbonate has been suggested for imidazolium and pyridinium based ionic liquids. In general, the presence of these functional groups in the side chain of typical ionic liquids can improve biodegradability as studied by Gathergood *et al.*, however it should be noted in this regard that the improvements are limited to the long side chain, whereas complete biodegradation of the core structure is not achieved.[74,75] The addition of an ester moiety can provide several additional benefits compared to simple surface-active ionic liquids with unfunctionalized alkyl chains, such as enhanced surface-activity through higher adsorption efficiency at the air/water interface and lower CMC and antimicrobial activity.[75,76] Similarly, also an amide moiety was introduced in the aliphatic group. Beside the enhanced surface-activity also a higher thermal stability of the final compound could be obtained. The possible intermolecular H-bonding offered by this functionality is considered to be responsible for its higher performance, however no major influence of the ring head was observed.[77,78] Similar trends were also observed on a series of ester and amide functionalized morpholinium surface-active ionic liquids.[38,79]

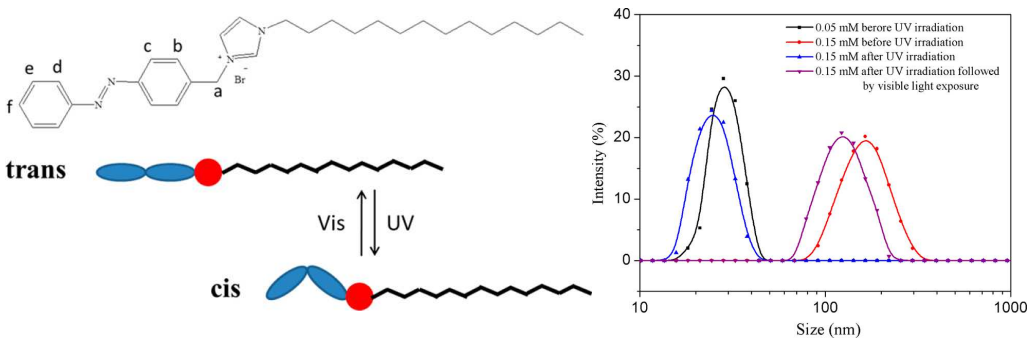

Figure 1.8: Molecular structure of photoresponsive SAIL [$C_{14}C_2$imAzoPh]Br (left) and aggregates size change with UV-Vis radiation (right) reported by Wu *et al.*[80]

Another modification that has been suggested both by Lin *et al.* and Wu *et al.* is the addition of an arylazo moiety on the imidazolium ring of surface-active ionic liquids. This class of compounds shows an enhanced surface-activity due to the increased hydrophobicity of the head group. Moreover, they have a specific photo-response to UV irradiaton as a consequence of the *cis-trans* isomerization of the azo double bond. The controlled switch between *cis* and *trans* isomer further decreases the CMC upon UV-irradiaton and changes the aggregates structure, as depicted in figure 1.8.[80,81]
Finally, the hydrocarbon chain was also modified by a siloxane moiety: the addition of trisiloxane groups at the end of the hydrocarbon reduces the melting point of the ionic liquids. These ionic liquids also showed an interesting surface-active behaviour: aggregate formation and a remarkably strong decrease of the water surface tension can be achieved already at rather short alkyl chain lengths. This is probably due to the different packing styles of the surfactants since the branched trisiloxane moieties are able to lie flat at the air/water interface.[82,83]

Table 1.4: CMC of functionalized surface-active ionic liquids measured by different techniques

IL	CMC [mM] method					Ref
	Surface tension	Conductivity	Fluorescence	Calorimetry	Other	
[C_{16}Vim]Br	0.48	0.49	0.41		0.40[a]	53
[C_{14}Vim]Br	1.85	2.06	1.86		1.85[a]	53
[C_{12}Vim]Br	7.00	8.15	11.33		8.75[a]	53
[C_{10}Vim]Br	27.20	33.22	24.13		26.86[a]	53
[HO-C_{16}Heim]Br	1.02	1.03	1.04			38
[HO-C_{14}Heim]Br	0.44	0.79	0.67			38
[HO-C_{12}Heim]Br	2.29	3.26	3.23			38
[HO-C_{16}Heim]Cl	0.70	1.75	1.48			38
[HO-C_{14}Heim]Cl	3.01	4.87	4.26			38
[HO-C_{12}Heim]Cl	1.34	3.18	2.29			38
[C_{14}Emim]Br	0.90	0.94	1.0			76
[C_{12}Emim]Br	2.5	3.8	1.0			76
[C_{10}Emim]Br	12	17	16			76
[C_8Emim]Br	43	77	74			76
[C_{14}EPyr]Br	0.90	0.91	0.87			76
[C_{12}EPyr]Br	3.4	4.1	3.4			76
[C_{10}EPyr]Br	14	17	14			76
[C_8EPyr]Br	60	73				76
[C_{14}Amim]Br	0.95	1.2	1.2			77
[C_{12}Amim]Br	5.5	5.2	6			77
[C_{12}Amim]Cl	3.43	5.80	4.55	5.14		78
[C_{10}Amim]Br	16	19	15			77
[C_8Amim]Br	65	77	80			77
[C_{14}APyr]Br	1	1.2	1.1			77
[C_{12}APyr]Br	4.8	4.6	3.4			77
[C_{10}APyr]Br	12	18	18			77
[C_8APyr]Br	70	73				77
[C_{14}Cmim]Cl	0.37	0.92	0.59		0.89[b]	75
[C_{12}Cmim]Cl	2.1	3.4	2.9		2.7[b]	75
[C_{10}Cmim]Cl	11.1	13.1	11.0		12.1[b]	75
[C_{12}Ampyrr]Cl	3.25	5.45	3.40	4.10		78
[C_{12}Ampip]Cl	3.10	5.20	4.05	3.680		78
[C_{12}Amorph]Cl	3.85	6.64	4.82	5.60		78
[C_{16}Emorph]Br	0.23	0.38	0.43	0.34		79
[C_{12}Emorph]Br	3.63	5.83	3.49	3.9		79
[C_8Emorph]Br	64.56	99.0	91.1	76.9		79
[C_{16}Amorph]Br	0.28	0.46	0.30	0.22		38
[C_{12}Amorph]Br	3.1	5.02	3.20	2.38		38
[C_8Amorph]Br	58.8	78.1	63.0	69.2		38
[C_{14}mimAzoPh]Br	0.15 (0.129[c])	0.147 (0.139[c])				81
[$C_{14}C_2$imAzoPh]Br	0.423 (0.307[c])	0.419 (0.402[c])				81
[C_{14}mimAzoPh]I	0.080 (0.072[c])	0.101				81
[$C_{14}C_2$imAzoPh]Br	0.111 (0.095[c])	0.102				81
[Si(3)C_3mim]Cl	15.5	19.7				82
[Si(3)C_3Pyr]Cl	24.8	30.2				82
[$((Me)_3SiO)_3$-C_3mpyrr]Cl	5.7	5.5				84

[a] UV-Vis absorbance
[b] Potentiometry
[c] After UV irradiation

Role of the anion

The anion plays a major role in the design and selection of any ionic liquid, as it is well known to alter and define their physical and chemical properties.[16] In the case of common hydrophobic ionic liquids with anions such as $N(Tf)_2^-$ and PF_6^- no micelle formation could be observed due to the poor solubility of the ionic liquids in water.[47] As for pure ionic liquids, the nature of the anion has a crucial impact on the aggregation behaviour of surface-active ionic liquids. The anion plays a major role in the neutralization of the charged head groups: anions that are able to shield this repulsion will facilitate micelle formation. This ability is correlated to the hydrophobicity and level of hydration of the anion. A less hydrated ion will then tend to stay closer to the micellar interface and shield the charged head groups more effectively, hence a lower CMC will be observed. In figure 1.9 and table 1.5 structures of different anions and CMC values of the corresponding cationic surface-active ionic liquids are reported.

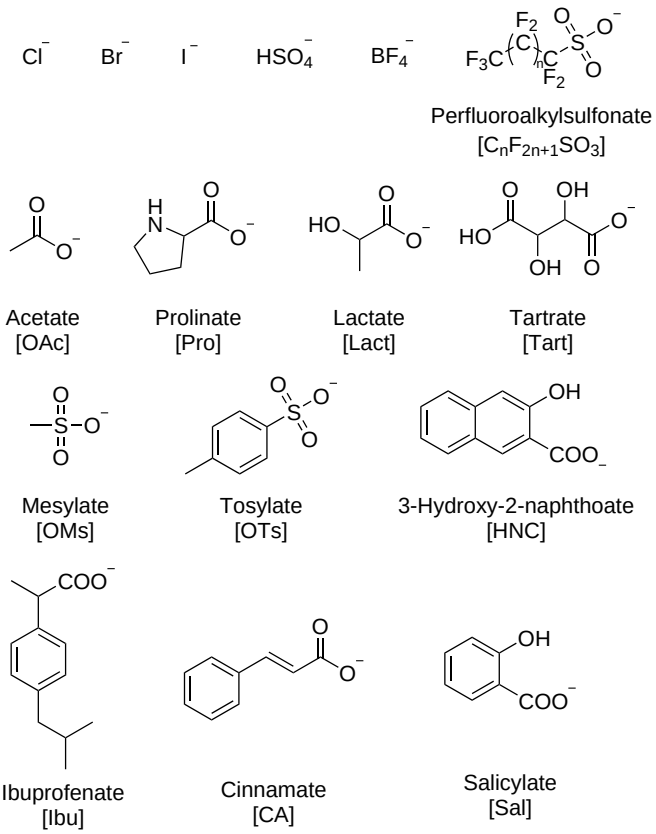

Figure 1.9: Reported anions for cationic surface-active ionic liquids.

In the case of halides, a larger and more polarizable anion such as iodide leads to stronger micellar interactions and hence lower CMC than a more hydrated chloride anion. Consequently, the CMC values decrease in the following order $Cl^- > Br^- > I^-$. Several anions have been reported each one showing specific behaviour, including hydrogen sulphate, BF_4^-, short chain alkylsulfonates, and carboxylates, both the simple acetate or amino acid based ones.
Aromatic anions provide a specific behaviour, since they add a rather strong hydrophobic character to the surfactant. The surface-activity is consequently significantly enhanced, especially due to the π-π interactions possible between the aromatic anions and the imidazolium ring. However, the steric hindrance of the anion should be taken into consideration, as this could hinder its screening efficiency.[85] A study from Singh *et al.* with a combination of stady-state fluorescence, isothermal titration calorimetry, ^{1}H NMR and dynamic light scattering has furthermore shown that these anions migrate into the micelle, forming ion pairs with the surfactant charged head, especially if substituents on the aromatic ring are present that further

increase the hydrophobicity of the anion.[86] Moreover, substituent positions on the aromatic ring may have an influence on the micellization behaviour, as it is the case for *m*- and *p*-hydroxybenzoate anions that show higher CMC in comparison to salicylate, when the same cation is present.[87]
In addition, a series of imidazolium based surface-active ionic liquids with biologically relevant aromatic anions has been reported by a number of authors including ibuprofene, salicylate, cinnamate and acetylsalicylate.[49,57,88,89] The presence of the large and rather hydrophobic anions could induce aggregation even with short alkyl chains of $n = 4$ in the cation. The same trend between anion hydrophobicity and CMC was observed for dicationic surface-active ionic liquids.[67]

Table 1.5: CMC of cationic surface-active ionic liquids with different anions.

	CMC [mM] method					
IL	Surface tension	Conductivity	Fluorescence	Calorimetry	Other	Ref
[C_{16}mim]HBS	0.38	0.36	0.41	0.34		86
[C_{16}mim]BS	0.33	0.38	0.33	0.32		86
[C_{16}mim]OTs	0.22	0.21	0.29	0.21		86
[C_{14}mim]HSO_4	1.23	2.18		2.34		90
[C_{12}mim]Cl	16.8	15.1				25
[C_{12}mim]Br	10.6	10.6				25
[C_{12}mim]I	4.6	5.2				25
[C_{12}mim]HSO_4	10.25	9.86		10.05		90
[C_{12}mim]BF_4	9.2	9.2				36
[C_{12}mim]OMs	14		19			24
[C_{12}mim]OAc	1.79					91
[C_{12}mim]Sal	2	2.21				85
[C_{12}mim]*m*HB	4.35		4.31			87
[C_{12}mim]*p*HB	4.96		5.92			87
[C_{12}mim][CA]	2.5	2.74				89
[C_{12}mim]HNC	0.35	0.36				85
[C_{12}mim][$C_4F_9SO_3$]		0.098				92
[C_{10}mim]HSO_4	37.4	37.7		45.3		90
[C_{10}mim]OMs	60		65			24
[C_8mim]HSO_4	205	206				90
[C_8mim]OMs	220					24
[C_8mim]I	100	150				50
[C_8mim]Ibu	12	14				49
[C_8mim][Tart]	25				22.9[a]	93
[C_8mim][Prol]	2.4				3.2[a]	93
[C_8mim][Lact]	3.3				4.6[a]	93
[C_8mim][$C_4F_9SO_3$]		2.41				92
[C_6mim]Ibu	38	41				49
[C_6mim][$C_4F_9SO_3$]		8.22				92
[C_4mim]Ibu	75	75				49
[C_{12}mpip]AcSal	1.23	1.27	1.28	1.52		57
[C_4mpyrr][$C_4F_9SO_3$]		10.09				92
[$(C_4)_4N$][$C_4F_9SO_3$]		2.43				92
[C_2mim][$C_4F_9SO_3$]	91.39	81.3		76.76		94
[C_2mim][$C_8F_{17}SO_3$]		1.33				94
[C_2mpy][$C_4F_9SO_3$]		13.82				94
[P_{14444}]OAc					3.2[b]	27
[P_{14666}]OAc					0.8[b]	27

[a] UV-Vis absorbance,
[b] Capillary electrophoresis,

A similar effect on surface-activity as was observed through the variation of the counterion of the surfactant, can also be obtained with the addition of external inorganic salts.[36] The addition of sodium inorganic salts decreases the surface tension and the CMC of imidazolium and pyridinium based ionic liquids. This is due to the positioning of the inorganic ions at the interfacial electric double layer of the micelle, thereby reducing the repulsion of the charged head group and thus favouring aggregation. The strength of this effect is dependent on the screening ability of the added ions. In case of sodium halides as additives, the Hofmeister series $<Cl^- < Br^- < NO_3^- < I^-$ is followed, since the hydration decreases with the charge neutralization

efficiency.[43,95] Through Small Angle Neutron Scattering (SANS) investigation it was shown for [C_8mim]Cl and Br that these salts do not change the shape of the aggregates but increase their aggreggation number and size and induce the micelle to organize into clusters.[40,95] The same effect of lowering the CMC with the addition of inorganic salts was also observed for dicationic, tricationic and zwitterionic surface-active ionic liquids, as well as for anionic surface-active ionic liquids with the addition of alkylammonium salts.[62,69,96,97]
The CMC can also be reduced by organic additives, in fact the solubility of aromatic compounds in water increases in the presence of surface-active ionic liquids because these can be hosted in the micellar core. At the same time the CMC is lowered because of hydrophobic interactions.[93,98,99] The effects of polar organic solvents methanol, ethanol, *n*-propanol, *n*-butanol, ethylene glycol and propylene glycol on the micellization and surface adsorption behaviour of the surface-active ionic liquid 1-dodecyl-3-methylimidazolium bromide and the traditional cationic surfactant dodecyltrimethylammonium bromide have also been studied. The results show that methanol, ethanol, ethylene glycol and propylene glycol act as co-solvents and slightly increase the CMC of both surfactants in aqueous solutions. However, more hydrophobic solvents such as *n*-propanol and *n*-butanol act as co-surfactants; consequently, the CMC of the respective surface-active ionic liquid is decreased by their presence.[100]
Alternatively, an alkyl chain can be replaced by a fluorinated one, and recently fluorinated surface-active ionic liquids composed of perfluorinated anions have been reported. An extensive study by Pereiro *et al.* showed that perfluorinated alkylsulfonates strongly decrease the CMC in comparison to the corresponding halide based ionic liquids, due to the high hydrophobicity of the fluorinated chain. Even for short-chain cations [C_2mim][$C_4F_9SO_3$] and [C_2mim][$C_8F_{17}SO_3$] a critical aggregation concentration could be detected.[92,94]

Anionic surface-active ionic liquids

While an alkyl chain with at least eight carbon atoms is generally a pre-requisite for the formation of surface-active ionic liquids, this can be either on the cation or on the anion. Even though the field of anionic surface-active ionic liquids has been less investigated, it shows remarkable advantages for the use of ionic liquids as surfactants: this class of surface-active ionic liquids has in fact lower CMC values than the corresponding cationic ones or anionic surfactants with an inorganic cation. Common anionic surface-active charged groups for ionic liquids are depicted in figure 1.10 and the corresponding CMC values are reported in table 1.6.
The first type of anionic surface-active ionic liquids reported were derived from conventional alkylsulphates. The common inorganic cations like sodium were replaced by larger organic cations that allowed for a better screening of the intramicellar electrostatic repulsion among the polar head groups, and hence a significantly lower CMC.[30] Surface-active anions can, and have been, further combined with an alkylimidazolium cation with different alkyl chain length. When both cation and anion reach a certain alkyl chain length the surfactant can be defined as catanionic since both show surface-activity. However, even though increasing the hydrophobic domain in cation and anion benefits the surface-activity, their solubility in water can decrease.[30,61,101]
In general, anionic surface-active ionic liquids based on alkylsulphates provide some benefits including higher thermal stability, low toxicity, and higher biodegradability. These aspects can be further increased by combination with amino acid derived cations.[56,106]
Alternatively, imidazolium alkylsulfonates ionic liquids have been extensively investigated by Blesic *et al.*. A matrix of ionic liquids with variable chain length in both the cation and the anion has been synthesized and characterized, confirming that a long alkyl chain on the anion is more efficient in decreasing the CMC than a similar alkyl chain on the cation.[24,113]
A series of protic ionic liquids based on long-alkyl chain carboxylates was further investigated

Table 1.6: CMC of anionic surface-active ionic liquids measured by different methods.

IL	CMC [mM] method					Ref
	Surface tension	Conductivity	Fluorescence	Calorimetry	Other	
$Na[C_{14}SO_4]$	1.5					102
$Na[C_{12}SO_4]$	7.5					102
$[C_4mim][C_{16}SO_4]$	0.14	0.17	0.21			103
$[C_6mim][C_{14}SO_4]$	0.40	0.42	0.45			103
$[C_4mim][C_{12}SO_4]$	1.8	2.1				104
		2.2				105
$[C_6mim][C_{12}SO_4]$		1.12				105
$[C_8mim][C_{12}SO_4]$	0.3	0.3	0.4			103
$[C_4mpyrr][C_{12}SO_4]$	2.7	3.8			31[a]	104
$[C_8Py][C_{12}SO_4]$	0.01					56
$[C_6Py][C_{12}SO_4]$	0.061					56
$[C_4Py][C_{12}SO_4]$	0.12					56
$[GlyC_4][C_{12}SO_4]$	0.43					106
$[AlaC_4][C_{12}SO_4]$	0.49					106
$[ValC_4][C_{12}SO_4]$	0.28					106
$[ProC_4][C_{12}SO_4]$	0.42					106
$[C_4mim][C_8SO_4]$		31			31[a]	30
	31.9	32.4				101
$[C_6mim][C_8SO_4]$	18.6	19.5				101
$[C_4mim][C_{12}SO_3]$	4.4	4.7				97
$[C_4mim][C_{12}SO_3]$	4.4	4.7				97
$[C_4mim][C_8SO_3]$	135		130			24
$[C_8mim][C_8SO_3]$	12		17			24
$[C_8mim][C_4SO_3]$	140		155			24
$[C_4mim][C_{12}BzSO_3]$	1.08			1.47		107
$[C_4Pyr][C_{12}BzSO_3]$	0.928			1.16		107
$[C_4mim][C_8H_{17}CO_2]$	45	42.2	44.9			108
$[C_4mim][C_{10}H_{21}CO_2]$	3.54	3.42	3.55			108
$[C_4mim][C_{12}H_{25}CO_2]$	0.44		0.45			108
$[im][C_8H_{17}CO_2]$	2.6	2.7				109
$[im][C_7H_{15}CO_2]$	4.6	4.5				109
$[im][C_6H_{13}CO_2]$	5.8	5.8				109
$[im][C_5H_{11}CO_2]$	11.2	11.2				109
$[pyrr][C_8H_{17}CO_2]$	2.1	2.2				109
$[pyrr][C_7H_{15}CO_2]$	2.8	2,8				109
$[pyrr][C_6H_{13}CO_2]$	4.8	4.6				109
$[pyrr][C_5H_{11}CO_2]$	9.3	9.5				109
$[Cho][C_5H_{11}SO_3]$		16.3				110
$[Cho][C_6H_{13}SO_3]$		4.6				110
$[Cho][C_7H_{15}SO_3]$		2.7				110
$[Cho][C_8H_{17}SO_3]$		1.0				110
[Gua]AOT	1.69	2.32				111
[Cho]AOT	1.87	2.38				111
$[C_4mim]$AOT	1.65	1.88				111
	1.7	1.9	1.8			108
		2.05	1.7			112
$[ProC_3]$AOT	1.45	1.43				111
$[C_4mim]$DEHP	9.3	9.6	13.5			108

[a] UV-Vis absorbance

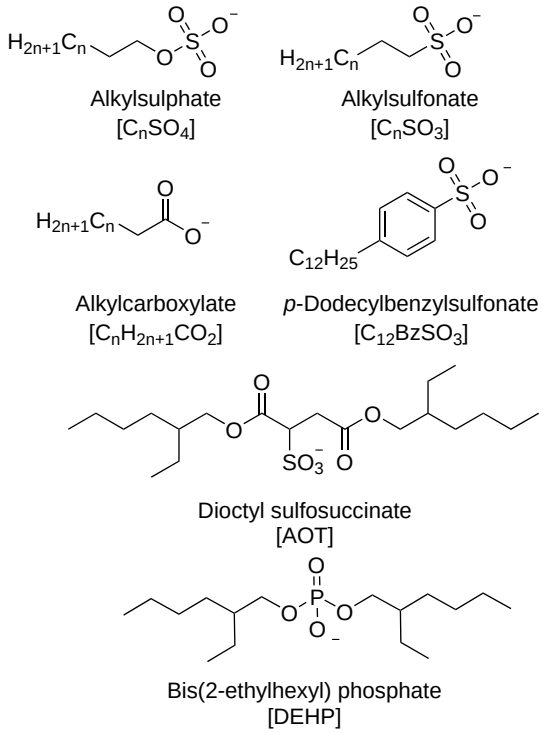

Figure 1.10: Reported groups for anionic surface-active ionic liquids.

with different cations such as imidazolium and pyrrolidinium. These ionic liquids showed a higher surface-activity than both the corresponding surfactants with inorganic cations and anionic surface-active ionic liquids based on alkylsulfates. In fact aggregation was also observed for alkyl chains with only 5 carbon atoms.[108,109]

The cholinium cation was combined with perfluoroalkanoate surface-active anions to yield a new class of high performance surfactant with a biodegradable cation.[110] Commonly used surface-active anions with two long alkyl chains such as dioctyl sulfosucccinate - also known as AOT - or bis(2-ethylhexyl) phosphate have been combined with typical ionic liquids such as imidazolium or cholinium as well, showing once more the superiority of these cations compared to metal ions.[108,111,112] Through an acid-base reaction between the lauryl monoester of diacetyl-(*L*)-tartaric acid and (*S*)-(-)-α-methylbenzylamine, an anionic surface-active ionic liquid with chiral centres both in the cation and the anion was obtained with a melting point of 55°C and a CMC of 0.32 mM detected by surface tension.[114]

1.3.2 Further characterization and properties of surface-active ionic liquids

While surface tension measurements and other analytical techniques such as as conductivity, fluorescence spectroscopy etc. allow for a practical and reliable determination of the critical micelle concentration, relatively little information is gained on size and shape of the aggregates. Scattering techniques such as SAXS and SANS are very powerful methods to characterize aggregate shape and size. The radiation of either the X-rays or neutrons scattered by the sample is registered by a detector; this is sensitive to electron-density differences and can therefore provide information on the sizes and shapes of particles in the nanometre range, but also on the internal structure of partially ordered systems and on the supramolecular organization pattern.[115] However, the application of SAXS and SANS for the characterization of surface-active ionic liquids is often hindered by the lack of a suitable contrast at low concentrations close to the CMC, especially for systems which form less compact micelles. Consequently, characterization of surface-active ionic liquids via SAXS and SANS is often reported at much higher concentrations. For [C_8mim]Cl and [C_8mim]I it was usually possible to fit the measured curves to a spherical or elipsoidal shape, however in the case of Cl^- sharp contrast was only obtained at a concentration of 500 mM, while for I^- 100 mM was sufficient. In the latter case particles radii ranging from 1.65 to 1.95 nm were found with increasing concentrations up to 3000 mM.[50] Goodchild *et al.* reported for [C_{10}mim]Br and [C_8mim]Br a particle radius of 1.34 nm and 1.05 nm respectively, and in both cases their shape shifted from spherical to elongated when increasing the concentration to 600 mM.[34] Fitting of SANS for octylpyridinium chloride was difficult and only a bi-layered structure at 4000 mM could be predicted.[40] For a series of [$C_n$mim][C_8SO_4] based surface-active ionic liquids at 50 mM a shift in the micelles' shape from spherical to ellipsoidal to vesicular structures was observed with the increase of the chain length on the imidazolium cation from 4 to 10 carbons.[101] Wang *et al.* were the first to report that alkylimidazolium bromide surface-active ionic liquids can form unilamellar vesicles in aqueous solutions. With the aid of cryo-Transmission Electron Microscopy (cryo-TEM) they could verify that the self-assembly can transfer from spherical micelles to rodlike micelles and then to vesicles with increasing concentration.[116] Multilamellar vesicle structures were also reported for the protic surface-active ionic liquids diisopropylethylamine nonecyl carboxylate.[109] Using DLS, cryo-TEM and SAXS investigations Sun *et al.* reported that [C_{16}im-C_3-SO_3] with the addition of sodium β-naphtalene, sulfonate forms initially micelles that evolve to worm-like shaped aggregates and then to hexagonal liquid crystalline structures with increasing concentration.[117]

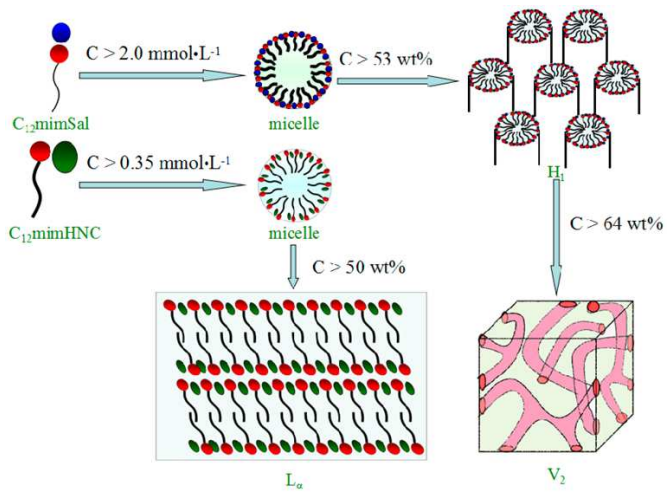

Figure 1.11: Liquid crystalline phase shifts reported by Xu *et al.*[85]

In case of 1-alkyl-3-methylimdiazolium based surface-active ionic liquids, lyotropic liquid crystalline phases including hexagonal liquid-crystalline phase (H1), cubic liquid-crystalline phase (V2) or lamellar liquid-crystalline (L($_alpha$)) phases have also been observed at higher concentrations.[34,85,89] As presented by Xu *et al.* in figure 1.11 when an aromatic anion is combined with the dodecylimidazolium cation different types of liquid crystalline phases can be observed. In the case of salicylate first a hexagonal (H_1) phase is formed. A further increase of the mass fraction of the ionic liquid in water results in the formation of a broad region of cubic liquid-crystalline phase (V_2). In contrast, in case of a larger anion such as 3-hydroxy-2-naphthoate a lamellar liquid-crystalline (L_α) is formed.[85,118]
Through temperature dependent conductivity or isothermal titration calorimetry (ITC) studies, a full thermodynamic characterization of the micellization process can be obtained, providing information on enthalpy, entropy and free energy of micelle formation.[46] The evaluation of these parameters has been addressed by several research groups and a similar thermodynamic behaviour to conventional surfactants has been identified for surface-active ionic liquids. The aggregation is the result of a balance between entropic and enthalpic contributions, in fact the CMC follows an U-shape dependence according to the temperature. The micellization process is usually entropy driven at low temperature and becomes enthalpy driven at higher temperatures, going through a minimum that is defined as the Krafft temperature. The reason for this behaviour is the gradual breakdown of the hydrogen-bond network of liquid water as temperature increases (entropic gain) which leads to an association enthalpy-driven micellization process at higher temperatures. The micellation process is endothermic (ΔH°_m>0) at low temperature and becomes exothermic at higher temperature (ΔH°_m<0), while entropy contributions are positive over the entire range but decrease with increasing temperature. The enthalpic term increases with increasing chain length.[48,61] Overall the free energy of micellization is always negative, as a consequence the process is spontaneous.[41] Table 1.7 summarizes the thermodynamic parameters for different surface-active ionic liquids with different structures from the comprehensive work of Galgano *et al.*. As it can be seen in the collected data, the ΔG°_m is decreasing regularly with a longer alkyl chain length. Each additional methylene group contributes around -3 kJ/mol to the free energy of micellization, and ΔH°_m is changing from positive to a negative value with increasing temperature. In contrast, the head group structure seems to have just a minor influence on the thermodynamics of micellization.[119]

Table 1.7: Thermodynamic parameters of micelle formation for different surface-active ionic liquids.

IL	T [°C]	ΔG°_m [kJ/mol]	ΔH°_m [kJ/mol]	-TΔS°_m [kJ/mol]	Ref
[C_{10}mim]Cl	25	-29.45	2.85	-32.30	119
[C_{10}mim]Cl	25	-25.0	3.5	-28.5	41
[C_{12}mim]Cl	25	-36.15	2.04	-38.19	119
[C_{14}mim]Cl	25	-41.82	0.54	-41.28	119
[C_{14}mim]Cl	25	-35.4	-0.5	-34.9	41
[C_{16}mim]Cl	15	-47.42	4.25	-51.67	119
[C_{16}mim]Cl	25	-48.63	-2.75	-45.88	119
[C_{16}mim]Cl	35	-49.64	-10.08	-39.56	119
[C_{16}mim]Cl	45	-50.41	-16.5	-33.91	119
[C_{16}mim]Cl	55	-50.67	-21.12	-29.55	119
[C_{16}mim]Cl	65	-50.75	-24.12	-26.63	119
[C_{16}mim]Cl	75	-50.71	-24.64	-26.07	119
[C_{18}mim]Cl	25	-43.3	-6.2	-37.1	41
[C_{16}Pyr]Cl	25	-47.31	-1.16	-46.15	119

1.3.3 Applications of surface-active ionic liquids

Surface-active ionic liquids are versatile surfactants with improved surface-active properties. Through their structural tunability compounds with unique micellization properties can be synthesized to target specific applications in different fields. The following section demonstrates the potential of surface-active ionic liquids for multiple applications, focusing on the most recent reports and developments in various fields.

Application in separations

Micellar solutions of ionic liquid based surfactants have been successfully used in separation science, mostly implemented as substitutes for conventional solvents in extraction processes. An initial finding that demonstrated the potential of surface-active ionic liquids in separation techniques addressed the solubilization of aromatic compounds in micellar solutions. The authors observed that the concentration of the aromatic hydrocarbons benzene, toluene and xylene gradually increased above the CMC for a series of alkylmethylimidazolium chloride based surface-active ionic liquids, with the highest solubilities found for benzene. Moreover, the number of moles of solute that can be incorporated in the micelle by one mole of ionic liquid was found to be significantly higher when compared to that of ionic surfactants of similar chain length, probably due to the additional $\pi - \pi$ interactions between the imidazolium head group and the aromatic solubilizate.[98]
The isolation of pharmaceutically active ingredients from different biomasses is a process that usually requires a relevant amount of organic solvents. In order to replace them with a more benign solvent like water, the implementation of ionic liquids micellar solutions has been suggested. Due to the hydrophobic core of the micelles formed in water higher solubility of the isolated organic molecules can be achieved, reaching extraction efficiencies comparable with those of conventional organic solvents. This strategy was successfully applied in several cases, and often a direct correlation between alkyl chain length, CMC and extraction efficiency was identified. In the extraction of piperidine from black pepper (*Piper nigrum*) with micellar solution of surface-active ionic liquids Ressmann *et al.* have shown that the extraction efficiency strongly increases after the CMC.[120] Bogdanov *et al.* investigated the extraction of sesquiterpenic acids in *Valeriana officialis* and could show that the micelles formation was the key factor increasing the extraction efficiency. In fact ionic liquids with short alkyl chains could not reach satisfactory performance even at high concentrations, while the amount of extracted sesquiterpenic acids strongly increased when surface-active ionic liquids were employed, this increase in performance was obtained already at concentrations slightly below the corresponding CMC.[121] De Faria *et al.* investigated the increased solubility of the triterpenic ursolic acid in surface-active ionic liquids micellar solutions, these were applied in the extraction of ursolic, oleanolic and betulinic acids from apple peels: surface-active ionic liquids outperformed both conventional cationic and anionic surfactants solutions and organic solvents.[122]
Apart from separations on preparative scale, surface-active ionic liquids were also successfully applied in analytical separations. Examples include their use as mobile or stationary phase modifiers in high performance liquid chromatography, but also as the micellar component in capillary electrophoresis.[124] The use of mixed hemimicelles of surface-active ionic liquids in a magnetic based micro-dispersive solid phase extraction for the determination of phenols in water samples was investigated by Trujillo-Rodríguez *et al.*. Cationic and dicationic ionic liquids as well as their mixtures in different ratios were tested. Under optimum conditions a very low amount of ionic liquids [$C_{12}C_{12}$mim]Br and [C_{16}mim]Br (less than 10 mg) was sufficient due to their particularly low CMC.[125] The surface-active ionic liquid [C_{14}mim]Br was used as pseudostationary phase in boronate affinity-assisted micellar electrokinetic chromatography

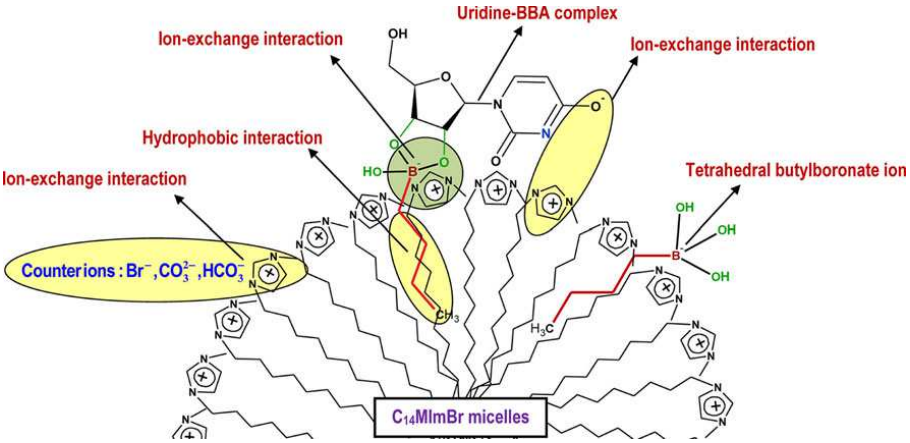

Figure 1.12: Schematic illustration of the mechanism of interaction of uridine-butylboronic acid (BBA) complex with [C_{14}mim]Br. Picture taken from Rageh *et al.*[123]

for the analysis of urinary nucleosides. The principle of separation depended on the different electrostatic and hydrophobic interactions between the positively charged micellar pseudostationary phase, the boronic acid additive that also acted as cosurfactant and the negatively charged nucleoside as depicted in figure 1.12.[123] Similarly, micellar solutions of [C_{12}mim]BF_4 were found suitable as pseudostationary phase in micellar electrokinetic chromatography for the separation of eleven carbamate pesticides in different fruit and vegetable juice samples.[126] Micellar solutions of surface-active imidazolium based ionic liquids were also found to modify the redox behaviour of dopamine and ascorbic acid. This allowed for the simultaneous electrochemical detection with a potentiostate without requiring a modification of the electrodes. Moreover, the effect was stronger when ionic liquids with longer alkyl chains were involved, so that low detection limits could be achieved.[127] The micellar solution of [$C_{12}C_4$mim]Br has been also used as dispersant prior to copper determination by flame atomic absorption spectrometry. This novel method resulted to be suitable for environmental and waste water analysis; however, in this case a non surface-active ionic liquid such as [C_6mim]PF_6 performed slightly better.[128]

Application in biomolecules stabilization

Keeping in mind the increasing interest in the use of ionic liquids for drug delivery, the interaction of surface-active ionic liquids with different drugs has been investigated. Studies on the complex formed by combining [C_{12}mim]Cl and ibuprofen with surface tension, steady-state fluorescence spectroscopy, UV-visible absorption, dynamic light scattering and ^{1}H NMR revealed that mixed catanionic complexes were formed both at the water/air interface as well as in the micelles. They showed an increased surface-activity due to a combination of equally relevant electrostatic, hydrophobic, cation - π and $\pi - \pi$ interactions. Size and shape of the aggregates were also changing with the mixture ratio: ibuprofen alone formed bigger aggregates compared to its mixture with the ionic liquid.[129] Similarly, synergistic interactions were found in the mixed micelle of [C_{12}mim]Br and bile salts, which could even improve the solubility of phenothiazine drug.[130] Comparable findings were reported for a mixture of [C_{14}mim]Br with different drugs such as dopamine hydrochloride and acetylcholine chloride. Studies revealed that the new imidazolium based surfactant is a better drug carrier than the common tetralkylammonium based systems. Moreover, it was suggested that hydrophilic drugs are adsorbed on the surface of the micelle, since a decrease in the CMC and changes in shielding of different protons in NMR were observed.[131] Dicationic surface-active ionic liquids have shown to have the same behaviour when mixed with the drug amitriptyline

hydrochloride.[132]
Surface-active ionic liquids, in particular dicationic ones, have been reported for their interactions with bio-macromolecules such as polypeptides, proteins, enzymes or nucleic acid. They are able to alter the structure and conformation of these macromolecules to induce a new activity and open up new opportunities in drug/gene delivery methods.[133] For example, surface-active ionic liquids micellar solutions were able to dissociate colloidal aggregates of the pure drug molecule rutaecarpine, therefore enhancing its activity.[134] Bovine serum albumin (BSA) is often taken as model globular protein since its structure is well known and characterized. The effect of [C_{12}mim]Cl and its ester and amide functionalized counterpart over bovine serum albumin was investigated. Structure modifications of the protein were dependent both on the ionic liquid concentration and type. While with the non-functionalized surface-active ionic liquids only unordered aggregates were observed, at specific concentration ranges the ester and amide functionalized surfactants induced the formation of ordered self-assembled structures such as long rods and right-handedly twisted helical amyloid fibres. These structures are depicted in figure 1.13. This modified aggregation behaviour is probably due to the different hydrogen bond capability of the different ionic liquids.[135] Further studies showed that the pH value strongly influences the interaction between this protein and [C_{16}mim]Br due to the change in the electrostatic interaction between the components, especially above the isoelectric point of BSA.[136]
The interaction of both cationic and anionic surface-active ionic liquids with human hemoglobin was investigated by Vashishat *et al.*, showing that a complex between the ionic liquid and the protein is formed. In the case of [C_6mim][$C_{12}H_{25}SO_4$] a stable network was observed while in the case of [C_{12}mim]Cl the heme group was released upon denaturation of the protein.[137] Also other proteins such as pepsin, β-casein and human serum albumin have shown to form complexes with surface-active ionic liquids. In all cases, their structure and conformation was altered above a threshold concentration.[138–140]

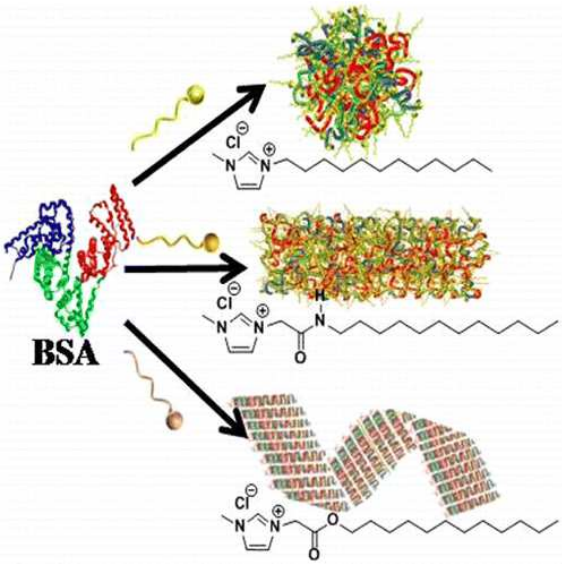

Figure 1.13: Different complex structures obtained with bovine serum albumin and various surface-active ionic liquids according to Singh *et al.*[135]

Enzymes have been coupled with surface-active ionic liquids and a synergistic combination was observed that would increase the catalytic activity of the enzyme. The structure of dicationic surface-active ionic liquids combined with *Rhizopus oryzae* lipase strongly influenced the activity of the enzymes. In fact ionic liquids with a shorter spacer would better improve the hydrolitic activity and thermal stability of the lipase, a longer spacer would modify the enzyme configuration more, resulting in a lower activity increase.[141]

Eventually also the effect of surface-active ionic liquids on nucleic acid was evaluated. In a study conducted by Roy *et al.* the interaction of the DNA nucleotide adenosine-5-monophosphate disodium with [C_{12}mim]Cl and [C_4mim][$C_8H_{17}SO_4$] was investigated. The nucleotide was incorporated in the ionic liquid micelles increasing their size and rendering them more rigid.[142] The concept was further deepened by Paradin *et al.* and Bhadani *et al.* who used dicationic surface-active ionic liquids for DNA stabilization, which were inspired by the fact that imidazolium is already present in various proteins and therefore plays a key role in their biological function. Through the positive charges placed on the surface of the formed vescicle the surfactants were able to interact with DNA to protect it from DNAse I enzyme cleavage.[59,143]

Application in organic synthesis and catalysis

So far, several studies addressed the implementation of surface-active ionic liquids in organic synthesis in water. They can have multiple roles, acting either solely as surface-active additives that improve water solubility of organic compounds or, based on some task-specific adjustments of the chemical structure, they can also actively take part in the reaction as catalyst. The micellar medium can provide a catalytic effect itself to the organic reaction in water through the micellar catalysis principle: substrates stabilized at the micelles will experience a much higher local concentration compared to the bulk solution, and therefore an overall reaction rate enhancement will be observed (figure 1.14).[15,144,145]

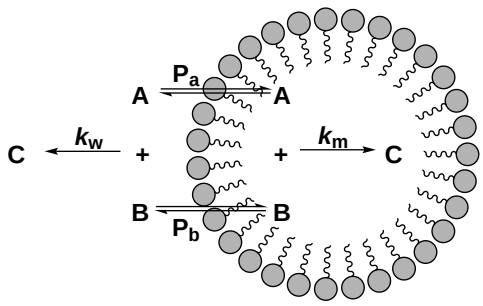

Figure 1.14: Scheme for micellar catalysis of a reaction taking place at the micelle and in the solvent at different reaction rate.

This principle has already been successfully applied to surface-active ionic liquids, in fact Bica *et al.* reported that reaction rates for a Diels-Alder reaction could be significantly increased compared to when water was used as the sole solvent. Also a major improvement was observed when using surface-active ionic liquids instead of conventional CTAB, SDS or zwitterionic Empigen®.[146]

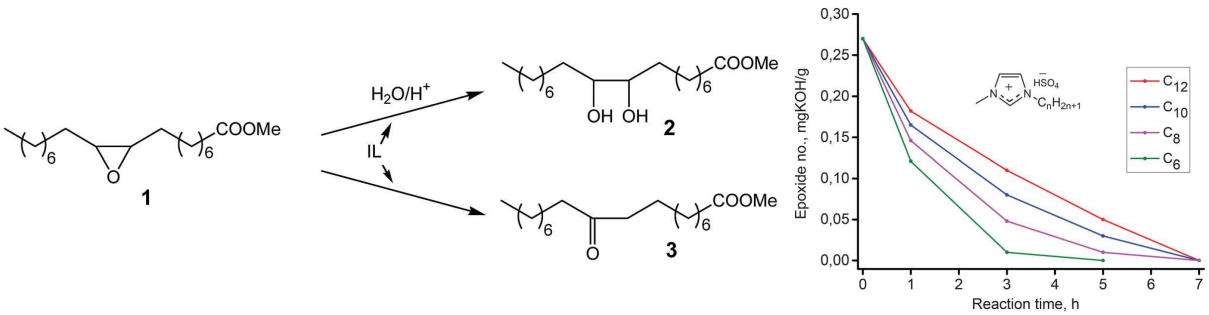

Figure 1.15: Oxirane ring opening reaction in epoxidized fatty acid methyl esters (left) and surface-active ionic liquid influence (right) reported from Nowicki *et al.*[90]

Nowicki *et al.* reported a series of dual functional alkylimidazolium based surface-active ionic liquids with a hydrogen sulphate anion which acts as co-catalyst in the oxirane ring

opening reaction in epoxidized fatty acid methyl esters (figure 1.15). The addition of the ionic liquids to the acid catalysed reaction strongly improved conversion and selectivity; moreover, a correlation between the alkyl chain length and the reaction performance could be identified.[90] The same type of surface-active ionic liquids was used as Brønsted acidic catalyst for the Mannich reaction of cyclohexanone in water, depicted in figure 1.16. High yields were obtained at room temperature for different substrates, moreover the reaction was selective for cyclohexanone and no product was observed when cyclopentanone was used.[147] Esterification of fatty acids with methanol and ethanol was also tested with this catalyst. Even in water as reaction medium, surprisingly high yields were obtained. This is a result of the dual functionality of the micelles which provide a hydrophobic core that facilitates organic molecules inclusion and water removal simultaneously. Additionally, the surfactant-containing water phase could be reused up to 4 times without loss in activity.[147]

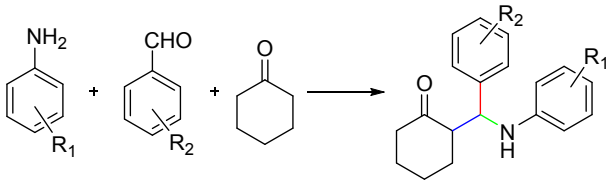

Figure 1.16: Mannich reaction reported from Vafaeezadeh *et al.*[147]

Sharma *et al.* modified an alkyl pyridinium SAILs with a nucleophilic oxime moiety in order to degrade organophosphorus pesticides (figure 1.17). The functionalized surface-active ionic liquids were used together with non-functionalized surfactants. The reaction rate increased with a longer alkyl chain length; moreover, when the unfunctionalized pyridinium derivative was used a synergetic effect took place and the system performed better than with tetraalkylammonium based surfactants.[148] Excellent performance has also been reported in this type of reaction with non-modified surface-active ionic liquids based on alkylmethylimidazolium with different anions. The oxime was used individually as nucleophile, and by careful choice of the anion and ionic liquid concentration a 34-fold increase in the reaction rate compared to pure water was achieved.[149]

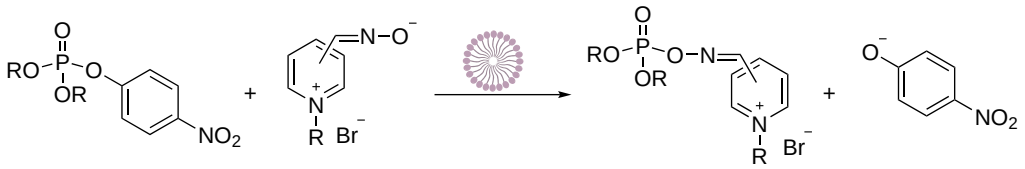

Figure 1.17: Alkylpyridinium functionalized SAILs for pesticides degradation reported from Sharma *et al.*[148]

Additionally, surface-active ionic liquids have been used by Bonnefond *et al.* as monomers for polymerization when they possess an unsaturated functional group like the 1-vinyl-3-dodecylimidazolium cation. Moreover, by selecting a series of metal halide counter ions, magnetic poly(ionic liquids) could be obtained.[150]

Application in nanotechnology

Owing to the self-assembly and distinct polarizability of imidazolium head groups, surface-active ionic liquids have been used in nanotechnology as supramolecular templates for the preparation of a broad variety of inorganic materials in water, including nanomaterials with a defined size and geometry. Alternatively, they have been used as ligands for nanoparticle

surface modification. For specific applications a targeted functionalization of the respective surface-active ionic liquid is often required.
The mechanism of interaction between surface-active ionic liquids and nanoparticles was investigate by Liu *et al.* for silica nanoparticles and [C_{12}mim]Br with turbidity measurements, isothermal titration microcalorimetry, fluorescence spectroscopy and dynamic light scattering. Stabilization of the silica nanoparticles was achieved through a combination of electrostatic attraction and hydrogen bonding interactions. Even at low surfactant concentration the ionic liquid was able to form micelle-like aggregates on the nanoparticle surface, as shown in figure 1.18. Moreover, the aggregation behaviour of the surfactant could be modulated by pH, alkyl chain length and additional salt. Due to the H-bond capability donor of the imidazolium cation stronger interactions were identified between this surfactant compared to an ammonium based analogous.[151]

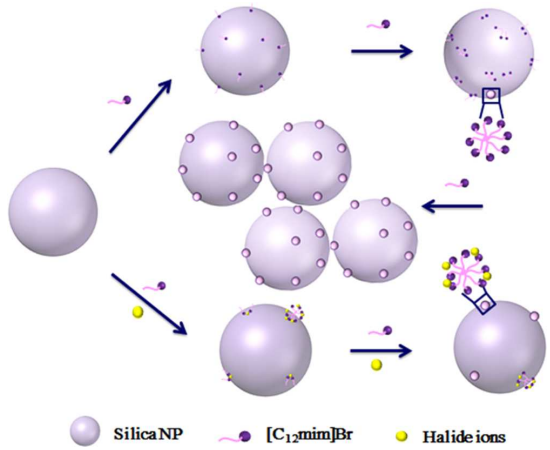

Figure 1.18: Binding interactions between silica nanoparticles and [C_{12}mim]Br as suggested by Liu *et al.*[151]

Gold nanoparticles were prepared in water by reduction of $HAuCl_4$ with $NaBH_4$ and stabilized for several months with both [C_{12}mim]Cl and [C_1mim-C_{12}-C_1mim]Br_2 already at concentrations below the respective CMCs, however poor polydispersity was obtained.[152] In an other study from Lin *et al.* using an arylazo functionalized surface-active ionic liquid, the shape of gold nanoparticles could be manipulated due to its repose to UV-Vis radiation.[81]
In general, dicationic surface-active ionic liquids are often implied in the synthesis and stabilization of nanoparticles in water. For example, Datta *et al.* reported silver nanoparticles stabilized by a series of [C_{16}im-C_n-$_{16}$im]Br_2 with different linkage and found a striking influence of the spacer length on the particles size and shape. In fact using monomeric or dicationic surfactant with a long spacer of at least 5 methylene units, spherical nanoparticles were obtained, while a short spacer with just two carbon atoms afforded ellipsoidal particles.[60]
Nanoparticles made of a polysaccharide like chitosan with a good and controllable geometry and size distribution could be synthesized and stabilized in water in the presence of surface-active ionic liquids. A complex between the polysaccharide and the ionic liquids was formed mainly due to the electrostatic and hydrophobic interactions. When using the anionic surface-active ionic liquid [C_4mim][C_8SO_4] these were much stronger due to the attraction between the positively charged chitosan and the alkyl sulphate chain, resulting in an insoluble complex at higher ionic liquid concentrations. In contrast, weaker interactions formed with the cationic surface-active ionic liquid [C_8mim]Cl prevented the complex precipitation.[153]
Surface-active ionic liquids have also shown promising application as surfactants in miniemulsion polymerization to form styrene based magnetic nanoparticles. As can be seen in figure 1.19 their size was dependent on the alkyl chain length of the ionic liquid used.[154]

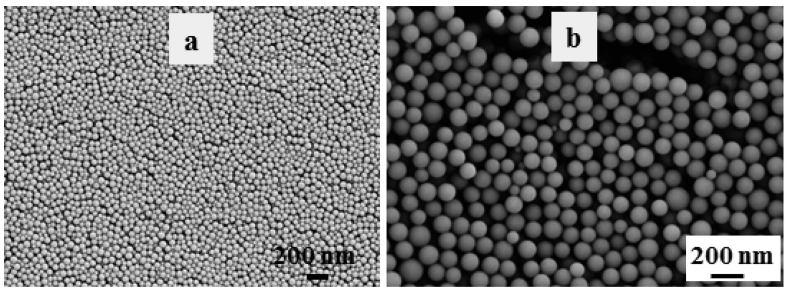

Figure 1.19: SEM image of polystyrene particles synthesized by (a) [C_{16}mim]Br and (b) [C_{12}mim]Br reported from Chakraborty *et al.*[154]

When using trisiloxane tailed surface-active ionic liquids it was possible to synthesize yolk-shell silica spheres consisting of a core and an outer shell in a water alkaline solution. Since the ionic liquid itself was used as silica source together with the conventional TEOS, the variation of templating agent concentration allowed to adjust the size of the core, the internal void and the outer sphere shell.[155]
Apart from nanoparticle synthesis, zeolites could be successfully synthesized using surface-active ionic liquids. In case of [C_{16}TEA]Cl, [C_{16}mim]Cl and [C_{16}mPy]Cl same textural properties were obtained for siliceous MCM-41 zeolites. This is in contrast to the preparation of mesoporous Y zeolites, where the pore size could be increased with the cation size.[156]
The role of surface-active ionic liquids in nanotechnology is not limited to the preparation or stabilization of nanoparticles. The obtained particles and/or inorganic materials can be subsequently applied in catalysis, thereby taking dual advantage of ionic liquid surfactant that acts not only as template and stabilizer, but also as additive to overcome the limited solubility of reagent encounters during catalysis. In fact, a dual catalytic effect combining nano- and micellar catalysis can be achieved.

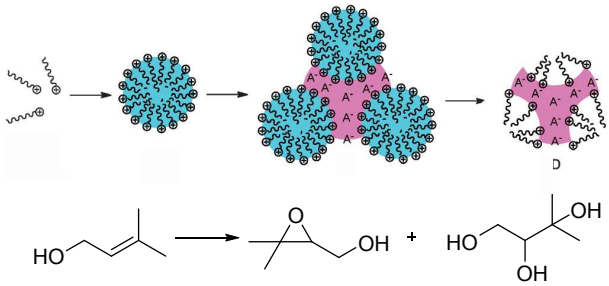

Figure 1.20: Proposed mechanism for the formation of surfactant-modified niobium peroxide hybrid catalysts (top) used for the epoxidation of allylic alcohols reaction (bottom) reported from Chen *et al.*[157]

Niobium peroxides were prepared by precipitation from a concentrated solution upon addition of the surface-active ionic liquid 1-dodecyl-3-methylimidazolium hydroxide. The micelles acted as a template providing high surface area of the solid catalyst, while the ionic liquid was also incapsulated in the surface to avoid aggregation, as shown in figure 1.20. When the system was tested in the epoxidation of allylic alcohols in hydrogen peroxide this catalyst showed an higher performance than the one prepared with conventional ammonium surfactants due to an higher surface area and the H-bond donor character of the proton on position 2 of the imidazolium ring that may activate the peroxide.[157]
Particularly suitable for Palladium nanoparticle stabilization in water are imidazolium based dicationic ionic liquids surfactants with a polyethylenglycol (PEG) linkage. The surface-active ionic liquid was successfully applied to the formation and stabilization of nanoparticles that were further applied in catalytic hydrogenations of styrene, as shown in figure 1.21 A. It is

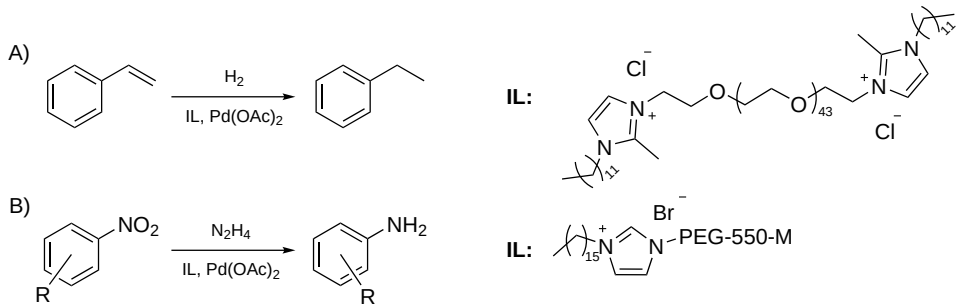

Figure 1.21: Catalytic hydrogenations catalyzed by Pd nanoparticles and PEG-derived surface-active ionic liquids reported by A) Zhu *et al.*[65] and B) Xu *et al.*[158]

interesting to note that when the imidazolium head was replaced by two simply hydrocarbon chains the nanoparticles were still well stabilized but their catalytic activity strongly decreased. In contrast pure PEG alone was not sufficient to stabilize the particles, thereby emphasizing the impact of tailored ionic liquid design in this reaction.[65] A similar approach was followed by Xu *et al.* who applied Pd nanoparticles stabilized by PEG-modified surface-active ionic liquids for the chemoselective transfer hydrogenation of nitroarenes using hydrazine hydrate as a hydrogen donor, as shown in figure 1.21 B. A higher ionic liquid concentration afforded smaller particles which increased the reaction performance.[158]

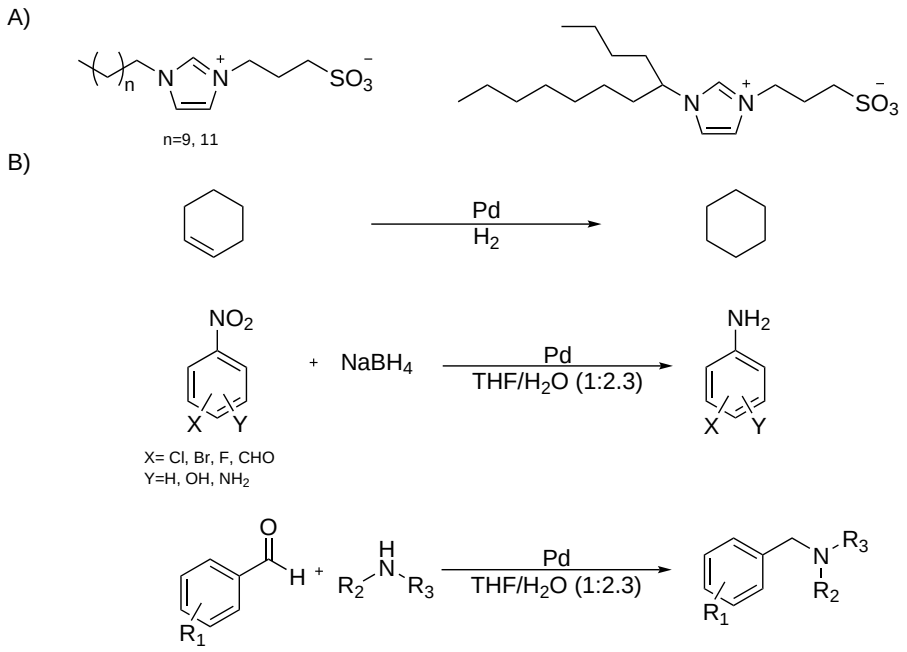

Figure 1.22: A) Zwitterionic surface-active ionic liquids used to stabilize Pd nanoparticles and B) reactions where they have been applied by Souza *et al.*[69–71,159]

Zwitterionic surface-active ionic liquids were also identified as suitable stabilizers for Palladium nanoparticles in water. Souza et al. reported the design and synthesis of [C_{12}im-C_3-SO_3] zwitterionic ionic liquids for Pd nanoparticle stabilization in water (figure 1.22). The authors showed that the ionic liquids formed a double layer around the particles. The system was successfully tested in the hydrogenation of cyclohexane. The addition of breached and more sterically demanding surfactant was necessary in order to obtain excellent yields over three repeating cycles. A similar catalytic system consisting of [C_{12}im-C_3-SO_3] zwitterionic ionic liquids and Pd nanoparticle was also suitable for the hydrogen transfer reductive amination of benzaldehydes, as well as for the reduction of aromatic nitro compounds.[69–71,159]

An hybrid material composed of a polyoxometalate (POM) and phosphotungstic acid ($H_3PW_{12}O_{40}$) stabilized by the oppositely charged COOH-functionalized surface-active ionic liquid 1-decyl-3-carboxymethyl imidazolium bromide in water was presented by Gong *et al.* Stabilization was achieved through electrostatic interactions and H-bond between the two components. Due to the change in the electrostatic repulsion between the POM and the protonated ionic liquid molecules, the hybrid material was pH-responsive, allowing to control its aggregation state by varying the pH, as shown in figure 1.23. This property could be used advantageously in the catalytic degradation of dyes, and adjusting the pH allowed to regenerate the catalyst after several reaction cycles.[160]

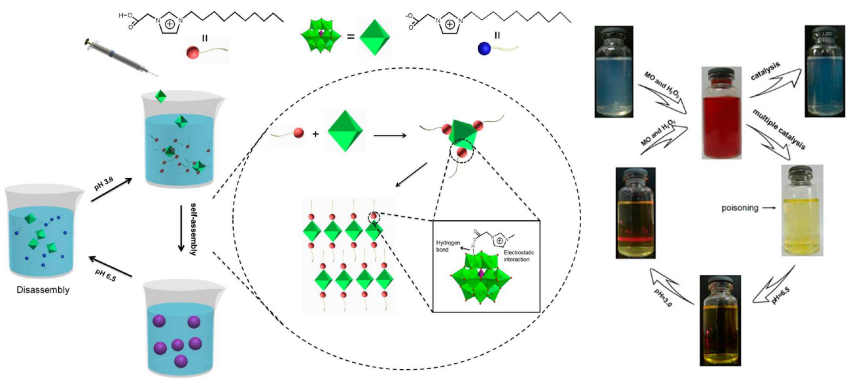

Figure 1.23: Schematic illustration of the formation mechanism of POM/IL hybrid materials and their pH response (left) and schematic illustration of pH-induced recycle of POM/IL materials (left) reported from Gong *et al.*[160]

The same group further extended the application of the carboxylic acid functionalized surface-active ionic liquid for production of a self-assembled material composed of the congo-red dye and ionic liquid. Due to the two components with opposite charge and their electrostatic, hydrophobic and $\pi - \pi$ interaction the system can react to pH and temperature stimulus to change its arrangement from 1D fibres to 2D planar structures. A controlled fluorescence emission was obtained.[161]

Beside metallic nanoparticles in catalysis, other functional materials for different applications can be stabilized by surface-active ionic liquids. For example graphene oxide magnetic sheets for the solid phase extraction of trace nickel were modified with dimethylglyoxime and 1-hexadecyl-3-methylimidazolium chloride. This allowed for an almost five-fold higher adsorption capacity with respect to non modified sorbent materials.[162]

1.4 Bibliography

[1] I. Chemical. "Global solvents - opportunities for greener solvents." (2013). Last accessed 05-07-2017, URL `https://www.ihs.com/products/chemical-special-reports-global-solvents.html`.

[2] C. Jimenez-Gonzalez, C. S. Ponder, Q. B. Broxterman, and J. B. Manley. "Using the right green yardstick: Why process mass intensity is used in the pharmaceutical industry to drive more sustainable processes." *Org. Process Res. Dev.*, **15**(2011), 912.

[3] D. Prat, J. Hayler, and A. Wells. "A survey of solvent selection guides." *Green Chem.*, **16**(2014), 4546.

[4] C. M. Alder, J. D. Hayler, R. K. Henderson, A. M. Redman, L. Shukla, L. E. Shuster, and H. F. Sneddon. "Updating and further expanding GSK's solvent sustainability guide." *Green Chem.*, **18**(2016), 3879.

[5] D. Prat, O. Pardigon, H.-W. Flemming, S. Letestu, V. Ducandas, P. Isnard, E. Guntrum, T. Senac, S. Ruisseau, P. Cruciani, and P. Hosek. "Sanofi's solvent selection guide: A step toward more sustainable processes." *Org. Process Res. Dev.*, **17**(2013), 1517.

[6] K. Alfonsi, J. Colberg, P. J. Dunn, T. Fevig, S. Jennings, T. A. Johnson, H. P. Kleine, C. Knight, M. A. Nagy, D. A. Perry, and M. Stefaniak. "Green chemistry tools to influence a medicinal chemistry and research chemistry based organisation." *Green Chem.*, **10**(2008), 31.

[7] D. J. C. Constable, C. Jimenez-Gonzalez, and R. K. Henderson. "Perspective on solvent use in the pharmaceutical industry." *Org. Process Res. Dev.*, **11**(2007), 133.

[8] R. A. Sheldon. "The E factor 25 years on: the rise of green chemistry and sustainability." *Green Chem.*, **19**(2017), 18.

[9] M. Seßler and J. Schatz. "Organometall-Reaktionen in Wasser: C-C-Verknüpfungen." *Chem. in unserer Zeit*, **46**(2012), 48.

[10] M. Petkovic, J. L. Ferguson, H. Q. N. Gunaratne, R. Ferreira, M. C. Leitao, K. R. Seddon, L. P. N. Rebelo, and C. S. Pereira. "Novel biocompatible cholinium-based ionic liquids-toxicity and biodegradability." *Green Chem.*, **12**(2010), 643.

[11] Q. Zhang, K. De Oliveira Vigier, S. Royer, and F. Jerome. "Deep eutectic solvents: syntheses, properties and applications." *Chem. Soc. Rev.*, **41**(2012), 7108.

[12] R. Breslow. "Hydrophobic effects on simple organic reactions in water." *Acc. Chem. Res.*, **24**(1991), 159.

[13] J. W. Wijnen and J. B. F. N. Engberts. "Retro-diels-alder reaction in aqueous solution: Toward a better understanding of organic reactivity in water." *J. Org. Chem.*, **62**(1997), 2039.

[14] J. B. Engberts. *Structure and Properties of Water*. Blackwell Publishing Ltd (2007).

[15] B. H. Lipshutz and S. Ghorai. "Transitioning organic synthesis from organic solvents to water. What's your E Factor?" *Green Chem.*, **16**(2014), 3660.

[16] J. P. Hallett and T. Welton. "Room-temperature ionic liquids: Solvents for synthesis and catalysis. 2." *Chem. Rev.*, **111**(2011), 3508.

[17] S. Chen, S. Zhang, X. Liu, J. Wang, J. Wang, K. Dong, J. Sun, and B. Xu. "Ionic liquid clusters: structure, formation mechanism, and effect on the behavior of ionic liquids." *Phys. Chem. Chem. Phys.*, **16**(2014), 5893.

[18] S. Feng and G. A. Voth. "Molecular dynamics simulations of imidazolium-based ionic liquid/water mixtures: Alkyl side chain length and anion effects." *Fluid Phase Equilib.*, **294**(2010), 148.

[19] Y. Kohno and H. Ohno. "Ionic liquid/water mixtures: from hostility to conciliation." *Chem. Commun.*, **48**(2012), 7119.

[20] A. Seddon, Kenneth R.and Stark and M.-J. Torres. "Influence of chloride, water, and organic solvents on the physical properties of ionic liquids." *Pure Appl. Chem.*, **72**(2009), 2275.

[21] J. Łuczak, J. Hupka, J. Thòming, and C. Jungnickel. "Self-organization of imidazolium ionic liquids in aqueous solution." *Colloids Surf., A*, **329**(2008), 125.

[22] M. Tariq, A. Podgoršek, J. Ferguson, A. Lopes, M. Costa Gomes, A. Pádua, L. Rebelo, and J. Canongia Lopes. "Characteristics of aggregation in aqueous solutions of dialkylpyrrolidinium bromides." *J. Colloid Interface Sci.*, **360**(2011), 606.

[23] M. J. Rosen and J. T. Kunjappu. *Surfactants and interfacial phenomena*. John Wiley & Sons, 4th edition (2012).

[24] M. Blesic, M. Swadźba-Kwaśny, J. D. Holbrey, J. N. Canongia Lopes, K. R. Seddon, and L. P. N. Rebelo. "New catanionic surfactants based on 1-alkyl-3-methylimidazolium alkylsulfonates, $[C_nH_{2n+1}mim][C_mH_{2m+1}SO_3]$: mesomorphism and aggregation." *Phys. Chem. Chem. Phys.*, **11**(2009), 426042.

[25] M. Ao and D. Kim. "Aggregation behavior of aqueous solutions of 1-Dodecyl-3-methylimidazolium salts with different halide anions." *J. Chem. Eng. Data*, **58**(2013), 1529.

[26] A. Domínguez, A. Fernández, N. González, E. Iglesias, and L. Montenegro. "Determination of critical micelle concentration of some surfactants by three techniques." *J. Chem. Educ.*, **74**(1997), 1227.

[27] S.-K. Mikkola, A. Robciuc, J. Lokajová, A. J. Holding, M. Lämmerhofer, I. Kilpeläinen, J. M. Holopainen, A. W. T. King, and S. K. Wiedmer. "Impact of amphiphilic biomass-dissolving ionic liquids on biological cells and liposomes." *Environ. Sci. Technol.*, **49**(2015), 1870.

[28] O. A. El Seoud, P. A. R. Pires, T. Abdel-Moghny, and E. L. Bastos. "Synthesis and micellar properties of surface-active ionic liquids: 1-Alkyl-3-methylimidazolium chlorides." *J. Colloid Interface Sci.*, **313**(2007), 296.

[29] N. J. Turro and A. Yekta. "Luminescent probes for detergent solutions. a simple procedure for determination of the mean aggregation number of micelles." *JACS*, **100**(1978), 5951.

[30] Z. Miskolczy, K. Sebõk Nagy, L. Biczók, and S. Göktürk. "Aggregation and micelle formation of ionic liquids in aqueous solution." *Chem. Phys. Lett.*, **400**(2004), 296.

[31] M. Blesic, A. Lopes, E. Melo, Z. Petrovski, N. V. Plechkova, J. N. Canongia Lopes, K. R. Seddon, and L. P. N. Rebelo. "On the self-aggregation and fluorescence quenching aptitude of surfactant ionic liquids." *J. Phys. Chem. B*, **112**(2008), 8645.

[32] B. Šarac and M. Bešter-Rogač. "Temperature and salt-induced micellization of dodecyltrimethylammonium chloride in aqueous solution: A thermodynamic study." *J. Colloid Interface Sci.*, **338**(2009), 216.

[33] A. Kessler, B. Zeeb, B. Kranz, O. Menéndez-Aguirre, L. Fischer, J. Hinrichs, and J. Weiss. "Isothermal titration calorimetry as a tool to determine the thermodynamics of demicellization processes." *Rev. Sci. Instrum.*, **83**(2012), 105104.

[34] I. Goodchild, L. Collier, S. L. Millar, I. Prokeš, J. C. Lord, C. P. Butts, J. Bowers, J. R. Webster, and R. K. Heenan. "Structural studies of the phase, aggregation and surface behaviour of 1-alkyl-3-methylimidazolium halide + water mixtures." *J. Colloid Interface Sci.*, **307**(2007), 455.

[35] A. Cornellas, L. Perez, F. Comelles, I. Ribosa, A. Manresa, and M. T. Garcia. "Self-aggregation and antimicrobial activity of imidazolium and pyridinium based ionic liquids in aqueous solution." *J. Colloid Interface Sci.*, **355**(2011), 164.

[36] B. Dong, N. Li, L. Zheng, L. Yu, and T. Inoue. "Surface adsorption and micelle formation of surface active ionic liquids in aqueous solution." *Langmuir*, **23**(2007), 4178.

[37] R. Vanyúr, L. Biczók, and Z. Miskolczy. "Micelle formation of 1-alkyl-3-methylimidazolium bromide ionic liquids in aqueous solution." *Colloids Surf., A*, **299**(2007), 256.

[38] R. Kamboj, S. Singh, and V. Chauhan. "Synthesis, characterization and surface properties of N-(2-hydroxyalkyl)-N-(2-hydroxyethyl)imidazolium surfactants." *Colloids Surf., A*, **441**(2014), 233.

[39] G. Singh, R. Kamboj, V. Singh Mithu, V. Chauhan, T. Kaur, G. Kaur, S. Singh, and T. Singh Kang. "Nicotine-based surface active ionic liquids: Synthesis, self-assembly and cytotoxicity studies." *J. Colloid Interface Sci.*, **496**(2017), 278.

[40] N. V. Sastry, N. M. Vaghela, P. M. Macwan, S. S. Soni, V. K. Aswal, and A. Gibaud. "Aggregation behavior of pyridinium based ionic liquids in water - Surface tension, ^{1}H NMR chemical shifts, SANS and SAXS measurements." *J. Colloid Interface Sci.*, **371**(2012), 52.

[41] J. Łuczak, C. Jungnickel, M. Joskowska, J. Thöming, and J. Hupka. "Thermodynamics of micellization of imidazolium ionic liquids in aqueous solutions." *J. Colloid Interface Sci.*, **336**(2009), 111.

[42] T. Asakawa, H. Kitano, A. Ohta, and S. Miyagishi. "Convenient estimation for counterion dissociation of cationic micelles using chloride-sensitive fluorescence probe." *J. Colloid Interface Sci.*, **242**(2001), 284.

[43] J. Łuczak, M. Markiewicz, J. Thöming, J. Hupka, and C. Jungnickel. "Influence of the hofmeister anions on self-organization of 1-decyl-3-methylimidazolium chloride in aqueous solutions." *J. Colloid Interface Sci.*, **362**(2011), 415.

[44] G. B. Ray, I. Chakraborty, S. Ghosh, S. P. Moulik, and R. Palepu. "Self-aggregation of alkyltrimethylammonium bromides (C10-, C12-, C14-, and C_{16}TAB) and their binary mixtures in aqueous medium: A critical and comprehensive assessment of interfacial behavior and bulk properties with reference to two types of micelle formation." *Langmuir*, **21**(2005), 10958.

[45] C. Jungnickel, J. Łuczak, J. Ranke, J. F. Fernández, A. Müller, and J. Thöming. "Micelle formation of imidazolium ionic liquids in aqueous solution." *Colloids Surf., A*, **316**(2008), 278.

[46] A. Heintz, J. K. Lehmann, S. A. Kozlova, E. V. Balantseva, A. B. Bazyleva, and D. Ondo. "Micelle formation of alkylimidazolium ionic liquids in water and in ethylammonium nitrate ionic liquid: A calorimetric study." *Fluid Phase Equilib.*, **294**(2010), 187.

[47] M. Blesic, M. H. Marques, N. V. Plechkova, K. R. Seddon, L. P. N. Rebelo, and A. Lopes. "Self-aggregation of ionic liquids: micelle formation in aqueous solution." *Green Chem.*, **9**(2007), 481.

[48] G. Bai, A. Lopes, and M. Bastos. "Thermodynamics of micellization of alkylimidazolium surfactants in aqueous solution." *J. Chem. Thermodyn.*, **40**(2008), 1509.

[49] C. Tourné-Péteilh, J.-M. Devoisselle, A. Vioux, P. Judeinstein, M. In, and L. Viau. "Surfactant properties of ionic liquids containing short alkyl chain imidazolium cations and ibuprofenate anions." *Phys. Chem. Chem. Phys.*, **13**(2011), 15523.

[50] J. Bowers, C. P. Butts, P. J. Martin, M. C. Vergara-Gutierrez, and R. K. Heenan. "Aggregation behavior of aqueous solutions of ionic liquids." *Langmuir*, **20**(2004), 2191.

[51] T. Inoue, H. Ebina, B. Dong, and L. Zheng. "Electrical conductivity study on micelle formation of long-chain imidazolium ionic liquids in aqueous solution." *J. Colloid Interface Sci.*, **314**(2007), 236.

[52] Q. Q. Baltazar, J. Chandawalla, K. Sawyer, and J. L. Anderson. "Interfacial and micellar properties of imidazolium-based monocationic and dicationic ionic liquids." *Colloids Surf., A*, **302**(2007), 150.

[53] N. I. Malek, Z. S. Vaid, U. U. More, and O. A. El Seoud. "Ionic-liquid-based surfactants with unsaturated head group: synthesis and micellar properties of 1-(n-alkyl)-3-vinylimidazolium bromides." *Colloid Polym. Sci.*, **293**(2015), 3213.

[54] J. Sirieixplenet. "Behaviour of a binary solvent mixture constituted by an amphiphilic ionic liquid, 1-decyl-3-methylimidazolium bromide and water Potentiometric and conductimetric studies." *Talanta*, **63**(2004), 979.

[55] H. Wang, J. Wang, S. Zhang, and X. Xuan. "Structural effects of anions and cations on the aggregation behavior of ionic liquids in aqueous solutions." *J. Phys. Chem. B*, **112**(2008), 16682.

[56] R. L. Vekariya and N. S. Kumar. "Micellization behaviour of surface active N-alkyl pyridinium dodecylsulphate task-specific ionic liquids in aqueous solutions." *Colloids Surf., A*, **529**(2017), 203.

[57] N. V. Sastry and D. K. Singh. "Surfactant and gelation properties of acetylsalicylate based room temperature ionic liquid in aqueous media." *Langmuir*, **32**(2016), 10000.

[58] S. Sunitha, P. S. Reddy, R. B. N. Prasad, and S. Kanjilal. "Synthesis and evaluation of new imidazolium-based aromatic ether functionalized cationic mono and gemini surfactants." *Eur. J. Lipid Sci. Technol.*, **113**(2011-06), 756.

[59] A. Bhadani, H. Kataria, and S. Singh. "Synthesis, characterization and comparative evaluation of phenoxy ring containing long chain gemini imidazolium and pyridinium amphiphiles." *J. Colloid Interface Sci.*, **361**(2011), 33.

[60] S. Datta, J. Biswas, and S. Bhattacharya. "How does spacer length of imidazolium gemini surfactants control the fabrication of 2D-langmuir films of silver-nanoparticles at the air-water interface?" *J. Colloid Interface Sci.*, **430**(2014), 85.

[61] B. K. Paul and S. P. Moulik, editors. *Ionic liquid-based surfactant science: formulation, characterization, and applications*. Wiley series on surface and interfacial chemistry. Wiley (2015).

[62] O. Nacham, A. Martín-Pérez, D. J. Steyer, M. J. Trujillo-Rodríguez, J. L. Anderson, V. Pino, and A. M. Afonso. "Interfacial and aggregation behavior of dicationic and tricationic ionic liquid-based surfactants in aqueous solution." *Colloids Surf., A*, **469**(2015), 224.

[63] S. M. Tawfik. "Simple one step synthesis of gemini cationic surfactant-based ionic liquids: Physicochemical, surface properties and biological activity." *J. Mol. Liq.*, **209**(2015), 320.

[64] C. Ren, F. Wang, Z. Zhang, H. Nie, N. Li, and M. Cui. "Synthesis, surface activity and aggregation behavior of gemini imidazolium surfactants 1,3-bis(3-alkylimidazolium-1-yl) propane bromide." *Colloids Surf., A*, **467**(2015), 1.

[65] W. Zhu, H. Yang, Y. Yu, L. Hua, H. Li, B. Feng, and Z. Hou. "Amphiphilic ionic liquid stabilizing palladium nanoparticles for highly efficient catalytic hydrogenation." *Phys. Chem. Chem. Phys.*, **13**(2011), 13492.

[66] A. Bhadani and S. Singh. "Synthesis and properties of thioether spacer containing gemini imidazolium surfactants." *Langmuir*, **27**(2011), 14033.

[67] P. Quagliotto, G. Viscardi, C. Barolo, E. Barni, S. Bellinvia, E. Fisicaro, and C. Compari. "Gemini pyridinium surfactants: Synthesis and conductometric study of a novel class of amphiphiles." *J. Org. Chem.*, **68**(2003), 7651.

[68] N. N. Al-Mohammed, R. S. Duali Hussen, Y. Alias, and Z. Abdullah. "Tris-imidazolium and benzimidazolium ionic liquids: a new class of biodegradable surfactants." *RSC Adv.*, **5**(2015), 2869.

[69] E. Drinkel, F. D. Souza, H. D. Fiedler, and F. Nome. "The chameleon effect in zwitterionic micelles: Binding of anions and cations and use as nanoparticle stabilizing agents." *Curr. Opin. Colloid Interface Sci.*, **18**(2013), 26.

[70] B. S. Souza, E. C. Leopoldino, D. W. Tondo, J. Dupont, and F. Nome. "Imidazolium-Based Zwitterionic Surfactant: A New Amphiphilic Pd Nanoparticle Stabilizing Agent." *Langmuir*, **28**(2012), 833.

[71] F. D. Souza, B. S. Souza, D. W. Tondo, E. C. Leopoldino, H. D. Fiedler, and F. Nome. "Imidazolium-based zwitterionic surfactants: Characterization of normal and reverse micelles and stabilization of nanoparticles." *Langmuir*, **31**(2015), 3587.

[72] C.-j. Cheng, G.-m. Qu, J.-j. Wei, T. Yu, and W. Ding. "Thermodynamics of micellization of sulfobetaine surfactants in aqueous solution." *J. Surfactants Deterg.*, **15**(2012), 757.

[73] K. S. Egorova and V. P. Ananikov. "Toxicity of ionic liquids: Eco(cyto)activity as complicated, but unavoidable parameter for task-specific optimization." *ChemSusChem*, **7**(2014), 336.

[74] A. Jordan and N. Gathergood. "Biodegradation of ionic liquids - a critical review." *Chem. Soc. Rev.*, **44**(2015), 8200.

[75] M. T. Garcia, I. Ribosa, L. Perez, A. Manresa, and F. Comelles. "Micellization and antimicrobial properties of surface-active ionic liquids containing cleavable carbonate linkages." *Langmuir*, (2017).

[76] M. T. Garcia, I. Ribosa, L. Perez, A. Manresa, and F. Comelles. "Aggregation behavior and antimicrobial activity of ester-functionalized imidazolium- and pyridinium-based ionic liquids in aqueous solution." *Langmuir*, **29**(2013), 2536.

[77] M. T. Garcia, I. Ribosa, L. Perez, A. Manresa, and F. Comelles. "Self-assembly and antimicrobial activity of long-chain amide-functionalized ionic liquids in aqueous solution." *Colloids Surf., B*, **123**(2014), 318.

[78] R. Kamboj, P. Bharmoria, V. Chauhan, G. Singh, A. Kumar, S. Singh, and T. S. Kang. "Effect of cationic head group on micellization behavior of new amide-functionalized surface active ionic liquids." *Phys. Chem. Chem. Phys.*, **16**(2014), 26040.

[79] V. Chauhan, R. Kamboj, S. P. Singh Rana, T. Kaur, G. Kaur, S. Singh, and T. S. Kang. "Aggregation behavior of non-cytotoxic ester functionalized morpholinium based ionic liquids in aqueous media." *J. Colloid Interface Sci.*, **446**(2015), 263.

[80] A. Wu, F. Lu, P. Sun, X. Gao, L. Shi, and L. Zheng. "Photoresponsive self-assembly of surface active ionic liquid." *Langmuir*, **32**(2016), 8163.

[81] C. Lin, L. Yang, M. Xu, Q. An, Z. Xiang, and X. Liu. "Properties and applications of designable and photo/redox dual responsive surfactants with the new head group 2-arylazo-imidazolium." *RSC Adv.*, **6**(2016), 51552.

[82] Z. Du, E. Li, Y. Cao, X. Li, and G. Wang. "Synthesis of trisiloxane-tailed surface active ionic liquids and their aggregation behavior in aqueous solution." *Colloids and Surfaces A: Physicochemical and Engineering Aspects*, **441**(2014), 744.

[83] G. Wang, P. Li, Z. Du, W. Wang, and G. Li. "Surface activity and aggregation behavior of siloxane-based ionic liquids in aqueous solution." *Langmuir*, **31**(2015), 8235.

[84] J. Tan and S. Feng. "Effect of counterions on micellization of pyrrolidinium based silicone ionic liquids in aqueous solutions." *J. Chem. Eng. Data*, **59**(2014), 1830.

[85] W. Xu, T. Wang, N. Cheng, Q. Hu, Y. Bi, Y. Gong, and L. Yu. "Experimental and dft studies on the aggregation behavior of imidazolium-based surface-active ionic liquids with aromatic counterions in aqueous solution." *Langmuir*, **31**(2015), 1272.

[86] G. Singh, G. Singh, and T. S. Kang. "Micellization behavior of surface active ionic liquids having aromatic counterions in aqueous media." *J. Phys. Chem. B*, **120**(2016), 1092.

[87] T. Wang, L. Wang, Y. Jin, P. Chen, W. Xu, and L. Yu. "Study the effect of substituent position in aromatic counterion to self-aggregation of cationic surface active ionic liquid in aqueous medium." *J. Mol. Liq.*, **204**(2015), 90 .

[88] C. Tourné-Péteilh, B. Coasne, M. In, D. Brevet, J.-M. Devoisselle, A. Vioux, and L. Viau. "Surfactant behavior of ionic liquids involving a drug: From molecular interactions to self-assembly." *Langmuir*, **30**(2014), 1229.

[89] Y. Bi, L. Zhao, Q. Hu, Y. Gao, and L. Yu. "Aggregation behavior of imidazolium-based surface-active ionic liquids with photoresponsive cinnamate counterions in the aqueous solution." *Langmuir*, **31**(2015), 12597.

[90] J. Nowicki, J. Łuczak, and D. Stańczyk. "Dual functionality of amphiphilic 1-alkyl-3-methylimidazolium hydrogen sulfate ionic liquids: surfactants with catalytic function." *RSC Adv.*, **6**(2016), 11591.

[91] I. Rodróguez-Palmeiro, I. Rodríguez-Escontrela, O. Rodríguez, A. Arce, and A. Soto. "Characterization and interfacial properties of the surfactant ionic liquid 1-dodecyl-3-methyl imidazolium acetate for enhanced oil recovery." *RSC Adv.*, **5**(2015), 37392.

[92] F. Teixeira, N. Vieira, O. Cortes, J. Araújo, I. Marrucho, L. Rebelo, and A. Pereiro. "Phase equilibria and surfactant behavior of fluorinated ionic liquids with water." *J. Chem. Thermodyn.*, **82**(2015), 99.

[93] T. Fan, C. Chen, T. Fan, F. Liu, and Q. Peng. "Novel surface-active ionic liquids used as solubilizers for water-insoluble pesticides." *J. Hazard. Mater.*, **297**(2015), 340.

[94] A. B. Pereiro, J. a. M. M. Araújo, F. S. Teixeira, I. M. Marrucho, M. M. Piñeiro, and L. P. N. Rebelo. "Aggregation behavior and total miscibility of fluorinated ionic liquids in water." *Langmuir*, **31**(2015), 1283.

[95] N. M. Vaghela, N. V. Sastry, and V. K. Aswal. "Effect of additives on the surface active and morphological features of 1-octyl-3-methylimidazolium halide aggregates in aqueous media." *Colloids Surf., A*, **373**(2011), 101.

[96] C. P. Frizzo, C. R. Bender, I. M. Gindri, P. R. S. Salbego, M. A. Villetti, and M. A. P. Martins. "Anion effect on the aggregation behavior of the long-chain spacers dicationic imidazolium-based ionic liquids." *Colloid Polym. Sci.*, **293**(2015), 2901.

[97] Y. Jin, L. Wang, T. Wang, P. Chen, Y. Bi, and L. Yu. "Aggregation behavior of dodecylsulfonate-based surface active ionic liquids in water." *J. Mol. Liq.*, **212**(2015), 23.

[98] J. Łuczak, C. Jungnickel, M. Markiewicz, and J. Hupka. "Solubilization of Benzene, Toluene, and Xylene (BTX) in Aqueous Micellar Solutions of Amphiphilic Imidazolium Ionic Liquids." *J. Phys. Chem. B*, **117**(2013), 5653.

[99] G. Chakraborty, M. Paulchowdhury, S. Bardhan, and S. K. Saha. "Surface activity and modifying effects of 1-Naphthol, 2-Naphthol and 2,3-dihydroxynaphthalene on self-assembled nanostructures of 1-Hexadecyl-3-methylimidazolium chloride." *Colloids Surf., A*, **516**(2017), 262.

[100] T. Nazemi and R. Sadeghi. "Effect of polar organic solvents on the surface adsorption and micelle formation of surface active ionic liquid 1-dodecyl-3-methylimidazolium bromide in aqueous solutions and comparison with the traditional cationic surfactant dodecyltrimethylammonium bromide." *Colloids Surf., A*, **462**(2014), 271.

[101] K. Thakkar, B. Bharatiya, V. K. Aswal, and P. Bahadur. "Aggregation of 1-alkyl-3-methylimidazolium octylsulphate ionic liquids and their interaction with Triton X-100 micelles." *RSC Adv.*, **6**(2016), 80585.

[102] J. Penfold, I. Tucker, R. K. Thomas, D. J. F. Taylor, X. L. Zhang, C. Bell, C. Breward, and P. Howell. "The Interaction between Sodium Alkyl Sulfate Surfactants and the Oppositely Charged Polyelectrolyte, polyDMDAAC, at the Air-Water Interface: The Role of Alkyl Chain Length and Electrolyte and Comparison with Theoretical Predictions." *Langmuir*, **23**(2007), 3128.

[103] W. Xu, Q. Zhang, H. Wei, J. Qin, and L. Yu. "Self-aggregation of catanionic surface active ionic liquids in aqueous solutions." *J. Surfactants Deterg.*, **18**(2015), 421.

[104] J. Jiao, B. Dong, H. Zhang, Y. Zhao, X. Wang, R. Wang, and L. Yu. "Aggregation behaviors of dodecyl sulfate-based anionic surface active ionic liquids in water." *J. Phys. Chem. B*, **116**(2012), 958.

[105] R. Sanan, T. S. Kang, and R. K. Mahajan. "Complexation, dimerisation and solubilisation of methylene blue in the presence of biamphiphilic ionic liquids: a detailed spectroscopic and electrochemical study." *Phys. Chem. Chem. Phys.*, **16**(2014), 5667.

[106] T. J. Trivedi, K. S. Rao, T. Singh, S. K. Mandal, N. Sutradhar, A. B. Panda, and A. Kumar. "Task-specific, biodegradable amino acid ionic liquid surfactants." *ChemSusChem*, **4**(2011), 604.

[107] K. S. Rao, P. S. Gehlot, H. Gupta, M. Drechsler, and A. Kumar. "Sodium bromide induced micelle to vesicle transitions of newly synthesized anionic surface active ionic liquids based on dodecylbenzenesulfonate." *J. Phys. Chem. B*, **119**(2015), 4263.

[108] N. Cheng, P. Yu, T. Wang, X. Sheng, Y. Bi, Y. Gong, and L. Yu. "Self-aggregation of new alkylcarboxylate-based anionic surface active ionic liquids: Experimental and theoretical investigations." *J. Phys. Chem. B*, **118**(2014), 2758.

[109] M. Anouti, J. Jones, A. Boisset, J. Jacquemin, M. Caillon-Caravanier, and D. Lemordant. "Aggregation behavior in water of new imidazolium and pyrrolidinium alkycarboxylates protic ionic liquids." *J. Colloid Interface Sci.*, **340**(2009), 104.

[110] C. Florindo, L. C. Tomẽ, and I. M. Marrucho. "Thermodynamic study of aggregation of cholinium perfluoroalkanoate ionic liquids." *J. Chem. Eng. Data*, **61**(2016), 3979.

[111] K. Srinivasa Rao, P. S. Gehlot, T. J. Trivedi, and A. Kumar. "Self-assembly of new surface active ionic liquids based on Aerosol-OT in aqueous media." *J. Colloid Interface Sci.*, **428**(2014), 267.

[112] T. Yin, J. Wu, S. Wang, and W. Shen. "Structural rearrangement in the aqueous solution of surface active ionic liquid 1-butyl-3-methylimidazolium bis(2-ethylhexyl) sulfosuccinate." *Soft Matter*, **11**(2015), 4717.

[113] M. Blesic, M. Swadźba-Kwaśny, T. Belhocine, H. Q. N. Gunaratne, J. N. C. Lopes, M. F. C. Gomes, A. A. H. Pádua, K. R. Seddon, and L. P. N. Rebelo. "1-Alkyl-3-methylimidazolium alkanesulfonate ionic liquids, [C_nH_{2n+1}mim][$C_kH_{2k+1}SO_3$]: synthesis and physicochemical properties." *Phys. Chem. Chem. Phys.*, **11**(2009), 8939.

[114] V. Raghavan and P. L. Polavarapu. "First room temperature chiral anionic liquid forming micelles and reverse micelles." *J. Phys. Chem. B*, **121**(2017), 1629.

[115] H. Schnablegger and Y. Sing, editors. *The SAXS Guide, Getting acquainted with the principles*. Anton Paar GmbH (2013).

[116] H. Wang, L. Zhang, J. Wang, Z. Li, and S. Zhang. "The first evidence for unilamellar vesicle formation of ionic liquids in aqueous solutions." *Chem. Commun.*, **49**(2013), 5222.

[117] P. Sun, F. Lu, A. Wu, L. Shi, and L. Zheng. "Spontaneous wormlike micelles formed in a single-tailed zwitterionic surface-active ionic liquid aqueous solution." *Soft Matter*, **13**(2017), 2543.

[118] W. Xu, Q. Yin, Y. Gao, and L. Yu. "Solvent and substituent effects on the aggregation behavior of surface-active ionic liquids with aromatic counterions and the dispersion of carbon nanotubes in their hexagonal liquid crystalline phase." *Langmuir*, **31**(2015), 12644.

[119] P. D. Galgano and O. A. El Seoud. "Surface active ionic liquids: Study of the micellar properties of 1-(1-alkyl)-3-methylimidazolium chlorides and comparison with structurally related surfactants." *J. Colloid Interface Sci.*, **361**(2011), 186.

[120] A. K. Ressmann, R. Zirbs, M. Pressler, P. Gaertner, and K. Bica. "Surface-active ionic liquids for micellar extraction of piperine from black pepper." *Z. Naturforsch., B: Chem. Sci.*, **68b**(2013), 1129.

[121] I. Svinyarov and M. G. Bogdanov. "Ionic liquid-assisted micellar extraction for the quantitative determination of sesquiterpenic acids in *Valeriana officinalis* l. (caprifoliaceae)." *Sep. Sci. Technol.*, (2017), 1.

[122] E. L. P. de Faria, S. V. Shabudin, A. F. M. Cláudio, M. Valega, F. M. Domingues, C. S. R. Freire, A. J. Silvestre, and M. G. Freire. "Aqueous solutions of surface-active ionic liquids: remarkable alternative solvents to improve the solubility of triterpenic acids and their extraction from biomass." *ACS Sustainable Chem. Eng.*, (2017). 10.1021/acssuschemeng.7b01616.

[123] A. H. Rageh and U. Pyell. "Boronate affinity-assisted mekc separation of highly hydrophilic urinary nucleosides using imidazolium-based ionic liquid type surfactant as pseudostationary phase." *Electrophoresis*, **36**(2015), 784.

[124] V. Pino, M. Germán-Hernández, A. Martín-Pérez, and J. L. Anderson. "Ionic liquid-based surfactants in separation science." *Sep. Sci. Technol.*, **47**(2012), 264.

[125] M. J. Trujillo-Rodríguez, V. Pino, J. L. Anderson, J. H. Ayala, and A. M. Afonso. "Double salts of ionic-liquid-based surfactants in microextraction: application of their mixed hemimicelles as novel sorbents in magnetic-assisted micro-dispersive solid-phase extraction for the determination of phenols." *Anal. Bioanal. Chem.*, **407**(2015), 8753.

[126] C. Tejada-Casado, D. Moreno-González, A. M. García-Campaña, and M. del Olmo-Iruela. "Use of an ionic liquid-based surfactant as pseudostationary phase in the analysis of carbamates by micellar electrokinetic chromatography." *Electrophoresis*, **36**(2015), 955.

[127] M. A. Rather, S. A. Bhat, S. A. Pandit, G. M. Rather, K. Z. Khan, and M. A. Bhat. "Imidazolium based surface active ionic liquids as novel micellar media for simultaneous and sensitive electrochemical detection of dopamine and ascorbic acid." *Electroanalysis*, **29**(2017), 1772.

[128] J. F. Ayala-Cabrera, M. J. Trujillo-Rodríguez, V. Pino, Ó. M. Hernández-Torres, A. M. Afonso, and J. Sirieix-Plénet. "Ionic liquids versus ionic liquid-based surfactants in dispersive liquid-liquid microextraction for determining copper in water by flame atomic absorption spectrometry." *Int. J. Environ. Anal. Chem.*, **96**(2016), 101.

[129] R. Sanan, R. Kaur, and R. K. Mahajan. "Micellar transitions in catanionic ionic liquid-ibuprofen aqueous mixtures; effects of composition and dilution." *RSC Adv.*, **4**(2014), 64877.

[130] R. Vashishat, R. Sanan, and R. K. Mahajan. "Bile salt-surface active ionic liquid mixtures: mixed micellization and solubilization of phenothiazine." *RSC Adv.*, **5**(2015), 72132.

[131] S. Mahajan, R. Sharma, and R. K. Mahajan. "An investigation of drug binding ability of a surface active ionic liquid: Micellization, electrochemical, and spectroscopic studies." *Langmuir*, **28**(2012), 17238.

[132] R. Patel, A. B. Khan, N. Dohare, M. Maroof Ali, and H. K. Rajor. "Mixed micellization and interfacial properties of ionic liquid-type imidazolium gemini surfactant with amphiphilic drug amitriptyline hydrochloride and its thermodynamics." *J. Surfactants Deterg.*, **18**(2015), 719.

[133] R. Patel, M. u. d. Parray, U. K. Singh, A. Islam, P. Venkatesu, S. Singh, and H. B. Bohidar. "Effect of 1,4-bis(3-dodecylimidazolium-1-yl) butane bromide on channel form of gramicidin vesicles." *Colloids Surf., A*, **508**(2016), 150.

[134] S. S. Dandpat and M. Sarkar. "Investigating the molecular and aggregated states of a drug molecule rutaecarpine using spectroscopy, microscopy, crystallography and computational studies." *Phys. Chem. Chem. Phys.*, **17**(2015), 13992.

[135] G. Singh and T. S. Kang. "Ionic liquid surfactant mediated structural transitions and self-assembly of bovine serum albumin in aqueous media: Effect of functionalization of ionic liquid surfactants." *J. Phys. Chem. B*, (2015), 10573.

[136] C. Cao, J. Lei, T. Huang, and F.-P. Du. "Impact of ionic liquid-type imidazolium surfactant addition on dynamic properties of bsa adsorption layers at different pH." *Soft Matter*, **10**(2014), 8896.

[137] R. Vashishat, S. Chabba, and R. K. Mahajan. "Surface active ionic liquid induced conformational transition in aqueous medium of hemoglobin." *RSC Adv.*, **7**(2017), 13041.

[138] T. Huang, C. Cao, Z.-l. Liu, Y. Li, and F.-p. Du. "Interaction of pepsin-[C_{16}mim]Br system: interfacial dilational rheology and conformational studies." *Soft Matter*, **10**(2014), 6810.

[139] C. Cao, T. Huang, and F.-P. Du. "Impact of ionic liquid-type imidazolium surfactant additions on dynamic properties of β-casein adsorption layer." *Food Hydrocolloids*, **36**(2014), 348.

[140] J. K. Maurya, M. U. H. Mir, N. Maurya, N. Dohare, A. Ali, and R. Patel. "A spectroscopic and molecular dynamic approach on the interaction between ionic liquid type gemini surfactant and human serum albumin." *J. Biomol. Struct. Dyn.*, **34**(2016), 2130.

[141] S. Adak, S. Datta, S. Bhattacharya, and R. Banerjee. "Role of spacer length in interaction between novel gemini imidazolium surfactants and rhizopus oryzae lipase." *Int. J. Biol. Macromol.*, **81**(2015), 560.

[142] A. Roy, P. Banerjee, R. Dutta, S. Kundu, and N. Sarkar. "Probing the interaction between a DNA nucleotide (adenosine-5'-monophosphate disodium) and surface active ionic liquids by rotational relaxation measurement and fluorescence correlation spectroscopy." *Langmuir*, **32**(2016), 10946.

[143] C. Pardin, L. Leclercq, and A. R. Schmitzer. "N-n-methylenediimidazolium salts: From self-assembly to an efficient DNAse protection system." *Chem. Eur. J.*, **16**(2010), 4686.

[144] G. La Sorella, G. Strukul, and A. Scarso. "Recent advances in catalysis in micellar media." *Green Chem.*, **17**(2015), 644.

[145] T. Dwars, E. Paetzold, and G. Oehme. "Reactions in micellar systems." *Angew. Chem. Int. Ed.*, **44**(2005), 7174.

[146] K. Bica, P. Gärtner, P. J. Gritsch, A. K. Ressmann, C. Schröder, and R. Zirbs. "Micellar catalysis in aqueous-ionic liquid systems." *Chemical Communications*, **48**(2012), 5013.

[147] M. Vafaeezadeh, M. Karbalaie-Reza, M. M. Hashemi, and K. Q. Soleimany. "Surfactant-like brønsted acidic ionic liquid as an efficient catalyst for selective mannich reaction and biodiesel production in water." *J. Iran. Chem. Soc.*, **14**(2017), 907.

[148] R. Sharma, B. Gupta, T. Yadav, S. Sinha, A. K. Sahu, Y. Karpichev, N. Gathergood, J. Marek, K. Kuca, and K. K. Ghosh. "Degradation of organophosphate pesticides using pyridinium based functional surfactants." *ACS Sustainable Chem. Eng.*, **4**(2016), 6962.

[149] A. Cognigni, P. Gaertner, R. Zirbs, H. Peterlik, K. Prochazka, C. Schröder, and K. Bica. "Surface-active ionic liquids in micellar catalysis: impact of anion selection on reaction rates in nucleophilic substitutions." *Phys. Chem. Chem. Phys.*, **18**(2016), 13375.

[150] A. Bonnefond, M. Ibarra, D. Mecerreyes, and J. R. Leiza. "Adding magnetic ionic liquid monomers to the emulsion polymerization tool-box: Towards polymer latexes and coatings with new properties." *J. Polym. Sci., Part A: Polym. Chem.*, **54**(2016), 1145.

[151] Y. Liu, L. Qiao, Y. Xiang, and R. Guo. "Adsorption behavior of low-concentration imidazolium-based ionic liquid surfactant on silica nanoparticles." *Langmuir*, **32**(2016), 2582.

[152] A. Safavi and S. Zeinali. "Synthesis of highly stable gold nanoparticles using conventional and geminal ionic liquids." *Colloids Surf., A*, **362**(2010), 121 .

[153] P. Bharmoria, T. Singh, and A. Kumar. "Complexation of chitosan with surfactant like ionic liquids: Molecular interactions and preparation of chitosan nanoparticles." *J. Colloid Interface Sci.*, **407**(2013), 361.

[154] S. Chakraborty, K. Jähnichen, H. Komber, A. A. Basfar, and B. Voit. "Synthesis of magnetic polystyrene nanoparticles using amphiphilic ionic liquid stabilized raft mediated miniemulsion polymerization." *Macromolecules*, **47**(2014), 4186.

[155] Z. Du, E. Li, G. Li, F. Cheng, and G. Wang. "One-step strategy for synthesis of yolk-shell silica spheres using trisiloxane-tailed ionic liquids as a template." *J. Mater. Sci.*, **49**(2014), 4919.

[156] A. Sachse, C. Wuttke, U. Díaz, and M. O. de Souza. "Mesoporous y zeolite through ionic liquid based surfactant templating." *Microporous Mesoporous Mater.*, **217**(2015), 81.

[157] C. Chen, X. Zhao, J. Chen, L. Hua, R. Zhang, L. Guo, B. Song, H. Gan, and Z. Hou. "Niobium peroxide-catalyzed selective epoxidation of allylic alcohols." *ChemCatChem*, **6**(2014), 3231.

[158] Z.-b. Xu, G.-p. Lu, and C. Cai. "Palladium nanoparticles stabilized by aqueous vesicles self-assembled from a PEGylated surfactant ionic liquid for the chemoselective reduction of nitroarenes." *Catal. Commun.*, **99**(2017), 57.

[159] E. E. Drinkel, R. R. Campedelli, A. M. Manfredi, H. D. Fiedler, and F. Nome. "Zwitterionic-surfactant-stabilized palladium nanoparticles as catalysts in the hydrogen transfer reductive amination of benzaldehydes." *J. Org. Chem.*, **79**(2014), 2574.

[160] Y. Gong, Y. Guo, Q. Hu, C. Wang, L. Zang, and L. Yu. "pH-Responsive Polyoxometalate-Based Supramolecular Hybrid Nanomaterials and Application as Renewable Catalyst for Dyes." *ACS Sust. Chem. Eng.*, **5**(2017), 3650.

[161] Y. Gong, Q. Hu, N. Cheng, T. Wang, W. Xu, Y. Bi, and L. Yu. "Fabrication of pH - and temperature-directed supramolecular materials from 1D fibers to exclusively 2D planar structures using an ionic self-assembly approach." *J. Mater. Chem. C*, **3**(2015), 3273.

[162] E. Aliyari, M. Alvand, and F. Shemirani. "Modified surface-active ionic liquid-coated magnetic graphene oxide as a new magnetic solid phase extraction sorbent for preconcentration of trace nickel." *RSC Adv.*, **6**(2016), 64193.

Chapter 2

Aim of the thesis

One of the key requirements for the reduction of the overall environmental impact of a chemical process is the replacement of organic solvents with more benign reaction media like water, however this suffers from solubility limitations. A powerful tool to overcome these issues in synthesis is micellar catalysis, where a small amount of surfactant species form aggregates in water with a lipophilic core that can act as a nanoreactor. Surface-active ionic liquids are prime candidates for this application due to the tunability of structure and properties of conventional ionic liquids that have already been established in catalysis. This suggests that ionic liquids-water micellar systems provide a novel and safer but yet cost-efficient reaction media and open a broad aspect for organic synthesis and catalysis. The new reaction environment, different from bulk water, will also show synergies and overcome drawbacks from both pure water and pure ionic liquids.

This thesis provides fundamental insight into the nature of self-organization of surface-active ionic liquids in water, with special focus on the design, development and evaluation of new ionic liquids-water micellar systems and their application in synthesis and catalysis.
The synthesis and characterization of a series of new 1-dodecylimidazolium based surface-active ionic liquids with different structural features will be reported, including different anions, dicationic and zwitterionic structures. The surface-activity and aggregation behaviour of the new surfactants will be defined by their CMC as well as by thermodynamic and spectroscopic studies. In order to test the broad applicability of ionic liquids-water micellar systems as reaction media different types of transformations will be tested:

- Organic synthesis: the influence of surface-active ionic liquids concentration, structure and properties on the reaction rate of a nucleophilic substitution reaction will be investigated
- Palladium catalysed reactions: besides providing a suitable reaction environment, aqueous-ionic liquid micellar media can play an active role in catalyst stabilization and speciation
- Catalytic water splitting: surface-active ionic liquids can be used to design catalysts for oxygen production via catalytic water splitting and simultaneously act as reaction media

Chapter 3

Surface-active ionic liquids in micellar catalysis

In this chapter the application of surface-active ionic liquids in organic reactions is presented. Particular attention is given to the role of the anion; consequently, a series of ionic liquids with the same cation $[C_{12}mim]^+$ and different anions has been synthesized, characterized and applied in a nucleophilic substitution reaction. A strong correlation between the reaction rate and the CMC could be observed. In order to support these findings, further characterization studies on the physical-chemical properties of the micellar solutions were conducted through external cooperations. Thermodynamic characterization of the micellar process was performed via isothermal titration calorimetry. Hydration degree of the micelles and anion mobility information were obtained via dielectric spectroscopy, allowing to rationalize the finding observed in nucleophilic substitution reactions.

The following manuscripts will be presented in this chapter:

- Cognigni, Alice; Gaertner, Peter; Zirbs, Ronald; Peterlik, Herwig; Prochazka, Katharina; Schroeder, Christian; Bica, Katharina; **Surface-active ionic liquids in micellar catalysis: impact of anion selection on reaction rates in nucleophilic substitutions** *Phys. Chem. Chem. Phys.* **2016**, *18* (19), 13375-13384.

As first author I planned and performed a major part of the experimental work, including the synthesis and characterization of the ionic liquid, as well as their application in nucleophilic substitution reactions. Furthermore I wrote the manuscript.

- Šarac, Bojan; Medoš, Žiga; Cognigni, Alice; Bica, Katharina; Chen, Li-Jen; Bešter-Rogač, Marija; **Thermodynamic study for micellization of imidazolium based surface active ionic liquids in water: Effect of alkyl chain length and anions** *Colloids Surf. A : Physicochem. Eng. Aspects* **2017**, DOI:10.1016/j.colsurfa.2017.01.062.

In this work arising from a collaboration with the university of Ljubljana I synthesized all involved ionic liquids and characterized them via conductivity and surface tension measurements. I also made a major contribution to parts of the manuscript.

- Friesen, Sergej; Buchecker, Thomas; Cognigni, Alice; Bica, Katharina and Buchner, Richard **Hydration and Counterion Binding of [C_{12}MIM] Micelles** *Langmuir* **2017**, DOI: 10.1021/acs.langmuir.7b02201.

In this manuscript arising from a cooperation with the university of Regensburg, I provided the involved surface-active ionic liquids. I also assisted in the manuscript preparation.

Supporting information for all manuscripts can be found in Appendix A.

PCCP

PAPER

View Article Online
View Journal | View Issue

Published on 28 April 2016. Downloaded by TU Wien University Library on 13/06/2016 09:08:38.

Cite this: *Phys. Chem. Chem. Phys.*, 2016, **18**, 13375

Surface-active ionic liquids in micellar catalysis: impact of anion selection on reaction rates in nucleophilic substitutions†

Alice Cognigni,[a] Peter Gaertner,[a] Ronald Zirbs,[b] Herwig Peterlik,[c] Katharina Prochazka,[c] Christian Schröder[d] and Katharina Bica*[a]

Received 22nd January 2016,
Accepted 5th April 2016

DOI: 10.1039/c6cp00493h

www.rsc.org/pccp

A series of surface-active ionic liquids based on the 1-dodecyl-3-methylimidazolium cation and different anions such as halides and alkylsulfates was synthesized. The aggregation behavior of these ionic liquids in water was characterized by surface tension, conductivity measurements and UV-Vis spectroscopy in order to determine the critical micelle concentration (CMC) and to provide aggregation parameters. The determination of surface activity and aggregation properties of amphiphilic ionic liquids was accompanied by SAXS studies on selected surface-active ionic liquids. The application of these surface-active ionic liquids with different anions was tested in nucleophilic substitution reactions for the degradation of organophosphorus compounds. Kinetic studies *via* UV-Vis spectrophotometry showed a strong acceleration of the reaction in the micellar system compared to pure water. In addition, an influence of the anion was observed, resulting in a correlation between the anion binding to the micelle and the reaction rate constants, indicating that the careful choice of the surface-active ionic liquid can considerably affect the outcome of reactions.

Introduction

In recent years the scope of ionic liquids as functional fluids has been expanded to include their mixtures with water for multiple applications.[1] The microstructure and heterogeneity in the liquid state, fundamental aspects of pure ionic liquids, continue to exist in aqueous solution, and several reviews have been published focusing on the structure and behaviour of ionic liquid clusters in water.[2] The self-assembly of ionic liquids in aqueous solution is particularly well investigated for long alkyl chain ionic liquids that have been found to display amphiphilic character analogous to conventional cationic surfactants.[3] The co-existence of an ionic hydrophilic head group and a long hydrophobic tail results in the formation of aggregates in water; however, as a general rule the alkyl chain must contain at least eight carbon atoms for aggregation in water.[4] A number of computational and experimental techniques, including molecular dynamics simulations, surface tension and conductivity measurements, potentiometry, UV-Vis spectroscopy, fluorescence probes, NMR spectroscopy, mass spectrometry, isothermal titration calorimetry, light scattering and small-angle X-ray and neutron scattering (SAXS and SANS) have been applied to understand the self-aggregation of surface-active ionic liquids in water.[4–11]

While traces of water in ionic liquids are often considered as problematic due to the difficulty in their removal and their large impact on physical properties, the deliberate combination of these two media in well-defined mixtures may result in unique properties that can be fully exploited by varying their composition.[12] For example, the limited solubility of many organic compounds in water could be enhanced with ionic liquids, whereas price or viscosity issues of ionic liquids could be balanced when used in aqueous solution. At the same time the specific properties of the highly tunable ionic liquids and the strong hydrogen bond of water can be combined to afford a reaction environment with new properties. Applications of well-defined ionic liquid/water mixtures have already been identified and range from biomolecule stabilization towards their application in catalysis or in novel separation processes.

[a] *Institute of Applied Synthetic Chemistry, Vienna University of Technology, Getreidemarkt 9/163, 1060 Vienna, Austria. E-mail: katharina.schroeder@tuwien.ac.at; Fax: +43 1 58801 16360; Tel: +43 1 58801 163601*

[b] *Group for Biologically Inspired Materials, Institute of Nanobiotechnology (DNBT), University of Natural Resources and Life Sciences, Muthgasse 11, 1190 Vienna, Austria*

[c] *Dynamics of Condensed Systems, University of Vienna, Boltzmanngasse 5, 1090 Vienna, Austria*

[d] *Institute of Computational Biological Chemistry, University of Vienna, Währingerstrasse 17, 1090 Vienna, Austria*

† Electronic supplementary information (ESI) available: Formulae for calculating aggregation parameters and fitting of kinetic constants and copies of NMR spectra. See DOI: 10.1039/c6cp00493h

Published on 28 April 2016. Downloaded by TU Wien University Library on 13/06/2016 09:08:38.

The impact of self-assembly of ionic liquids in aqueous solution has also been exploited by our group, showing that surface-active ionic liquids can be efficiently applied in micellar catalysis of Diels Alder reactions, for asymmetric transfer hydrogenations in water, and also for extraction of natural products.[13,14]

Studies on the self-assembly and structural organization of ionic liquids in water have so far dealt mainly with monocationic alkyl imidazolium based ionic liquids, however also other structures have already been investigated. Full critical micellar concentration (CMC) characterization and extensive thermodynamic studies allow identifying specific features that influence the properties of these ionic liquids. Several studies showed that the CMC is strongly influenced by the structure of the ionic liquid, in particular in terms of the alkyl chain length of the hydrophobic tail unit.[3–6,15–19] As for traditional cationic surfactants, the Klevens equation was found to be valid.[20] A linear relationship between the number of carbon atoms on the alkyl chain and the logarithm of the CMC has been verified[19] which can be applied for predicting the CMC for a homologous series of linear-single chain amphiphiles at a fixed temperature. Cations with different structures have also been reported.[5,6,21] Blesic *et al.*[21] investigated the effect of different cationic rings by comparing alkylmethylimidazolium with alkylmethylpyridinium, alkylmethylpiperidinium and alkylmethylpyrrolidinium core groups. The results show that pyrrolidinium has the lowest CMC while the others present an almost identical surface tension profile, however due to the very complex interactions a univocal explanation based on geometry and/or electronic distribution could not be provided. This is in accordance with a study of Cornellas *et al.*[5] where no substantial difference was identified in the behaviour for surface-active ionic liquids with imidazolium and pyridinium head groups. The introduction of an ester or amide functionality in the side chain of these head groups resulted in improved surface activity according to the studies of Comelles *et al.*[22,23]; moreover biodegradability was improved by the ester functionality, while the amide group provided a higher thermal stability. On the other hand El Seoud *et al.*[24] showed that the introduction of a vinyl moiety on the imidazolium cation resulted in higher CMC values compared to the corresponding ethyl analogues due to the less hydrophobic character of the vinyl group. Baltazar *et al.*[25] also investigated the aggregation behaviour of dicationic alkylimidazolium ionic liquids, and CMC values were found to depend not only on the chain length of the imidazolium cation, but also on the length of the linkage chain between the two head groups. Similar results were also obtained by Anderson *et al.*[26] who investigated tricationic surface active ionic liquids. Besides showing a better surface activity compared to dicationic ones, this could be further improved by increasing the size and aromaticity of the internal linker. In addition, surface-active ionic liquids with different anions have been investigated, but studies on the role of the anion are less systematic. Blesic *et al.*[4] compared the aggregation behaviour of 1-dodecycl-3-methylimidazolium ($[C_{12}mim]^+$) based ionic liquids with Cl^-, $[PF_6]^-$, and $[NTf_2]^-$ as counterions. Aggregates in aqueous solution were found only in the case of chloride anions, whereas the low solubility of the ionic liquids containing the $[PF_6]^-$ and $[NTf_2]^-$ anions resulted in phase separation prior to the formation of aggregates. In a different study on different halide counterions Kim *et al.* reported higher surface activity for $[C_{12}mim]I$ than for the same ionic liquids containing Br^- or Cl^- as a counter anion; this was explained by the higher polarizability and binding to the micelles of iodide ions.[27]

In a study conducted by Frizzo *et al.*[28] concerning dicationic imidazolium based surface-active ionic liquids dissolved in 4.75% ethanol–water solution, a correlation between the aggregation and the anion hydrophobicity was identified. Recently Nowicki *et al.*[29] reported a series of alkylimidazolium surface-active ionic liquids with HSO_4^- as a counterion. These ionic liquids had a key role as co-catalysts in an oxirane ring opening reaction of epoxidized methyl oleate, and their performance was dependent on the length of the alkyl chain attached to the imidazolium cation. Using a bulky amphiphilic anion such as ibuprofenate allows detection of a critical aggregation concentration even when coupled with $[C_4mim]^+$ or $[C_6mim]^+$ cations; moreover it was suggested that ionic liquids containing an active pharmaceutical ingredient can be incorporated into ionogels and used for drug delivery applications.[30]

In contrast, fewer studies exist on ionic liquids with surface-active anions in the literature. Early examples report surface-activity of octylsulfate combined with $[C_4mim]^+$, which also contributes to a decrease in the toxicity of the ionic liquid.[10,31] Comprehensive work was conducted by Blesic *et al.*[32,33] on alkylimidazolium alkylsulfonate ionic liquids. A matrix of ionic liquids with variable chain length in both the cation and the anion was synthesized and the physico-chemical properties were determined. Again, a strong dependence of the CMC on the chain length of the cation was identified, but the surface activity could be considerably improved by simultaneously introducing a long alkyl chain in the anion. A series of protic ionic liquids based on long-alkyl chain carboxylates was investigated with different cations such as imidazolium and pyrrolidinium. These ionic liquids not only showed a higher surface activity than cationic surfactants, but also performed better than the corresponding surfactants with inorganic cations.[34] When diisopropylethylammonium was used as a cation, the formation of bilayer vesicle-like aggregates was also demonstrated.[35]

Eventually, fluorinated surface-active ionic liquids composed of perfluorinated anions have only recently been investigated.[36,37] An extensive study by Pereiro *et al.* showed that perfluorinated alkylsulfonates strongly decrease the CMC in comparison to the corresponding halide-based ionic liquids, and even for $[C_2mim][C_4F_9SO_3]$ and $[C_2mim][C_8F_{17}SO_3]$ a critical aggregation concentration could be detected.

Herein, we intend to present further insights into the nature of self-organization of ionic liquids in water and its impact on micellar catalysis of nucleophilic substitution reactions in water. In particular, we focused on the role of the counteranion and aimed for a correlation between anion binding to the micelle and reaction rate constants, suggesting that the careful choice of the surface-active ionic liquid can considerably affect the outcome of reactions.

 This journal is © the Owner Societies 2016

Published on 28 April 2016. Downloaded by TU Wien University Library on 13/06/2016 09:08:38.

Results and discussion

Synthesis of surface-active ionic liquids

We focused on 1-dodecycl-3-methylimidazolium-based ionic liquid [C_{12}mim]X, as this is a known and already characterized surface-active cation and we functionalized it with different anions. Our synthetic route is based on two different approaches (Scheme 1). In the case of the surface active [C_{12}mim]Cl **1**, [C_{12}mim]Br **2** and [C_{12}mim]I **3** the classical alkylation of *N*-methylimidazole with the corresponding dodecyl halides was performed. In contrast, surface-active ionic liquids [C_{12}mim]OMs **4** and [C_{12}mim]OTs **5** and [C_{12}mim]OTf **6** were prepared in a two-step synthesis route, including the initial synthesis of *N*-dodecylimidazole by alkylation of imidazole. Afterwards the final ionic liquids were obtained *via* direct alkylation of *N*-dodecylimidazole with the methyl esters of the corresponding anions. This second route offers a halide free pathway for the synthesis of ionic liquids. In any case, good yields between 83 and 98% were obtained. The final products were purified by repeated crystallization from organic solvents to isolate all ionic liquids as colourless crystals in high purity. In contrast, crystallization was not possible for [C_{12}mim]OTf **6**; however, the highly volatile anion precursors could be easily removed under reduced pressure, allowing isolation of the ionic liquid as a low-melting colourless solid.

Characterization of surface-activity

Prior to their application in micellar catalysis all ionic liquids were characterized by different experimental techniques in order to investigate the formation of aggregates in water. Several techniques can and have been used for the determination of the CMC of alkyl methyl imidazolium-based ionic liquids, and the reported literature values for a specific ionic liquid vary considerably according to the different techniques as can be seen from the ionic liquid [C_{14}mim]Cl, where CMC values ranging from 2.98–4.6 mM have been reported. Herein, we selected three different techniques, including surface tension, conductivity and UV-Vis spectroscopy. The results are summarized in Table 1 and will be discussed in the following paragraphs in detail.

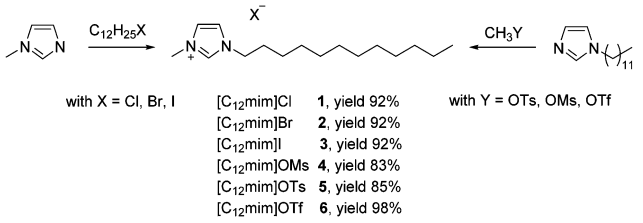

Scheme 1 Synthesis with surface-active ionic liquids based on the 1-dodecycl-3-methylimidazolium cation with variable anions.

Conductivity measurements

Conductivity measurements can be utilized for the characterization of ionic surfactants due to the different mobility of the individual ions and their aggregates. Curves of the specific conductivity (κ) *versus* the ionic liquid concentration are reported in Fig. 1 (left). Two different linear regimes could be typically identified that allowed calculating the CMC values *via* their breaking point. In principle, two phenomena are responsible for this curve shape: formed micelles have a lower mobility than single ions. Moreover, parts of the anions are adsorbed on the surface of the aggregates, decreasing the total species contributing to the solution conductivity upon formation of micelles. The degree of counterion binding (β) can be estimated from the ratio of the slopes[27] and indicates the amount of anions on the surface of the micelles. The observed CMC values for ionic liquids already reported are in agreement with the results obtained by other research groups.[27,32] A clear trend can be seen in the halide series, and CMC values decrease in the order Cl > Br > I. Similarly, a trend is visible for sulfonates where tosylate (OTs^-) and triflate (OTf^-) based ionic liquids have a lower CMC than [C_{12}mim]OMs **4**. A larger and more hydrophobic anion such as OTs^- tends to adsorb on the micellar surface instead of being hydrated, and consequently favours the formation of aggregates by shielding the electrostatic repulsion forces of the charged headgroups.[38] This behaviour is also supported by the degree of counterion binding (β): a higher value corresponds to a lower CMC due to the higher amount of anions bound to the micellar surface. Additionally, the Gibbs energy of micellization (ΔG^0_{mic}) could be calculated from the conductivity data, proving that the formation of micelles is a spontaneous process that is accompanied by a negative free energy change (see the ESI† for details).[39]

Table 1 Physical-chemical characterization of the surface-active ionic liquids

	Surface tension[b]				Conductivity[c]			UV-Vis[d]
Ionic liquid[a]	CMC (mM)	$\prod_{CMC}$ (mN m^{-1})	A_{min} (nm^2)	P	CMC (mM)	β	ΔG^0_{mic} (kJ mol^{-1})	CMC (mM)
[C_{12}mim]Cl **1**	13.25 (Lit. 13.17)[6]	28.6	0.72	0.29	14.53	0.43	−29.1	—
[C_{12}mim]Br **2**	9.29	29.3	0.71	0.30	10.29	0.70	−36.2	10.24
[C_{12}mim]I **3**	4.76	37.7	0.62	0.34	5.19	0.84	−42.3	4.12
[C_{12}mim]OMs **4**	12.50	29.4	1.13	0.18	14.71	0.45	−29.5	15.26
[C_{12}mim]OTf **5**	2.37	40.2	0.55	0.38	3.31	0.73	−41.7	2.69
[C_{12}mim]OTs **6**	2.25	38.3	0.65	0.32	3.44	0.89	−45.4	—

[a] Solutions were prepared with doubly-distilled Millipore Milli-Q water and left under shaking with 360 min^{-1} for 24 h to equilibrate. Samples were equilibrated at 25.0 ± 0.1 °C using a HAAKE K15 thermostat before measurements. [b] Surface tension was determined using the Du Noüy ring method on a Krüss tensiometer. [c] Conductivity measurement were performed at 25 °C using a Mettler Toledo SevenExcellence InLAB® 741-ISM electrode. [d] UV-Vis measurements were performed at 25 °C, following the absorbance at 312 nm using benzoylacetone. $\prod_{CMC}$ is the effectiveness of the surface tension reduction, A_{min} is the area per molecule residing at the surface, P is the packing parameter, β is the degree of counterion binding, ΔG^0_{mic} is Gibbs energy of micellization (for details see the ESI).

Published on 28 April 2016. Downloaded by TU Wien University Library on 13/06/2016 09:08:38.

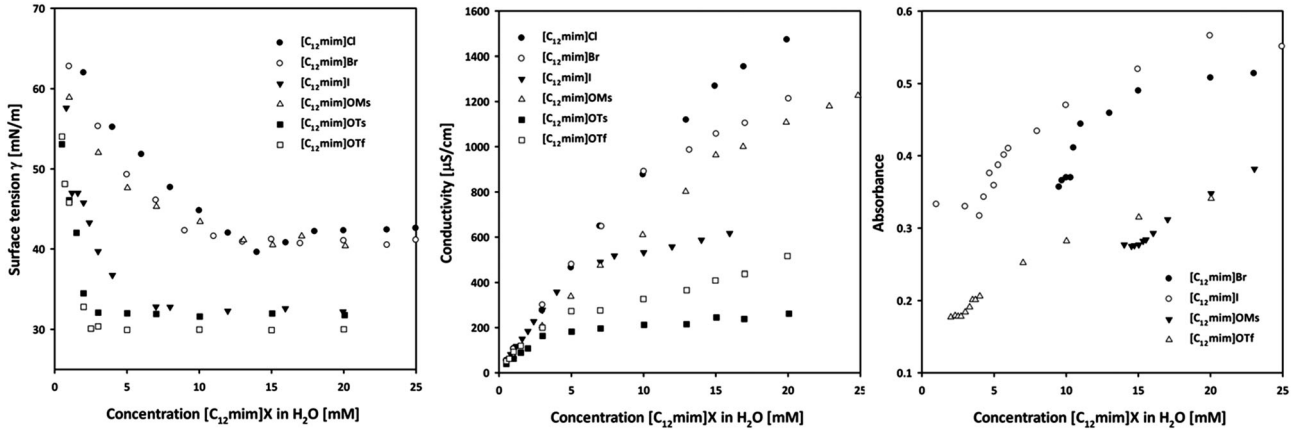

Fig. 1 Surface tension (left), conductivity (center) and UV-Vis profiles (right) of the investigated ionic liquids at 25 °C.

Surface-tension measurements

Fig. 1 (center) displays the surface tension (γ) curves as a function of the concentration of ionic liquids. As a consequence of absorption of ionic liquids at the surface, the surface tension decreases with increasing ionic liquid concentration, until a stable value is obtained after surface saturation. The breaking point of the curve can be used to determine the CMC value of the respective surfactant (see the ESI† for details). This characteristic behaviour allowed calculating CMC values for all ionic liquids. In general, the obtained CMC values were systematically slightly lower than those measured *via* the conductivity, however the same trend can be observed for the anions. According to the effectiveness of the surface tension reduction ($\prod_{CMC}$) all investigated ionic liquids reduce the water surface tension of 30–40 mN m^{-1}. The effectiveness can also be related to the degree of packing of adsorbed surfactant molecules at the interface. The Gibbs adsorption isotherm equation can be used to estimate the average area per molecule residing at the surface (A_{min}), assuming that the structure pattern corresponds to a monolayer.[40] A lower A_{min} value corresponds to a closer packing of monomers at the interface. This value could be used to estimate the shape of the formed aggregates according to the packing parameter[41] (P) which includes the volume (v) of the hydrocarbon chain embedded in the hydrocarbon core of the aggregate and the maximum effective length (l_c) that the chain can assume, calculated according to the Tanford equation (see the ESI† for details).[42] In general, a packing parameter $P < 0.33$ corresponds to spherical micelles, an intermediate value of $0.33 < P < 0.5$ corresponds to non-spherical, ellipsoidal micelles, while higher values correspond to rod-like micelles and various interconnected structures.[41] The results in Table 1 show that both spherical and ellipsoidal aggregates are presumably formed and depend on the anion size. According to this methodology, smaller anions such as bromide or mesylate form spherical micelles, while bigger anions, *e.g.* iodide or tosylate, favor the formation of ellipsoidal aggregates. This is to some extent in agreement with a study on the shape of alkyl imidazolium bromides by Goodchild *et al.*,[9] who performed SANS experiments and found that [C_{12}mim]Br forms spherical particles at low concentration near the CMC, while the shape tends to turn into elongated micelles at higher concentrations.

UV-Vis measurements

The determination of the CMC of surfactants using UV-Vis spectroscopy is based on the ketoenolic equilibrium of benzoylacetone. The enolic form can be stabilized by intramolecular hydrogen bonding forming a 6-membered ring. This structure is favoured inside the micelles where no competition for hydrogen bonding with the solvent is present. Consequently the formation of micelles with increasing ionic liquid concentration will shift the ketoenolic equilibrium towards the enol form. This results in an increase of the absorbance at 312 nm which can be used to calculate the CMC value from the breaking point of the curves.[43,44] The values depicted in Fig. 1 (right) are in good agreement with those obtained using the previous techniques, with the exception of [C_{12}mim]Cl **1**, where we were not able to find an unambiguous break point. However, we could not perform measurements for [C_{12}mim]OTs due to the overlap of the absorption spectrum of the ionic liquids with that of benzoylacetone.

Small-angle X-ray scattering

The determination of the surface activity and aggregation properties of amphiphilic ionic liquids was accompanied by SAXS studies. As the SAXS measurements and the evaluation were more time consuming, we decided to select three representative ionic liquids **1**, **2** and **6**, which cover the observed range of different conductivities (high, medium, and low conductivity in Fig. 1, center).

The SAXS intensities (Fig. 2) were fitted using a model describing spherical micelles with a radius of the core R_c, a Schulz distribution for the radii and a shell thickness δ. The core radius is about 1 nm and exhibits a more uniform and narrow size distribution with increasing concentration (see Fig. S1a to c in the ESI†). The shell has a similar size, about 1 nm for [C_{12}mim]Cl **1** and slightly higher for [C_{12}mim]Br **2** and [C_{12}mim]OTs **6**. The most important information is the parameter γ, which describes the electron differences between the core, shell and surrounding medium[45] and is defined in

 This journal is © the Owner Societies 2016

Published on 28 April 2016. Downloaded by TU Wien University Library on 13/06/2016 09:08:38.

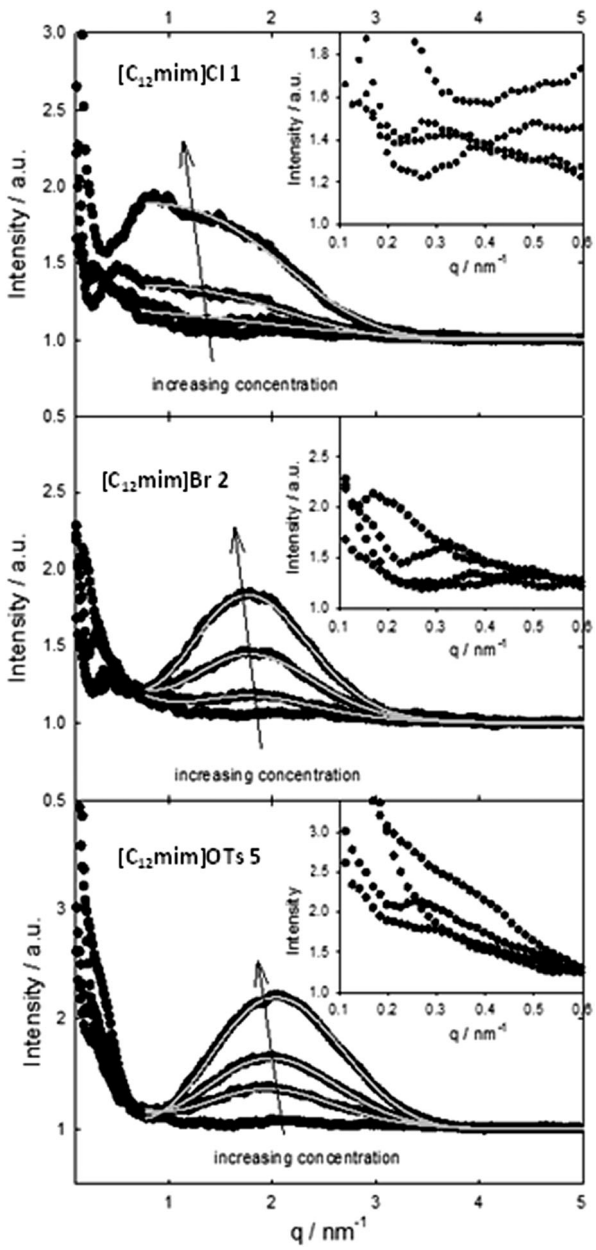

Fig. 2 Small-angle X-ray intensities for the different ionic liquids. The experimental intensities are shown as filled circles, the fit from the core–shell model with grey fit lines and the insets show the scattering intensities towards very low q-values.

the ESI:† it decreases with increasing concentration as well as it is significantly lower for $[C_{12}mim]Cl$ (even close to zero for $[C_{12}mim]Cl$ at 100 mM concentration) than for both other ionic liquids. As a value of $\gamma = 0$ means that the scattering only arises from the core[45] and the density of the shell is the same as the density of the surrounding solution, one may conclude that Cl is mobile and distributed in the solution, whereas OTs is only very weakly affected by different concentrations (Table 2). The inset in Fig. 2 shows the scattering intensities towards very low q-values. A weak maximum is also visible, which shifts towards smaller q-values for higher concentrations. This can be interpreted

Table 2 Fit parameters for spheres with a core shell structure and a Schulz distribution of the radius of the core (parameters core radius R_c, Z). γ is the scaled medium contrast (γ = 1, the scatter origins only from the shell, γ = 0, only from the core)[35]

Ionic liquid	Concentration/mM	Core radius R_c/nm	Z	Shell thickness δ/nm	γ
$[C_{12}mim]OTs$	25	0.95	15	1.23	0.16
$[C_{12}mim]OTs$	50	0.97	28	1.26	0.13
$[C_{12}mim]OTs$	100	1.02	84	1.22	0.12
$[C_{12}mim]Br$	25	0.97	8.3	1.27	0.20
$[C_{12}mim]Br$	50	0.97	13	1.39	0.13
$[C_{12}mim]Br$	100	0.98	25	1.59	0.09
$[C_{12}mim]Cl$	25	1.14	52	0.95	0.07
$[C_{12}mim]Cl$	50	1.18	250	0.94	0.06
$[C_{12}mim]Cl$	100	1.14	51	0.94	0.007

as a weak tendency for agglomeration of micelles with a cluster size of approximately 15 nm for the 25 mM concentration and considerably larger for higher concentration.

Application in nucleophilic substitutions

Micellar catalysis has already been proven to be a very powerful tool to overcome issues of conventional synthesis in both pure organic solvents and water, and recent developments in the fields have been thoroughly reviewed.[46–48] The problems created by the massive use of volatile, toxic and flammable organic solvents in industrial processes have increased the demand for more benign reaction media, and water is a prime candidate here. However, issues related to the poor solubility of organic compounds in water are well known, a problem that can be overcome *via* the addition of surfactants. It has already been reported that surface active ionic liquid aggregates can increase the solubility of apolar organic compounds that exhibit very poor solubility in water.[49] Furthermore micelles have the capability to drastically alter reaction rates of organic reactions, as the local concentration experienced by the reactants at/in the micellar zone is higher than in a bulk solution. Surfactants based on ionic liquids can also be finely tuned by adjustments on the head group, alkyl chain or counterion structure in order to offer an optimal reaction environment increasing parameters such as yield, rate and selectivity. Successful results were already obtained in our previous research on Diels–Alder reactions.[14] The highest reaction rate occurred above the CMC, clearly showing the positive effect of ionic liquid-derived micelles.

Nucleophilic substitutions of organophosphorus compounds can be accelerated by cationic surfactants and are strongly influenced by different anions present in the reaction mixture.[50] Optimal conditions for the substitution of organophosphorus compounds are obtained with α-nucleophiles, *i.e.* nucleophiles possessing a heteroatom with an unshared electron pair adjacent to the nucleophilic centre that exhibit a higher nucleophilic reactivity compared with common nucleophiles of similar basicity, a concept that is also known as the "α-effect". More specifically, oximates have been shown to efficiently promote the hydrolysis of phosphate triesters as they prevent the competition with other nucleophiles such as OH^- or halides.[51–53] Studies on the effect of several oximes[54] and substrate features[51,53] have been reported.

Published on 28 April 2016. Downloaded by TU Wien University Library on 13/06/2016 09:08:38.

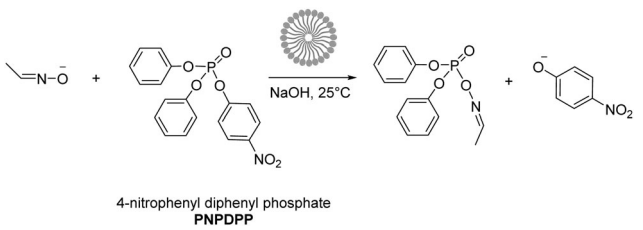

Scheme 2 Nucleophilic substitution of 4-nitrophenyl diphenyl phosphate (PNPDPP) with acetaldoxime.

In this study, we investigated the reaction between 4-nitrophenyl diphenyl phosphate (PNPDPP) and acetaldoxime (pK_a = 11.82) in different surface-active ionic liquid/water mixtures (Scheme 2). PNPDPP is a highly lipophilic substrate which tends to interact strongly with micellar aggregates in aqueous solution. Moreover, it has an analogous structure to pesticides such as paraoxon or fenitron, both being toxic organophosphorous compounds that are widely used as pesticides in agriculture for field crop and fruit protection against a variety of insects and show considerable toxicity towards human and other mammals.[54] In the literature second order kinetic constants of the reaction occurring in the micellar phase and in the bulk water are reported to be very similar, consequently, we were only interested in the observed pseudo first order kinetic constant that shows the overall reaction rate acceleration.[53,54] The substitution reaction was conducted under pseudo-first order conditions where the oxime was used in 100-fold excess – an oxime concentration high enough to act as a buffer itself. Different possible reaction pathways have been reported for nucleophilic substitutions of organophosphorus compounds. In our case the only possible pathway is the attack of the nucleophile at the phosphorous centre, which follows a $S_N2(P)$ mechanism,[54] while the attack on the aromatic carbons is very unlikely.[53,55,56] In principle, two leaving groups are possible, either the favored *p*-nitrophenolate, whose formation can be observed at 402.5 nm or phenolate, which cannot be seen due to the spectral overlap with other components in the reaction mixture. We observed that the final absorbance reached during the kinetic runs did not correspond to the maximum theoretical one, suggesting the formation of a by-product. This was verified through ^{31}P experiments, where the formation of both *p*-nitrophenyl phenyl phosphate and diphenyl phosphate as by-products was observed, although the formation of the latter one was considerably slower. Eventually, rate constants for both the desired reaction and the by-product formation were calculated through the least-squares exponential fit of the experimental data: results reported here as observed reaction rates k_{obs} refer to the desired nucleophilic reaction only (see the ESI† for details).

In order to investigate the effect of our IL anions we initially investigated the reaction in all halide based ionic liquids $[C_{12}mim]X$ with X = Cl, Br and I in the concentration range from 0 to 100 mM. The observed reaction rates are shown in Fig. 3, and three interesting factors can be identified: in all cases a strong increase in the reaction rate was observed with increasing concentration of ionic liquids, resulting in strongly

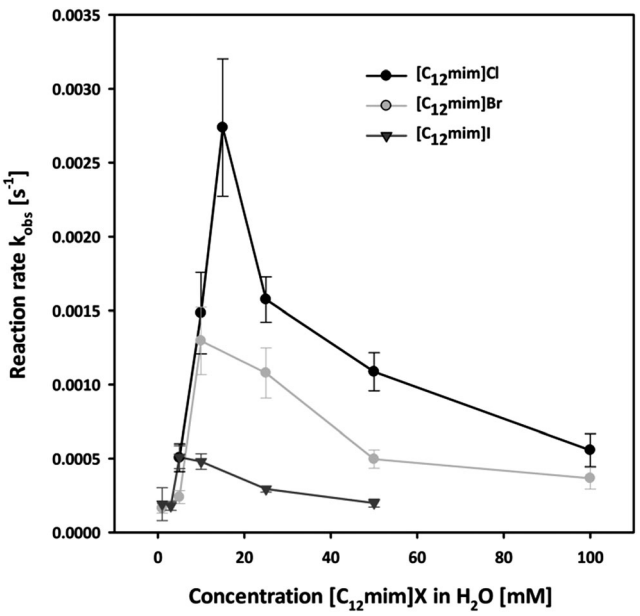

Fig. 3 Pseudo first order reaction rate constant of the nucleophilic substitution of nitrophenyl diphenyl phosphate (PNPDPP) with acetaldoxime as a function of $[C_{12}mim]X$ with X = Cl, Br and I in water.

enhanced reaction rates compared to pure water. This rate enhancement in the micellar medium arises from two effects: on the one side the lipophilic substrate accumulates in the micelles, and at the same time the electrostatic attraction of the cationic head groups to the negatively charged nucleophile leads to the increment of its concentration at the micellar interface where the reaction takes place.

Moreover, it can be observed that in all three cases the maximum acceleration for each ionic liquid corresponds to their CMC. Below the CMC the formation of aggregates induced by the presence of the solute causes the rate enhancement compared to water, while above the CMC most probably both a dilution effect over more micelles and a higher competition with the higher amount of inert anions take place. This effect is in accordance with the concept of micellar catalysis and has also been observed in our previous work on Diels–Alder reaction in surface-active ionic liquid/water mixtures.[14]

Most importantly, the highest enhancement of the reaction rate was observed with chloride-based ionic liquids, suggesting that the choice of anion plays a fundamental role. It has been reported that the presence of the inert anions influences the reaction rate due to a competition at the micellar interface with the reactive oximate.[53,57] As a consequence different rate enhancement will take place depending on the extent to which the inert anions are bound to the micellar surface.[50,58] The observed reaction rates are therefore in accordance with the physico-chemical data of the respective ionic liquid, as the chloride anion is less bound to the micellar surface and hence more readily exchangeable compared to bromide or iodide as it can also be seen from the β value calculated from the conductivity data.

This trend also exists when kinetic studies were extended to all surface-active ionic liquids involved in this study. Table 3 reports

 This journal is © the Owner Societies 2016

Published on 28 April 2016. Downloaded by TU Wien University Library on 13/06/2016 09:08:38.

Table 3 Comparison of pseudo first order reaction rate constant of the nucleophilic substitution of nitrophenyl diphenyl phosphate (PNPDPP) with acetaldoxime at the CMC of different surface-active ionic liquids

Ionic liquid	Concentration (mM)	Rate constant 10^3 k_{obs} (s^{-1})
$[C_{12}mim]Cl$ **1**	15	2.74 ± 0.46
$[C_{12}mim]Br$ **2**	10	1.30 ± 0.23
$[C_{12}mim]I$ **3**	5	0.51 ± 0.08
$[C_{12}mim]OMs$ **4**	15	1.68 ± 0.29
$[C_{12}mim]OTs$ **5**	3	0.42 ± 0.07
$[C_{12}mim]OTf$ **6**	2.5	0.18 ± 0.03
Water	—	0.08 ± 0.01

Kinetics experiments were done using UV-Visible spectroscopy on a Shimadzu UV1800 spectrometer at 25 °C. All kinetic runs were performed under pseudo first order conditions, the initial concentrations of PNPDPP and oxime in the cuvette were 2.3×10^{-5} M and 2.3×10^{-3} M respectively. The appearance of the product *p*-nitrophenolate was monitored at 402.5 nm.

the maximum rate constants for all ionic liquids $[C_{12}mim]X$ **1–6** at a concentration close to their respective CMC, as this should correspond to the highest rate constants.

The results reported in Table 2 show again the dependence between the CMC and the rate enhancement, as ionic liquids with lower CMC show poorer performance than those with higher CMC, due to the ability of the anion to exchange with the nucleophile. Moreover, the correlation between the degree of anion binding to the micelle and the reaction rate constants exists also in the sulfonate-based series with $[C_{12}mim]X$ **4–6**. The highest rate among these surface-active ionic liquids was observed for $[C_{12}mim]OMs$, indicating again that the careful choice of the surface-active ionic liquid can considerably affect the outcome of reactions. In fact, this suggests that it would be possible to govern the rate of a desired reaction by applying a definite micellar system with targeted surface-active ionic liquids, and various projects in this regard are currently investigated in our lab.

Experimental

Materials and methods

Commercially available reagents and solvents were used as received from Sigma Aldrich unless otherwise specified. Doubly-distilled deionized water was obtained from a Millipore Milli-Q water purification system (Millipore, USA). ^{1}H and ^{13}C NMR spectra were recorded on a Bruker AC 200 at 200 MHz, using the solvent peak as reference. *N*-Dodecylimidazole was synthesized according to a procedure already reported in the literature and distilled before use.[59] All ionic liquids were dried for at least 48 h at room temperature and 0.01 mbar before use and were stored under an argon atmosphere.

Synthetic procedures

Synthesis of $[C_{12}mim]X$, X = Cl^-, Br^-, I^-. The halide-based imidazolium salts were synthesized according to standard methodologies,[60] which include the alkylation of *N*-methylimidazole with the appropriate alkyl halide to afford the corresponding imidazolium halide. The ILs were repeatedly crystallized in order to obtain colorless solids.

1-Dodecyl-3-methylimidazolium chloride (1). After following the general procedure the product was recrystallized from THF and obtained in 92% yield. ^{1}H NMR (200 Hz, $CDCl_3$): δ (ppm) = 0.81 (3H, t, J = 6.36 Hz, $-C_{11}H_{22}-CH_3$), 1.18 (18H, m, $-C_2H_4-C_9H_{18}-CH_3$), 1.84 (2H, t, J = 6.26 Hz, $-CH_2-CH_2-C_{10}H_{21}$), 4.06 (3H, s, N–CH_3), 4.25 (2H, t, J = 7.35 Hz, $-CH_2-C_{11}H_{23}$), 7.29 (1H, s, –N–C*H*–CH–), 7.45 (1H, s, –N–C*H*–CH–), 10.54 (1H, s, –N–C*H*–N–). The data were in accordance with the literature.[61]

1-Dodecyl-3-methylimidazolium bromide (2). After following the general procedure the product was recrystallized from THF and obtained in 92% yield. ^{1}H NMR (200 Hz, $CDCl_3$): δ (ppm) = 0.81 (3H, t, J = 7.41 Hz, $-C_{11}H_{22}-CH_3$), 1.18 (18H, m, $-C_2H_4-C_9H_{18}-CH_3$), 1.85 (2H, t, J = 6.95 Hz, $-CH_2-CH_2-C_{10}H_{21}$), 4.07 (3H, s, N–CH_3), 4.25 (2H, t, J = 7.41 Hz, $-CH_2-C_{11}H_{23}$), 7.31 (1H, s, –N–C*H*–CH–), 7.46 (1H, s, –N–C*H*–CH–), 10.35 (1H, s, –N–C*H*–N–). The data were in accordance with the literature.[5]

1-Dodecyl-3-methylimidazolium iodide (3). After following the general procedure the product was crystallized from toluene and further washed with *n*-hexane and obtained in 95% yield. Mp: 39 °C. $C_{16}H_{31}IN_2$ (378.34): calcd C 50.79, H 8.26, N 7.40%; calcd (including 1.2 × H_2O) C 48.05, H 8.42, N 7.00% found C 48.08, H 8.06, N 6.90. ν_{max} (cm^{-1}): 3415 (O–H), 2916 (C–H), 1565(C═C), 1163 (C–N). ^{1}H NMR (200 Hz, $CDCl_3$): δ (ppm) = 0.82 (3H, m, $-C_{11}H_{22}-CH_3$), 1.19 (18H, m, $-C_2H_4-C_9H_{18}-CH_3$), 1.88 (2H, m, $-CH_2-CH_2-C_{10}H_{21}$), 4.08 (3H, s, N–CH_3), 4.27 (2H, t, J = 7.36 Hz, $-CH_2-C_{11}H_{23}$), 7.45 (1H, s, –N–C*H*–CH–), 7.59 (1H, s, –N–C*H*–CH–), 9.94 (1H, s, –N–C*H*–N–). ^{13}C NMR (200 Hz, $CDCl_3$): δ (ppm) = 136.59, 123.84, 122.18, 50.20, 37.07, 31.82, 30.23, 29.52 (2C), 29.44, 29.32, 29.25, 28.93, 26.18, 22.60, 14.06.

1-Dodecyl-3-methylimidazolium methanesulfonate (4). *N*-Dodecylimidazole (27.06 g, 30 mmol) was dissolved in 8 ml ethyl acetate, and a solution of methyl methanesulfonate (3.47 g, 31.5 mmol) in 8 ml ethyl acetate was added dropwise at RT. The reaction mixture was then stirred for 6 h at 50 °C. The product precipitated upon cooling and was recrystallized two more times to obtain the product in high purity. After removal of solvent traces under reduced pressure for at least 2 d at 0.01 mbar, 1-dodecyl-3-methylimidazolium methanesulfonate was obtained as a colorless powder in 83% yield. ^{1}H NMR (200 Hz, $CDCl_3$): δ (ppm) = 0.88 (3H, t, J = 6.17 Hz, $-C_{11}H_{22}-CH_3$), 1.25 (18H, m, $-C_2H_4-C_9H_{18}-CH_3$), 1.88 (2H, m, $-CH_2-CH_2-C_{10}H_{21}$), 2.83 (3H, s, –S–CH_3), 4.06 (3H, s, N–CH_3), 4.26 (2H, t, J = 7.33 Hz, $-CH_2-C_{11}H_{23}$), 7.21 (1H, s, –N–C*H*–CH–), 7.27 (1H, s, –N–C*H*–CH–), 10.10 (1H, s, –N–C*H*–N–). The data were in accordance with the literature.[32]

1-Dodecyl-3-methylimidazolium *p*-toluenesulfonate (5). *N*-Dodecylimidazole (2.85 g, 12 mmol) was dissolved in 8 ml ethyl acetate, and a solution of methyl *p*-toluenesulfonate (2.37 g, 12.6 mmol) in 8 ml ethyl acetate was added dropwise at RT. The reaction mixture was then stirred for 3 h at 50 °C. The product precipitated upon cooling and was recrystallized two more times to obtain the product in high purity. After removal of solvent traces under reduced pressure for at least 2 d at 0.01 mbar, 1-dodecyl-3-methylimidazolium *p*-toluenesulfonate was obtained as a colorless crystal in 85% yield. Mp: 97 °C. $C_{23}H_{38}N_2O_3S$ (422.63): calcd C 65.37, H 9.06, N 6.63%; found

Published on 28 April 2016. Downloaded by TU Wien University Library on 13/06/2016 09:08:38.

C 65.42, H 9.20, N 6.66. ν_{max} (cm^{-1}): 2919 (C–H), 1575 (C═C), 1498 (S═O), 1194 (Ar–C–C), 1034 (C–N). ^{1}H NMR (200 Hz, $CDCl_3$): δ (ppm) = 0.81 (3H, t, J = 12.8 Hz, –$C_{11}H_{22}$–CH_3), 1.16 (18H, m, –C_2H_4– C_9H_{18}–CH_3), 1.71 (2H, t, J = 6.55 Hz, –CH_2–CH_2–$C_{10}H_{21}$), 2.27 (3H, s, –C_6H_6–CH_3), 3.91 (3H, s, N–CH_3), 4.09 (2H, t, J = 14.87 Hz, –CH_2–$C_{11}H_{23}$), 7.07 (2H, d, J = 7.98 Hz, aromatic proton), 7.18 (1H, s, –N–C*H*–CH–), 7.32 (1H, s, –N–C*H*–CH–), 7.71 (2H, d, J = 8.12 Hz, aromatic proton), 9.78 (1H, s, –N–C*H*–N–). ^{13}C NMR (50 Hz, $CDCl_3$): δ (ppm) = 143.91, 139.25, 137.6, 137.44, 128.60, 125.73, 123.79, 122.01, 49.74, 36.15, 31.83, 30.87, 30.14, 29.55–29.48 (3C), 29.34–29.27 (2C), 28.93, 26.13, 22.61, 21.21, 14.06.

1-Dodecyl-3-methylimidazolium trifluoromethane sulfonate (6). *N*-Dodecylimidazole (5.16 g, 21.8 mmol) was dissolved in 25 ml anhydrous DCM in argon and freshly distilled methyl trifluoromethane sulfonate (4.3 g, 3 ml, 26.2 mmol) was added dropwise while cooling in an ice bath. The reaction mixture was then stirred for 3 h at RT until NMR showed complete conversion. The volatile materials were removed under reduced pressure, and the product was repeatedly washed with *n*-hexane. 1-Dodecyl-3-methylimidazolium trifluoromethane sulfonate was obtained *via* filtration as a pale solid in 97% yield. ^{1}NMR ($CDCl_3$): δ (ppm) = 0.87 (3H, t, J = 6.36 Hz, –$C_{11}H_{22}$–CH_3), 1.25 (18H, m, –C_2H_4–C_9H_{18}–CH_3), 1.87 (2H, br, –CH_2–CH_2–$C_{10}H_{21}$), 3.98 (3H, s, N–CH_3), 4.18 (2H, t, J = 7.24 Hz, –CH_2–$C_{11}H_{23}$), 7.31 (1H, s, –N–C*H*–CH–), 7.38 (1H, s, –N–C*H*–CH–), 9.13 (1H, s, –N–C*H*–N–). The data were in accordance with the literature.[62]

Characterization of surface-activity

Solutions at various concentrations of the ionic liquids were prepared with doubly-distilled Millipore Milli-Q water and left under shaking at 360 min^{-1} for 24 h at RT to equilibrate.

Conductivity measurements. The samples were previously equilibrated at (25 ± 0.1) °C in a HAAKE K15 thermostat, then conductivity measurements were performed on a Mettler Toledo Seven Excellence system, equipped with an InLAB® 741-ISM electrode (cell constant k = 0.105). The conductometer was calibrated with a standard KCl solution and two independent measurements were performed. The CMC was calculated as the intersection point of the two linear regimes in the conductivity/concentration graph. The degree of counter ion binding was calculated using the following equation $\beta = 1 - \alpha$, where α is the degree of ionization and corresponds to the ratio of the slopes between the two linear fragments of the conductivity curves.

Surface tension measurements. Surface tension was determined using the Du Noüy ring method on a Krüss manual tensiometer K6 at RT. Each measurement was repeated 5 times.

UV-Vis measurements. For the UV-Vis measurements a stock solution of benzoylacetone (31 mM) in 1,4-dioxane was prepared, which was used to prepare a diluted solution in water (0.5 mM). For UV-Vis measurements 0.2 ml of benzoylacetone solution in water were added to the ionic liquid solution to obtain a final volume of 1.5 ml. These solutions were equilibrated at 25 °C for at least 1 h, and then transferred to the cuvette for measurement. The final concentration of benzoylacetone in the cuvette was 0.07 mM, while the reference cuvette contained all reagents except for benzoylacetone.

Small angle X-ray scattering. Small-angle scattering experiments were performed using a Bruker Nanostar (Bruker AXS), equipped with a microfocus X-ray source (Incoatec IμS High Brilliance) with CuKα radiation with a wavelength of 0.1542 nm and a 2D-position sensitive detector (Vantec 2000). The scattering patterns were recorded for 2 hours. The data were azimuthally integrated and corrected for background scattering resulting in scattering intensities $I(q)$ depending on the scattering vector $q = (4\pi/\lambda)\sin\theta$ in the range from q = 0.1 to 20 nm^{-1}, with 2θ being the scattering angle. In the figures, only the range up to q = 5 nm^{-1} is shown for clarity.

Micellar catalysis. 4-Nitrophenyl diphenyl phosphate (PNPDPP) was synthesized according to an already reported procedure[63] and crystallized from ethanol. Due to its low solubility in water a stock solution in acetonitrile was prepared (11.5×10^{-3} M). In parallel, a stock buffer solution of acetaldehydeoxime (552×10^{-3} M) in water was prepared by using a NaOH solution as solvent in order to obtain a NaOH : oxime ratio of 1 : 2.

Kinetic measurements. Kinetics experiments were performed by UV-Visible spectroscopy using a Shimadzu UV1800 spectrometer equipped with a thermostate at 25 °C. All kinetic runs were performed under pseudo first order conditions in which the concentration of the oxime was at least 100 times greater than the initial concentration $[PNPDPP]_0$. Reaction mixtures were always freshly prepared by first mixing the 2.4 ml ionic liquid solution with 10 μl oxime stock solutions. The kinetic run was then started by adding 2 μl of the PNPDPP stock solution to 1 ml of ionic liquid–oxime solution in a quartz cuvette. The initial concentrations of PNPDPP and oxime in the cuvette were 2.3×10^{-5} M and 2.3×10^{-3} M respectively. The formation of the product *p*-nitrophenolate NP was monitored at a fixed wavelength of 402.5 nm. Generally each reaction was followed until no change in the final absorbance was observed anymore. The rate constants for both the desired reaction, and the by-product formation, were calculated through least-squares exponential fitting, the system was assimilated in the case of parallel reactions. The following formula afforded the rate constants for the formation of product *p*-nitrophenolate NP:

$$[\mathrm{NP}](t) = [\mathrm{PNPDPP}]_0 \frac{k_{\mathrm{obs}}}{k' + k_{\mathrm{obs}}}\left(1 - \mathrm{e}^{-(k'+k_{\mathrm{obs}})t}\right)$$

The reported values are an average of at least 3 runs. The values of the rate constant of the parallel reaction k' were always at least one order of magnitude smaller than k_{obs}.

Theoretical final absorbance. The theoretical final absorbance values for the reaction between PNPDPP and the oxime were measured by injecting 2 μl of an acetonitrile solution of *p*-nitrophenol (11.5×10^{-3} M, equivalent to the PNPDPP in the kinetic study) in 1 ml of the corresponding IL–oxime solution. Each value was taken two times.

^{31}P NMR measurements. Samples in DMSO–water [10 : 90 (w/w)] were measured containing either the starting material or the reaction mixture. The peaks were referred to a capillary with

 This journal is © the Owner Societies 2016

Published on 28 April 2016. Downloaded by TU Wien University Library on 13/06/2016 09:08:38.

H_3PO_4 as external standard. The obtained chemical shifts are in good agreement with those reported in the literature, and no other products were identified.

Conclusions

We have reported a study on the counterion role in surface-active ionic liquids based on 1-dodecyl-3-methylimidazolium. The two investigated series based on halides and sulfonate anions show a correlation between the tendency of the anions to reside closer to the micellar interface and their surface activity. These properties were reflected also when the surface-active ionic liquids were implied in micellar catalysis, in fact, a different rate acceleration was obtained using the different ionic liquids in nucleophilic substitutions in micellar media.

Acknowledgements

Financial support from the Austrian Science Fund (FWF project P25504-N28) is gratefully acknowledged.

Notes and references

1 Y. Kohno and H. Ohno, *Chem. Commun.*, 2012, **48**, 7119.
2 S. Chen, S. Zhang, X. Liu, J. Wang, J. Wang, K. Dong, J. Sun and B. Xu, *Phys. Chem. Chem. Phys.*, 2014, **16**, 5893.
3 J. Łuczak, J. Hupka, J. Thöming and C. Jungnickel, *Colloids Surf., A*, 2008, **329**, 125.
4 M. Blesic, M. H. Marques, N. V. Plechkova, K. R. Seddon, L. P. N. Rebelo and A. Lopes, *Green Chem.*, 2007, **9**, 481.
5 A. Cornellas, L. Perez, F. Comelles, I. Ribosa, A. Manresa and M. T. Garcia, *J. Colloid Interface Sci.*, 2011, **355**, 164.
6 O. A. El Seoud, P. A. R. Pires, T. Abdel-Moghny and E. L. Bastos, *J. Colloid Interface Sci.*, 2007, **313**, 296.
7 J. Sirieix-Plénet, *Talanta*, 2004, **63**, 979–986.
8 J. Bowers, C. P. Butts, P. J. Martin, M. C. Vergara-Gutierrez and R. K. Heenan, *Langmuir*, 2004, **20**, 2191.
9 I. Goodchild, L. Collier, S. L. Millar, I. Prokeš, J. C. D. Lord, C. P. Butts, J. Bowers, J. R. P. Webster and R. K. Heenan, *J. Colloid Interface Sci.*, 2007, **307**, 455.
10 Z. Miskolczy, K. Sebők-Nagy, L. Biczók and S. Göktürk, *Chem. Phys. Lett.*, 2004, **400**, 296.
11 M. Tariq, M. G. Freire, B. Saramago, J. A. P. Coutinho, J. N. C. Lopes and L. P. N. Rebelo, *Chem. Soc. Rev.*, 2012, **41**, 829.
12 K. R. Seddon, A. Stark and M.-J. Torres, *Pure Appl. Chem.*, 2000, **72**, 2275.
13 A. K. Ressmann, R. Zirbs, M. Pressler, P. Gaertner and K. Bica, *Z. Naturforsch., B: J. Chem. Sci.*, 2013, **68b**, 1129.
14 K. Bica, P. Gärtner, P. J. Gritsch, A. K. Ressmann, C. Schröder and R. Zirbs, *Chem. Commun.*, 2012, **48**, 5013.
15 T. Inoue, H. Ebina, B. Dong and L. Zheng, *J. Colloid Interface Sci.*, 2007, **314**, 236.
16 J. Łuczak, C. Jungnickel, M. Joskowska, J. Thöming and J. Hupka, *J. Colloid Interface Sci.*, 2009, **336**, 111.
17 C. Jungnickel, J. Łuczak, J. Ranke, J. F. Fernández, A. Müller and J. Thöming, *Colloids Surf., A*, 2008, **316**, 278.
18 G. Bai, A. Lopes and M. Bastos, *J. Chem. Thermodyn.*, 2008, **40**, 1509.
19 R. Vanyúr, L. Biczók and Z. Miskolczy, *Colloids Surf., A*, 2007, **299**, 256.
20 P. D. T. Huibers, *Langmuir*, 1999, **15**, 7546.
21 M. Blesic, A. Lopes, E. Melo, Z. Petrovski, N. V. Plechkova, J. N. Canongia Lopes, K. R. Seddon and L. P. N. Rebelo, *J. Phys. Chem. B*, 2008, **112**, 8645.
22 M. T. Garcia, I. Ribosa, L. Perez, A. Manresa and F. Comelles, *Colloids Surf., B*, 2014, **123**, 318.
23 M. T. Garcia, I. Ribosa, L. Perez, A. Manresa and F. Comelles, *Langmuir*, 2013, **29**, 2536.
24 N. I. Malek, Z. S. Vaid, U. U. More and O. A. El Seoud, *Colloid Polym. Sci.*, 2015, **293**, 3213.
25 Q. Q. Baltazar, J. Chandawalla, K. Sawyer and J. L. Anderson, *Colloids Surf., A*, 2007, **302**, 150.
26 O. Nacham, A. Martín-Pérez, D. J. Steyer, M. J. Trujillo-Rodríguez, J. L. Anderson, V. Pino and A. M. Afonso, *Colloids Surf., A*, 2015, **469**, 224.
27 M. Ao and D. Kim, *J. Chem. Eng. Data*, 2013, **58**, 1529.
28 C. P. Frizzo, C. R. Bender, I. M. Gindri, P. R. S. Salbego, M. A. Villetti and M. A. P. Martins, *Colloid Polym. Sci.*, 2015, **293**, 2901.
29 J. Nowicki, J. Łuczak and D. Stańczyk, *RSC Adv.*, 2016, **6**, 11591.
30 C. Tourné-Péteilh, J.-M. Devoisselle, A. Vioux, P. Judeinstein, M. In and L. Viau, *Phys. Chem. Chem. Phys.*, 2011, **13**, 15523.
31 A. Heintz, J. K. Lehmann, S. A. Kozlova, E. V. Balantseva, A. B. Bazyleva and D. Ondo, *Fluid Phase Equilib.*, 2010, **294**, 187.
32 M. Blesic, M. Swadźba-Kwaśny, J. D. Holbrey, J. N. Canongia Lopes, K. R. Seddon and L. P. N. Rebelo, *Phys. Chem. Chem. Phys.*, 2009, **11**, 4260.
33 M. Blesic, M. Swadźba-Kwaśny, T. Belhocine, H. Q. N. Gunaratne, J. N. C. Lopes, M. F. C. Gomes, A. A. H. Pádua, K. R. Seddon and L. P. N. Rebelo, *Phys. Chem. Chem. Phys.*, 2009, **11**, 8939.
34 M. Anouti, J. Jones, A. Boisset, J. Jacquemin, M. Caillon-Caravanier and D. Lemordant, *J. Colloid Interface Sci.*, 2009, **340**, 104.
35 M. Anouti, P.-Y. Sizaret, C. Ghimbeu, H. Galiano and D. Lemordant, *Colloids Surf., A*, 2012, **395**, 190.
36 A. B. Pereiro, J. M. M. Araújo, F. S. Teixeira, I. M. Marrucho, M. M. Piñeiro and L. P. N. Rebelo, *Langmuir*, 2015, **31**, 1283.
37 F. S. Teixeira, N. S. M. Vieira, O. A. Cortes, J. M. M. Araújo, I. M. Marrucho, L. P. N. Rebelo and A. B. Pereiro, *J. Chem. Thermodyn.*, 2015, **82**, 99.
38 J. Łuczak, M. Markiewicz, J. Thöming, J. Hupka and C. Jungnickel, *J. Colloid Interface Sci.*, 2011, **362**, 415.
39 R. Zana, *Langmuir*, 1996, **12**, 1208.
40 M. J. Rosen and J. T. Kunjappu, *Surfactants and interfacial phenomena*, John Wiley & Sons, 4th edn, 2012.
41 J. N. Israelachvili, *Intermolecular and Surface Forces*, Elsevier, 2011, p. 535.

Published on 28 April 2016. Downloaded by TU Wien University Library on 13/06/2016 09:08:38.

42 C. Tanford, *J. Phys. Chem.*, 1972, **76**, 3020.
43 E. Iglesias, *J. Phys. Chem.*, 1996, **100**, 12592.
44 A. Dominguez, A. Fernandez, N. Gonzalez, E. Iglesias and L. Montenegro, *J. Chem. Educ.*, 1997, **74**, 1227.
45 P. Bartlett and R. H. Ottewill, *J. Chem. Phys.*, 1992, **96**, 3306.
46 G. La Sorella, G. Strukul and A. Scarso, *Green Chem.*, 2015, **17**, 644.
47 B. H. Lipshutz and S. Ghorai, *Green Chem.*, 2014, **16**, 3660.
48 T. Dwars, E. Paetzold and G. Oehme, *Angew. Chem., Int. Ed.*, 2005, **44**, 7174.
49 J. Łuczak, C. Jungnickel, M. Markiewicz and J. Hupka, *J. Phys. Chem. B*, 2013, **117**, 5653.
50 C. A. Bunton and L. Robinson, *J. Org. Chem.*, 1969, **34**, 773.
51 S. Couderc and J. Toullec, *Langmuir*, 2001, **17**, 3819.
52 F. Terrier, P. Rodriguez-Dafonte, E. Le Guével and G. Moutiers, *Org. Biomol. Chem.*, 2006, **4**, 4352.
53 V. K. Balakrishnan, X. Han, G. W. VanLoon, J. M. Dust, J. Toullec and E. Buncel, *Langmuir*, 2004, **20**, 6586.
54 X. Han, V. K. Balakrishnan, G. W. vanLoon and E. Buncel, *Langmuir*, 2006, **22**, 9009.
55 J. E. Omakor, I. Onyido, G. W. vanLoon and E. Buncel, *J. Chem. Soc., Perkin Trans. 2*, 2001, 324.
56 B. A. Burnside, L. L. Szafraniec, B. L. Knier, H. D. Durst, R. A. Mackay and F. R. Longo, *J. Org. Chem.*, 1988, **53**, 2009.
57 C. A. Bunton, F. Nome, F. H. Quina and L. S. Romsted, *Acc. Chem. Res.*, 1991, **24**, 357.
58 N. Ouarti, A. Marques, I. Blagoeva and M.-F. Ruasse, *Langmuir*, 2000, **16**, 2157.
59 B. S. Souza, E. C. Leopoldino, D. W. Tondo, J. Dupont and F. Nome, *Langmuir*, 2012, **28**, 833.
60 B. F. Gilmore, G. P. Andrews, G. Borberly, M. J. Earle, M. A. Gilea, S. P. Gorman, A. F. Lowry, M. McLaughlin and K. R. Seddon, *New J. Chem.*, 2013, **37**, 873.
61 A. E. Bradley, C. Hardacre, J. D. Holbrey, S. Johnston, S. E. J. McMath and M. Nieuwenhuyzen, *Chem. Mater.*, 2002, **14**, 629.
62 A. E. Bradley, C. Hardacre, J. D. Holbrey, S. Johnston, S. E. J. McMath and M. Nieuwenhuyzen, *Chem. Mater.*, 2002, **14**, 629.
63 S. Jones and D. Selitsianos, *Org. Lett.*, 2002, **4**, 3671.

 This journal is © the Owner Societies 2016

G Model
COLSUA-21326; No. of Pages 9
ARTICLE IN PRESS
Colloids and Surfaces A: Physicochem. Eng. Aspects xxx (2017) xxx–xxx
Contents lists available at ScienceDirect
Colloids and Surfaces A: Physicochemical and Engineering Aspects
journal homepage: www.elsevier.com/locate/colsurfa

Thermodynamic study for micellization of imidazolium based surface active ionic liquids in water: Effect of alkyl chain length and anions

Bojan Šarac[a], Žiga Medoš[a], Alice Cognigni[b], Katharina Bica[b,*], Li-Jen Chen[c], Marija Bešter-Rogač[a,*]

[a] Faculty of Chemistry and Chemical Technology, University of Ljubljana, Večna pot 113, SI-1000 Ljubljana, Slovenia
[b] Institute of Applied Synthetic Chemistry, Vienna University of Technology, Getreidemarkt 9/163, A-1060 Vienna, Austria
[c] Department of Chemical Engineering, National Taiwan University, Taipei 10617, Taiwan

HIGHLIGHTS

- Micellization process in water has been investigated on imidazolium based SAILs.
- The influence of counter-ion is studied.
- The standard thermodynamic parameters of micellization process are derived.
- Entropy-enthalpy compensation effect is discussed.
- Heat capacity change is linked to the solvent accessible surface area.

GRAPHICAL ABSTRACT

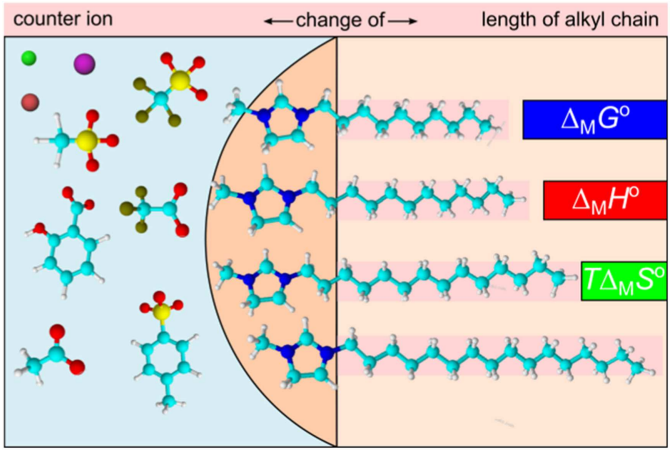

ARTICLE INFO

Article history:
Received 5 November 2016
Received in revised form 7 January 2017
Accepted 22 January 2017
Available online xxx

Keywords:
Surface active imidazolium based ionic liquids
Micellization
Isothermal titration calorimetry
Thermodynamic study
Solvent accessible surface area

ABSTRACT

A systematic investigation of influence of the length of the side alkyl chain and the counter-ions on the thermodynamics of the micellization process at imidazolium based surface active ionic liquids (SAILs) in aqueous solutions was carried out by isothermal titration calorimetry (ITC) in a broad temperature range.

The effect of alkyl chain length on the micellization process in water has been investigated on 1-decyl-3-methylimidazolium ([C_{10}mim]Cl), 1-dodecyl-3-methylimidazolium ([C_{12}mim]Cl), 1-tetradecyl-3-methylimidazolium ([C_{14}mim]Cl) and 1-hexadecyl-3-methylimidazolium ([C_{16}mim]Cl) chlorides, whereas the influence of counter-ion was studied at the micellization of 1-dodecyl-3-methylimidazolium chloride ([C_{12}mim]Cl), bromide ([C_{12}mim]Br), iodide ([C_{12}mim]I), acetate ([C_{12}mim]OAc), methanesulfonate ([C_{12}mim]OMs), toluen sulfonate (([C_{12}mim]OTs), trifluromethane sulfonate ([C_{12}mim]OTf), trifluoro acetate (([C_{12}mim]TFA) and salicylate ([C_{12}mim]Sal) in water.

From ITC experimental data, the corresponding standard thermodynamic parameters of micellization (enthalpy, $\Delta_M H^0$; Gibbs free energy, $\Delta_M G^0$; entropy, $\Delta_M S^0$; heat capacity change, $\Delta_M c_p^0$) were estimated by help of the mass-action model. It was found that SAILs behave mainly like common cationic surfactants, where cmc values are decreasing with the length of the side alkyl chain and exhibit U-shape dependence

* Corresponding authors.
E-mail addresses: katharina.schroeder@tuwien.ac.at (K. Bica), marija.bester@fkkt.uni-lj.si (M. Bešter-Rogač).

http://dx.doi.org/10.1016/j.colsurfa.2017.01.062
0927-7757/© 2017 Elsevier B.V. All rights reserved.

Please cite this article in press as: B. Šarac, et al., Thermodynamic study for micellization of imidazolium based surface active ionic liquids in water: Effect of alkyl chain length and anions, Colloids Surf. A: Physicochem. Eng. Aspects (2017), http://dx.doi.org/10.1016/j.colsurfa.2017.01.062

on temperature. Remarkable influence of counter-ions on cmc and all thermodynamic functions was observed, however the entropy-enthalpy compensation turned out as a matter of fact, arising from the relationship $\Delta G = \Delta H - T\Delta S$. $\Delta_M c_p^0$ values were further discussed in terms of the removal of solvent accessible surface areas of SAILs and counter-ion from the contact with water after micellization.
© 2017 Elsevier B.V. All rights reserved.

1. Introduction

Ionic liquids have recently attracted much attention as new class of surfactants. It has in fact been demonstrated that ionic liquids containing long alkyl chains behave similar to conventional surfactants forming aggregates in water [1]. Several structures have been investigated changing alkyl chain length, charged head group structure, functional groups, both cationic and anionic surface active ionic liquids have been described [2,3,4,5–7,8]. An attractive factor for continuous research in this field is that these ionic liquids have generally been found to have a superior surface activity in comparison to corresponding alkyltrimethylammonium based surfactants, or corresponding anionic surfactants with inorganic cations [9]. Moreover, the high tunability of ionic liquids opens up a broad range of applications for surface active ionic liquids (SAILs), such as in micellar catalysis or in separation processes [10–12].

There are already some studies dealing with thermodynamic properties of imidazolium-based SAILs in the literature [13–15] investigating quite narrow selections of anions (Cl^-, Br^-).

Thus, we decided to carry out a systematic thermodynamic investigation of influence of the length of the side alkyl chain and the counter-ions on the micellization process of imidazolium based SAILs in aqueous solution by isothermal titration calorimetry (ITC) as one of the most valuable techniques for thermodynamic analysis.

ITC experiments were performed within the temperature range of 278.15–318.15 K in 10 K steps on 1-decyl-3-methylimidazolium ([C_{10}mim]Cl), 1-dodecyl-3-methylimidazolium ([C_{12}mim]Cl), 1-tetradecyl-3-methylimidazolium ([C_{14}mim]Cl) and 1-hexadecyl-3-methylimidazolium ([C_{16}mim]Cl) chlorides. To obtain more information about the influence of counter-ion on the micellization, measurements were carried out also for 1-dodecyl-3-methylimidazolium bromide ([C_{12}mim]Br), iodide([C_{12}mim]I), acetate ([C_{12}mim]OAc), methanesulfonate ([C_{12}mim]OMs), toluensulfonate (tosylate, [C_{12}mim]OTs), trifluromethane sulfonate ([C_{12}mim]OTf), trifluoro acetate ([C_{12}mim]TFA) and salicylate ([C_{12}mim]Sal). The structures of investigated SAILs and anions are presented on Scheme 1. The corresponding standard thermodynamic parameters of micellization (enthalpy, $\Delta_M H^0$; Gibbs free energy, $\Delta_M G^0$; entropy, $\Delta_M S^0$; heat capacity change, $\Delta_M c_p^0$) were estimated by fitting of the model function based on the mass-action model to the experimental data. Enthalpy-Entropy Compensation (EEC) effect was discussed in terms of the side alkyl chain length and the effect of counter-ions on EEC was presented. In addition, $\Delta_M c_p^0$ was further correlated to the changes in solvent accessible surface upon micelle formation.

2. Experimental section

2.1. Materials

Commercially available reagents and solvents were used as received from Sigma Aldrich unless otherwise specified. Deionized water was obtained from a Millipore Milli-Q water purification system (Millipore, USA). ^{1}H and ^{13}C NMR spectra were recorded on a Bruker AC 200 at 200 MHz, using the solvent peak as reference. All ionic liquids were dried for at least 48 h at room temperature and 0.01 mbar before use and were stored under argon atmosphere.

2.2. Synthetic procedures

2.2.1. Synthesis of [C_{12}mim]X, X = Cl^-, Br^-, I^-

The halide-based imidazolium salts were synthesized according to standard methodologies, which include the alkylation of N-methylimidazole with the appropriate alkyl halide to afford the corresponding imidazolium halide. The ILs were repeatedly crystallized in order to obtain colorless solids. Detailed results are reported in our previous work [12].

2.2.2. Synthesis of C_{12}mim]X, X = OMs^-, OTs^-, OTf^-, TFA^-

Surface-active ionic liquids [C_{12}mim]OMs, [C_{12}mim]OTs, [C_{12}mim]OTf and [C_{12}mim]TFA were prepared in a two steps synthesis route, including the initial synthesis of *N*-dodecylimidazole by alkylation of imidazole. Afterwards the final ionic liquids were obtained via direct alkylation of *N*-dodecylimidazole with the methyl esters of the corresponding anions. Detailed results are reported in our previous work [12].

2.2.3. Synthesis of [C_{12}mim]TFA

N-dodecylimidazole (1.31 g, 5.5 mmol) was dissolved in 5 mL anhydrous acetonitrile and freshly distilled methyl trifluoroacetic acid (4.8 g, 3.8 mL, 38 mmol) was added drop wise while cooling in an ice bath. The reaction mixture was then stirred for 7 days at 70 °C until NMR showed complete conversion. The volatile materials were removed under reduced pressure, and the product was repeatedly washed with *n*-hexane. 1-Dodecyl-3-methylimidazolium trifluoroacetate was obtained via filtration as pale solid in 98% yield. mp: 37.3 °C. $C_{18}H_{31}F_3N_2O_2$ (464.45): calcd. C 59.32, H 8.57, N 7.69%; found C 59.13, H 8.69, N 7.59. ν_{max} (cm^{-1}): 2918 (C—H), 1679 (CO_2^-), 1578 (C=C), 1159 (C—N), 1115 (C—F). ^{1}H NMR (200 MHz, $CDCl_3$): δ(ppm) = 0.81 (3H, t, *J* = 6.06 Hz, $-C_{11}H_{22}-CH_3$), 1.19 (18H,m, $-C_2H_4-C_9H_{18}-CH_3$), 1.80 (2H, br, $-CH_2-CH_2-C_{10}H_{21}$), 3.94 (3H, s, $N-CH_3$), 4.15 (2H, t, *J* = 7.34 Hz, $-CH_2-C_{11}H_{23}$), 7.33 (1H, s, —N—CH=CH—), 7.41 (1H, s, —N—CH—CH), 9.90 (1H, s, —N—CH—N—). ^{13}C NMR (100 Hz, $CDCl_3$): δ (ppm) = 160.93 (q, *J* = 34.16 Hz), 137.79, 125.64, 123.55, 116.86 (q, *J* = 294.37 Hz), 49.96, 36.11, 31.80, 30.10, 29.48 (2C), 29.38, 29.23 (2C), 28.83, 26.07, 22.58, 14.01.

2.2.4. Synthesis of [C_{12}mim]Sal and [C_{12}mim]OAc

Both ionic liquids were prepared adapting a procedure from Ferguson et al. [16] which includes the neutralization of the corresponding hydroxide ionic liquid with the desired acid as counter-ion.

General procedure: [C_{12}mim]Cl (1 equivalent) was slowly mixed with 1 equivalent of concentrated sulfuric acid in a round bottom flask. The round-bottomed flask was fitted with a stopcock, the other end of which was connected to an open tube packed with NaOH pellets. The flask was heated up to 90 °C and stirred for 2 h, after which the open end of the NaOH packed tube was connected to a small diaphragm pump. The mixture was left overnight under vacuum at 90 °C. The obtained [C_{12}mim][HSO_4] was dissolved in hot deionized water (95–100 °C, 25 mL) and slowly added to a solution

Please cite this article in press as: B. Šarac, et al., Thermodynamic study for micellization of imidazolium based surface active ionic liquids in water: Effect of alkyl chain length and anions, Colloids Surf. A: Physicochem. Eng. Aspects (2017), http://dx.doi.org/10.1016/j.colsurfa.2017.01.062

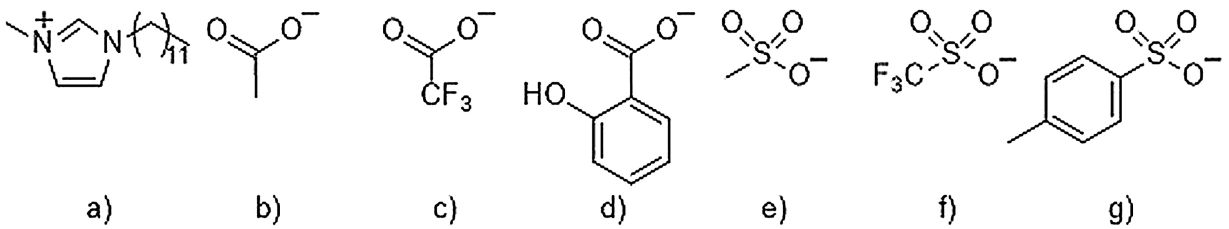

Scheme 1. Structures of investigated systems: a) n = 9 ([C_{10}mim]), n = 11 ([C_{12}mim]), n = 13 ([C_{14}mim]) and n = 15 ([C_{16}mim]) cations in ([$C_X$mim]Cl) and b) OAc, c) TFA, d) Sal, e) OMs, f) OTf, and g) OTs anions in [C_{12}mim]X systems.

of barium hydroxide octahydrate dissolved in hot deionized water (95–100 °C, 55 mL). The cloudy reaction mixture was stirred, and allowed to cool to room temperature, then refrigerated. The white solid precipitate was removed via vacuum filtration (P4 glass sintered funnel with a 0.5 cm celite layer), washed with water (ca. 20 °C, 50 mL), and discarded. The highly basic hydroxide solution generated from the procedure was then diluted to 250 mL in a volumetric flask. From this 3 mL were taken, diluted with ca. 50 mL of water and titrated with HCl 0.05 M followed by pH meter. From the equivalence point the required amount of the desired acid was calculated and added to the volumetric flask. Water was removed via lyophilisation, and the obtained product was dried at high vacuum (0.01 mbar) overnight. The crude product was re-dissolved in anhydrous DCM (100 mL), filtered, and the solvent was removed via evaporation. Remaining traces of volatiles were removed under high vacuum (0.01 mbar) overnight.

Following the general procedure [C_{12}mim]OAc was obtained as off-white solid in 83% yield. $C_{18}H_{34}N_2O_2$ (310.48): calculated C 69.63, H 11.04, N 9.02%; calculated (including 0.5 x H_2O) C 67.67, H 11.04, 8.77%; found C 67.52, H 11.56, N 9.03. ν_{max} (cm^{-1}): 2922 (C—H), 1666 (CO_2^-) 1578 (C=C), 1176 (C—N). ^{1}H NMR ($CDCl_3$): δ (ppm) = 0.81 (3H, br, —$C_{11}H_{22}$—CH_3), 1.18 (18H, m, —C_2H_4— C_9H_{18}—CH_3), 1.80 (2H, br, –CH_2—CH_2—$C_{10}H_{21}$), 1.91 (2H, s, CH_3COO), 3.99 (3H, s, N—CH_3), 4.21 (2H, t, J = 4.21 Hz, —CH_2—$C_{11}H_{23}$), 7.14 (1H, s, —N—CH=CH—), 7.23 (1H, s, —N=CH—CH), 10.91 (1H, s, –N—CH—N—). ^{13}C NMR (200 Hz, $CDCl_3$): δ (ppm) = 177.54, 139.36, 123.12, 121.32, 49.79, 36.20, 31.79, 30.22, 29.49 (3C), 29.41, 29.28, 29.22, 28.93, 26.17, 24.96, 22.57, 14.02,

Following the general procedure [C_{12}mim]Sal was obtained as a yellow pale very viscous liquid in 63% yield. $C_{23}H_{36}N_2O_3$ (388.55): calculated C 71.10, H 9.34, N 7.21%; calculated (including 0.1 x H_2O) C 70.77, H 9.35, N 7.18%; found C 70.70, H 10.28, N 7.23%, Cl 150 ppm ν_{max} (cm^{-1}): 3394 (O—H), 2923 (C—H), 1575 (COO^-), 1455 (C=C), 1385(Ar—C—C), 1169 (C—N). ^{1}NMR (200 MHz, $CDCl_3$): δ (ppm) = 0.81 (3H, t, J = 6.26 Hz, —$C_{11}H_{22}$—CH_3), 1.16 (18H,m, —C_2H_4— C_9H_{18}—CH_3), 1.75 (2H, br, —CH_2—CH_2—$C_{10}H_{21}$), 3.94 (3H, s, N—CH_3), 4.12 (2H, t, J = 7.38 Hz, —CH_2—$C_{11}H_{23}$), 6.63-6.78 (2H, m, Ar), 7.03–7.20 (3H, m, Ar), 7.86 (1H, d, J = 6.30, —N—CH—CH—), 10.52 (1H, s, —N—CH—N). ^{13}δ (ppm) = 174.08, 162.15, 138.17, 132.24, 130.46, 123.14, 121.52, 119.83, 117.33, 116.23, 49.99, 36.30, 31.89, 30.15, 29.58 (2C), 29.47, 29.33 (2C), 28.93, 26.20, 22.67, 14.11

2.3. Conductivity measurements

The samples were previously equilibrated at (25.0 ± 0.1) °C in a HAAKE K15 thermostat, then conductivity measurement were performed using a Mettler Toledo Seven Excellence system, equipped with a InLAB® 741-ISM electrode (cell constant κ = 0.105 cm^{-1}, determined with a standard KCl solution). The sample was stirred before measurement to ensure homogeneous mixing. The plot of electrical conductivity versus surfactant concentration, typically consists of a two distinct linear regions. Critical micelle concentration (cmc) values were calculated as the intersection point of these two linear regimes in the conductivity/concentration graph and the degree of micelle ionization, β (=z/n, where z is the effective charge of the micelles and n is the number of surfactant monomer in the micellar aggregate) was estimated from the ratio of slopes [17].

2.4. Surface tension measurements

Surface tension was determined with the Du Noüy ring method on a Krüss manual tensiometer K6 at room temperature. Each measurement was repeated five times, considering the arithmetic mean of the results with a relative standard deviation less than 0.5%.

2.5. Viscosity determination

The viscosity of solutions was determined by using a micro Ostwald viscometer (SI Analytics GmbH, Mainz, Germany, type and capillary no. 516 10/I) and an automatic flow time measuring system ViscoSystem® AVS 370. The procedure is described in detail in literature [18].

2.6. Isothermal titration calorimetry (ITC)

The heat changes upon micellization were measured using a VP-ITC microcalorimeter from MicroCal, LLC (Northampton, MA, USA). Periodical calibration of the instrument has been proposed electrically by administering a known quantity of power through a resistive heater element located on the cell [19]. The precision of instrument has been also validated through binding of the cytidine 2′-monophosphate to the ribonuclease A active site. The standard chemical reaction is described elsewhere [20]. Degassed water in the titration cell was titrated with the degassed surfactant solution in the corresponding solvent from a 0.300 mL syringe at temperatures between 278.15 and 318.15 K. Successive aliquots of surfactant solution were added into the calorimeter cell (V = 1.386 mL) under constant stirring through a motor driven syringe. The experimental data was analysed using the Origin 7.0 software provided by MicroCal. A detailed description of the procedure is given in our previous work [21].

3. Thermodynamic analysis

The experimental ITC data were fitted with a model function, derived on the basis of the mass-action model for micellization of cationic surfactant. To make the applied procedure clearer, the thermodynamic analysis here is divided into three sections, whereas a detailed explanation of is given in the Supplementary material together with the algorithm of the fitting.

a) Model description. According to the mass-action model [22–25] the micellization process of a cationic surfactant at constant temperature, T, and pressure, p, may be described as

$$nS^+ + (n-z)C^- \rightleftarrows M^z \quad (1)$$

where S^+ represents the monomeric state of surfactant, C^- the corresponding counter-ions and M^z the micellar aggregate of n sur-

factant monomers with an effective charge of z. The equilibrium between species can be expressed by the apparent equilibrium constant (apparent because we are using molalities instead of activities – approximation acceptable at low concentrations), K_M,

$$K_M = \frac{m_M}{m_S^n m_C^{n-z}} \tag{2}$$

where m_S is the molality of surfactant ions in monomeric form, m_C the molality of counter-ions and m_M the molality of micelles.

Surfactant solution with concentration above critical micelle concentration, cmc, can be considered as a mixed electrolyte solution with the total surfactant molality, m, containing fraction of surfactant in micellar form, $\alpha_M = n \cdot m_M/m$.

It follows that K_M can be expressed as

$$K_M = \frac{\alpha_M m^{1-n}}{n(1-\alpha_M)^n \left(m\left(1-\alpha_M\left(1-\beta\right)\right)\right)^{n(1-\beta)}} \tag{3}$$

$$H_i = n_1\bar{H}_1 + n_S\bar{H}_S + n_C\bar{H}_C + n_M\bar{H}_M \tag{4}$$

where n_1 is the number of moles of solvent, n_S the number of moles of surfactant ions in monomeric form, n_C the number of moles of free counter-ions, and n_M the number of moles of surfactant ions in micellar form and $\bar{H}_1$, $\bar{H}_S$, $\bar{H}_C$, and $\bar{H}_M$the corresponding partial molar enthalpies. By taking into account the total number of moles of surfactant, $n_2 = n_S + n_M$, and counter-ions, $n_C = n_S + \beta n_M$, Eq. (4) becomes

$$H_i = n_1\bar{H}_1 + n_2\left(\bar{H}_S + \bar{H}_C\right) + n_M\Delta_M H \tag{5}$$

where the enthalpy of micelle formation, $\Delta_M H$, is defined as

$$\Delta_M H = \left(\bar{H}_M - \bar{H}_S - \left(1-\beta\right)\bar{H}_C\right). \tag{6}$$

Partial derivative of enthalpy with respect to n_2 at constant p, T, and n_1 in combination with Gibbs-Duhem equation (detailed explanation is given in the Supplementary material), leads to the relation for measured relative molar enthalpy, ΔH, including the enthalpy of micellization, $\Delta_M H$, which is assumed to be concentration independent and thus equal to its value in the standard state ($\Delta_M H = \Delta_M H^0$),

$$\Delta H = \left(\bar{H}_S + \bar{H}_C - \text{const}\right) + \Delta_M H^0\left(\frac{\partial n_M}{\partial n_2}\right)_{n_1,p,T} \tag{7}$$

Standard state is hypothetical state and is 1 M solution, which behaves as the solution at infinite dilution. Eq. (7) is ITC model function primarily used to fit our experimental data. The fitting parameters within the model function are calculated by using set of equations which are presented in continuation.

Using the Gibbs-Helmholtz relation and the Guggenheim approximation for surfactant mean activity coefficient [26], the $(\bar{H}_S + \bar{H}_C)$ contribution below cmc can be expressed as

$$\bar{H}_S + \bar{H}_C = \bar{H}_2^0 + 2 \cdot RT^2\left(\frac{A'_{(T)}\sqrt{m}}{1+\sqrt{m}} + B'_{(T)}m\right) \tag{8}$$

where $\bar{H}_2^0$ represents the partial molar enthalpy of surfactant in its standard state. The coefficients $A'_{(T)}$ and $B'_{(T)}$ are temperature derivatives of the constants $A_{(T)}$ and $B_{(T)}$, that reflect solvent properties and ion–ion interactions, respectively [26]. Since the values of coefficients $A'_{(T)}$ and $B'_{(T)}$ are almost constant at all temperatures and they do not affect the values of other thermodynamic parameters significantly, we have concluded that Guggenheim approximation is adequate to represent ionic interactions in SAIL system.

Due to the small changes in concentrations of S^+ and C^- ions above cmc, their concentration and thus also their mean activity coefficient are assumed to remain constant and equal to its value at the cmc. Consequently the contribution $(\bar{H}_S + \bar{H}_C)$ above cmc can be also regarded as constant.

c) Fitting procedure. By help of well-known relation $\Delta_M G^0 = -RT/n \ln K_M$, the ITC model function (Eq. (7)) may be described in terms of adjustable (fitting) parameters n, $\Delta_M H^0$, $\Delta_M G^0$, the coefficients $A'_{(T)}$ and $B'_{(T)}$ (Eq. (8)) and $\Delta_M c_p^0$ in the case of global fitting (see explanation further). The $\left(\partial n_M/\partial n_2\right)_{n_1,p,T}$ derivative in Eq. (7) represents the fraction of surfactant molecules in micellar state M and can be derived from the apparent equilibrium constant K_M considering the mass-balance relations (see Supplementary material).

To perform a global fitting of the data (fitting of curves at all temperatures simultaneously) we must also include Kirchhoff's law and the integrated Gibbs-Helmholtz equation

$$\Delta_M H^0(T) = \Delta_M H^0(T_r) + \Delta_M c_p^0(T - T_r) \tag{9}$$

$$\Delta_M G^0(T) = T\left(\Delta_M G^0(T_r)/T_r + \Delta_M H^0(T_r)\left[1/T - 1/T_r\right] + \Delta_M c_p^0\left[1 - T_r/T - \ln\left(T/T_r\right)\right]\right) \tag{10}$$

where $\Delta_M H^0(T_r)$ and $\Delta_M G^0(T_r)$ are the standard enthalpy and the standard Gibbs free energy of micellization at some reference temperature T_r. $\Delta_M c_p^0$ is heat capacity change for micellization and was considered as constant. All above-mentioned adjustable parameters were obtained by fitting of Eq. (7) to the experimental data points using the Levenberg-Marquardt non-linear regression algorithm [27] for minimizing χ^2 function (Eq. z in Supplementary material). At this point, it must be emphasized that the Eqs. (2)–(8) and consequently the standard Gibbs free energies and entropies are based on the molality scale. We also fitted our experimental data on mole fraction scale and obtained parameters which were within the calculated error, but for clarity reason only parameters on molality scale are shown.

In this work, a global fitting of the model equation to the corresponding experimental curves at all the examined temperatures was performed giving a greater confidence in the proposed model and consequently in all the adjustable parameters [28]. The main presumption concerning the global fitting was temperature independence of the aggregation number, which turned out to be acceptable since the individual and global fitting parameter didn't differentiate too much. This approach was already successfully used in our previous work [29].

4. Results and discussion

The dependence of experimental heat of dilution, ΔH, on surfactant concentration (enthalpogram) for titration of [C_{12}mim]Cl in water in the investigated temperature range is shown in Fig. 1(a). Similar enthalpy patterns were also obtained for other investigated systems at the same temperatures (Fig. S1 in the Supplementary material). In Fig. 1(b) the comparison of enthalpograms for [$C_X$mim]Cl systems is presented. As can be seen on Fig. 1(a), the heat effect at 298.15 K at [$C_X$mim]Cl systems is relatively weak and therefore the effect at 288.15 K is compared in Fig. 1(b).

As it can be seen from Figs. 1 and S1 in Supplementary material, anomalies from purely sigmoidal behavior at some titration curves were observed, which cannot be fitted well (for example [C_{10}mim]Cl at higher temperatures, [C_{12}mim]OMs at 288.15 K and at 308.15 K, [C_{12}mim]OAc at 288.15 K and at 298.15 K]). The experiment can be described as usually: the surfactant undergoes demicellization initially, which is followed by monomer dilution (at surfactant concentrations in the calorimetric cell below the cmc). Thus, at the beginning of experiment the heat changes measured result from demicellization of surfactant micelles, dilution of monomers, corresponding counter-ions and their mutual interactions. After surfactant concentration in the calorimetric cell reaches

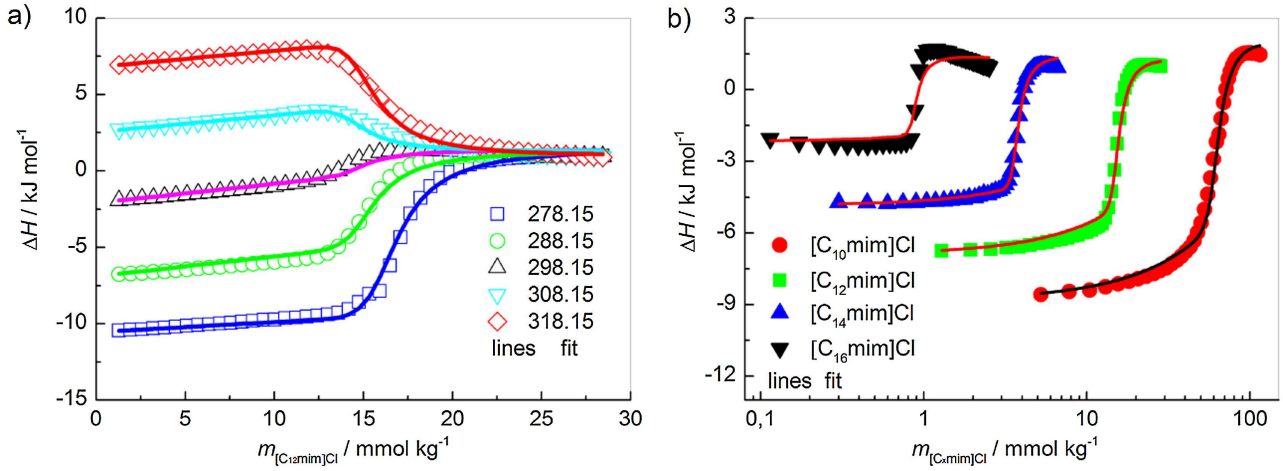

Fig. 1. a) Temperature dependent enthalpograms for $[C_{12}mim]Cl$; b) enthalpograms for $[C_x mim]Cl$ at 288.15 K in water. Solid lines represent the fits according to the model function (Eq. (7)).

the cmc, solution undergoes micellar dilution only (and no further demicellization) with an appreciable change in enthalpy that remains nearly constant with increasing surfactant concentration.

Therefore, the whole enthalpy curve (Figs. 1 and S1 in Supplementary material) consists of a three regions: two approximately horizontal or at least linear parts linked by a declining or increasing one. Evidently, investigated systems in general obey the same pattern as it has been observed for classical surfactants and was also represented in our previous work for alkyltrimethylammonium chlorides in water [21,30]. Obviously here the process at $[C_{12}mim]X$ systems is strongly affected by the counter-ions. The values of cmc and $\Delta_M H^0$ were simultaneously determined by the fitting procedure and are listed together with other thermodynamic parameters in Table S1 in Supplementary material for all systems at all investigated temperatures. Here also the comparison with the (available) literature data and cmc values as obtained from different techniques are reported. In Fig. 2, values of the degree of micelle ionization, as estimated from conductivity measurements and cmc values from ITC at 298.15 K are presented.

From Figs. Fig. 1(b) and Fig. 2(b) (and in Table S1 in Supplementary material) it is evident that cmc is decreasing with the length of side alkyl chain in the imidazolium cation at $[C_x mim]Cl$, as it is usual for "classical" surfactants. The values of cmc, estimated in this work, are in reasonable agreement with the literature data. There is no explicit relation between degree of micelle ionization, β, and side alkyl chain length.

On the other hand, at $[C_{12}mim]X$ systems cmc values decrease with increasing hydrophobicity of counter-ions. Thus OAc^- is strongly hydrated (cosmotrop) and possesses thus the highest cmc, OTs^-, OTf^- and Sal^- are hydrophobic and their cmc values are lower. If hydrogen is replaced by fluoride the hydrophobic character of counter-ion is more pronounced which affects cmc crucially (OAc^- vs. TFA^-; OMs^- vs. OTf^-). At 298.15 K cmc can be ranked in $OAc^- \approx OMs^- \approx Cl^- > Br > TFA^- > I^- > OTs^- \approx OTf^- > Sal^-$.

The values of the degree of micelle ionization, β, at $[C_{12}mim]X$ systems are strongly dependent on the counter-ions and can be ranked in the order $Cl^- > OAc^- \approx OMs^- > TFA^- > Br^- > OTf^- > I^- > OTs^- > Sal^-$. Weakly hydrated counter-ions (I^-, OTs^-) can be adsorbed more readily on the micellar surface, resulting in decreased charge repulsion between the ionic surfactant head groups. In contrast, the charge on the heavily hydrated Cl^- is partially screened by the surrounding polar water molecules and these counter-ions are thus less effective in reducing the charge repulsion. Cl^- cannot approach the highly charged surface of the micelle as closely as less hydrated ions. Therefore, it can neither screen the charge at the surface of micelles nor reduce the surface potential as effectively as other, less hydrated ions. This results not only in higher values of β but also in higher values of cmc (Fig. 2). $[C_{12}mim]OTs$ and $[C_{12}mim]Sal$ express the outstanding low value of β what can be ascribed to possible intercalation of anion possessing an aromatic ring in the micelle what has been already confirmed at dodecyltrimethylammonium chloride (DTACl) in the presence of NaSal [31].

In our previous work weak temperature dependence of β at ionic surfactants was observed [32,33]. Thus, in this work β values were determined at 298.15 K only and were regarded as temperature independent quantities since their values do not affect the thermodynamic analysis crucially.

The temperature dependence of cmc shows typical U-shaped form (Fig. S2 in Supplementary material) reaching the minimum value cmc* at the temperature T^*. These values, obtained from the corresponding derivative of the polynomial $cmc = A + BT + CT^2$, are listed in Table 1, whereas the coefficients of polynomial are given in Table S2 in Supplementary material.

The comparison of thermodynamic functions at 298.15 K is given in Fig. 3. The reported errors in Table S1 in Supplementary material correspond to the precision of the experimental data and the fitting procedure assuming the proposed model is correct.

The micellization process of studied systems is endothermic at low temperatures and becomes exothermic at high temperatures, as it is evident from Table S1 in Supplementary material and Fig. S3 in Supplementary material. Such behavior could be ascribed to the delicate balance between hydrophobic hydration of non-polar parts (endothermic) and couter ion binding (exothermic) upon micellization, where former effect diminishes with temperature [34]. Interestingly, for $[C_{12}mim]I$ and $[C_{12}mim]Sal$ the micellization process would be endothermic at relatively low temperature, ~270 K.

Similar change in the sign of $\Delta_M H^0$ with increasing temperature has been already observed for number of ionic surfactants also [21,29,30,32,35]. As it is evident form Table 1, the temperature T_0 at which $\Delta_M H^0 = 0$ is in excellent agreement with T^* confirming that the micellization can be described well by applied mass-action model. According to the model, the Gibbs free energy of micellization, $\Delta_M G^0$, is a function of temperature, therefore the cmc minimum leads to a minimum in the $\Delta_M G^0/T$. Following the Gibbs-Helmholtz relation, thus $\Delta_M H^0$ must pass through zero. Here, temperature T_0 at which $\Delta H_M^0 = 0$ is in the range of room temperature for all systems, except for $[C_{12}mim]I$ and $[C_{12}mim]Sal$,

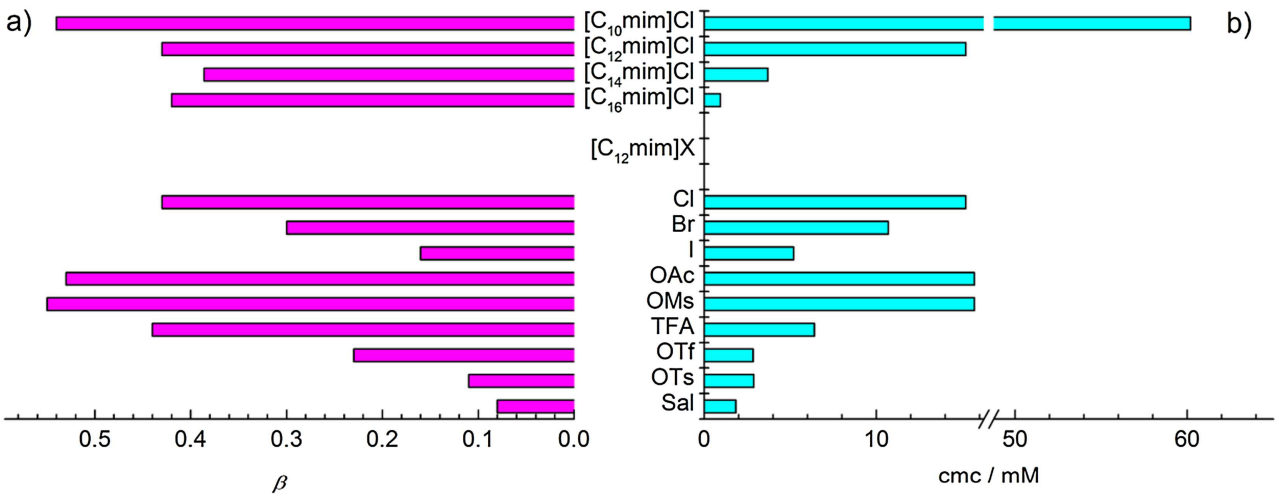

Fig. 2. a) Values for degree of micelle ionization, β, and b) critical micelle concentrations, cmc, for all investigated systems at 298.15 K.

Table 1
Aggregation number for of micelles, n_{agg}, the temperature, T^*(cmc), at the minimum critical micelle concentration, cmc*, temperature T_0 at $\Delta_M H^0 = 0$, together with the "chemical part" of the micellization process, $\Delta_M H_c$, compensation temperature, T_c, and standard heat capacity change upon micelle formation, $\Delta_M c_p^0$, for the investigated systems.[a]

	n_{agg}	T^*(cmc)	cmc*	T_0	$\Delta_M H_c$	T_c	$\Delta_M c_p^0$
[C_{10}mim]Cl	13.4 ± 0.1	309.0	58.2 ± 0.1	309.0	−8.9 ± 0.1	298 ± 3	−353 ± 2
[C_{12}mim]Cl	16.33 ± 0.06	302.9	15.2 ± 0.8	302.3	−15.0 ± 0.2	297 ± 3	−417 ± 2
[C_{12}mim]Br	16.82 ± 0.01	291.9	10.5 ± 0.5	291.8	−17.0 ± 0.2	297 ± 4	−398 ± 3
[C_{12}mim]I	17.6 ± 0.2	271.0	4.6 ± 0.3	270.4	−22.9 ± 0.2	297 ± 4	−387 ± 2
[C_{12}mim]OAc	10.4 ± 0.3	311.3	16.7 ± 0.9	311.2	−13.0 ± 0.2	297 ± 4	−476 ± 2
[C_{12}mim]OMs	21.8 ± 0.1	306.3	15.2 ± 0.8	306.3	−13.7 ± 0.2	298 ± 3	−430 ± 2
[C_{12}mim]OTs	8.20 ± 0.02	290.2	2.8 ± 0.1	290.5	−26.1 ± 0.2	298 ± 3	−621 ± 1
[C_{12}mim]OTf	16.9 ± 0.1	286.3	2.7 ± 0.1	286.5	−23.0 ± 0.2	299 ± 4	−494 ± 2
[C_{12}mim]TFA	17.2 ± 0.2	301.3	6.4 ± 0.3	300.6	−18.5 ± 0.3	298 ± 4	−528 ± 1
[C_{12}mim]Sal	9.3 ± 0.8	275.5	1.66 ± 0.09	273.2	−27.7 ± 0.2	298 ± 3	−526 ± 2
[C_{14}mim]Cl	20.6 ± 0.1	297.6	3.7 ± 0.2	298.0	−20.9 ± 0.2	298 ± 3	−516 ± 2
[C_{16}mim]Cl	11.1 ± 0.1	292.7	0.92 ± 0.05	293.1	−26.1 ± 0.2	302 ± 3	−608 ± 2

[a] Units: T^*(cmc), K; cmc*, mmol kg^{-1}; T_0, K; $\Delta_M H_c$, kJ mol^{-1}; T_c, K; $\Delta_M c_p^0$, J K^{-1} mol^{-1}.

where $T_0 = \sim 270$ K could be estimated (Table S1, Fig. S3 in Supplementary material).

From Fig. 3 it is evident that an interplay between enthalpy and entropy results in the negative values of Gibbs free energy, is characteristic of spontaneous processes at constant p and T. For micellization process these linear relationship between the changes in entropy and enthalpy can be represented by

$$\Delta_M H^0 = \Delta_M H_c + T_c \Delta_M S^0 \quad (11)$$

where T_c is called the compensation temperature and can be obtained from the slope of the straight line with $\Delta_M H_c$ as the intercept [36,37]. T_c can be interpreted as a characteristic of solute-solvent interactions, i.e., proposed as a measure of the "desolvation" part of the process of micellization and correlates to thus to the dehydration of the non-polar parts of the self-assembled molecules [37]. $\Delta_M H_c$ characterizes the solute–solute interactions and is considered as an index of the "chemical" part of the process of micellization, connected to the formation of micelle of monomers [37].

Entropy-enthalpy plots for all investigated systems are presented in Fig. S4 in Supplementary material for all investigated SAILs, whereas the estimated values of T_c and $\Delta_M H_c$ are listed in Table 1.

Evidently, for all investigated systems values of T_c are close together, $T_c = 300 \pm 3$ K. According to Lumry and Rajender [36], for a variety of processes involving aqueous solutions of small molecules T_c values lie in a narrow range between 250 and 350 K. Even more, Lumry's law states that, for processes dominated by hydration, a value of $T_c \cong 280$ K should be assumed [36,38,39]. Thus, the value obtained here for studied SAILs is indicative for processes dominated by dehydration [36].

It was assumed [37], that $\Delta_M H_c$ represents the strength of the solute–solute interactions at surfactant aggregation when the entropic contribution to micellization is zero i.e., $\Delta_M S^0 = 0$. The increase in $\Delta_M H_c$ corresponds thus to a decrease in the stability of the structure of the micelles. From Table 1 is evident that $\Delta_M H_c$ is ranked in the order [C_{10}mim]Cl > [C_{12}mim]Cl, [C_{14}mim]Cl > [C_{16}mim]Cl. It can be assumed that the self-assembled structures with C_{16} are more densely packed then those with C_{10}, as it is usual also at "classical" ionic surfactants [37,40].

In other words, the effect of this so-called "chemical part" of the process in micellization diminishes as the alkyl chain length decreases. In our previous work [37] it was found, that the value of $\Delta_M H_c$ decreases by ~3.9 kJ mol^{-1} when the alkyl chain length increases by one methylene unit for an ionic surfactant, and less (~2.9 kJ mol^{-1}) for a non-ionic surfactant C_iE_8.

As it is evident from Table 1, for investigated SAILs value of $\Delta_M H_c$ decreases for 3.1 kJ mol^{-1} at increasing the side alkyl chain for one methylene group from [C_{10}mim]Cl to [C_{12}mim]Cl, for 2.9 kJ mol^{-1} from [C_{12}mim]Cl to [C_{14}mim]Cl, and for 2.6 kJ mol^{-1} from [C_{14}mim]Cl to [C_{16}mim]Cl, what is in reasonable agreement with reported findings [37].

For surfactants possessing C_{12}-alkyl chain, value of $\Delta_M H_c = \sim -35$ kJ mol^{-1} is reported [37], but it was determined on very narrow

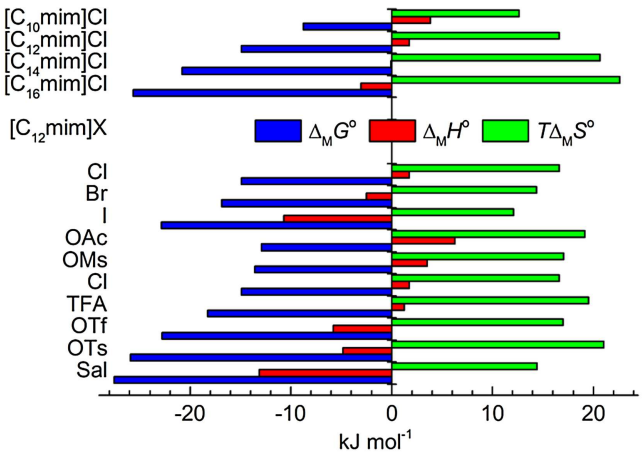

Fig. 3. Thermodynamic parameters of micellization for investigated systems in water at 298.15 K: standard enthalpy, $\Delta_M H^0$, Gibbs free energy, $\Delta_M G^0$, and entropy contributions, $T\Delta_M S^0$, for micellization at investigated systems in water as obtained by the fitting procedure.

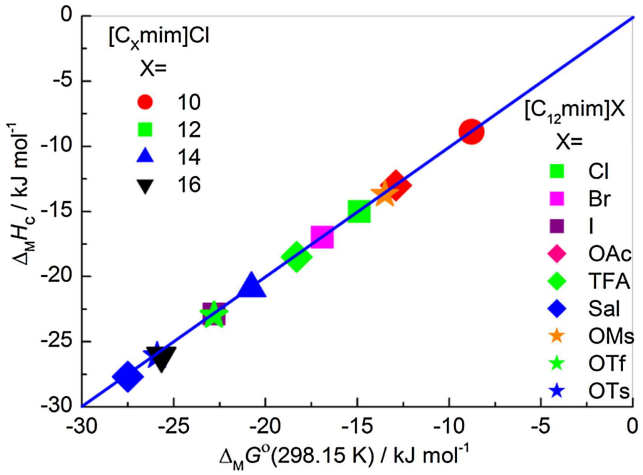

Fig. 4. Intercepts of the EEC plot, $\Delta_M H_c$, as a function of $\Delta_M G^0$(298.15 K) for all investigated systems.

choice of counter-ions (Br^-, Na^+). In this work for $\Delta_M H_c$ values from -13.0 kJ mol^{-1} ([C_{12}mim]OAc) to -27.7 kJ mol^{-1} ([C_{12}mim]Sal) were estimated. Thus $\Delta_M H_c$ depends strongly on the counter-ion, as it is evident also from Table 1.

Unfortunately, there is no data on the effect of the counter-ions on the enthalpy-entropy compensation effect in the literature. But having the look on Fig. 4, presenting the $\Delta_M H_c$ as a function of $\Delta_M G^0$(298.15 K), we can see that all values are excellent fitted to the same line starting in the origin with the slope of 1. There is no doubt that the length of alkyl chain and the counter-ions influence the micellization process. As it is evident form Figs. 2 and 3 and results in Table S1 in Supplementary material, cmc, β, and all thermodynamic functions are strongly dependent on properties of system. But there is no evidence that there is some extra-thermodynamic mechanism for ΔH-ΔS compensation. Values of $\Delta_M H_c$, determined in these work for SAILs with four different alkyl chain and for nine different counter-ions for the SAILs with C_{12}-alkyl chain are practically identical to the value of $\Delta_M G^0$ near T_c. Thus it can be concluded that in this case EEC is a matter of fact arising from the relationship $\Delta G = \Delta H - T\Delta S$. An inspections of values for $\Delta_M G^0$ in Table S1 in Supplementary material reveals, that for a separate system micellization process occurs at the nearly constant $\Delta_M G^0$ ($\pm\sim 2$ kJ mol^{-1}), but there are bigger differences among them, for example ~15 kJ mol^{-1} between [C_{10}mim]Cl and [C_{16}mim]Cl and also between [C_{12}mim]OAc and [C_{12}mim]Sal.

Nevertheless, the main driving force for the formation of micelles is the apparent disaffinity of water for the non-polar (interacting) surfaces known as hydrophobic effect. The parameter that illustrates this effect is the heat capacity of micellization, $\Delta_M c_p^0$, which is highly negative (Table 1), what can be ascribed to the removal of water molecules from contact with non-polar surface area upon micelle formation [41]. However, their values are considerably dependent on the counter-ions.

By modeling the micellization processes as a transfer of surfactant molecules into the micellar phase, the heat capacity can be expressed in terms of the change of water accessible non-polar and polar surface areas, derived by Spolar et al. [42] from protein folding

$$\Delta_M c_p^o(\mathrm{J\,K^{-1}\,mol^{-1}}) = -1.34(\pm 0.33)\,\Delta A_{np}(\mathring{A}^2) + 0.59(\pm 0.17)\,\Delta A_p(\mathring{A}^2) \quad (12)$$

where ΔA_{np} stand for the loss of water accessible non-polar and ΔA_p for polar surface area upon protein folding. Because the hydrophilic head groups of non-ionic surfactants remain hydrated upon micelle formation, the "theoretical" contribution of water accessible non-polar surface area change to the heat capacity change upon micelle formation, $\Delta_M c_p^0(\mathrm{th_{np}})$, can be assumed to reflect only the change in exposure of the hydrophobic tails to water. Consequently, Eq. (12) is reduced to

$$\Delta_M c_p^o(\mathrm{th_{np}})(\mathrm{J\ K^{-1}\ mol^{-1}}) = -1.34(\pm 0.33)\,\Delta A_{np}(\mathring{A}^2) \quad (13)$$

This approach turned out as useful for a series of non-ionic surfactants [43,44].

According to Richards [45], water accessible surface area of a methylene group is 30 Å^2 and 88 Å^2 for a methyl group. Thus ΔA_{np} of the hydrophobic tails of the surfactants investigated in this study is 358, 418, 478 and 538 Å^2 for the C_{10}, C_{12}, C_{14} and C_{16} alkyl chain, respectively, giving the values of ($\mathrm{th_{np}}$) = −479, −560, −640 and −720 J K^{-1} mol^{-1} for C_{10}, C_{12}, C_{14} and C_{16} alkyl chain, respectively. Comparison of $\Delta_M c_p^0(\mathrm{th_{np}})$, estimated by Eq. (13), with $\Delta_M c_p^0$(exp), as illustrated in Fig. 5, reveals that there is an evident discrepancy between $\Delta_M c_p^0(\mathrm{th_{np}})$ and $\Delta_M c_p^0$(exp). This discrepancy can be explained in two ways:

a) It can be assumed that there are still water molecules in the interior of the micelle upon micellization and thus the ΔA_{np} calculated by approach of Richards [45] mentioned above, is overestimated. That is, the "real" ΔA_{np} is smaller than that of Richards. Actually, the low aggregation numbers, n_{agg}, of studied surfactants obtained by the fitting procedure (see Table 1) support the above presumption of loose aggregates with lots of water molecules still in contact with hydrocarbon skeleton even after micelles are formed for [$C_x$mim]Cl.
b) The Eq. (13) holds well for non-ionic surfactants [43,44], but it is not valid for ionic surfactants. Positive contribution of removal of water accessible polar surface area to the heat capacity change of micellization should also be considered and cannot be neglected, consistent with the findings for the heat capacity change upon protein folding [42]. It is believed that ionic surfactant are fully dissociated in aqueous solution when the surfactant concentration is below its cmc. But this is not the case upon micellization, where the partially binding of counter-ions to the micelles results in the values of degree of micelle ionization lower then 1 ($0.1 < \beta < 0.6$), Fig. 2(b). Thus, the contribution of the removal of water accessible polar surface area, ΔA_p, should not be neglected in the case of ionic surfactants. However no direct correlation between $\Delta_M c_p^0$ and β can be deduced (Figs. 2, 5 and S5 in Supplementary material). Interestingly, the difference between $\Delta_M c_p^0$(exp) and $\Delta_M c_p^0(\mathrm{th_{np}})$ for the [$C_x$mim]Cl systems, as illustrated in Fig. 5(a), is almost constant

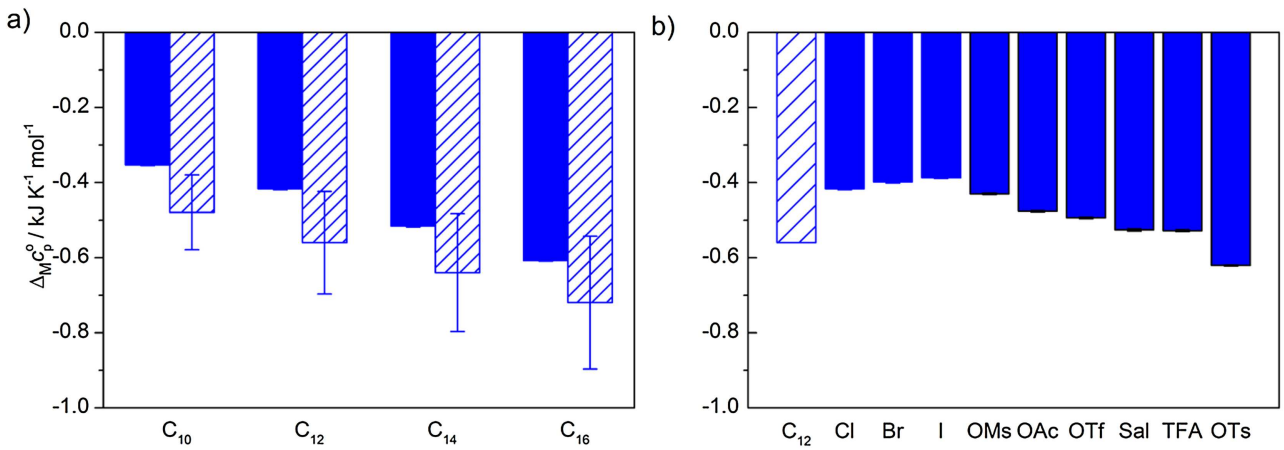

Fig. 5. Comparison of theoretical and experimental values of heat capacity changes upon micellization process, $\Delta_M c_p^0$, for a) [$C_x$mim]Cl and b) [C_{12} mim]X.

$127 \pm 12\,J\,mol^{-1}K^{-1}$, that implies the removal of water accessible polar surface area due to the partial binding of counter-ions (Cl^-) to the micelles is almost independent of alkyl chain length of ionic liquid [$C_x$mim]Cl. In addition, the influence of counter-ion on $\Delta_M c_p^0$ for [C_{12}mim]X systems is illustrated in Fig. 5(b). If simply consider three systems: [C_{12}mim]Cl, [C_{12}mim]Br and [C_{12}mim]I, it is obvious to observe that the difference between $\Delta_M c_p^0$(exp) and $\Delta_M c_p^0$(th_{np}) for the systems increases along with an increase in size of anion. It is plausible to conjecture that the removal of water accessible polar surface area also increases along with an increase in size of counter-ion binding onto the micelle, but it can be concluded that ΔA_p part here cannot be neglected.

Recently, the incorporation of hydrophobic part of counter-ion (benzene ring) in the micelle was confirmed for hydroxybenzoates [31,46] and parabens [18] at micellization of dodecyltrimethylammonium chloride (DTACl) in water. In this case the contribution for the removal of the hydrophobic part of counter-ion from the contact with water after micellization to the $\Delta_M c_p^0$ can be assumed. Thus, the "hydrophobic" anions (OTs^-, OTf^-, TFA^- and Sal^-) can be partially incorporated in the micelle and therefore the hydrophobic part of anion can contribute to the ΔA_{np}. The result of such incorporation frequently leads to the formation of elongated or rod-like micelles at higher concentrations, which also indicate our viscosity measurements (Fig. S6 in Supplementary material). This was, for example, already confirmed for [C_{16}mim]OTs by Singh et al. using various methods [47].

5. Conclusions

The present work clearly shows the great potential of surface active ionic liquids (SAILs) for investigation of thermodynamics of micellization process in solutions due to possible variations in the structure of chain length and counter-ions. In many ways their behavior is identical to those observed by "usual" cationic surfactants: the critical micelle concentration is decreasing with the length of hydrophobic chain and expresses a minimum in the temperature dependence. In general, the micellization process is endothermic at low temperatures and exothermic at high temperatures, but in this work it was verified that the influence of counter-ions plays an extremely important role. It was confirmed, that the hydrophobicity of counter-ions evidently contribute to the heat capacity change and the water accessible surface area removal upon burial of non-polar group from the contact with water at micellization process. Even more, it can be assumed that all hydrophobic anions (OTs^-, OTf^-, TFA^- and Sal^-) are partially incorporated in the micelles.

Enthalpy-entropy compensation (EEC) plots exhibit nearly parallel slopes for all studied SAILs giving compensation temperatures $T_c = 300 \pm 3$ K, indicating the domination of dehydration by micellization process at all studied SAILs. The interceptions of these plots, $\Delta_M H_c$ as the measure for so-called "chemical part" of the micellization, turned out as being strongly correlated to the $\Delta_M G^0$, leading to the conclusion that at micellization process entropy-enthalpy compensation is the fact, arising from the relationship $\Delta G = \Delta H - T\Delta S$.

Finally, $\Delta_M c_p^0$ was correlated with the removal of solvent accessible surface areas of SAILs and counter-ion from the contact with water after micellization. From the discrepancies between experimental and theoretical values of $\Delta_M c_p^0$ it can be assumed, that there are still water molecules in the interior of the micelle upon micellization or/and that also the contribution of the removal of polar water accessible surface should be taken into account in the case of ionic surfactants.

Conflict of interest

The authors declare no competing interests.

Acknowledgements

The financial support by the Slovenian Research Agency through Grant No. P1-0201 and the Austrian Science Fund (FWF Project P25504-N28) is gratefully acknowledged. The work was partially supported by COST Action CM1206.

Appendix A. Supplementary data

Supplementary data associated with this article can be found, in the online version, at http://dx.doi.org/10.1016/j.colsurfa.2017.01.062.

References

[1] M. Blesic, M.H. Marques, N.V. Plechkova, K.R. Seddon, L.P.N. Rebelo, A. Lopes, Self-aggregation of ionic liquids: micelle formation in aqueous solution, Green Chem. 9 (2007) 481–490.
[2] A. Cornellas, L. Perez, F. Comelles, I. Ribosa, A. Manresa, M.T. Garcia, Self-aggregation and antimicrobial activity of imidazolium and pyridinium based ionic liquids in aqueous solution, J. Colloid Interface Sci. 355 (2011) 164–171.
[3] O.A. El Seoud, P.A.R. Pires, T. Abdel-Moghny, E.L. Bastos, Synthesis and micellar properties of surface-active ionic liquids: 1-Alkyl-3-methylimidazolium chlorides, J. Colloid Interface Sci. 313 (2007) 296–304.

[4] M. Blesic, A. Lopes, E. Melo, Z. Petrovski, N.V. Plechkova, J.N. Canongia Lopes, K.R. Seddon, L.P.N. Rebelo, On the self-aggregation and fluorescence quenching aptitude of surfactant ionic liquids, J. Phys. Chem. B 112 (2008) 8645–8650.
[5] M.T. Garcia, I. Ribosa, L. Perez, A. Manresa, F. Comelles, Self-assembly and antimicrobial activity of long-chain amide-functionalized ionic liquids in aqueous solution, Colloids Surf. B 123 (2014) 318–325.
[6] J. Nowicki, J. Łuczak, D. Stańczyk, Dual functionality of amphiphilic 1-alkyl-3-methylimidazolium hydrogen sulfate ionic liquids: surfactants with catalytic function, RSC Adv. 6 (2016) 11591–11601.
[7] M. Blesic, M. Swadźba-Kwaśny, J.D. Holbrey, J.N. Canongia Lopes, K.R. Seddon, L.P.N. Rebelo, New catanionic surfactants based on 1-alkyl-3-methylimidazolium alkylsulfonates, [C(n)H(2n + 1)mim][C(m)H(2m + 1)SO(3)]: Mesomorphism and aggregation, Phys. Chem. Chem. Phys. 11 (2009) 4260–4268.
[8] A.B. Pereiro, J.M.M. Araújo, F.S. Teixeira, I.M. Marrucho, M.M. Piñeiro, L.P.N. Rebelo, Aggregation behavior and total miscibility of fluorinated ionic liquids in water, Langmuir 31 (2015) 1283–1295.
[9] M. Anouti, J. Jones, A. Boisset, J. Jacquemin, M. Caillon-Caravanier, D. Lemordant, Aggregation behavior in water of new imidazolium and pyrrolidinium alkycarboxylates protic ionic liquids, J. Colloid Interface Sci. 340 (2009) 104–111.
[10] A.K. Ressmann, R. Zirbs, M. Pressler, P. Gaertner, K. Bica, Surface-active ionic liquids for micellar extraction of piperine from black pepper, Z. Naturforsch. B 68b (2013) 1129–1137.
[11] K. Bica, P. Gärtner, P.J. Gritsch, A.K. Ressmann, C. Schröder, R. Zirbs, Micellar catalysis in aqueous–ionic liquid systems, Chem. Commun 48 (2012) 5013–5015.
[12] A. Cognigni, P. Gärtner, R. Zirbs, H. Peterlik, K. Prochazka, C. Schröder, K. Bica, Surface-active ionic liquids in micellar catalysis: impact of anion selection on reaction rates in nucleophilic substitutions, Phys. Chem. Chem. Phys. 18 (2016) 13375–13384.
[13] F. Geng, J. Liu, L. Zheng, L. Yu, Z. Li, G. Li, C. Tung, Micelle formation of long-chain imidazolium ionic liquids in aqueous solution measured by isothermal titration Microcalorimetry, J. Chem. Eng. Data. 55 (2010) 147–151.
[14] J. Łuczak, C. Jungnickel, M. Joskowska, J. Thöming, J. Hupka, Thermodynamics of micellization of imidazolium ionic liquids in aqueous solutions, J. Colloid Interface Sci. 336 (2009) 111–116.
[15] P.D. Galgano, O.A. El Seoud, Surface active ionic liquids: study of the micellar properties of 1-1-alkyl]-3-methylimidazolium chlorides and comparison with structurally related surfactants, J. Colloid Interface Sci. 361 (2011) 186–194.
[16] J.L. Ferguson, J.D. Holbrey, S. Ng, N.V. Plechkova, K.R. Seddon, A.A. Tomaszowska, D.F. Wassell, A greener, halide-free approach to ionic liquid synthesis, Pure Appl. Chem. 84 (2011) 723–744.
[17] M. Benrraou, B.L. Bales, R. Zana, Effect of the nature of the counterion on the properties of anionic surfactants. 1. cmc, ionization degree at the cmc and aggregation number of micelles of sodium, cesium, tetramethylammonium, tetraethylammonium, tetrapropylammonium, and tetrabutylammonium dodecyl sulfates, J.Phys. Chem. B 107 (2003) 13432–13440.
[18] A. Kroflič, B. Šarac, J. Cerkovnik, M. Bešter-Rogač, Hydrophobicity of counterions as a driving force in the self-assembly process: dodecyltrimethylammonium chloride and parabens, Colloid Surf. A 460 (2014) 108–117.
[19] L. Baranauskiene, V. Petrikaite, J. Matuliene, D. Matulis, Titration calorimetry standards and the precision of isothermal titration calorimetry data, Int. J. Mol. Sci. 10 (2009) 12752–12762.
[20] T. Wiseman, S. Williston, J.F. Brandts, L.-N. Lin, Rapid measurement of binding constants and heats of binding using a new titration calorimeter, Anal. Biochem. 179 (1989) 131–137.
[21] B. Šarac, M. Bešter-Rogač, Temperature and salt-induced micellization of dodecyltrimethylammonium chloride in aqueous solution: a thermodynamic study, J. Colloid Interface Sci. 338 (2009) 216–221.
[22] R.J. Hunter, Introduction to Modern Colloid Science, Oxford University Press, 1993.
[23] J.N. Phillips, The energetics of micelle formation, J. Trans. Soc. 51 (1954) 561–569.
[24] J. Lah, C. Pohar, G. Vesnaver, Calorimetric study of the micellization of alkylpyridinium and alkyltrimethylammonium bromides in water, J. Phys. Chem. B 104 (2000) 2522–2526.
[25] J. Lah, M. Bešter-Rogač, T.-M. Perger, G. Vesnaver, Energetics in correlation with structural features: the case of micellization, J. Phys. Chem. B 110 (2006) 23279–23291.
[26] E.M. Woolley, T.E. Burchfield, Model for thermodynamics of ionic surfactant solutions. 2. Enthalpies, heat capacities, and volumes, J. Phys. Chem. 88 (1984) 2155–2163.
[27] W.H. Press, B.P. Flannery, S.A. Teukolsky, W.T. Vetterling, Numerical Recipes, Cambridge University Press, Oxford, 1992.
[28] I. Drobnak, G. Vesnaver, J. Lah, Model-based thermodynamic analysis of reversible unfolding processes, J. Phys. Chem. 114 (2010) 8713–8722.
[29] A. Kroflič, B. Šarac, M. Bešter-Rogač, Thermodynamic characterization of CHAPS micellization ising isothermal titration calorimetry: temperature, salt, and pH dependence, Langmuir 28 (2012) 10363–10371.
[30] A. Kroflič, B. Šarac, M. Bešter-Rogač, Influence of the alkyl chain length, temperature, and added salt on the thermodynamics of micellization: alkyltrimethylammonium chlorides in NaCl aqueous solutions, J. Chem. Thermodyn. 43 (2011) 1557–1563.
[31] B. Šarac, G. Meriguet, A. Bernard, M. Bešter-Rogač, Salicylate isomer-specific effect on the micellization of dodecyltrimethylammonium chloride: large effects from small changes, Langmuir 29 (2013) 4460–4469.
[32] T.-M. Perger, M. Bešter-Rogač, Thermodynamic of micelle formation of alkyltrimethylammonium chlorides from high performance electric conductivity measurements, J. Colloid Interface Sci. 313 (2007) 288–295.
[33] A. Kroflič, B. Šarac, M. Bešter-Rogač, What affects the degree of micelle ionization: conductivty study of alkyltrimethylammonium chlorides, Acta Chim. Slov. 59 (2012) 564–570.
[34] D. Ben-Amotz, Water-mediated hydrophobic interactions, Annu. Rev. Phys. Chem. 67 (2016) 617–638.
[35] R. Zielinski, Effect of temperature on micelle formation in aqueous nabr solutions of octyltrimethylammonium bromide, J. Colloid Interface Sci. 235 (2001) 201–209.
[36] R. Lumry, S. Rajender, Enthalpy–entropy compensation phenomena in water solutions of proteins and small molecules: A ubiquitous property of water, Biopolymers 9 (1970) 1125–1227.
[37] L.J. Chen, S.-Y. Lin, C.-C. Huang, Effect of hydrophobic chain length of surfactants on enthalpy-entropy compensation of micellization, J. Phys. Chem. 102 (1998) 4350–4356.
[38] C.V. Krishnan, H.L. Friedman, Enthalpies of alkyl sulfonates in water, heavy water, and water-alcohol mixtures and the interaction of water with methylene groups, J. Solution Chem. 2 (1973) 37–51.
[39] C.V. Krishnan, H.L. Friedman, Studies of hydrophobic bonding in aqueous alcohols: Enthalpy measurements and model calculations, J. Solution Chem. 2 (1973) 119–140.
[40] C. Baar, R. Buchner, W. Kunz, Dielectric relaxation of cationic surfactants in aqueous solution. 2. Solute relaxation, J. Phys. Chem. B 105 (2001) 2914–2922.
[41] Z. Kiraly, I. Dekany, I. A thermometric titration study on the micelle formation of sodium decyl sulfate in water, J. Colloid Interface Sci. 242 (2001) 214–219.
[42] R.S. Spolar, J.R. Livingstone, M.T. Record Jr., Use of liquid hydrocarbon and amide transfer data to estimate contributions to thermodynamic functions of protein folding from the removal of nonpolar and polar surface from water, Biochemistry 31 (1992) 3947–3955.
[43] L.J. Chen, Y.-H. Sheu, P.-J. Li, Heat capacity changes accompanying micelle formation upon burial of hydrophobic tail of nonionic surfactants, J. Phys. Chem. 108 (2004) 19096–19098.
[44] G.C. Kresheck, Isothermal titration calorimetry studies of neutral salt effects on the thermodynamics of micelle formation, J. Phys. Chem. B 113 (2009) 6732–6735.
[45] a) F.M. Richards, The interpretation of protein structures: total volume, group volume distributions and packing density, J. Mol Biol. 82 (82) (1974) 1–14;
b) F.M. Richards, Areas, volumes, packing and protein structure, Annu. Rev. Biophys Bioeng. 6 (1977) 151–176;
c) F.M. Richards, Calculation of molecular volumes and areas for structures of known geometry, Methods Enzymol. 115 (1985) 440–446.
[46] J. Gujt, J.M. Bešter-Rogač, E. Spohr, Structure and stability of long rod-like dodecyltrimethylammonium chloride micelles in solutions of hydroxybenzoates: a molecular, dynamics simulation study, Langmuir 32 (2016) 8275–8286.
[47] G. Singh, T.S. Kang, Micellization behavior of surface active ionic liquids having aromatic counterions in aqueous media, J. Phys. Chem. B 120 (2016) 1092–1105.

Please cite this article in press as: B. Šarac, et al., Thermodynamic study for micellization of imidazolium based surface active ionic liquids in water: Effect of alkyl chain length and anions, Colloids Surf. A: Physicochem. Eng. Aspects (2017), http://dx.doi.org/10.1016/j.colsurfa.2017.01.062

LANGMUIR

Universitätsbibliothek TU Wien

Subscriber access provided by TU Wien University Library

Article

Hydration and Counterion Binding of [CMIM] Micelles

Sergej Friesen, Thomas Buchecker, Alice Cognigni, Katharina Bica, and Richard Buchner

Langmuir, **Just Accepted Manuscript** • DOI: 10.1021/acs.langmuir.7b02201 • Publication Date (Web): 08 Aug 2017

Downloaded from http://pubs.acs.org on August 18, 2017

Just Accepted

"Just Accepted" manuscripts have been peer-reviewed and accepted for publication. They are posted online prior to technical editing, formatting for publication and author proofing. The American Chemical Society provides "Just Accepted" as a free service to the research community to expedite the dissemination of scientific material as soon as possible after acceptance. "Just Accepted" manuscripts appear in full in PDF format accompanied by an HTML abstract. "Just Accepted" manuscripts have been fully peer reviewed, but should not be considered the official version of record. They are accessible to all readers and citable by the Digital Object Identifier (DOI®). "Just Accepted" is an optional service offered to authors. Therefore, the "Just Accepted" Web site may not include all articles that will be published in the journal. After a manuscript is technically edited and formatted, it will be removed from the "Just Accepted" Web site and published as an ASAP article. Note that technical editing may introduce minor changes to the manuscript text and/or graphics which could affect content, and all legal disclaimers and ethical guidelines that apply to the journal pertain. ACS cannot be held responsible for errors or consequences arising from the use of information contained in these "Just Accepted" manuscripts.

ACS Publications

Langmuir is published by the American Chemical Society. 1155 Sixteenth Street N.W., Washington, DC 20036

Published by American Chemical Society. Copyright © American Chemical Society. However, no copyright claim is made to original U.S. Government works, or works produced by employees of any Commonwealth realm Crown government in the course of their duties.

Hydration and Counterion Binding of [C_{12}MIM] Micelles

Sergej Friesen,[†] Thomas Buchecker,[‡] Alice Cognigni,[¶] Katharina Bica,[¶] and Richard Buchner[*,†]

Institut für Physikalische und Theoretische Chemie, Universität Regensburg, Regensburg, Germany, Institut für Anorganische Chemie, Universität Regensburg, Regensburg, Germany, and Institut für Angewandte Synthesechemie, Technische Universität Wien, Vienna, Austria

E-mail: richard.buchner@chemie.uni-regensburg.de

Abstract

Surface-active ionic liquids based on imidazolium cations are promising targets for micellar catalysis in aqueous solution, yielding enhanced rate constants compared to surfactants based on *n*–alkyltrimethylammonium cations and exhibiting a pronounced counterion dependence.[1,2] Probably most relevant to that is the interplay of headgroup hydration and counterion binding. To get more detailed information on these effects aqueous solutions of 1-dodecyl-3-methylimidazolium ([C_{12}MIM]) bromide, iodide and triflate (TfO^-) were investigated at 45 °C using broadband dielectric spectroscopy, viscosity measurements and small-angle X-ray scattering experiments. Effective hydration numbers were determined and information on the location and mobility of the condensed counterions, X^-, was derived. It turned out that [C_{12}MIM]-halide micelles

[*]To whom correspondence should be addressed
[†]Institut für Physikalische und Theoretische Chemie, Universität Regensburg, Regensburg, Germany
[‡]Institut für Anorganische Chemie, Universität Regensburg, Regensburg, Germany
[¶]Institut für Angewandte Synthesechemie, Technische Universität Wien, Vienna, Austria

were less hydrated than corresponding *n*-dodecyl-trimethylammonium ([C_{12}TA]X) aggregates. Together with their somewhat weaker counterion condensation this probably explains their higher catalytic activity. Whilst [C_{12}MIM]Br micelles remained roughly spherical in the studied concentration range, rod-like aggregates were formed at high concentrations of the iodide and in particular the triflate surfactant. It appears that the much lower mobility of condensed TfO^- counterions is the reason for the very low catalytic activity of [C_{12}MIM]TfO micelles.

Introduction

Since the discovery of ionic liquids (ILs) by Paul Walden in 1914,[3] these compounds continue attracting the attention of chemists around the world. Defined as salts melting below 100 °C,[4] their unique physico-chemical properties, such as negligible vapor pressure, high thermal and chemical stability, low flammability and high charge density,[5,6] have aroused increasing industrial and fundamental interest. Possible applications of ILs range from their use as alternative solvents in extraction/separation, electrochemical and catalytical processes to materials engineering.[5,7] Research into that direction is mainly focused on pure ILs or on situations where these compounds are a major mixture component but also dilute IL solutions are gaining increasing interest.[8–10]

Due to their structure, consisting of a hydrophobic residue —often an alkyl chain— attached to a charged moiety, many ions used as building blocks of ILs are amphiphilic and thus prone to self-association,[11] including the formation of micelles in dilute aqueous solution.[9,12] Typical examples of such surface-active ionic liquids (SAILs), which form micelles for $n \geq 8$, are 1-alkyl-3-methylimidazolium ILs, [C_nMIM]X, where X is the anion and n the number of carbon atoms in the alkyl chain.[13–16] In that respect but also from a structural point of view they resemble *n*-alkyl-trimethylammonium salts, [C_nTA]X, a classical family of cationic surfactants[17] serving here as a convenient reference.

Recent studies revealed the outstanding performance of [C_{12}MIM]X SAILs in mi-

cellar extraction processes[18,19] and for the micellar catalysis of Diels Alder reactions,[1] oxidations[20–22] and nucleophilic substitution (S_N) reactions.[2] In the latter case, a marked influence of the anion on the reaction rate constant, k, of a model S_N reaction was observed, with $k(Cl^-) > k(Br^-) > k(I^-) > k(TfO^-)$ (TfO^- - triflate, trifluoromethanesulfonate). For charged micelles to be stable counterions have to condense on their surface, reducing thus Coulomb repulsion between the surfactant headgroups.[23] Therefore, it is reasonable to assume that the anion effect observed for k is related to the extent and also the strength of counterion binding on the micellar surface. For the latter not only the Coulomb interactions between the anions and the cationic surfactant headgroups are relevant but also the hydration of both.

Broadband dielectric relaxation spectroscopy (DRS) probes the interaction of the sample with a small-amplitude electromagnetic field and thus provides information on the structure and collective dynamics of the studied system.[24] This technique has proven to be a very useful tool for the investigation of solute-solute, solute-solvent and solvent-solvent interactions in systems ranging from pure dipolar fluids[25] to electrolyte solutions.[26,27] In the case of ionic surfactant systems DRS allows the determination of effective hydration numbers and —via micelle-specific modes— yields insights into the location and mobility of condensed couterions.[28–33] Accordingly, we present in this contribution a dielectric study of aqueous solutions of the SAILs 1-dodecyl-3-methylimidazolium bromide ($[C_{12}MIM]Br$), 1-dodecyl-3-methylimidazolium iodide ($[C_{12}MIM]I$) and 1-dodecyl-3-methylimidazolium trifluoromethanesulfonate ($[C_{12}MIM]TfO$) at 45 °C to elucidate the impact of different counterions on the dynamics and hydration of the formed micelles. Measurements covered the concentration range $cmc < c < 250$ mM (*i.e.* 10^{-3} mol/L) where cmc is critical micellar concentration (Table 1). The triflate counterion was chosen as it exhibited the lowest reaction rate constant in the investigation of Cognigni *et al.*[2] on micellar catalysis. Although the Br^- ion yielded only the second fastest rate in the latter study, it was preferred over Cl^- for the present investigation as dielectric data for dodecyl-trimethylammonium

bromide ([C_{12}TA]Br) were available for comparison.[28,29,32] The rate constant for I^- was intermediate to those of Br^- and TfO^-. Additionally, dielectric measurements of selected samples were performed in the temperature range of (25 to 65) °C to determine Eyring activation enthalpies and entropies of the observed relaxation processes.[34] These investigations were complemented by viscosity measurements and small-and-wide-angle X-ray scattering (SWAXS) experiments to gain further information on the aggregation behavior.

Experimental

Materials. Except for 1-bromdodecane, which was distilled at 170 °C under reduced pressure (55 mbar), all chemicals required for the synthesis of the surfactants were used as received. The halide-based imidazolium ILs were synthesized by reacting 1-methylimidazole (Carl Roth, ≥ 99%) with a slight molar excess (1.2 equivalents) of the appropriate 1-halododecane (Sigma-Aldrich, > 97%).[35] After the reaction [C_{12}MIM]Br was recrystallized three times from ethyl acetate (Acros Organics, 99.97%), whereas toluene (VWR Chemicals, ≥ 99.5%) was used to recrystallize [C_{12}MIM]I thrice. The latter compound was subsequently washed three times with *n*-hexane (VWR Chemicals, 99%). In both cases colorless crystalline solids were obtained which were then dried at room temperature under reduced pressure ($p \leq 2 \cdot 10^{-6}$ bar) over P_2O_5 (Siccapent, Merck) as a desiccant for four days. The water content determined by Karl Fischer titration was found to be < 370 ppm for [C_{12}MIM]Br and < 70 ppm for [C_{12}MIM]I.

[C_{12}MIM]TfO was prepared according to ref. 2. The required chemicals methyl triflouromethane sulfonate and dichlormethane were acquired from Carbolution Chemicals (97 %) and Acros Organics (> 99.8%) respectively. *N*-dodecylimidazole was synthesized as described by Souza *et al.*[36] and subsequently distilled at 140 °C under $3 \cdot 10^{-5}$ bar. The freshly synthesized [C_{12}MIM]TfO was washed four times with *n*-hexane (VWR Chemicals, 99%) to give a colorless solid which was subsequently dried under high vacuum

($p \leq 10^{-8}$ bar) at 45 °C for four days. The water content of the final product was < 260 ppm.

For all synthesized ILs purity was checked by ^{1}H-NMR, ^{13}C-NMR and elemental analysis. The water used for sample preparation was purified with a Millipore Q-MILLI purification unit and showed a specific electrical resistance of ≥ 18 MΩcm. Aqueous [C_{12}MIM]X solutions of solute molality, m (in mol·kg^{-1} solvent), were prepared gravimetrically without buoyancy correction.

Auxiliary Measurements. To obtain the molar solute concentration, c (in mol·L^{-1} = M), of the sample of molality m solution densities, ρ, were determined with an Anton Paar DMA 5000 vibrating tube densimeter having $5 \cdot 10^{-6}$ g·cm^{-3} nominal uncertainty and 0.005 K temperature stability. Viscosities, η, of the micellar solutions were obtained with an Anton Paar AMVn rolling ball viscometer having an uncertainty of 0.05 K in temperature, T, and a relative uncertainty of 0.02 in η. The electrical conductivity, κ, of the samples used for DRS was determined with the equipment described previously, having a temperature uncertainty of 0.005 K and a relative uncertainty in κ of 0.015.[37] The thus obtained data for ρ, η and κ are summarized in Tables S1-S6 of the Supporting Information.

Additionally, the critical micellar concentration, *cmc*, of the three surfactants in water at (45.0 ± 0.1) °C was determined by conductivity measurements with a WTW inoLab Cond 730 conductivity meter. The *cmc* was obtained from the intersection of the two straight lines observed for $\kappa(c)$ at $c < cmc$ and $c > cmc$ respectively (Figure S1 of the Supporting Information). The obtained *cmc* values and the degree of counterion binding, β, estimated from the ratio of the slopes above and below *cmc*,[38] are presented in Table 1. As expected for ionic surfactants,[23] the *cmc* decreased with increasing β, *i.e.* decreasing headgroup repulsion, yielding the anion sequence $Br^- > I^- > TfO^-$. The obtained data for *cmc* and β compare reasonably with literature values for 25 °C, except for the rather small β value published for [C_{12}MIM]TfO (Table 1).[1]

Small-and-wide angle X-ray Scattering. Small-and-wide-angle X-ray scattering (SWAXS) is one of the most established methods to examine the mesoscale structure of soft matter.

The instrumentation used for the present SWAXS measurements was described in details elsewhere.[39] The scattered intensities were recorded as a function of the magnitude of the scattering vector, $q = [(4\pi)/\lambda] \times \sin(\theta/2)$, where λ is the wavelength of incident radiation and θ the scattering angle. Quartz capillaries of 2 mm diameter were used as sample containers. The usual corrections for the background (empty cell and detector noise) and an intensity normalization, using a high-density polyethylene film as a standard, were applied. Silver behenate in a sealed capillary was used to calibrate the scattering vector. The experimental resolution was $\Delta q/q = 0.05$. All measurements were performed at room temperature. The FIT2D software[40] was used for data analysis.

Table 1: Critical micelle concentrations, *cmc*, and degrees of counterion binding, β, of the investigated SAILs at 45 °C in comparison with literature data.

	45 °C		25 °C	
SAIL	*cmc* / mM	β	*cmc* / mM	β
$[C_{12}MIM]Br$	10.03	0.64	10.29[a]	0.70[a], 0.75[b]
$[C_{12}MIM]I$	7.13	0.78	5.19[a]	0.84[a], 0.85[b]
$[C_{12}MIM]TfO$	3.58	0.80	3.31[a]	0.73[a]

[a] taken from Ref. 2; [b] taken from Ref. 41.

Dielectric Relaxation Spectroscopy. DRS probes the macroscopic polarization of a sample induced by an applied electric field of frequency ν.[24] This response is conveniently expressed in terms of the generalized complex permittivity[42]

$$\hat{\eta}(\nu) = \hat{\varepsilon}(\nu) - \frac{\mathrm{i}\kappa}{2\pi\nu\varepsilon_0} = \varepsilon'(\nu) - \mathrm{i}[\varepsilon''(\nu) + \frac{\kappa}{2\pi\nu\varepsilon_0}] \quad (1)$$

In eq 1, $\varepsilon'(\nu)$ is the relative permittivity of the sample and $\varepsilon''(\nu)$ the associated dielectric loss; ε_0 denotes the permittivity of vacuum. The last term in the equation describes energy dissipation arising from the dc ($\nu = 0$) conductivity, κ, of the sample whereas the complex permittivity, $\hat{\varepsilon}(\nu) = \varepsilon'(\nu) - \mathrm{i}\varepsilon''(\nu)$, comprises all contributions that explicitly depend on

frequency and thus provides information on the cooperative dynamics of the investigated system.

The generalized permittivity was recorded in the frequency range of $0.02 \leq \nu/\mathrm{GHz} \leq 89$. For $\nu \leq 50$ GHz a frequency-domain reflectometer was used. This setup is based on an Agilent E8364B vector network analyzer (VNA) in combination with two open-ended coaxial dielectric probes, Agilent 85070E-20 (0.2-20 GHz) and 85070-50 (5-50 GHz),[43] and a coaxial cut-off cell for 0.02-1 GHz. For $60 \leq \nu/\mathrm{GHz} \leq 89$ a waveguide interferometer with variable-pathlength transmission cell was used. For all three surfactants $\hat{\varepsilon}(\nu)$ was recorded as a function of solute concentration in the range $cmc \lesssim c \lesssim 260$ mM at the temperature of 318.15 K. Additionally, for each SAIL one of these solutions ([C_{12}MIM]Br: 0.1033 mol·kg^{-1}, corresponding to c = 99.2 mM at 318.15 K; [C_{12}MIM]I: 0.1038 mol·kg^{-1}/99.5 mM at 318.15 K; [C_{12}MIM]TfO: 0.0749 mol·kg^{-1}/74.4 mM at 318.15 K) was studied as a function of temperature for $298.15 \leq T/\mathrm{K} \leq 338.15$. The temperature uncertainty of the dielectric experiments was 0.05 K.

After concatenating the data obtained with the different instruments $\hat{\eta}(\nu)$ was corrected for dc conductivity to yield $\varepsilon''(\nu)$. Where required, $\varepsilon'(\nu)$ was additionally corrected for electrode polarization as described in ref. 24 (Fig. S2). For the thus obtained dielectric spectra, $\hat{\varepsilon}(\nu)$, the associated relaxation-time distribution function, $P(\tau)$, was determined using Zasetzky's method[44] to restrict the number of relaxation models to be tested in subsequent fits of $\hat{\varepsilon}(\nu)$ with sums of n Havriliak-Negami equations.[26] At $c > cmc$ the obtained $P(\tau)$ spectra, Figs. S3–S8, suggest the presence of four relaxations centered at approximately 5 ps (corresponding to ~30 GHz), 100 ps (1.5 GHz), 400 ps (0.4 GHz) and 1-3 ns (0.09-0.16 GHz) for all studied solutions. Subsequent testing of all possible models with $2 \leq n \leq 5$ assumed modes along the criteria described in detail previously[25] revealed that these spectra could be consistently fitted with a superposition of four Debye equations

$$\hat{\varepsilon}(\nu) = \sum_{j=1}^{4} \frac{S_j}{1 + \mathrm{i}2\pi\nu\tau_j} + \varepsilon_\infty \tag{2}$$

In this D+D+D+D model S_j is the amplitude and τ_j the relaxation time of the modes $j = 1 \ldots 4$ resolved at increasing frequencies; $\varepsilon_\infty = \lim_{\nu\to\infty} \varepsilon'(\nu)$ is the high-frequency permittivity. The static relative permittivity of the sample is given as $\varepsilon = \varepsilon_\infty + \sum S_j$. Examples of the dielectric spectra spectra and their fits are shown in Figs. 1-3. The obtained parameters are summarized in Tables S7–S12.

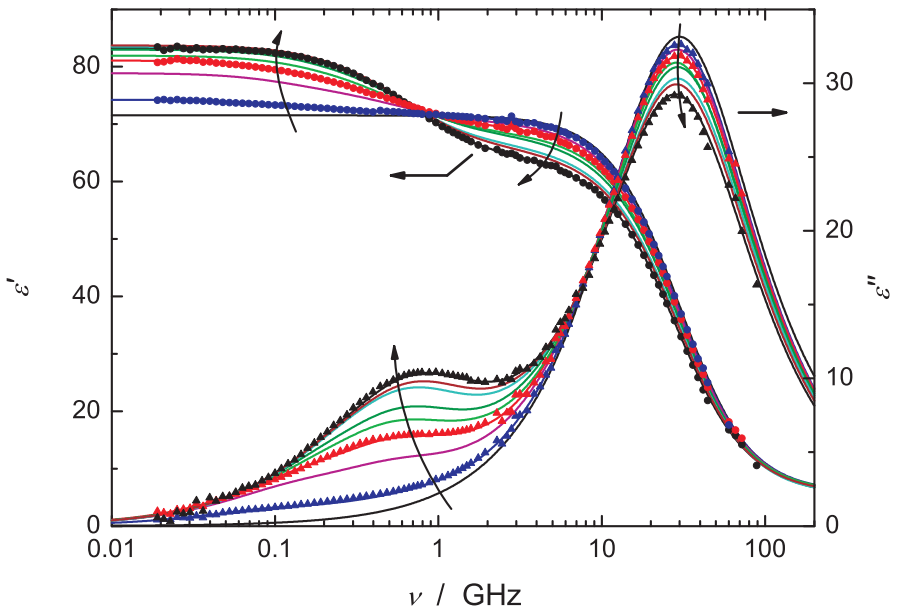

Figure 1: Spectra of relative permittivity, $\varepsilon'(\nu)$ (▲), and dielectric loss, $\varepsilon''(\nu)$ (●), and their fits with eq 2 (lines) of aqueous [C_{12}MIM]Br solutions at 45 °C and concentrations c = (0, 19.9, 49.4, 74.7, 99.2, 125.0, 173.8, 199.6 and 242.1) mM in arrow direction. For clarity experimental data are only shown for selected samples.

For the three IL samples with $c \approx cmc$ mode $j = 3$ could not be resolved and also S_1 and S_2 are very small and biased. Accordingly, the parameters of the D+D+D fit to these spectra were not considered in the further analysis but their values are given in Tables S7–S9 for completeness. Note that for higher concentrations the D+D+CC model, *i.e.* two Debye functions for the micelle-specific modes and a symmetrically broadened Cole-Cole function for the solvent, produced fits of a quality similar to the D+D+D+D model. However, the derived hydration numbers were un-physical so that the D+D+CC model was discarded.

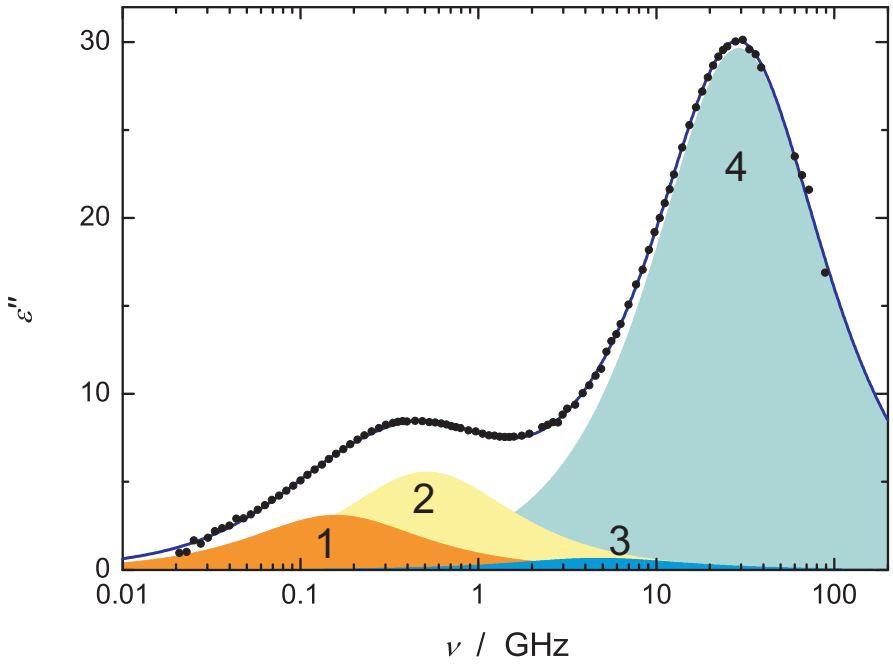

Figure 2: Dielectric loss, $\varepsilon''(\nu)$ (●), spectrum of 230.1 mM aqueous $[C_{12}MIM]I$ at 45 °C and associated fit with the D+D+D+D model (line). The shaded areas show the contributions of the resolved modes, $j = 1 \ldots 4$.

Results

Dielectric Spectroscopy

Assignment of Relaxation Modes. The dominating relaxation process at ~ 30 GHz ($\tau_3 \approx$ 5.4 ps) can be readily assigned to the cooperative (c) rearrangement of the H-bond network of bulk-like water as for pure H_2O at 45 °C the corresponding relaxation time is τ_c = 5.33 ps[45] and the present data for τ_3 smoothly evolve from that value (Tables S7–S9). Since the present spectra extend only to 89 GHz the fast (f) water mode (τ_f = 0.165 ps at $c = 0$) could not be resolved but its presence is obvious from the obtained high-frequency permittivity values ($\varepsilon_\infty(c) \approx 5$) which significantly exceed the pure-water value ($\varepsilon_\infty(0)$ = 2.78).

Upon surfactant addition a broad micelle-specific contribution appeared at $c > cmc$ in the 0.05 to 5 GHz region of the dielectric spectra (Fig. 1). This feature shifted to lower

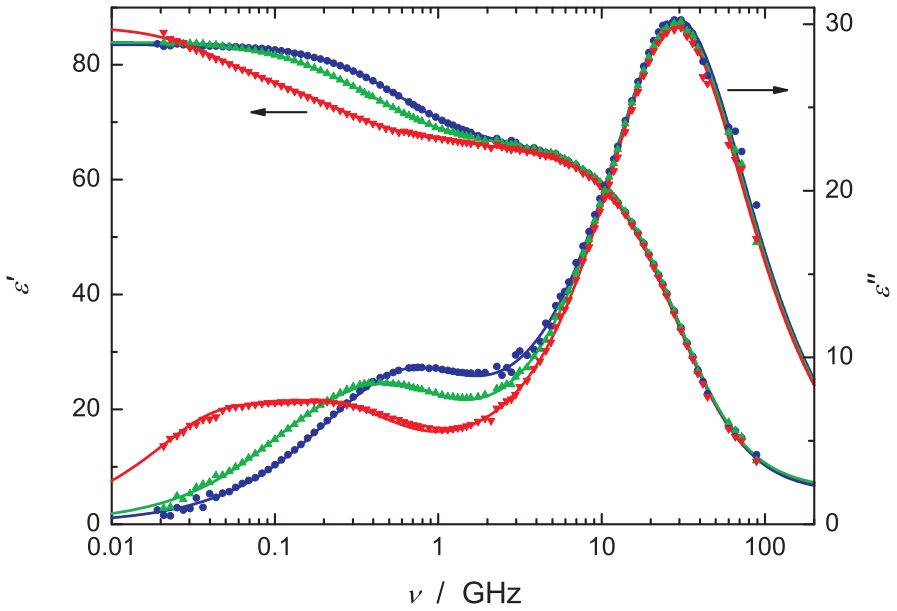

Figure 3: Dielectric loss, $\varepsilon''(\nu)$ (symbols), spectra and their fits with eq 2 (lines) of aqueous solutions of 173.8 mM [C_{12}MIM]Br (●), 173.9 mM [C_{12}MIM]I (▲) and 173.9 mM [C_{12}MIM]TfO (▼) at 45 °C.

frequencies when going from Br^- to I^- to TfO^- (Fig. 3) and —as predicted by the theory of Grosse[46] for suspensions of charged colloids— was well described by two additional Debye relaxations (Fig. 2). Accordingly, we assigned the lowest-frequency mode centered at ~ 0.1 GHz to fluctuations of the diffuse counterion cloud surrounding the micelles, whereas the intermediate-frequency mode at ~0.4 GHz was attributed to the hopping of condensed counterions on the surface of the micelle.[29,31]

Only with the assumption of an additional weak mode, (S_3, τ_3), located between the micelle-specific relaxations and the dominating contribution from bulk-like water consistent sets of relaxation parameters as a function of concentration (Tables S7–S9) and temperature (Tables S10–S12) could be obtained. Due to its small amplitude, $S_3 < 3$, the obtained parameters were very noisy and in some cases τ_3 had to be fixed in the fit to get reasonable S_3 values. Despite the large variation of τ_3 with the anion and (partly) with c and T we assign this relaxation to retarded (slow) H_2O molecules hydrating the micelles for the reasons discussed below.

The contribution of free SAIL cations to the dielectric spectra could be neglected as their concentration is comparable to the *cmc* and thus very low.[47] Also the contribution of free triflate anions is negligible.[48]

Eyring Activation Parameters. The relaxation times, τ_j ($j = 1 \ldots 4$), of the solutions investigated as a function of temperature in the range $298.15 \leq T/\mathrm{K} \leq 338.15$ (Tables S10–S12) were fitted to the Eyring equation[34]

$$\ln(\tau_j/\mathrm{s}) = \ln\left(\frac{h}{k_\mathrm{B}T}\right) - \frac{\Delta S^{\neq}}{R} + \frac{\Delta H^{\neq}}{RT} \tag{3}$$

where the activation entropy, $\Delta S^{\neq}$, and the activation enthalpy, $\Delta H^{\neq}$, were assumed to be independent of T; h, k_b and R have their usual meaning. The obtained activation parameters are summarized in Table 2; corresponding fits are shown in Figs. S9-S11. The results for τ_3 have to be taken with a grain of salt as the amplitude of this mode is very small. Therefore, not only S_3 but also the corresponding relaxation time is very sensitive to experimental error. For some spectra values of τ_3 (open symbols in Figs. S10 & S11) even had to be fixed to get reasonable fits with eq 2, which obviously might bias $\Delta H^{\neq}$ and $\Delta S^{\neq}$.

In line with current understanding of water dynamics, which assumes jump reorientation via a triangular transition state,[50] not only the activation enthalpy for the cooperative water relaxation but also the corresponding entropy was found to be positive for the three investigated SAIL solutions. Within experimental uncertainty $\Delta S^{\neq}(\tau_4)$ and $\Delta H^{\neq}(\tau_4)$ are independent of the anion but both quantities are somewhat reduced compared to pure water.[51] Thus, all three solutes facilitate bulk-water reorientation to some extent. Almost certainly, this is mainly due to the labile hydration shells of the present anions, Br^-,[52] I^-,[50,52] and TfO^-,[53] which cannot be distinguished from bulk water by DRS.[26]

Activation enthalpy and entropy of the slow-water mode strongly depend on the anion. Both quantities decrease in the sequence $Br^- < I^- < TfO^-$. Although other possible sources for the pronounced change of τ_3 with temperature, in particular for Br^-, cannot be excluded

Table 2: Eyring activation enthalpy, $\Delta H^{\neq}$, and activation entropy, $\Delta S^{\neq}$, of relaxation times, $\tau_j(T)$ ($j = 1 \ldots 4$), of the solutions investigated as a function of T.

system	τ_j	$\Delta H^{\neq}$ / kJ mol^{-1}	$\Delta S^{\neq}$ / J mol^{-1}K^{-1}
water	τ_b [a]	15.9 ± 0.2	20.4 ± 0.7
[C_{12}MIM]Br	τ_1	20 ± 6	−8 ± 18
b = 0.1033 mol/kg	τ_2	20.6 ± 0.8	−2 ± 3
(99.2 mM at 45 °C)	τ_3	71 ± 10	174 ± 31
	τ_4	14.0 ± 0.4	14.1 ± 1.2
[C_{12}MIM]I	τ_1	10 ± 3	−44 ± 8
b = 0.1038 mol/kg	τ_2	13.7 ± 0.8	−20 ± 3
(99.5 mM at 45 °C)	τ_3	19.8 ± 1.4	17 ± 4
	τ_4	14.0 ± 0.5	14 ± 2
[C_{12}MIM]TfO	τ_1	15 ± 2	−38 ± 6
b = 0.0749 mol/kg	τ_2	15 ± 3	−21 ± 9
(74.4 mM at 45 °C)	τ_3	13 ± 3	−14 ± 10
	τ_4	13.6 ± 0.3	12.8 ± 1.1

[a] Ref. 49.

the data appear to be reasonable (see Discussion).

The activation parameters obtained for the two micelle-specific modes are not very reliable but trends can be noted from Table 2. For both relaxation times, τ_1 & τ_2, the sequence $I^- < TfO^- < Br^-$ was found for $\Delta H^{\neq}$. On the other hand for bromide $\Delta S^{\neq}$ is negligible for both micelle relaxations whereas for the other two anions the activation entropies are clearly negative and similar in magnitude, with $\Delta S^{\neq}(\tau_1) \approx 2\Delta S^{\neq}(\tau_2)$.

Water Relaxation and Hydration Numbers. The amplitudes, S_i, of relaxation processes associated with the reorientation of molecular dipoles can be analyzed with the equation

$$\frac{\varepsilon + A_i(1-\varepsilon)}{\varepsilon} S_i = \frac{N_A c_i}{3\varepsilon_0 k_B T} \cdot \mu_{\mathrm{eff},i}^2 \tag{4}$$

where c_i is the molar concentration of the involved species, i, $\mu_{\mathrm{eff},i}$ its effective dipole moment and A_i the associated cavity field factor; N_A is the Avogadro constant.[27] For

water molecules the assumption of a spherical cavity, $A = 1/3$, is reasonable and for the evaluation of solvent modes normalization to the pure state is convenient as it allows elimination of $\mu_{\mathrm{eff},i}$.

For water the fast jump reorientation of a molecule, probably associated with the fast relaxation (τ_f = 165 fs at 45 °C), and the subsequent settling of the H-bond network and waiting for the next jump, governed by τ_c = 5.33 ps, form a continuous sequence of events and accordingly the sum of both amplitudes, $S_b = S_c + S_f$, has to be evaluated with eq 4.[27] This is also the case for solution spectra. Since no fast water mode was resolved from the present solution spectra the amplitude of bulk water was approximated as $S_b(c) = S_4(c) + \varepsilon_\infty(c) - \varepsilon_\infty(0)$.

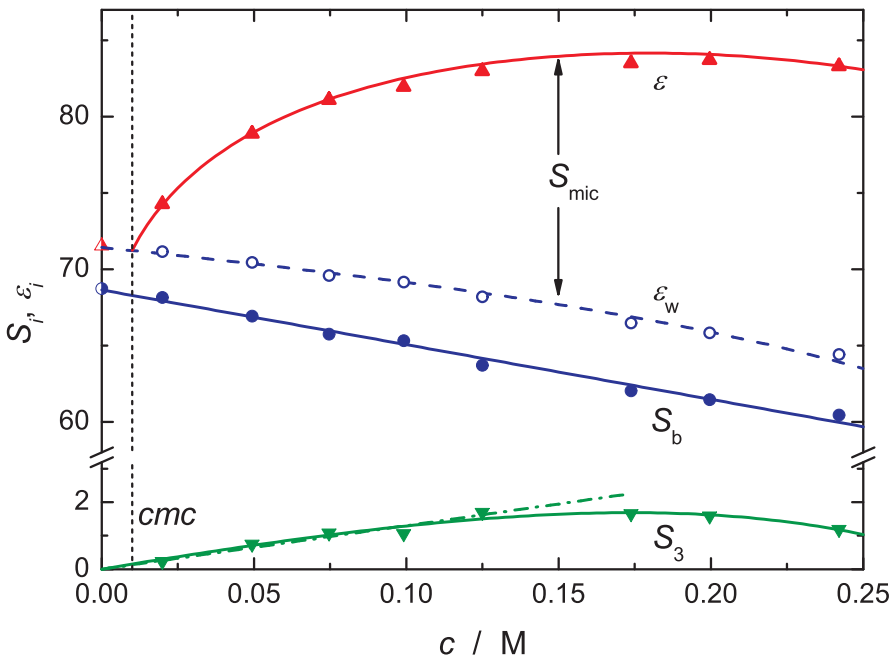

Figure 4: Static permittivity of the solution, ε (▲), and corresponding contribution of water, $\varepsilon_w = \varepsilon - S_1 - S_2$ (○), for aqueous [C_{12}MIM]Br solutions at 45 °C. Also shown are the corresponding amplitudes of bulk, S_b (●), and slow water, S_3 (▼). Lines are a guide to the eye, with the dash-dotted line highlighting the linear increase of S_3 at $c \leq 125$ mM and the vertical line indicating the *cmc*.

From S_b the concentration of bulk-like water, c_b, can be obtained whereas S_3 yields the concentration of moderately retarded (slow) solvent, c_s. These quantities then allow

calculating the total effective hydration number, $Z_t = (c_w - c_b)/c$ (c_w is the analytical solvent concentration), and the number of retarded H_2O molecules per equivalent of solute, $Z_s = c_s/c$.[26,27] The difference $Z_{ib} = Z_t - Z_s$ gives the number of water dipoles which are so strongly impeded (irrotationally bound, ib) in their rotation that they disappear from the spectrum.

A problem with the direct calculation of Z_t and Z_s is that with decreasing solute concentration their uncertainties strongly increase as the amplitude error remains constant whereas $(c_w - c_b)$ respectively c_s get smaller and smaller. However, for all three SAILs investigated S_b decreases linearly with solute concentration (Fig. 4). Additionally, S_3 increases linearly over the entire range investigated for [C_{12}MIM]I and [C_{12}MIM]TfO. For [C_{12}MIM]Br this is only true for $c \leq 125$ mM (Fig. 4). Since also solution density, ρ, and conductivity, κ, exhibit straight lines over the entire concentration range it is convenient to focus on the well-defined slopes of these quantities. To do so, eq 4 was rearranged to give the $c \to 0$ limit

$$Z_t^0 = \lim_{c\to 0}\left(\frac{\mathrm{d}c_w}{\mathrm{d}c}\right) - \lim_{c\to 0}\left(\frac{\mathrm{d}c_b^{eq}}{\mathrm{d}c}\right) \tag{5}$$

where

$$\lim_{c\to 0}\left(\frac{\mathrm{d}c_w}{\mathrm{d}c}\right) = \left[\lim_{c\to 0}\left(\frac{\mathrm{d}\rho}{\mathrm{d}c}\right) - M\right]/M_s \tag{6}$$

with M and M_s as the molar masses of solute and solvent, and

$$\lim_{c\to 0}\left(\frac{\mathrm{d}c_b^{eq}}{\mathrm{d}c}\right) = \frac{c_w(0)}{S_b(0)} \times \left[\lim_{c\to 0}\left(\frac{\mathrm{d}S_b}{\mathrm{d}c}\right) + \xi \times \lim_{c\to 0}\left(\frac{\mathrm{d}\kappa}{\mathrm{d}c}\right)\right] \tag{7}$$

In this approach the second summand in eq 7, with

$$\xi = p \times \frac{\varepsilon(0) - \varepsilon_\infty(0)}{\varepsilon(0)} \times \frac{\tau(0)}{\varepsilon_0} \tag{8}$$

corrects for kinetic depolarization assuming slip boundary conditions ($p = 2/3$) for ion transport.[54] Similarly, for linearly increasing S_3 the low-c limit of the slow-water solvation

number is given by

$$Z_s^0 = \lim_{c\to 0}\left(\frac{dc_s}{dc}\right) = \frac{c_w(0)}{S_b(0)} \times \lim_{c\to 0}\left(\frac{dS_3}{dc}\right) \quad (9)$$

Obviously, for $[C_{12}MIM]Br$ at $c > 125$ mM values for $Z_s(c)$ had to be calculated directly as described in detail in Ref. 27.

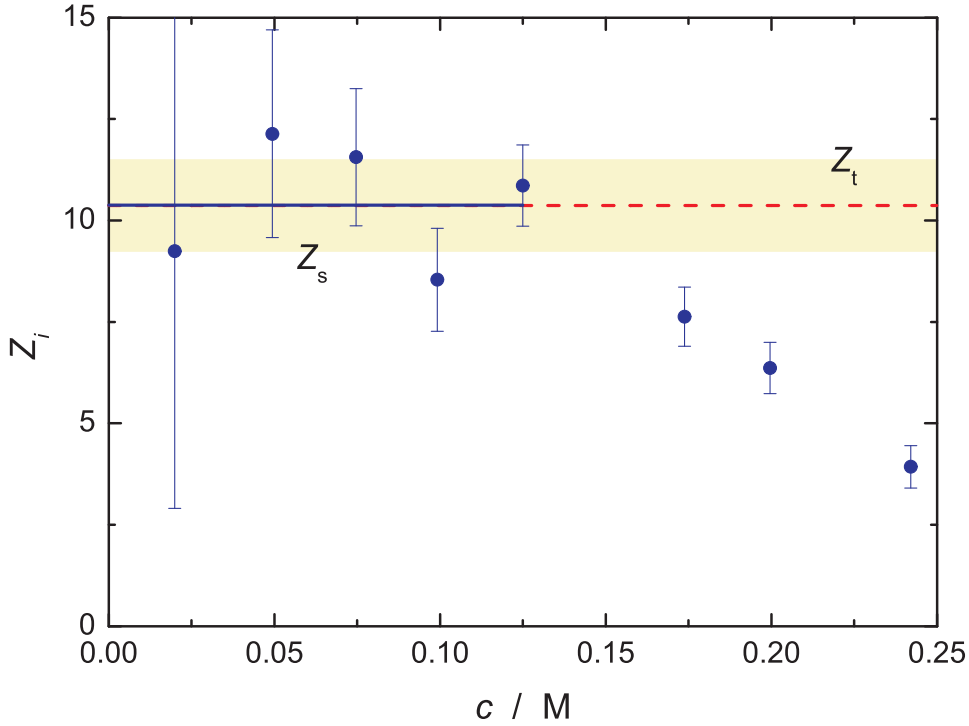

Figure 5: Total hydration number, Z_t (broken line), and associated standard uncertainty (shaded area) of $[C_{12}MIM]Br$ in aqueous solution at 45 °C. Also indicated is the corresponding number of slow (retarded) H_2O molecules per equivalent of solute, Z_s, obtained with eq 9 from the slope dS_3/dc for $c \leq 125$ mM (solid line; on top of Z_t) and directly calculated values (●).

Table 3 summarizes the obtained Z_t^0 and Z_s^0 values. Figure 5 compares for $[C_{12}MIM]Br$ the result obtained with eq 9 for $c \leq 125$ mM with directly calculated Z_s values for the entire concentration range. For $[C_{12}MIM]Br$ up to 125 mM and for all $[C_{12}MIM]TfO$ solutions $Z_t^0 = Z_s^0$ within experimental uncertainty. On the other hand, for $[C_{12}MIM]I$ $Z_{ib} \approx 6$ at all studied c and for $[C_{12}MIM]Br$ the number of strongly bound water molecules, $Z_{ib} = Z_t - Z_s$, increases from zero at $c \leq 125$ mM to ~ 6 at 242 mM whilst the total hydration number

Table 3: Effective total hydration numbers, Z_t^0, and numbers of slow (moderately retarded) water, Z_s^0, of the investigated [C_{12}MIM]X surfactants at 45 °C and of comparable [C_{12}TA]X surfactants from the literature.

	[C_{12}MIM]X		[C_{12}TA]X	
X^-	Z_t^0	Z_s^0	Z_t^0	Z_s^0
Br^-	10.4 ± 1.4	10.4 ± 0.6	22 ± 3 [a]	12 ± 2 [a]
			21 ± 3 [b]	11 ± 2 [b]
I^-	11.8 ± 0.7	5.8 ± 0.3		
TfO^-	10.2 ± 0.7	9.2 ± 0.4	11 ± 2 [b]	not detected[b]

[a] At 25 °C;[28] [b] at c = 0.1 M and 45 °C.[32]

remains constant (Fig. 5).

Solute Relaxation. The micelle-specific relaxations 1 & 2 were analyzed using Grosse's theory for charged colloids.[46] This model considers a dispersion of charged spherical particles of radius, R_G, and relative permittivity, ε_P, suspended in a medium of relative permittivity, ε_M, and dc conductivity, κ_M. An infinitely thin conducting layer with surface conductance λ_S, resulting from the lateral motion of condensed counterions, is assumed to be located at the surface of the charged particle. The latter is surrounded by a diffuse spherical cloud formed by the remaining dissociated (free) counterions and characterized by its Debye length, which in this model is approximated as

$$\chi^{-1} = \sqrt{\frac{\varepsilon_0 \varepsilon_M D}{\kappa_M}} \tag{10}$$

D is the diffusion coefficient of the free counterions.

Grosse showed that such a system exhibits two distinct dielectric relaxation processes and for small particle volume fractions, $\phi \ll 1$, assuming $R_G \gg \chi^{-1}$, he obtained analytical expressions for the amplitudes and relaxation times of both processes.[46] The lower-frequency mode, j = 1 of this study, arises from fluctuations of the diffuse ion cloud

with relaxation time

$$\tau_1 \approx \frac{R_G^2}{D} \tag{11}$$

and amplitude

$$S_1 = \frac{9\phi\varepsilon_M \left(\frac{2\chi\lambda_S}{\kappa_M}\right)^4}{16\left[\frac{2\chi\lambda_S}{\kappa_M}\left(\frac{2\lambda_S}{\kappa_M R_G}+1\right)+2\right]^2} \tag{12}$$

The higher-frequency mode, $j = 2$, is due to the tangential hopping motion, expressed as surface conductance, λ_S, of condensed counterions on the surface of the particle, located at R_G. Its relaxation time is given by

$$\tau_2 = \frac{\varepsilon_0\varepsilon_M\left(\frac{\varepsilon_P}{\varepsilon_M}+2\right)}{\kappa_M\left(\frac{2\lambda_S}{R_G\kappa_M}+2\right)} \tag{13}$$

and the corresponding amplitude is

$$S_2 = \frac{9\phi\varepsilon_M\left(\frac{2\lambda_S}{R_G\kappa_M}-\frac{\varepsilon_P}{\varepsilon_M}\right)^2}{\left(\frac{\varepsilon_P}{\varepsilon_M}+2\right)\left(\frac{2\lambda_S}{R_G\kappa_M}+2\right)^2} \tag{14}$$

The Grosse model assumes R_G as the effective radius of the micelle, *i.e.* also the layer occupied by the condensed counterions and the solvent therein is attributed to the micelle. Thus the corresponding volume fraction of micelles in the solution is given by

$$\phi = \frac{4}{3}\pi R_G^3 N_A \cdot \frac{c - cmc}{N} \tag{15}$$

with N as the aggregation number. This view is supported by a recently published combined DRS and SAXS study.[55] The surface conductance can be directly linked to a surface diffusion coefficient, D^S, of the bound counterions by

$$D^S = \frac{4\pi k_B T \lambda_S R_G^2}{\beta e_0^2 N} \tag{16}$$

where e_0 is the elementary chargeand β was taken from Table 1.[31]

Using the experimentally acquired relaxation parameters (τ_1, S_1, τ_2, S_2) as input data either all four equations of the Grosse model, eqs 11-14, or selections of them were simultaneously solved in a weighted fit (see Supporting Information for details) to yield the micelle-specific parameters Grosse radius, R_G, aggregation number, N, and surface conductance, λ_S. In this procedure the conductivity of the medium, κ_M, was set equal to the dc conductivity of the solution, *i.e.* $\kappa_M = \kappa(c)$. For the relative permittivity of the medium the value of pure water at 45 °C, $\varepsilon_M = 71.523$, was taken whereas $\varepsilon_P = 2$, typical for pure liquid hydrocarbons was assumed.[56] The diffusion coefficients of the free counterions, of charge number $z = -1$, at 45 °C were calculated according to

$$D = \frac{RT}{F^2} \cdot \frac{\lambda^\infty}{|z|} \tag{17}$$

from their ionic conductivities at infinite dilution, λ^∞, using published 25 °C values for the anions[56,57] scaled to 45 °C using Walden's rule.[58] In eq 17 F is the Faraday constant. Obtained values for D are (3.32, 3.26 & 1.89)$\times 10^{-9}$ m^{2}s^{-1} for Br^-, I^- & TfO^- respectively.

Table 4: Grosse radius, R_G, aggregation number, N, surface conductance, λ_S, surface diffusion coefficient, D^S, of the condensed counterions, and ratio D^S/D of the diffusion coefficients of condensed and free counterions for the investigated [C_{12}MIM]X micelles at 45 °C and for comparable [C_{12}TA]X micelles from the literature.

.

surfactant	$\frac{R_G}{10^{-9}\text{m}}$	N	$\frac{\lambda_S}{10^{-9}\Omega^{-1}}$	$\frac{D^S}{10^{-9}\text{m}^2\text{s}^{-1}}$	D^S/D
[C_{12}MIM]Br	1.83	29	3.59	1.40	0.42
[C_{12}MIM]I	2.32	72	3.64	0.76	0.23
[C_{12}MIM]TfO	2.88	180	2.05	0.26	0.14
[C_{12}TA]Br	2.17[a]	47[a]	2.43[a]	0.64[b]	0.32[b]
	2.26[c]	52[c]	3.00[c]	1.08[c]	0.37[c]
[C_{12}TA]TfO	2.21[c]	55[c,d]	2.12[c]	0.45[c]	0.27[c]

[a] Ref. 29 and [b] Ref. 31, both for 25 °C; [c] Ref. 32 (45 °C); [d] N fixed.

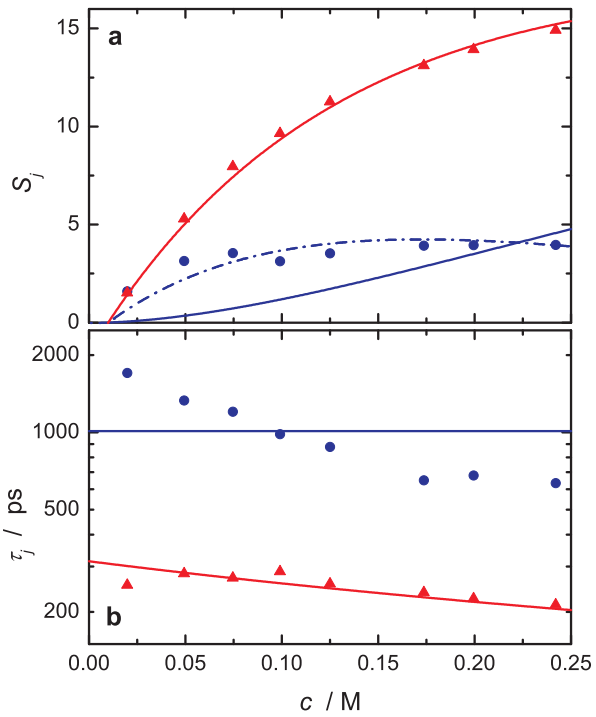

Figure 6: (a) Experimental amplitudes, S_j, and (b) relaxation times, τ_j, of the micellar relaxation processes $j = 1$ (●) and $j = 2$ (▲) of [C_{12}MIM]Br at 45 °C. The correspondingly colored lines represent the description with Grosse's model when S_1 is omitted in the fit. The dash-dotted line gives the fit of S_1 with adjusted Debye length, χ_{emp}^{-1}.

Figures 6, S12 & S13 show the outcome of these fits. For all three SAILs it turned out that, similar to sodium dodecylsulfate (SDS) solutions,[30] the Grosse model was not able to capture S_1 as the calculated amplitude had the wrong curvature. Additionally, τ_1 was largely overestimated when all four equations, eqs 11-14, were simultaneously solved, see Fig. S12. Significantly better descriptions of τ_1, τ_2 and S_2 were obtained when eq 12 was omitted. Since the Debye length only enters eq 12 and for SDS a good description of S_1 was obtained with an (albeit counter-intuitive) empirical modification[30] of χ^{-1} it is reasonable to assume that also for the present surfactants neither the conventional expression[58] for the Debye length nor Grosse's modification, eq 10, is valid. Accordingly, we focus the discussion on fits involving only eqs 11, 14 & 13, which yielded the Grosse radii, R_G, association numbers, N, and surface conductivities, λ_S, summarized in Table 4. However, note that with these R_G, N and λ_S values also a good description of the ion-cloud amplitude, S_1, can be achieved if for the effective Debye length a concentration dependence of the form

$$\chi_{\text{emp}}^{-1} = a_0 + a_1 \times c \tag{18}$$

is assumed (dash-dotted lines in Figs. 6, S12 & S13). The corresponding parameters, a_0 & a_1, are summarized in Table S13.

In the case of [C_{12}MIM]Br the amplitude S_2 was well reproduced over the entire concentration region (Fig. 6). However, for the other two surfactants S_2 was systematically overestimated at $c \gtrsim 100$ mM (Figs. S12 & S13). Similar deviations were found for [C_{12}TA]X solutions, albeit at significantly higher concentration.[29] The relaxation time of the surface-hopping mode, τ_2, was always well met but in particular for the bromide the experimental τ_1 values exhibit a marked decrease with c, whereas the Grosse model predicts a constant value.[59] This contrasts the behavior of [C_{12}TA]X and SDS solutions where the experimental τ_1 does not vary much.[29,30,32]

Viscosity

Figure 7 reveals rather different rheological behavior of the three SAILs. The viscosity of [C_{12}MIM]Br solutions increases only weakly with concentration, whereas for [C_{12}MIM]I η considerably rises at c > 150 mM although the entire concentration range could still be fitted with an exponential function. In contrast to that, the viscosity of [C_{12}MIM]TfO solutions rapidly takes off at $c \approx$ 30 mM, following a power law up to ~ 100 mM but then remains essentially constant. This suggest a gradual transition from spherical to rod-like micelles for the iodide, whereas for the triflate this transition is much sharper and apparently associated with a rapid growth of the average rod length.[60] According to Kern *et al.*[61] the subsequent plateau of η indicates that for triflate the maximum rod length is reached and orientational correlations among the micelles due to electrostatic interactions now dominate rheology.

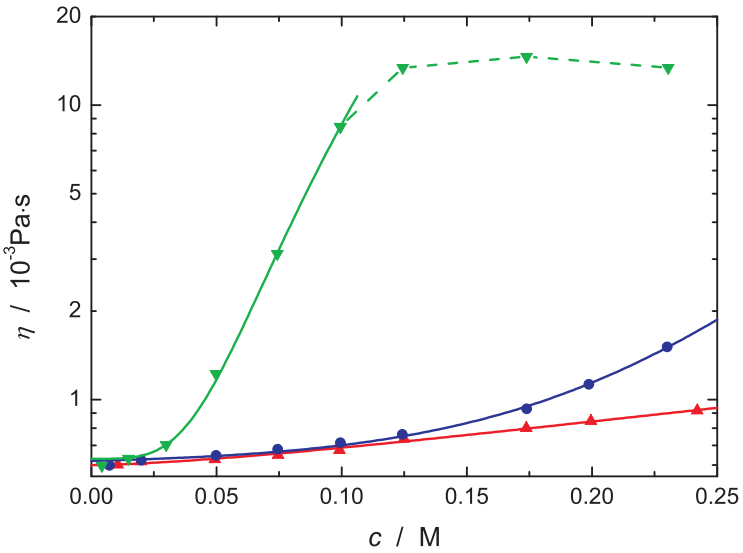

Figure 7: Viscosity, η, as function of solute concentration, c, of aqueous solutions of [C_{12}MIM]Br (▲), [C_{12}MIM]I (●) and [C_{12}MIM]TfO (▼) at 45 °C (lines as a guide to the eye, with solid lines representing fits with exponential functions).

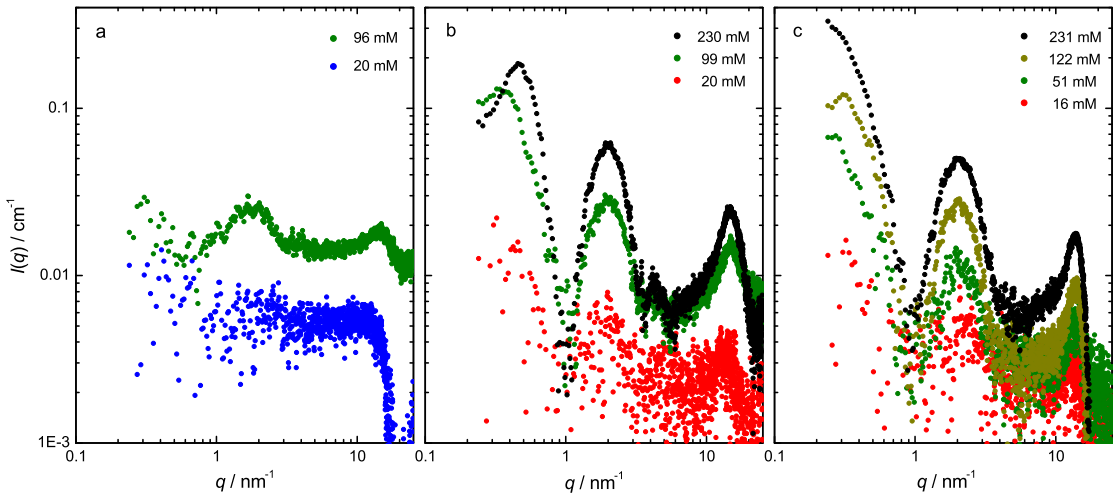

Figure 8: Small-and-wide angle X-ray scattering spectra of aqueous (a) [C_{12}MIM]Br, (b) [C_{12}MIM]I and (c) [C_{12}MIM]TfO solutions at room temperature. $I(q)$ is the absolute SWAXS intensity. The contribution of water to $I(q)$ was removed for clarity.

SWAXS

Figure 8 shows the obtained SWAXS spectra of aqueous [C_{12}MIM]Br (panel a), [C_{12}MIM]I (b) and [C_{12}MIM]TfO (c) solutions, where the peak at 20 nm^{-1} associated with the O–O pair correlation of the solvent was subtracted for clarity. Due to the limited sensitivity of the instrument and the low scattering contrast of [C12MIM]Br micelles against H_2O, no change in the intensity compared to water was observed for [C_{12}MIM]Br at the solute concentration of 20 mM but at 96 mM two weak oscillations at $q \approx 2\,nm^{-1}$ and (just detectable) ~4.2 nm^{-1} were found. Similar oscillations were also observed for iodide and triflate but much stronger and rapidly increasing with concentration. Such a scattering pattern is indicative for scatterers consisting of a core-shell system with excess electron density in the shell.[62–64] For the present [C_{12}MIM]X micelles this observation reflects the high degree of counterion condensation, in particular for I^- and TfO^- (Table 1).

For [C_{12}MIM]I and [C_{12}MIM]TfO a strong rise of the scattering intensity was observed at $q < 1\,nm^{-1}$ when m exceeded 50 mM (Fig. 8b & c). This indicated formation of objects larger than ~ 5 to 10 nm. Their average radius clearly exceeded the radius of ~ 2.1 nm

expected for a spherical micelle of $[C_{12}MIM]^+$ ions from geometry.[65] Due to the limited q range of our instrument the region of constant $I(q)$ at $q \to 0$ was not reached and thus an unambiguous determination of the characteristic parameters of the scatterers impossible. Nevertheless, the obtained data support the inference from rheology of a transition from spherical to ellipsoidal or even rod-like micelles with increasing concentrations of $[C_{12}MIM]I$ and $[C_{12}MIM]TfO$.[62–64] For $[C_{12}MIM]Br$ solutions the very low scattering length density difference between micelles and solvent prevented detection of the characteristic low-q pattern by SWAXS but the small-angle neutron scattering study of Kusano *et al.*[66] provided clear evidence for the transition from spherical to ellipsoidal micelles also for this SAIL. However, with $R_{max}/R_{min} < 1.8$ the axis ratio remained small for $[C_{12}MIM]Br$ micelles. The latter finding probably explains the only moderate increase of the present viscosity data with c.

Discussion

Hydration. The results presented in Table 3 and Fig. 5 show that the total hydration numbers of all three SAILs are essentially the same and independent of concentration for $c \leq 250$ mM. By definition DRS hydration numbers, Z_i (i =t, s & ib), refer to one equivalent of solute and for salts are thus the sum of cation and anion contributions, Z_i^+ & Z_i^-. The present finding, $Z_t \approx 10 \ldots 12$, already suggests that the hydration of free anions might be negligible. Indeed, it is well known that the present anions are only weakly hydrated[50,52,53] Accordingly, previous DRS studies yielded $Z_t^- = 0$ for Br^-[26] and I^-.[67] To our knowledge no DRS data are available for TfO^- but $Z_t^- \approx 0$ can probably also be assumed for this ion.[32,53] The effective hydration numbers of Table 3 can thus be safely attributed to the micelles, more exactly: to the polar region formed by the cationic headgroups and condensed counterions. Interestingly, the present data significantly exceed the value of $Z_t^+ \approx 2$ found for the $[C_4MIM]^+$ cation, which does not form micelles.[68] This indicates a significant

degree of cooperativity in the hydration of $[C_{12}MIM]^+$ micelles. With regard to the total hydration number, Z_t, this cooperative effect does obviously not depend on the condensed anion. However, the amount of frozen water, expressed by Z_{ib}, varies markedly from nil for the TfO^- SAIL via increasingly relevant at $c > 125$ mM for Br^- to permanently present for I^-. This clearly indicates that at least for the two halide SAILs bound water molecules simultaneously interact with charged imidazolium headgroups of the micelle **and** condensed counterions and thus get trapped.

In that context, it is interesting to note that according to MD simulations even at a molar ratio of 1:200 of solute to solvent a significant fraction of the cations is still coordinated to anions in aqueous $[C_4MIM]Br$.[69] In these solutions, where no micelles are formed, H_2O molecules act as a bridge between anion and cation. Indications for such cooperative water binding by ion pairs also come from a Car-Parinello study[70] of aqueous $[C_2MIM]Cl$. Additionally, the formation of ib water for $[C_nTA]$-halide micelles was interpreted in that way.[28,32] Interestingly, however, the latter are much stronger hydrated than the present imidazolium micelles, with Z_t values of 20 to 27 and in particular $Z_{ib} \approx 10...14$, see Table 3. The large Z_t values for $[C_nTA]$ halide micelles indicated penetration of H_2O molecules beyond the rather flexible headgroup layer,[28,31] confirming thus information from other methods on these surfactants.[71–73] In contrast to that, Bhargava and Klein found no water molecules and counterions inside the quasi-spherical cation aggregates of $[C_nMIM]Br$ (n = 10, 12, 14, 16) forming spontaneously in their molecular dynamics simulations.[74] Apparently, the surface of $[C_{12}MIM]^+$ micelles is better "sealed" against water penetration (and as a consequence presumably more rigid). A possible reason might be $\pi - \pi$ interactions among the planar imidazolium rings which were found to be relevant for $[C_1MIM]Cl$ (albeit in the gas phase)[75] and for $[C_nMIM]Br/p$-xylene/water mixtures with n = 12, 14 & 16.[76] However, it must be noted that for binary aqueous $[C_nMIM]Br$ solutions such interactions were only identified for n = 16.[74]

Interestingly, the Z_t values of $[C_{12}MIM]TfO$ and $[C_{12}TA]TfO$ agree within error limits,

Table 3. Based on information from various techniques, Lima *et al.* suggested that in the case of [C_{12}TA]TfO the slightly amphiphilic triflate anions insert into the headgroup layer, leading to large disc-shaped micelles with a rather "sealed" surface in contact with the solvent.[32,33,77] Hydration is thus reduced here mainly for steric reasons. A similar situation may apply also for [C_{12}MIM]TfO although the observed rheology (Fig. 7) suggests rod-like micelles for this surfactant. Obviously, DRS cannot directly monitor whether triflate anions insert into the imidazolium layer but it is interesting to note that in contrast to the other SAILs no ib water was found. Instead, the retardation factor, $r = \tau_3/\tau_4 \approx 18$, for the hydrating slow H_2O molecules is rather large and independent of T and c. Their activation enthalpy, $\Delta H^{\neq}(\tau_3)$, of this mode is similar to bulk water, thus the binding strength to the micelle surface is similar to H_2O-H_2O interactions. On the other hand, the activation entropy is definitely smaller than the bulk value, if not even negative (Table 2). This suggests that —in contrast to the halide SAILs— for [C_{12}MIM]TfO the large r value arises from a shielding of the hydrating H_2O against approaching new H-bond partners by the micelles. Accordingly, τ_3 is here dominated by the volume excluded to the rotation of these water molecules.[50]

For the halide SAILs $\Delta H^{\neq}(\tau_3) > \Delta H^{\neq}(\tau_4)$ (Table 2). Whilst for the iodide the activation enthalpy of the slow-water relaxation exceeds the bulk-water value only by ~40 % with a moderate and roughly constant retardation factor of $r \approx 6$, $\Delta H^{\neq}(\tau_3)$ is five times larger for the bromide with a strongly T-dependent retardation factor, dropping from $r \approx 39$ at 25 °C to ~3.3 at 65 °C. For both SAILs the activation entropy of τ_3 is clearly positive, suggesting that the transition state for the rotation of these hydrating H_2O molecules is less "ordered". Thus, hydrogen-bond breaking is probably involved in the rate-determining step. Keeping in mind that, similar to aqueous [C_4MIM]Br[69] and [C_2MIM]Cl,[70] the involved H_2O molecules probably bind simultaneously to a cation in the headgroup layer and a condensed anion sitting on top of that, this would also explain the high $\Delta H^{\neq}(\tau_3)$ values. However, without detailed molecular-level information, *e.g.* from MD simulations

or time-resolved vibrational spectroscopy, this remains speculation as does an answer to the question why for I^- ib water is observed over the entire concentration range whereas for Br^- this becomes detectably only for $c > 125$ mM. In any case, hydration seems to be a "local" property of the micelle surface which does not reflect the apparently large variation of micelle shape with c for $[C_{12}MIM]I$ and in particular for $[C_{12}MIM]TfO$ that is suggested by the rheological behavior of these SAILs (Fig. 7).

Micelle Properties. The estimated Grosse radii, R_G, and aggregation numbers, N, rise in the order of $[C_{12}MIM]Br < [C_{12}MIM]I < [C_{12}MIM]TfO$ (Table 4). The surface conductivities, λ_S, of the bromide and iodide SAILs are practically the same but that of the triflate is significantly reduced. This is compatible with the assumption that, similar to $[C_{12}TA]TfO$,[32,33,77] also for $[C_{12}MIM]TfO$ micelles the condensed anions are inserted in the headgroup layer. Compared to their bulk values the diffusion coefficients of the anions on the micelle surface are always considerably reduced, with D^S/D decreasing in the order $Br^- > I^- > TfO^-$.

Grosse theory[46] assumes micelles to be spherical, with R_G giving the location of the center of the condensed counterions relative to the center of the micelles. The Debye length should be negligible compared to R_G and micelle-micelle interactions absent. Clearly, these conditions are not really met by the present SAIL solutions. The observed rheology (Fig. 7) and the SWAXS data (Fig. 8) suggest non-spherical micelles for the iodide and, in particular, for the triflate. Additionally, in the covered concentration range $R_G < \chi^{-1}$ in all cases. Even more, almost from the *cmc* the average center-to-center distance, d, of (assumed spherical) micelles with aggregation number N (Table 4) is smaller than $2(R_G + \chi^{-1})$ (Fig. 9). Thus, ion clouds overlap and therefore micelle-micelle interactions are present. This probably explains why the ion-cloud amplitude, S_1, cannot be reproduced with eq 10 or the conventional expression[58] for χ^{-1} but also raises the question how relevant the present Grosse parameters, Table 4, are. As discussed below, it turns out that indeed useful information can be extracted from the analysis of the two micelle-specific modes.

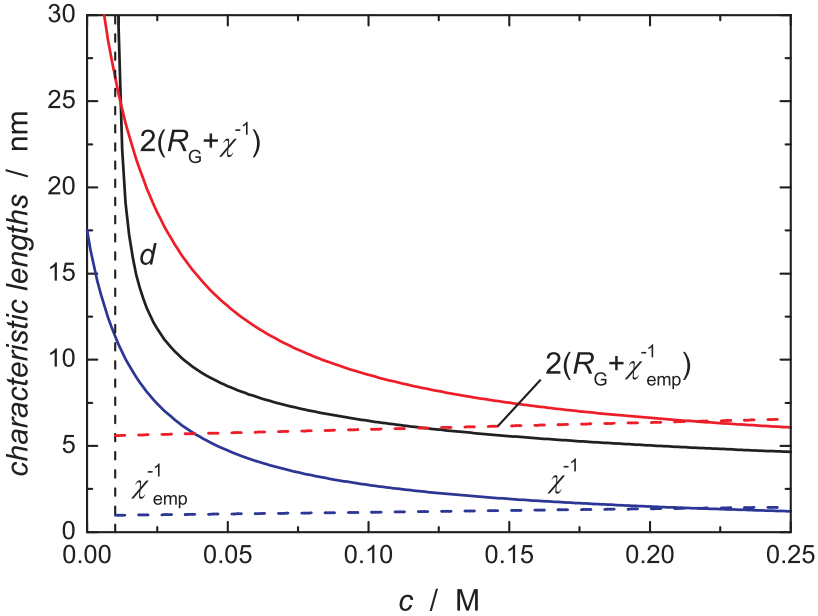

Figure 9: Characteristic lengths in aqueous [C_{12}MIM]Br solutions assuming spherical micelles of aggregation number N = 29: micelle center-to-center distance, d; Debye length according to eq 10, χ^{-1}, and empirical value derived from S_1 with eq 12, χ^{-1}_{emp}; effective micelle diameters, $2(R_{\mathrm{G}} + \chi^{-1})$ and $2(R_{\mathrm{G}} + \chi^{-1}_{\mathrm{emp}})$.

For [C_{12}MIM]Br a number of literature data on micelle size and shape are available. Using luminescence quenching Vanyur *et al.*[78] and Wang et al.[79] reported N = 44, whereas Šarac *et al.*[16] determined a value of 16.82 with conductivity measurements. According to the MD simulations of Bhargava *et al.*[74] [C_{12}MIM]Br forms quasi-spherical but rather open aggregates with a most probable aggregation number of N = 22 at c = 716 mM. This contrasts the small-angle neutron scattering (SANS) results of Kusano *et al.*,[66] where micelles change from spherical (N = 85.96) at 42.5 mM to ellipsoidal at $c \geq$ 91.6 mM, reaching an axis ratio of 1.74 and an aggregation number of 154.3 at 1040 mM. With ~2.0 nm the minor radius of the ellipsoid found in that study remains practically constant and is somewhat shorter than the length of a stretched cation, 2.10 nm,[80] but significantly larger than the present R_{G} value of 1.83 nm. Cognigni *et al.* did not report aggregation numbers but deduced an effective radius increasing from 2.24 nm at 25 mM to 2.57 nm at 100 mM with constant core radius, ~0.97 nm, for the spherical core-shell model fitted to

their SAXS data.[2]

Obviously, the aggregation number of [C_{12}MIM]Br micelles is not well known. In part, this certainly reflects that reported values were determined at different concentrations but certainly more relevant is the applied method. On the other hand, there seems to be consensus on the spherical shape of [C_{12}MIM]Br micelles close to *cmc*. According to Kusano *et al.*[66] the aggregates get more and more ellipsoidal with rising surfactant concentration but even at 1040 M the micelles are far from cylindrical shape. This explains why viscosity rises only weakly with c for this compound (Fig. 7) despite expected micelle-micelle interactions (Fig. 9). In the concentration range covered by the present investigation, $c < 250$ mM, the axis ratio of the ellipsoidal micelles reaches ~1.6 at maximum.[66] Apparently, this is close enough to spherical for the assumptions of Grosse's theory[46] as amplitude, S_2, and relaxation time, τ_2, of the mode solely governed by micelle-specific parameters ($N = 29$, $R_G = 1.83$ nm, $\lambda_S = 3.59 \times 10^{-9}\,\Omega^{-1}$) are well described by eqs 14 & 13 at all c (Fig. 6).

Compared to the data for [C_{12}TA]Br (Table 4) the present values for N and R_G of [C_{12}MIM]Br are rather low. In Fig. 10 the corresponding effective volume fraction of micelles, calculated with eq 15 is compared with the result

$$\phi(c) = \frac{c_b(cmc) - c_b(c)}{c_w(0)} \tag{19}$$

obtained from the DRS-detected concentration of bulk-like water, c_b.[28] Except for the highest concentration the two independent approaches yield the same ϕ values for [C_{12}MIM]Br micelles. A similar agreement was previously obtained for the much better characterized [C_{12}TA]Br micelles,[31] lending thus credit to the Grosse parameters of Table 4 and the assumption of essentially spherical aggregates up to 250 mM for this imidazolium SAIL.

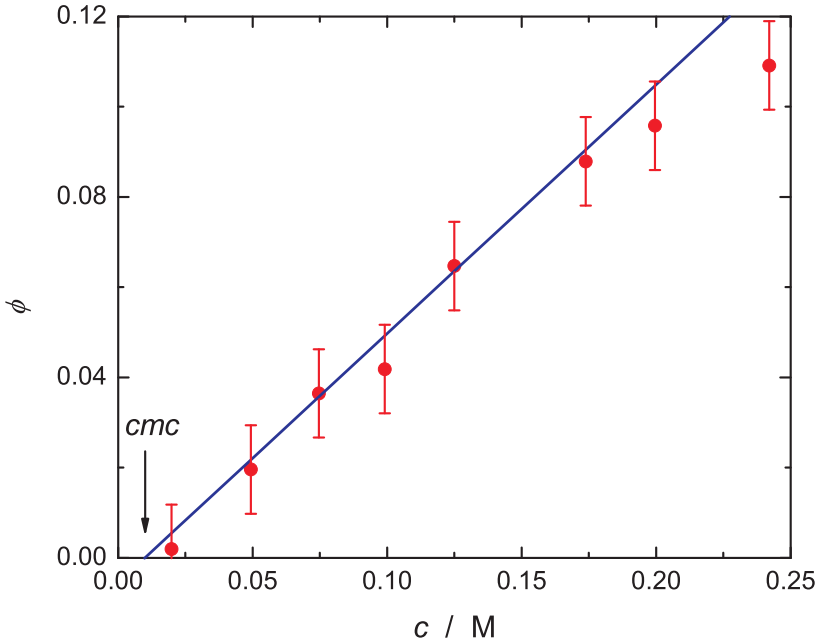

Figure 10: Effective volume fraction, ϕ, of [C_{12}MIM]Br micelles in aqueous solution calculated from Grosse radius, R_G, and aggregation number, N, with eq 15 (solid line), and independently from the bulk water amplitude, S_b, via eq 19 (●).

Further support for the present R_G and N values of [C_{12}MIM]Br comes from the favorable comparison of the associated effective monomer volume, $V_G^m = (4\pi R_G^3)/(3N) = 0.855\,\mathrm{nm}^3$ (Table 5) with the volume of the bare, $V_\phi^m = V_\phi^{mic}/N_A$, and the hydrated monomer

$$V_{\phi,\mathrm{hyd}}^m = \left[V_\phi^{mic} + Z_t \times V^\circ(H_2O)\right]/N_A \tag{20}$$

calculated from the apparent molar volume of the surfactant in the micelle, V_ϕ^{mic}, and the molar volume of water at 45 °C, $V^\circ(H_2O) = 18.193\,\mathrm{cm^3mol^{-1}}$ (Table 5).[81] Note that for [C_{12}MIM]Br the difference between V_G^m and $V_{\phi,\mathrm{hyd}}^m$ corresponds to a single additional hydrating H_2O molecule, which is within the uncertainty of Z_t for this surfactant.

To the best of our knowledge no numerical information on the size and shape of [C_{12}MIM]I and [C_{12}MIM]TfO micelles is available in the literature. Also the present SWAXS data (Fig. 8) did not allow reliable extraction of this information. Using isothermal titration calorimetry, Šarac *et al.*[16] obtained aggregation numbers of 17.6 for the first and of

Table 5: Effective monomer volume in the micelle from Grosse's model, V_G^m, and molecular volumes V_ϕ^m and $V_{\phi,hyd}^m$ calculated from the apparent molar volume of the micelle without and with taking micelle hydration into account, see text.

.

surfactant	$\frac{V_G^m}{nm^3}$	$\frac{V_\phi^m}{nm^3}$	$\frac{V_{\phi,hyd}^m}{nm^3}$
$[C_{12}MIM]Br$	0.855	0.511	0.825
$[C_{12}MIM]I$	0.726	0.532	0.889
$[C_{12}MIM]TfO$	0.556	0.598	0.907

16.9 for the second SAIL but judging from the available data for the bromide surfactant, see above, these numbers appear to be rather small. On the other hand, also the present N and R_G values (Table 4) for $[C_{12}MIM]I$ and in particular for $[C_{12}MIM]TfO$ are unrealistic because only at low c the effective volume fraction of micelles, ϕ, derived from the bulk-water amplitude, eq 19, agrees with that derived from the Grosse radius, eq 15. With increasing concentration the values obtained from S_b grow considerably faster than those calculated from the micelle relaxation (Figs. S14 & S15). By the same token, the effective monomer volumes, V_G^m, calculated from R_G and N are significantly smaller than the $V_{\phi,hyd}^m$ values obtained from apparent molar volumes (Table 5). Since the Grosse model also failed reproducing S_2 at $c > 75$ mM for $[C_{12}MIM]I$ (Fig. S12) and $c > 125$ mM for $[C_{12}MIM]TfO$ (Fig. S13), these observations are probably a consequence of the tendency of these surfactants to form rod-like micelles, as suggested by their rheology (Fig. 7) and SWAXS data (Fig. 8). Due to the limited data base no systematic study of the impact of micelle shape on surface conductance, λ_S, and diffusion coefficient, D^S, is possible yet but almost certainly the values (Table 4) for $[C_{12}MIM]I$ and $[C_{12}MIM]TfO$ are unreliable at $c > 75$ mM respectively 125 mM.

At 25 °C a linear correlation between the relative surface diffusion coefficient, D^S/D, and the degree of counterion dissociation, $1-\beta$, was observed for $[C_nTA]X$ surfactants with halide anions.[31] Interestingly, the present data for $[C_{12}MIM]Br$ and $[C_{12}MIM]I$ together

with those for [C_{12}TA]Cl and [C_{12}TA]Br at 45 °C[32] form a straight line shifted parallel to the room-temperature data (Fig. S16), whereas those for [C_{12}MIM]TfO, [C_{12}TA]TfO and [C_{12}TA]MS (MS: methylsulfate) are off, with both triflates in opposite directions. The increase of D^S/D with $(1-\beta)$ appears reasonable as reduced counterion condensation means more unoccupied and thus accessible binding sites for the hopping anions. [C_{12}TA]TfO micelles are disk-shaped with the triflate counterions inserted in the headgroup layer,[73,77] whereas the present rheological data (Fig. 7) suggest rods for [C_{12}MIM]TfO.[60,61] This may explain their opposing deviations in Fig. S16. In any case, for [C_{12}MIM]TfO the surface diffusion coefficient of the anion is significantly smaller than that of the two studied halides, suggesting insertion of TfO^- anions into the headgroup layer.

As already indicated, the ion-cloud amplitude, S_1, cannot be reproduced with eq 10 or the conventional expression[58] for χ^{-1} (Figs. 6, S12 & S13). For micellar solutions of SDS it was found that the assumption of a linearly increasing Debye length, eq 18, provided an excellent description of S_1 over the entire concentration range studied.[30] This was also the case for [C_{12}MIM]Br, Fig. 6. For the two other SAILs the fit was excellent for $c < 150$ mM but then the experimental S_1 deviated from the prediction, Figs. S12 & S13. However, in all three cases eq 18 predicts the correct concave curvature of the experimental data. The intercepts, a_0, and slopes, a_1, obtained by fitting S_1 with eq 12, using the R_G and N values of Table 4 as fixed input, are summarized in Table S13. Most noteworthy, this empirical expression for χ^{-1} does not show the marked decrease with rising c expected from Debye theory but a weak increase, reaching the values given by eq 10 only at $c \approx 200$ mM (Fig. 9). As a consequence, the average separation, d, of the micelles exceeds the effective micelle diameter, $2(R_G + \chi^{-1}_{emp})$, at $c \lesssim 100$ mM for all three SAILs. At present, it cannot be decided whether the need for eq 18 to describe S_1 indicates a general failure of the Grosse model or if at low c Coulomb screening is indeed much weaker for these micelles than conventionally predicted. However, it should be noted that, based on surface-force measurements between charged plates, a recent scaling analysis suggested that also for

concentrated electrolyte solutions the characteristic length of charge screening, *i.e.* the effective Debye length, increases linearly with concentration.[82]

Concluding Remarks

For the investigated [C_{12}MIM]X SAILs the effective total hydration numbers, Z_t^0 (Table 3, Fig. 5), determined from the bulk-water amplitude can be safely assigned to the micelles as the free anions are only weakly hydrated and contributions of the free cations are negligible because of the small *cmc*. All three surfactants bind approximately 10-11 H_2O molecules per imidazolium headgroup. However, there are differences in binding quality. Whilst for the triflate SAIL all bound water is only retarded by a factor of $r \approx 18$, approximately half of the hydrating H_2O is completely frozen (ib) for [C_{12}MIM]I. The bromide SAIL is intermediate as here ib water was detected only for $c > 150$ mM but for lower c solvent retardation is very large ($r \approx 39$) at room temperature. Counterion condensation is much stronger for TfO^- compared to Br^- and I^- (Table 1). At the same time, the surface diffusion coefficient of triflate is much smaller (Table 4). Possibly, this suggests that, similar to [C_{12}TA]TfO,[73,77] also for [C_{12}MIM]TfO the condensed counterions are inserted into the headgroup layer. Halide ions apparently sit on top of the micelles with ib water molecules simultaneously binding to them and the imidazolium cations, comparable to the situation for aqueous [C_2MIM]Cl[70] and [C_4MIM]Br.[69]

Analysis of the two micelle-specific relaxations suggests that —within the sensitivity of Grosse's model— [C_{12}MIM]Br micelles remain essentially spherical in the investigated concentration range. Viscosity data (Fig. 7) but also Grosse radii and aggregation numbers (Table 4), as well as volumetric data (Table 5) indicate that this is not the case for the other two SAILs. In particular [C_{12}MIM]TfO almost certainly forms rod-like micelles (Fig. 8). Apparently for all three surfactants micelle-micelle distances are so small that Grosse's (but also the conventional) expression, eq 10, for the Debye screening length breaks down.

Recently, some of us observed that micelles of [C_{12}MIM]X SAILs were promising catalysts for nucleophilic substitution reactions.[2] However, at least for the chosen model reaction of nitrophenyl diphenyl phosphate (PNPDPP, assumed to be solubilized in the micelle) with acetaldoxime, the catalytic activity strongly depended on the counterion, dropping from a 34-fold rate enhancement for Cl^-, compared to the non-catalyzed reaction, to only 2.3-fold for TfO^-. At least for the halides it appears that the superior performance of [C_{12}MIM]X micelles is due to their weaker hydration compared to [C_{12}TA]X (Table 3), permitting thus easier access of the acetaldoxime anions dissolved in the aqueous phase to the PNPDPP molecules sitting in the micelle. By the same token, due to the increasing condensation of counterions and their simultaneously decreasing mobility (Tables 1 & 4) the surface-charge density of the cationic [C_{12}MIM] micelle becomes less positive and thus less attractive for the aldoxime anion when going from Br^- via I^- to TfO^- as the surfactant counterion in the [C_{12}MIM]X series.

Acknowledgement

The authors thank Pierre Bauduin, Olivier Diat and Bruno Corso for their help with SWAXS measurements. Financial support from the COST action no. CM1206, *Exchange on Ionic Liquids*, is gratefully acknowledged. KB also acknowledges financial support by the Austrian Science Fund (FWF) with grant no. P25504-N28 and TB thanks the BFHZ (Bayerisch-französisches Hochschulzentrum) for grant FK41_15, covering travel expenses, and the DFG Graduate School GRK1626, Chemical Photocatalysis, for financial support.

Supporting Information Available

Tables with data for density, viscosity and conductivity of the investigated solutions. Tables with parameters of the D+D+D+D model fitted to the dielectric spectra and additional Figures illustrating data analysis. This material is available free of charge via the Internet

at http://pubs.acs.org/.

Notes and References

(1) Bica, K.; Gärtner, P.; Gritsch, P. J.; Ressmann, A. K.; Schröder, C.; Zirbs, R. Micellar Catalysis in Aqueous-Ionic Liquid Systems. *Chem. Commun.* **2012**, *48*, 5013–5015.

(2) Cognigni, A.; Gärtner, P.; Zirbs, R.; Peterlik, H.; Prochazka, K.; Schröder, C.; Bica, K. Surface-active Ionic Liquids in Micellar Catalysis: Impact of Anion Selection on Reaction Rates in Nucleophilic Substitutions. *Phys. Chem. Chem. Phys.* **2016**, *18*, 13375–13384.

(3) Walden, P. Molecular Weights and Electrical Conductivity of Several Fused Salts. *Bulletin of the Russian Academy of Sciences: Physics* **1914**, 405–422.

(4) Seddon, K. R.; Stark, A.; Torres, M.-J. Influence of Chloride, Water, and Organic Solvents on the Physical Properties of Ionic Liquids. *Pure Appl. Chem.* **2000**, *72*, 2275–2287.

(5) Welton, T. Room-Temperature Ionic Liquids. Solvents for Synthesis and Catalysis. *Chem. Rev.* **1999**, *99*, 2071–2084.

(6) Wasserscheid, P.; Welton, T. *Ionic Liquids in Synthesis*; Wiley-VCH, 2007.

(7) Plechkova, N. V.; Seddon, K. R. Applications of Ionic Liquids in the Chemical Industry. *Chem. Soc. Rev.* **2007**, *37*, 123–150.

(8) Kohno, Y.; Ohno, H. Ionic Liquid/Water Mixtures: From Hostility to Conciliation. *Chem. Commun.* **2012**, *48*, 7119–7130.

(9) Chaban, V. V.; Prezhdo, O. V. Ionic and Molecular Liquids: Working Together for Robust Engineering. *J. Phys. Chem. Lett.* **2013**, *4*, 1423–1431.

(10) Hayes, R.; Warr, G. G.; Atkin, R. Structure and Nanostructure in Ionic Liquids. *Chem. Rev.* **2015**, *115*, 6357–6426.

(11) Bruce, D. W.; Cabry, C. P.; Canongia Lopes, J. N.; Costen, M. L.; D'Andrea, L.; Grillo, I.; Marshall, P. C.; McKendrick, K. G.; Minton, T. K.; Purcell, S. M.; Rogers, S.; Slattery, J. M.; Shimizu, K.; Smoll, E.; Tesa-Serrate, M. A. Nanosegregation and Structuring in the Bulk and at the Surface of Ionic-Liquid Mixtures. *J. Phys. Chem. B* **2017**, *121*, 6002–6020.

(12) Greaves, T. L.; Drummond, C. J. Solvent Nanostructure, the Solvophobic Effect and Amphiphile Self-assembly in Ionic Liquids. *Chem. Soc. Rev.* **2013**, *42*, 1096–1120.

(13) Blesic, M.; Marques, M. H.; Plechkova, N. V.; Seddon, K. R.; Rebelo, L. P. N.; Lopes, A. Self-aggregation of Ionic Liquids: Micelle Formation in Aqueous Solution. *Green Chem.* **2007**, *9*, 481–490.

(14) Łuczak, J.; Hupka, J.; Thöming, J.; Jungnickel, C. Self-organization of Imidazolium Ionic Liquids in Aqueous Solution. *Colloids Surf., A* **2008**, *329*, 125–133.

(15) Tariq, M.; Freire, M. G.; Saramago, B.; Coutinho, J. A. P.; Canongia Lopes, J. N.; Rebelo, L. P. N. Surface Tension of Ionic Liquids and Ionic Liquid Solutions. *Chem. Soc. Rev. 41*, 829–868.

(16) Šarac, B.; Medoš, Ž.; Cognigni, A.; Bica, K.; Chen, L.-J.; Bešter-Rogač, M. Thermodynamic Study for Micellization of Imidazolium Based Surfaceactive Ionic Liquids in Water: Effect of Alkyl Chain Length and Anions. *Colloids Surf. A: Physicochem. Eng. Aspects* **2017**, *http://dx.doi.org/10.1016/j.colsurfa.2017.01.062*.

(17) Tanford, C. *The Hydrophobic Effect: Formation of Micelles and Biological Membranes*; Wiley: New York, 1980.

(18) Łuczak, J.; Jungnickel, C.; Markiewicz, M.; Hupka, J. Solubilization of benzene, toluene, and xylene (BTX) in aqueous micellar solutions of amphiphilic imidazolium ionic liquids. *J. Phys. Chem. B* **2013**, *117*, 5653–5658.

(19) Svinyarov, I.; Bogdanov, M. G. Ionic Liquid-assisted Micellar Extraction for the Quantitative Determination of Sesquiterpenic Acids in *Valeriana officinalis* L. (Caprifoliaceae). *Sep. Sci. Technol.* **2017**, *http://dx.doi.org/10.1080/01496395.2017.1295995*.

(20) Nowicki, J.; Łuczak, J.; Stańczyk, D. Dual functionality of amphiphilic 1-alkyl-3-methylimidazolium hydrogen sulfate ionic liquids: surfactants with catalytic function. *RSC Adv.* **2016**, *6*, 11591–11601.

(21) Cokoja, M.; Reich, R. M.; Wilhelm, M. E.; Kaposi, M.; Schäffer, J.; Morris, D. S.; Münchmeyer, C. J.; Anthofer, M. H.; Markovits, I. I. E.; Kühn, F. E.; Herrmann, W. A.; Jess, A.; Love, J. B. Olefin epoxidation in aqueous phase using ionic-liquid catalysts. *ChemSusChem* **2016**, *9*, 1773–1776.

(22) Cognigni, A.; Kampichler, S.; Bica, K. Surface-active ionic liquids in catalysis: Impact of structure and concentration on the aerobic oxidation of octanol in water. *J. Coll. Interface. Sci.* **2017**, *492*, 136–145.

(23) Evans, D. F.; Wennerström, H. *The Colloidal Domain*, 2nd ed.; Wiley-VCH: New York, 1999.

(24) Kremer, F.; Schönhals, A. *Broadband Dielectric Spectroscopy*; Springer: Berlin, 2002.

(25) Stoppa, A.; Nazet, A.; Buchner, R.; Thoman, A.; Walther, M. Dielectric Response and Collective Dynamics of Acetonitrile. *J. Mol. Liq.* **2015**, *212*, 963–968.

(26) Buchner, R.; Hefter, G. Interactions and Dynamics in Electrolyte Solutions by Dielectric Spectroscopy. *Phys. Chem. Chem. Phys.* **2009**, *11*, 8984–8999.

(27) Eiberweiser, A.; Nazet, A.; Hefter, G.; Buchner, R. Ion Hydration and Association in Aqueous Potassium Phosphate Solutions. *J. Phys. Chem. B* **2015**, *119*, 5270–5281.

(28) Baar, C.; Buchner, R.; Kunz, W. Dielectric Relaxation of Cationic Surfactants in Aqueous Solution. 1. Solvent Relaxation. *J. Phys. Chem. B* **2001**, *105*, 2906–2913.

(29) Baar, C.; Buchner, R.; Kunz, W. Dielectric Relaxation of Cationic Surfactants in Aqueous Solution. 2. Solute Relaxation. *J. Phys. Chem. B* **2001**, *105*, 2914–2922.

(30) Fernandez, P.; Schrödle, S.; Buchner, R.; Kunz, W. Micelle and Solvent Relaxation in Aqueous Sodium Dodecylsulfate Solutions. *ChemPhysChem* **2003**, *4*, 1065–1072.

(31) Buchner, R.; Baar, C.; Fernandez, P.; Schrödle, S.; Kunz, W. Dielectric Spectroscopy of Micelle Hydration and Dynamics in Aqueous Ionic Surfactant Solutions. *J. Mol. Liq.* **2005**, *118*, 179–187.

(32) Lima, F. S.; Chaimovich, H.; Cuccovia, I. M.; Buchner, R. Dielectric Relaxation Spectroscopy Shows a Sparingly Hydrated Interface and Low Counterion Mobility in Triflate Micelles. *Langmuir* **2013**, *29*, 10037–10046.

(33) Lima, F. S.; Cuccovia, I. M.; Buchner, R.; Antunes, F. E.; Lindman, B.; Miguel, M. G.; Horinek, D.; Chaimovich, H. Sodium Triflate Decreases Interaggregate Repulsion and Induces Phase Separation in Cationic Micelles. *Langmuir* **2015**, *31*, 2609–2614.

(34) Glasstone, S.; Laidler, K. J.; Eyring, H. *The theory of rate processes*; McGraw Hill: New York, 1941.

(35) Huddleston, J. G.; Willauer, H. D.; Swatloski, R. P.; Visser, A. E.; Rogers, R. D. Room Temperature Ionic Liquids as Novel Media for 'Clean' Liquid-liquid Extraction. *Chem. Commun.* **1998**, *16*, 1765–1766.

(36) Souza, B. S.; Leopoldino, E. C.; Tondo, D. W.; Dupont, J.; Nome, F. Imidazolium-Based

Zwitterionic Surfactant: A New Amphiphilic Pd Nanoparticle Stabilizing Agent. *Langmuir* **2012**, *28*, 833–840.

(37) Nazet, A.; Sokolov, S.; Sonnleitner, T.; Makino, T.; Kanakubo, M.; Buchner, R. Densities, Viscosities, and Conductivities of the Imidazolium Ionic Liquids [Emim][Ac], [Emim][FAP], [Bmim][BETI], [Bmim][FSI], [Hmim][TFSI], and [Omim][TFSI]. *J. Chem. Eng. Data* **2015**, *60*, 2400–2411.

(38) Zana, R. Ionization of Cationic Micelles: Effect of the Detergent Structure. *J. Colloid Interface Sci.* **1980**, *78*, 330–337.

(39) Buchecker, T.; Krickl, S.; Winkler, R.; Grillo, I.; Bauduin, P.; Touraud, D.; Pfitzner, A.; Kunz, W. The Impact of the Structuring of Hydrotropes in Water on the Mesoscale Solubilisation of a Third Hydrophobic Component. *Phys. Chem. Chem. Phys.* **2017**, *19*, 1806–1816.

(40) Hammersley, A. P. FIT2D: an introduction and overview. *European Synchrotron Radiation Facility Internal Report ESRF97HA02T* **1997**, *68*.

(41) Ao, M.; Kim, D. Aggregation Behavior of Aqueous Solutions of 1-Dodecyl-3-methylimidazolium Salts with Different Halide Anions. *J. Chem. Eng. Data* **2013**, *58*, 1529–1534.

(42) Böttcher, C. F. J.; Bordewijk, P. *Theory of Electric Polarization, Vol. 2*; Elsevier: Amsterdam, 1978.

(43) Sonnleitner, T.; Turton, D. A.; Waselikowski, S.; Hunger, J.; Stoppa, A.; Walther, M.; Wynne, K.; Buchner, R. Dynamics of RTILs: A Comparative Dielectric and OKE Study. *J. Mol. Liq.* **2014**, *192*, 19–25.

(44) Zasetsky, A. Y.; Buchner, R. Quasi-linear Least Squares and Computer Code for

Numerical Evaluation of Relaxation Time Distribution from Broadband Dielectric Spectra. *J. Phys.: Condens. Matter* **2011**, *23*, 025903.

(45) Data for $0.1 \leq \nu/\mathrm{GHz} \leq 89$ from this laboratory[83,84] were extended to 2 THz by interpolated data of Rønne *et al.*[85] The thus obtained spectrum was fitted to a D+D model, keeping the static permittivity fixed to $\varepsilon_s(0) = 71.523$.[86] Obtained parameters for 45 °C are $S_1 = S_c = 66.113$, $\tau_1 = \tau_c = 5.33$ ps, $S_2 = S_f = 2.63$, $\tau_2 = \tau_f = 0.165$ ps and $\varepsilon_\infty = 2.78$.

(46) Grosse, C. Permittivity of a Suspension of Charged Spherical Particles in Electrolyte Solution. 2. Influence of the Surface Conductivity and Asymmetry of the Electrolyte on the Low- and High-frequency Relaxations. *J. Phys. Chem.* **1988**, *92*, 3905–3910.

(47) Zana, R. Critical Micellization Concentration of Surfactants in Aqueous Solution and Free Energy of Micellization. *Langmuir* **1996**, *12*, 1208–1211.

(48) Assuming an effective dipole moment of 5.05 D (MOPAC, COSMO-PM6 functional) for TfO^- the relaxation amplitude at the highest concentration, $c = 250$ mM, is ~0.14 and thus negligible within experimental uncertainty.

(49) Buchner, R.; Barthel, J.; Stauber, J. The Dielectric Relaxation of Water between 0 °C and 35 °C. *Chem. Phys. Lett.* **1999**, *306*, 57–63.

(50) Laage, D.; Stirnemann, G.; Sterpone, F.; Rey, R.; Hynes, J. T. Reorientation and Allied Dynamics in Water and Aqueous Solutions. *Annu. Rev. Phys. Chem.* **2011**, *62*, 395–416.

(51) For pure water, where very precise data are available, plots of τ_s and η *vs.* T^{-1} are notably curved, suggesting a temperature dependence of $\Delta H^{\neq}$ and $\Delta S^{\neq}$ as discussed in Ref. 49.

(52) Migliorati, V.; Sessa, F.; Aquilanti, G.; D'Angelo, P. Unraveling Halide Hydration: A High Dilution Approach. *J. Chem. Phys.* **2014**, *141*, 044509.

(53) Bergström, P.-Å.; Lindgren, J. An Infrared Spectroscopic Study of the Hydration of the Triflate Ion ($CF_3SO_3^-$) in Aqueous Solution. *J. Mol. Struct.* **1990**, *239*, 103–111.

(54) Hubbard, J. B.; Colonomos, P.; Wolynes, P. G. Molecular theory of solvated ion dynamics. III. The kinetic dielectric decrement. *J. Chem. Phys.* **1979**, *71*, 2652–2661.

(55) Sato, T.; Akahane, T.; Amano, K.; Hyodo, R.; Yanase, K.; Ogura, T. Scattering and Spectroscopic Study on the Hydration and Phase Behavior of Aqueous Alcohol Ethoxylate and Methyl Ester Ethoxylate: Effects of Terminal Groups in Hydrophilic Chains. *J. Phys. Chem. B* **2016**, *120*, 5444–5454.

(56) Lide, D. R. *CRC Handbook of Chemistry and Physics, 85th Edition*; CRC Press: Boca Raton, 2004.

(57) Okan, S. E.; Champeney, D. C. Molar Conductance of Aqueous Solutions of Sodium, Potassium, and Nickel Trifluoromethanesulfonate at 25 °C. *J. Solution Chem.* **1997**, *26*, 405–414.

(58) Bockris, J. O.; Reddy, A. K. N. *Modern Electrochemistry*, 2nd ed.; Plenum: New York, 1998; Vol. 1.

(59) Replacement of the present infinite-dilution diffusion coefficients by experimental $D(c)$ values does not improve the situation as diffusion coefficients of free ions generally depend only weakly on concentration.[58]

(60) Rehage, H.; Hoffmann, H. Rheological Properties of Viscoelastic Surfactant Systems. *J. Phys. Chem.* **1988**, *92*, 4712–4719.

(61) Kern, F.; Lequeux, F.; Zana, R.; Candau, S. J. Dynamic Properties of Salt-free Viscoelastic Micellar Solutions. *Langmuir* **1994**, *10*, 1714–1723.

(62) Naskar, B.; Diat, O.; Nardello-Rataj, V.; Bauduin, P. Nanometer-Size Polyoxometalate

Anions Adsorb Strongly on Neutral Soft Surfaces. *J. Phys. Chem. C* **2015**, *119*, 20985–20992.

(63) Bauer, C.; Bauduin, P.; Girard, L.; Diat, O.; Zemb, T. Hydration of sugar based surfactants under osmotic stress: A SAXS study. *Colloids and Surfaces A: Physicochemical and Engineering Aspects* **2012**, *413*, 92–100.

(64) Pedersen, J. S. Analysis of small-angle scattering data from colloids and polymer solutions: modeling and least-squares fitting. *Adv. Colloid Interface Sci.* **1997**, *70*, 171–210.

(65) Schulz, P. C. Steric Fitting of the Spherical Micelle Size. *Colloid Polym. Sci.* **1991**, *269*, 612–619.

(66) Kusano, T.; Fujii, K.; Tabata, M.; Shibayama, M. Small-Angle Neutron Scattering Study on Aggregation of 1-Alkyl-3-methylimidazolium Based Ionic Liquids in Aqueous Solution. *J. Solution Chem.* **2013**, *42*, 1888–1901.

(67) Brandes, E.; Stage, C.; Motschmann, H.; Rieder, J.; Buchner, R. Is Surface Layering of Aqueous Alkali Halides Determined by Ion Pairing in the Bulk Solution? *J. Chem. Phys.* **2014**, *141*, 18C509.

(68) Bešter-Rogač, M.; Stoppa, A.; Hunger, J.; Hefter, G.; Buchner, R. Association of Ionic Liquids in Solution: A Combined Dielectric and Conductivity Study of [bmim][Cl] in Water and in Acetonitrile. *Phys. Chem. Chem. Phys.* **2011**, *13*, 17588–17598.

(69) Migliorati, V.; Zitolo, A.; D'Angelo, P. Using a Combined Theoretical and Experimental Approach to Understand the Structure and Dynamics of Imidazolium-Based Ionic Liquids/Water Mixtures. 1. MD Simulations. *J. Phys. Chem. B* **2013**, *117*, 12505–12515.

(70) Spickermann, C.; Thar, J.; Lehmann, S. B. C.; Zahn, S.; Hunger, J.; Buchner, R.; Hunt, P. A.; Welton, T.; Kirchner, B. Why are Ionic Liquids Mainly Associated in

Water? A Car-Parinello Study of 1-Ethyl-3-methyl-imidazolium Chloride Water Mixture. *J. Chem. Phys.* **2008**, *129*, 104505.

(71) Halle, B.; Carlström, G. Hydration of Ionic Surfactant Micelles from Water Oxygen-17 Magnetic Relaxation. *J. Phys. Chem.* **1981**, *85*, 2142–2147.

(72) Pal, S.; Bagchi, B.; Balasubramanian, S. Hydration Layer of a Cationic Micelle, C_{10}TAB: Structure, Rigidity, Slow Reorientation, Hydrogen Bond Lifetime, and Solvation Dynamics. *J. Phys. Chem. B* **2005**, *109*, 12879–12890.

(73) Lima, F. S.; Chaimovich, H.; Cuccovia, I. M.; Horinek, D. Molecular Dynamics Shows That Ion Pairing and Counterion Anchoring Control the Properties of Trifalte Micelles: A Comparison with Triflate at the Air/Water Interface. *Langmuir* **2014**, *30*, 1239–1249.

(74) Bhargava, B. L.; Klein, M. L. Initial Stages of Aggregation in Aqueous Solutions of Ionic Liquids: Molecular Dynamics Studies. *J. Phys. Chem. B* **2009**, *113*, 9499–9505.

(75) Matthews, R. P.; Welton, T.; Hunt, P. A. Competitive pi Interactions and Hydrogen Bonding within Imidazolium Ionic Liquids. *Phys. Chem. Chem. Phys.* **2014**, *16*, 3238–3253.

(76) Li, X.-W.; Zhang, J.; Dong, B.; Zheng, L.-Q.; Tung, C.-H. Characterization of Lyotropic Liquid Crystals Formed in the Mixtures of 1-Alkyl-3-methylimidazolium Bromide/p-Xylene/Water. *Colloids Surf., A* **2009**, *335*, 80–87.

(77) Lima, F. S.; Cuccovia, I. M.; Horinek, D.; Amaral, L. Q.; Riske, K. A.; Schreier, S.; Salinas, R. K.; Bastos, E. L.; Pires, P. A. R.; Bozelli, J. C.; Favaro, D. C.; Rodrigues, A. C. B.; Dias, L. G.; El Seoud, O. A.; Chaimovich, H. Effect of Counterions on the Shape, Hydration, and Degree of Order at the Interface of Cationic Micelles: The Triflate Case. *Langmuir* **2013**, *29*, 4193–4203.

(78) Vanyur, R.; Biczok, L.; Miskolczy, Z. Micelle Formation of 1-Alkyl-3-methylimidazolium Bromide Ionic Liquids in Aqueous Solution. *Colloids Surf. A* **2007**, *299*, 256–261.

(79) Wang, J.; Wang, H.; Zhang, S.; Zhang, H.; Zhao, Y. Conductivities, Volumes, Fluorescence, and Aggregation Behavior of Ionic Liquids [C_4mim][BF_4] and [$C_n$mim]Br (n = 4, 6, 8, 10, 12) in Aqueous Solutions. *J. Chem. Phys. B* **2007**, *111*, 6181–6188.

(80) Stewart, J. J. *MOPAC 2012*; Stewart Computational Chemistry: Colorado Springs, CO, USA, 2012.

(81) In this calculation it was assumed that the apparent molar volumes of the ILs, calculated from the density values of Tables S1-S3, are equal to V_ϕ^{mic} as for $c > cmc$ the obtained data were constant within error limits.

(82) Lee, A. L.; Perez-Martinez, C. S.; Smith, A. M.; Perkin, S. Scaling Analysis of the Screening Length in Concentrated Electrolytes. *Phys. Rev. Lett.* **2017**, *119*, 026002.

(83) Hölzl, C. Optimierung einer TDR-Apparatur zur Untersuchung der dielektrischen Relaxationvon H_2O, D_2O und wässrigen Tetraalkylammoniumbromidlösungen. Ph.D. thesis, Regensburg University, 1998.

(84) Schrödle, S. Effects of Non-ionic Surfactants and Related Compounds on the Cooperative and Molecular Dynamics of their Aqueous Solutions. Ph.D. thesis, Regensburg University, 2005.

(85) Rønne, C.; Åstrand, P.-O.; Keiding, S. R. THz Spectroscopy of H_2O and D_2O. *Phys. Rev. Lett.* **1999**, *82*, 2888–2891.

(86) Ellison, W. J.; Lamkaouchi, K.; Moreau, J.-M. Water: A Dielectric Reference. *J. Mol. Liq.* **1996**, *68*, 171–279.

Graphical TOC Entry

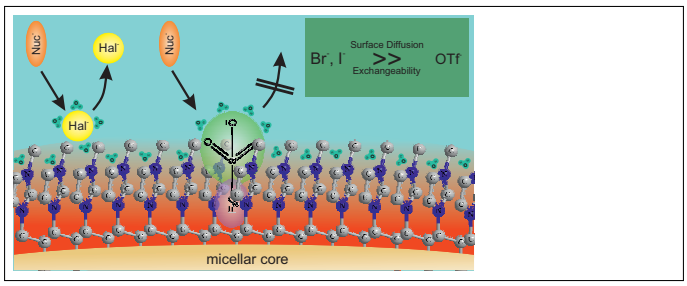

Chapter 4

Application of surface-active ionic liquids in transition metal catalysis

In this chapter the application of surface-active ionic liquids is expanded to palladium catalysed reactions in water. The oxidation of 1-octanol to octanoic acid and the Heck cross coupling reaction between ethyl acrylate and iodobenzene were selected to study the impact of surface-active ionic liquids in transition metal catalysed reactions. In both cases a strong influence of the ionic liquid concentration on the reaction performance was observed. Moreover, a different catalytic behaviour was found depending on the ability of the imidazolium based ionic liquids to form a carbene. After optimization of reaction conditions and ionic liquid concentration, superior performance compared to conventional ammonium surfactant was verified for both processes.

The following manuscripts will be presented in this chapter:

- Cognigni, Alice; Kampichler, Sebastian; Bica, Katharina, **Surface-active ionic liquids in catalysis: Impact of structure and concentration on the aerobic oxidation of octanol in water** *J. Colloid Interface Sci.* **2017**, *492*, 136-145.

As first author I planned and performed a major part of the experimental work, including the tests of catalytic activity with [C_{12}mim]Cl and [$C_{12}m_2$im]Cl both at atmospheric and higher pressure. Additionally, I was solely responsible for the characterization of surface-active ionic liquids. Furthermore I wrote the manuscript.

- Taskin, Meltem; Cognigni, Alice; Zirbs, Ronald; Reimhult, Erik and Bica, Katharina **Surface-active ionic liquids for Palladium-catalysed cross coupling in water: Effect of ionic liquid concentration on the catalytically active species** *RSC Adv.* **2017**, *7*, 41144-41151.

I characterized the aggregation behaviour of the surface-active ionic liquids and performed a major part of the experimental work. I also made a major contribution to the manuscript.

Supporting information for all manuscripts can be found in Appendix B.

Journal of Colloid and Interface Science 492 (2017) 136–145

Contents lists available at ScienceDirect

Journal of Colloid and Interface Science

journal homepage: www.elsevier.com/locate/jcis

Surface-active ionic liquids in catalysis: Impact of structure and concentration on the aerobic oxidation of octanol in water

Alice Cognigni, Sebastian Kampichler, Katharina Bica *

Institute of Applied Synthetic Chemistry, Vienna University of Technology, Getreidemarkt 9/163, 1060 Vienna, Austria

GRAPHICAL ABSTRACT

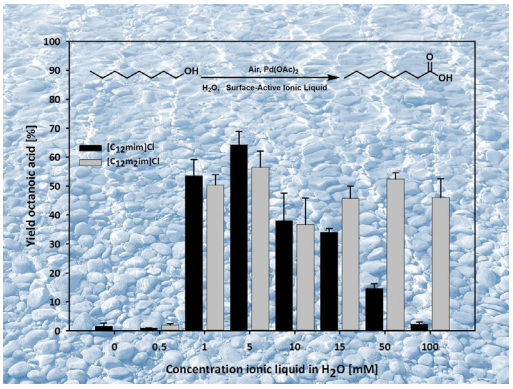

ARTICLE INFO

Article history:
Received 25 November 2016
Revised 23 December 2016
Accepted 26 December 2016
Available online 29 December 2016

2010 MSC:
00-01
99-00

Keywords:
Micellar catalysis
Water
Surfactants
Ionic liquids
Aerobic oxidation
Palladium

ABSTRACT

We present design and synthesis of surface-active ionic liquids for the application in micellar catalysis. A series of 1-methyl-3-dodecylimidazolium based ionic liquids with variable core structures including dicationic and zwitterionic ones was synthesized and characterized. These surface-active ionic liquids where applied in the aerobic oxidation of aliphatic alcohols to carbonyl compounds. A strong dependence on the ionic liquid concentration and structure was identified, which is in accordance with the concepts of micellar catalysis. Optimum conditions for the oxidation of 1-octanol could be identified, and the use of surface-active ionic liquids strongly improved the reaction performance compared to pure water. Under optimized conditions, it was possible to isolate up to 75% of octanoic acid using only small amounts of surface-active ionic liquid in a 0.05 mM solution in water without further ligands.

© 2016 Published by Elsevier Inc.

* Corresponding author.
E-mail address: katharina.schroeder@tuwien.ac.at (K. Bica).

http://dx.doi.org/10.1016/j.jcis.2016.12.063
0021-9797/© 2016 Published by Elsevier Inc.

1. Introduction

Solvent consumption accounts for a relevant part of the overall environmental impact of a chemical process. Replacing traditional volatile organic solvents with more benign ones such as water can be a key step towards the development of sustainable processes, although problems with substrate solubility may exist [1]. The addition of commercially available surfactants provides a powerful tool to overcome the solubility issue of many organic substrates in water, as the formation of aggregates in water enables the solubilization of reaction mixtures in water. Micelles or higher aggregates have the capability to drastically alter reaction rates, as the local concentration experienced by the reactants in the supramolecular assembly is higher than in a bulk solution [2]. Moreover, recent developments on the engineering of designer surfactants for a specific reaction showed a drastic impact on activity and selectivity through specific interactions between micelle, substrates and catalysts [3].

For this purpose ionic liquids with a long alkyl chain have been recently intensely investigated. It has been demonstrated that ionic liquids with alkyl chains longer than 8 carbon atoms behave like amphiphiles and are able to form micelles in aqueous solution, which renders them ideal candidates as tailor-made surfactants for a number of applications [4,5]. Micellar aggregates of surface-active ionic liquids can increase the solubility of organic compounds such as toluene in water [6], and are even suitable for the extraction of natural compounds [7]. Moreover, the lipophilic core of ionic liquid aggregates in water can act as nanoreactor and exhibit strong kinetic effects on organic reactions [8–11]. While research on the aggregation behavior of ionic liquids in water focuses mainly on monocationic alkyl imidazolium based ionic liquids, studies on the adjustments of head group, side chain or counterion structure have also been performed. This high tunability of ionic liquids provides a powerful tool for the design of the optimal environment for a specific reaction in water [12].

Based on these considerations, we expanded our recent research on the design of surface-active ionic liquids for micellar catalysis towards the application in aerobic oxidations. In here, we report a study on the ligand free, unsupported, monometallic Pd catalyzed oxidation of 1-octanol to octanoic acid in water with the aid of surface-active imidazolium-based ionic liquids and discuss impact of ionic liquid structure and concentration in water.

Oxidation reactions are among the most useful transformations and a key step for the synthesis of intermediates in organic chemistry. However, conventional methods relying on reagents such as Dess-Martin periodinane, Swern reagent, or the tetrapropylammonium perruthenate (TPAP)/N-methylmorpholine-N-oxide system exhibit low atom economy. These methods suffer from high waste production due to the by-products formed by the deactivation of the oxidizing agent after the reaction and are difficult to implement at industrial level [13]. As a result, research has focused on the development of more benign oxidations protocols, particularly on catalytic versions that operate under milder conditions and reduce waste [14,15]. Among different proposed catalysts Palladium is a prime candidate, and homogenous catalysts based on Palladium with a number of ligands have been intensely investigated. Recently Muldoon et al. and Cámpora et al. reported a new series of N,O-ligated Pd(II) complexes based on pyridine-carboxylate and quinoline ligands which are competitive with the so far reported ones in term of turn-over frequency (TOF) [16–18]. In general, dioxygen is considered as the most appealing oxidant used in combination with homogenous Palladium-catalysts as it is cheap, abundant and produces just water as by-product. However, due to safety issues, it should be used in diluted gas mixtures and/or in combination with non-flammable solvents such as water. As a consequence, Sheldon et al. reported highly efficient ligand systems based on bathophenanthroline disulfonate, which allows to perform the Palladium-catalyzed oxidation of alcohols under aqueous conditions [19–21]. To obtain acceptable reaction rates for poor water soluble alcohols addition of co-solvents or additives were required. Recent research on Palladium-catalyzed aerobic oxidations of alcohols under aqueous conditions also suggest the use of water-soluble *N*-heterocyclic carbene ligands [22]. Han et al. reported the Palladium catalyzed aerobic oxidation of 1-heptanol in water using 1,3-dialkylimidazolium-based ligands with a quaternary ammonium moiety [23]. Alternatively, heterogeneous catalysts relying on Palladium-based nanomaterials have been reported for the oxidation of alcohols to carbonyl compounds [24].

A number of aspects render surface-active ionic liquids in water an interesting alternative as reaction media in aerobic oxidations under aqueous conditions. Apart from the solubilization of the reaction mixture in water, surface-active ionic liquids, can, and have been, used to increase reaction rates, activity, and selectivity according to the concepts of micellar catalysis [25,26]. Moreover, the impact of improved solubility is not limited to starting materials or catalyst species: Even though oxygen has generally low solubility in aqueous solutions, it has been reported that micelles can improve the oxygen concentration dissolved in the solution, therefore facilitating the oxidation of substrates solubilized in the aggregates [27]. Eventually, the role of the surface-active ionic liquid is not limited to the use as mere surfactant; moreover it can interact with the catalytically active species in oxidation reactions, either as *N*-heterocyclic carbene ligands or as stabilizer of in situ formed catalytically active Palladium nanoparticles.

2. Materials and methods

2.1. General

Commercially available reagents and solvents were used as received from Sigma Aldrich unless otherwise specified. Doubly-distilled deionized water was obtained from a Millipore Milli-Q water purification system (Millipore, USA). All ionic liquids were dried for at least 48 h at room temperature and 0.01 mbar before use and were stored under an argon atmosphere.

For the characterization of the surface activity of the investigated ionic liquids the same procedure used in our previous work was followed [9]. Solutions at various concentration of the ionic liquids were prepared with doubly-distilled Millipore Milli-Q water and left under shaking at 360 min^{-1} for 24 h at room temperature (RT) to equilibrate. For conductivity measurements, samples were previously equilibrated at (25 ± 0.1) °C in a HAAKE K15 thermostat. Conductivity measurement were performed on a Mettler Toledo Seven Excellence system, equipped with a InLAB 741-ISM electrode (cell constant κ = 0.105). The conductimeter was calibrated with a standard KCl solution and two independent measurements were performed. The CMC was calculated as the intersection point of the two linear regimes in the conductivity/concentration graph. The degree of counter ion binding was calculated with the following equation $\beta = 1 - \alpha$, where α is the degree of ionization and corresponds to the ratio of the slopes between the two linear fragments of the conductivity curves. Surface tension was determined with the Du Noüy ring method on a Krüss manual tensiometer K6 at room temperature. Each measurement was repeated 5 times.

^{1}H and ^{13}C NMR spectra were recorded on a Bruker AC 200 or 400, using the solvent peak as reference. Infrared spectra were recorded on a Perkin-Elmer Spectrum 65 FT IR spectrometer equipped with a Specac MK II Golden Gate Single Reflection ATR

unit. Gas chromatography analyses were carried out using a Thermo Scientific Focus gas chromatograph equipped with a BGB5 column BGB-5 (30 m × 0.25 mm i.d., 0.5 m film thickness) cross-bonded dimethyl polysiloxane capillary column and a FID detector. The following conditions were employed: Inlet temperature, 260 °C; split ratio 20; He carrier gas, 2 ml/min; detector temperature, 280 °C. The temperature program applied for the detection of octanal (t_r = 5.2 min), 1-octanol (t_r = 5.9 min), methyl benzoate (internal standard, t_r = 6.2 min), octanoic acid (t_r = 6.8 - min) and octanoic acid octyl ester (t_r = 9.9 min) was the following: Initial column temperature 60 °C, heating to 170 °C at a rate of 15 °C/min, heating to 300 °C at a rate of 50 °C/min, final temperature held 5 min.

2.2. Synthesis of ionic liquids

Synthesis of [C_{12}mim]X, with X = Cl^- (**1**) and Br^- (**3**): The halide-based imidazolium salts were synthesized following standard procedures, including the alkylation of *N*-methylimidazole or 1,2-dimethyl imidazole with the appropriate alkyl halide to yield the corresponding imidazolium halide that were repeatedly crystallized for purification. Details can be found in our previous work [9].

2.2.1. 1-Dodecyl-2,3-dimethylimidazolium chloride (*2*)

1,2-Dimethylimidazole (7.99 g, 8.3 mmol) was placed in a three necks round bottom flask equipped with a condenser and an dropping funnel. 1-Chlorododecane (18.7 g, 9.1 mmol, 1.1 eq) were slowly added at room temperature. The reaction was left stirring at 100 °C for 4 days until NMR analysis showed complete conversion. Remaining volatiles were removed under reduced pressure, and the crude product was recrystallized from THF to obtain a colorless crystalline solid in 95% yield. ^{1}H NMR (200 MHz, $CDCl_3$): δ(ppm) = 7.86 (1H, d, *J* = 1.90 Hz, NC*H*=CH), 7.49 (1H, d, *J* = 1.92 Hz, NCH=C*H*), 4.17 (2H, t, *J* = 7.41 Hz, $CH_2C_{11}H_{23}$), 4.01 (3H, s, NCH_3), 2.77 (3H, s, N=C—CH_3), 1.75 (2H, t, *J* = 6.88 Hz, CH_2-$CH_2C_{10}H_{21}$), 1.19 (18H, m, $C_2H_4C_9H_{18}CH_3$), 0.81 (3H, t, *J* = 6.10 Hz, $C_{11}H_{22}CH_3$). Analytical data was in accordance with literature [28].

Synthesis of dicationic and zwitterionic surface-active ionic liquids: The remaining ionic liquids were synthesized through a two step procedure involving the alkylation of 1-dodecylimidazole, which was previously synthesized following a procedure reported in literature and distilled before use [29].

2.2.2. 1,3-Bis(3-dodecanimidazolium-1-yl) methane dibromide (*4*)

1-Dodecylimidazole (4.32 g, 18.3 mmol, 2.1 eq) was dissolved in 15 ml of THF and 1.59 g of dibromomethane (9.1 mmol, 1 eq) were added at room temperature. The mixture was heated to 65 °C for 5 days. After evaporation of the solvent, the product was dissolved in a small amount of CH_2Cl_2 and precipitated by adding EtOAc. The product was obtained via filtration in 10% yield as a colorless solid. ^{1}H NMR (400 MHz, $CDCl_3$): δ(ppm) = 10.77 (s, 2H, —N—C*H*=N—), 8.95 (s, 2H, —N—CH_2—N—), 7.53 (s, 2H, NC*H*=CH), 7.44 (s, 2H, NC*H*=CH), 4.22 (t, 4H, *J* = 7.64 Hz, $CH_2C_{11}H_{23}$), 1.88 (m, 4H, $CH_2CH_2C_{10}H_{21}$), 1.22–1.13 (m, 36H, $C_2H_4C_9H_{18}CH_3$), 0.80 (t, 6H, *J* = 6.78 Hz, $C_{11}H_{22}CH_3$). Analytical data was in accordance with literature [30].

2.2.3. 1,3-Bis(3-dodecanimidazolium-1yl) propane dibromide (*5*)

1-Dodecylimidazole (3.5 g, 14.8 mmol, 2.1 eq) were dissolved in 30 ml of THF and 1.49 g of 1,3-dibromopropane (7.4 mmol, 1 eq) were added at room temperature. The mixture was heated to 65 °C for 5 days. After evaporation of the solvent, the product was dissolved in a small amount of CH_2Cl_2 and precipitated by adding EtOAc. The product was collected via filtration and obtained in 84% yield as a colorless solid. mp = 62.6 °C. ν_{max} (cm^{-1}) = 3132 (C—H Ar), 2919 (C—H), 2851 (C—H), 1571 (C=C), 1468 (C=C), 1161 (C—N). ^{1}H NMR (400 MHz, $CDCl_3$): δ (ppm) = 10.15 (s, N—C*H*=N—), 8.22 (s, 2H, —NC*H*=CH—), 7.30 (s, 2H, —NC*H*=CH—), 4.67 (t, 4H, *J* = 7.22 Hz, —N—CH_2—CH_2—CH_2—N—), 4.20 (t, 4H, *J* = 7.48 Hz, $CH_2C_{11}H_{23}$), 2.83 (quint, 2H, *J* = 7.25 Hz, —N—CH_2—CH_2-—CH_2—N—) 1.85 (m, 4H, —$CH_2CH_2C_{10}H_{21}$), 1.27–1.13 (m, 36H, C_2-$H_4C_9H_{18}CH_3$), 0.80 (t, 6H, *J* = 6.80 Hz, $C_{11}H_{22}CH_3$). ^{13}C NMR (100 MHz, $CDCl_3$): δ(ppm) = 136.5,123.8, 121.6, 50.3, 46.7, 31.8, 30.9, 30.1, 29.5, 29.4, 29.3, 29.3, 28.9, 26.3, 22.6, 14.1.

2.2.4. 1,5-Bis(3-dodecanimidazolium-1-yl) pentane dibromide (*6*)

1-Dodecyimidazole (3.5 g, 14.27 mmol, 2.1 eq) was dissolved in 30 ml of THF and 1.64 g of 1,5-dibromopentane (7.13 mmol, 1 eq) were added at room temperature. The mixture was heated to 65 °C for 5 days. After evaporation of the solvent, the product was dissolved in a small amount of CH_2Cl_2 and precipitated by adding EtOAc. The product was collected via filtration and obtained in 80% yield as a colorless solid. mp = 95.8 °C. ν_{max} (cm^{-1}): 3120 (C—H Ar), 2921 (C—H), 2852 (C—H), 1561 (C=C), 1459 (C=C), 1158 (C—N). ^{1}H NMR (400 MHz, $CDCl_3$): δ(ppm) = 10.31 (s, 2H, —N—C*H*=N—), 8.10 (s, 2H, NC*H*=CH—), 7.32 (s, 2H, —NC*H*=CH—), 4.44 (t, 4H, *J* = 7.06 Hz, —N—CH_2—C_3H_6—CH_2—N—), 4.23 (t, 4H, *J* = 7.46 Hz, $CH_2C_{11}H_{23}$), 2.05 (m, 4H, —N—C_2H_4—CH_2—C_2H_4—N—), 1.85 (m, 4H, —$CH_2CH_2C_{10}H_{21}$), 1.43 (m, 2H, —N—C_2H_4—CH_2—C_2H_4-—N—) 1.27–1.13 (m, 36H, C_2H_4 $C_9H_{18}CH_3$), 0.80 (t, 6H, *J* = 6.82 Hz, $C_{11}H_{22}CH_3$). ^{13}C NMR (100 MHz, $CDCl_3$): δ(ppm) = 136.6, 123.5, 121.5, 50.0, 49.0, 31.8, 30.2, 29.5, 29.4, 29.3, 29.2, 29.1, 28.9, 26.2, 22.6, 22.0, 14.0.

2.2.5. 4-(1-Dodecyl-3-midazolium) butansulfonate (*7*)

1-Dodedecylimidazole (3.17 g, 13.42 mmol, 1 eq) were dissolved in 5 ml of THF and a solution of 2.01 g 1,4-butansultone (14.76 mmol, 1.1 eq) in 5 ml of THF was added dropwise at 0 °C. The reaction mixture was warmed to room temperature and stirred for 6 days at 65 °C. The obtained precipitate was collected via filtration. The crude product was washed with diethylether three times to obtain the product in 77% yield as a colorless solid. mp = 106.3 °C. ν_{max} (cm^{-1}): 3133 (C—H Ar), 2919 (C—H), 2848 (C—H), 1567 (C=C), 1469 (C=C), 1185 (C—N, S=O), 1037 (S—O). ^{1}H NMR (100 Hz, $CDCl_3$): δ(ppm) = 9.72 (s, 1H, —N—C*H*=N—), 7.72 (s, 1H, —NC*H*=CH—), 7.23 (s, 1H, —NC*H*=CH—), 4.32 (t, 2H, *J* = 7.18 Hz, —N—CH_2—C_3H_6—SO_3), 4.15 (t, 2H, *J* = 7.38 Hz, CH_2C_{11}-H_{23}), 2.80 (t, 2H, *J* = 7.46 Hz, —N—C_3H_6—CH_2—SO_3) 2.04 (q, 2H, *J* = 7.36 Hz, —N—CH_2—CH_2—C_2H_4—SO_3) 1.80 (m, 4H, O_3S—CH_2-—CH_2—C_2H_4—N—CH—N—$CH_2CH_2C_{10}H_{21}$), 1.24–1.13 (m, 18H, C_2H_2-$C_9H_{18}CH_3$), 0.80 (t, 3H, *J* = 6.82 Hz, $C_{11}H_{22}CH_3$). ^{13}C NMR (100 MHz, $CDCl_3$): δ(ppm) = 137.2, 123.1, 121.5, 50.9, 49.9, 49.4, 31.2, 30.2, 29.6, 29.5, 29.4, 29.3, 29.3, 29.0, 26.3, 22.6, 22.2, 14.1.

2.2.6. Poly(ethylene glycol) functionalized dicationic ionic liquid [C_{11}im-PEG1000—C_{11}im]Cl_2 *8*)

The synthesis was performed adapting procedures already described in literature for the derivatization of PEG1000 to dichloro-PEG1000 [31,32]. Subsequently 1.77 g of dichloro-PEG1000 (1.7 mmol, 1 eq) were mixed with 0.93 g of 1-dodecylimidazole (3.9 mmol, 2.3 eq) and stirred for 4 days at 90 °C under argon. The product was washed several times with EtOAc and obtained as an orange viscose liquid in 89% yield. mp = 28.4 °C. ν_{max} (cm^{-1}): 2921 (C—H), 2854 (C—H), 1563 (C=C), 1457 (C=C), 1103 (C—O—C).^{1}H NMR (400 Hz, $CDCl_3$): δ(ppm) = 10.54 (s, 2H, —N=C*H*—N—), 7.65 (s, 2H, —NC*H*=CH—), 7.21 (s, 2H, —NC*H*=CH—), 4.60 (t, 4H, *J* = 4.42 Hz, —CH_2—), 4.19 (t, 6H, *J* = 7.58 Hz, —CH_2—), 3.92 (t, 4H, *J* = 4.46 Hz, —CH_2—), 3.60 3.53 (m, PEG), 1.83 (t, 4H, *J* = 6.36 Hz, $CH_2CH_2C_{10}H_{21}$), 1.18 (m, 41H, C_2-$H_4C_9H_{18}CH_3$), 0.88 (t, 6H, *J* = 6.84 Hz, $C_{11}H_{22}CH_3$).

2.3. Oxidation procedures

2.3.1. Representing procedure for the oxidation of 1-octanol at atmospheric pressure

As general procedure to perform the oxidation of 1-octanol at 1 bar a stock solution of $Pd(OAc)_2$ (4.48 mg/ml) in EtOAc was prepared. This stock solution (1 ml) was placed in a 20 ml vial. The vial was placed under reduced pressure for 5 h to remove the solvent. Stock solutions of ionic liquids at different concentrations were prepared in water that also contained the base K_2CO_3 (13.8 mg/ml). The stock solution of ionic liquid and base in water (2 ml) was added to a vial containing the catalyst, followed by 63.3 µl of 1-octanol. A balloon filled with O_2 was placed on top of the vial with a syringe needle through a septum. The vials were then placed in a pre-heated stirring block for the desired time and temperature. When the reaction was finished the vials were allowed to cool to room temperature before opening. An excess of 2 M HCl was added to neutralize the base and the product was extracted with 10 ml EtOAc. An aliquot of the organic layer was taken for GC analysis using methylbenzoate as internal standard.

2.3.2. Representing procedure for the oxidation of 1-octanol under pressure

A 40 ml autoclave was charged with catalyst 22.4 mg (0.1 mmol) and 138 mg (1 mmol) of K_2CO_3. The ionic liquid solution in water (10 ml) and 261 mg (2 mmol) of 1-octanol were added. The autoclave was loaded with air at the desired pressure and left stirring on a heating block for the desired time and temperature. The autoclave was cooled to room temperature prior to the release of the pressure. An excess of 2 M HCl was added to neutralize the base and the product was extracted with EtOAc. The organic fractions were collected together and diluted to 50 ml. An aliquote of this solution was taken for GC analysis using methylbenzoate as internal standard.

In order to isolate the product a different work-up procedure was followed: After pressure release an excess of base was added and remaining 1-octanol and by-products were extracted with EtOAc. Afterwards an excess of HCl was added and octanoic acid was successively extracted with EtOAc. The combined organic fractions were collected and diluted to 50 ml. An aliquot (0.4 µl) of this solution was taken for GC analysis using methylbenzoate as internal standard. The remaining solution was dried over Na_2SO_4. Solvents were removed under reduced pressure to obtain octanoic acid in spectroscopically pure form. ^{1}H NMR (200 MHz, $CDCl_3$): δ(ppm) = 11.32 (s, 1H, COO*H*), 2.27 (t, 2H, *J* = 7.56 MHz, —CH_2—COOH), 1.56 (quin, 2H, *J* = 7.35 MHz, —CH_2—CH_2—COOH), 1.23 (m, 8H, CH_3—C_4H_8—CH_2—), 0.80 (t, 3H, *J* = 6.88 Hz, —CH_3). Analytical data was in accordance with literature [33].

3. Results and discussion

3.1. Design and synthesis of surface-active ionic liquids

Based on our previous experience in cross-coupling chemistry and on recent literature data concerning Palladium-catalyzed oxidation, we focused on the use of imidazolium-based 1-alkylmethylimidazolium-based ionic liquids. These surface-active ionic liquids should not only act as amphiphiles to overcome solubility issues of the alcohol in water, but may directly act as ligands for Palladium. Consequently, a series of known and new surface-active ionic liquids based on the 1-dodecyl-3-methylimidazolium ($[C_{12}mim]^+$) cation including dicationic and zwitterionic structures was synthesized adapting procedures already reported in literature [34,35,29,32]. Different approaches were used and are depicted in Fig. 1.

In case of surface-active ionic liquids $[C_{12}mim]Cl$ **1**, $[C_{12}mim]Br$ **2** and $[C_{12}m_2im]Cl$ **3** the direct alkylation of 1-methylimidazole or 1,2-dimethylimidazole with the desired dodecyl halides gave a straightforward access to the desired surface-active ionic liquids. The products could be obtained as colorless crystals in excellent yields after recrystallization from suitable solvents. The remaining surface-active ionic liquids were synthesized through a two step procedure relying on 1-dodecylimidazole as precursor: For the dicationic surface-active ionic liquids $[C_{12}im\text{-}C_1\text{-}C_{12}im]Br_2$ **4**, $[C_{12}im\text{-}C_3\text{-}C_{12}im]Br_2$ **5** and $[C_{12}im\text{-}C_5\text{-}C_{12}im]Br_2$ **6** the corresponding dibromoalkane was used as alkylating agent with 2 equivalents of 1-dodecylimidazole. Precipitation in ethyl acetate afforded all products as colorless solids. Good yields were obtained for surface-active ionic liquids **5** and **6**, while in the case of **4** the high volatility of the starting material dibromomethane strongly limited the reaction results. The zwitterionic ionic liquid $[C_{12}im\text{-}C_4\text{-}SO_3]$ **7** was obtained through the ring opening reaction of 1,4-butane sultone with 1-dodecylimidazole to yield the product as a colorless solid in 77% yield. In order to synthesize $[C_{12}im\text{-PEG1000-}C_{12}im]Cl_2$ **8** an additional step for the derivatization of PEG1000 to the dichloro-PEG1000 prior to the alkylation with 1-dodecylimidazole was necessary. The product was obtained in the second step after washing with EtOAc as an orange wax in 89% yield.

3.2. Characterization of surface-active ionic liquids

The synthesized ionic liquids were characterized with regard to their surface activity. For this purpose critical micelle concentrations (CMC) were measured with two techniques, surface tension and conductivity, and results are depicted in Fig. 2 and 3, and summarized in Table 1.

In general, imidazolium-based surfactants show a higher surface activity compared to the corresponding ammonium ones due to the delocalized charge on the imidazolium group [36]. The addition of a methyl group on the position 2 of the imidazolium ring slightly lowers the CMC. In addition, the anion plays a relevant role in the aggregation ability of surfactants, since it screens the electrostatic repulsion of the head groups in the micelles. Consequently, a less hydrated anion such as bromide favors micellization over chloride [9].

Dicationic or gemini surfactants consist of two polar head groups with hydrophobic chains, covalently connected through a spacer [35]. In general, dicationic surfactants show a lower CMC than the monoatomic analogous and tend to aggregate forming vesicles like lipids [30]. The length of the spacer has a critical role in the determination of the flexibility of the molecule and hence on the formation of aggregates. As a consequence of these characteristic, a similar CMC was observed for the $[C_{12}im\text{-}C_n\text{-}C_{12}im]Br_2$ series with $n = 1$ and 5, while $n = 3$ shows a minimum. A similar behavior was already identified in a study on $[C_{16}im\text{-}C_n\text{-}C_{16}im]Br_2$ dicationic surfactants with variable spacer length [37]. Since zwitterionic surfactants are not suitable for conductivity measurement, the CMC of ionic liquid $[C_{12}im\text{-}C_4\text{-}SO_3]$ **7** could only be determined by surface tension. Due to the overall neutral charge of the head group zwitterionic surfactants have a higher surface activity compared to cationic surfactants, as can be seen in the comparison of surface-active ionic liquids $[C_{12}m_2im]Cl$ and $[C_{12}im\text{-}C_4\text{-}SO_3]$. Moreover, replacing the ammonium group of sulfobetaine with the imidazolium-based head group resulted in an decrease of the CMC, which is in accordance with literature data on cationic surfactants [38].

3.3. Optimization of reaction parameters in the aerobic oxidation of 1-octanol

With this set of surface-active ionic liquids with variable structure of the cationic head group in hand, we turned our attention

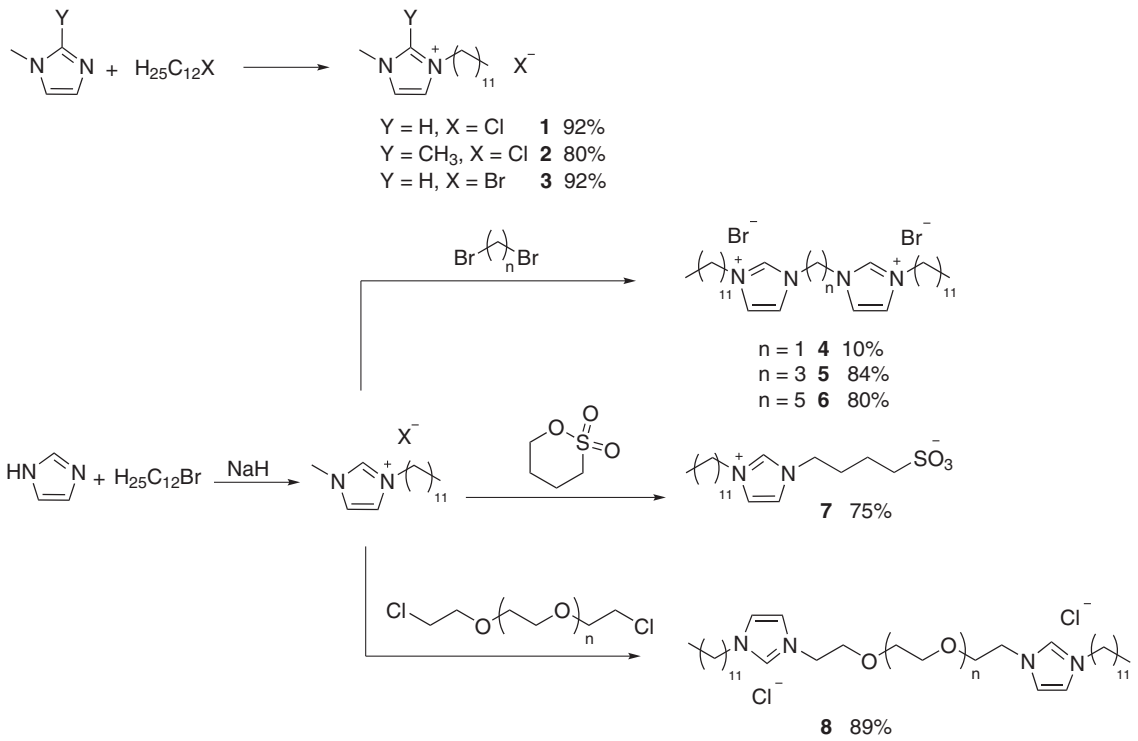

Fig. 1. Synthesis of surface-active ionic liquids.

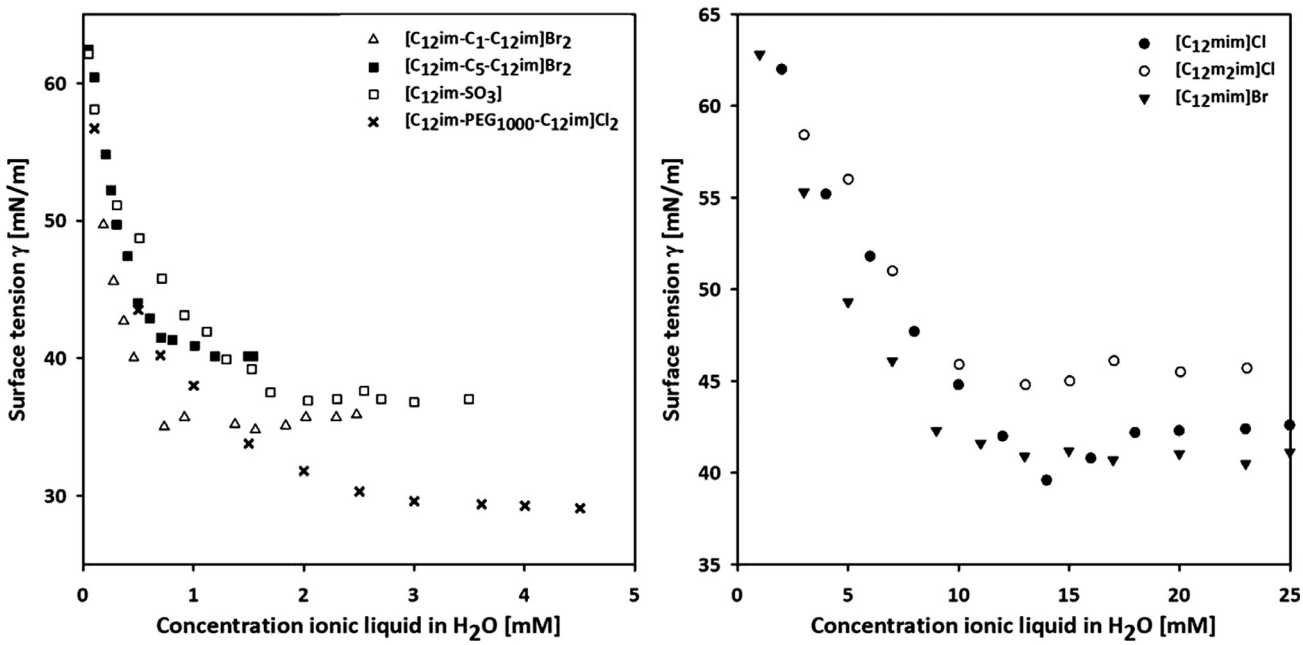

Fig. 2. Surface tension of the investigated ionic liquids at 25 °C.

towards the palladium-catalyzed aerobic oxidation of alcohols in water. We have chosen aliphatic inactivated alcohols, as these are less reactive in catalytic systems and notoriously difficult to oxidize. Our initial experiments focused on the optimization of reaction parameters for the oxidation of 1-octanol at atmospheric pressure. Reactions were carried out using 2 ml of aqueous ionic liquid solution in magnetically stirred vials placed in a metal heating block. Oxygen was used as oxidizing agent and introduced in the system with a balloon through a septum. Results of the initial screening of reaction parameters are summarized in Table 2.

After running the reaction for the indicated time, the crude reaction mixtures were analyzed by GC. While traces of side products such as octanal and octyloctanoate ester below 5% were found, the oxidation proceeded smoothly towards octanoic acid as main product. As already suggested in literature, we found a strong influence of the base. Best results were obtained with potassium

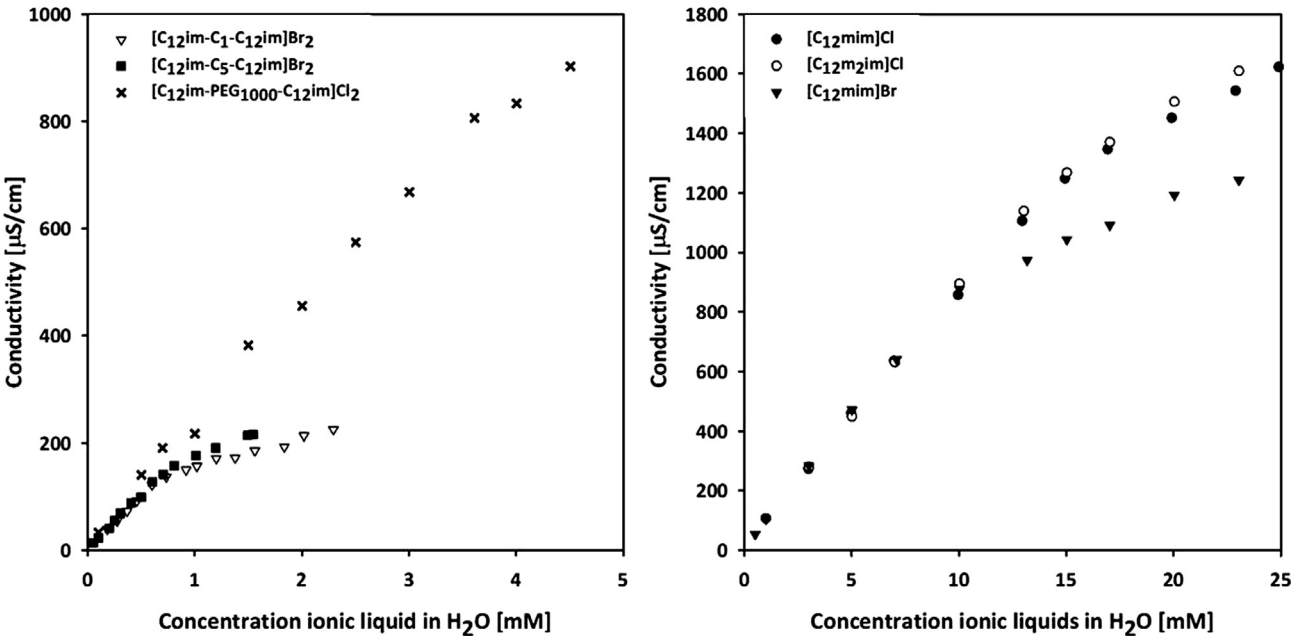

Fig. 3. Conductivity of the investigated ionic liquids at 25 °C.

Table 1
Critical micelle concentration (CMC) obtained by surface tension and conductivity for surface-active ionic liquids **1**–**8**.

Ionic liquid	Surface tension [mM]	Conductivity [mM]
[C_{12}mim]Cl **1**	13.25 [9]	14.53 [9]
[$C_{12}m_2$im]Cl **2**	10.33	13.75
[C_{12}mim]Br **3**	9.29 [9]	10.29 [9]
[C_{12}im-C_1-C_{12}im]Br_2 **4**	0.70	0.74
[C_{12}im-C_3-C_{12}im]Br_2 **5**	0.53 [39]	0.61 [39]
[C_{12}im-C_5-C_{12}im]Br_2 **6**	0.63	0.70
[C_{12}im-C_4-SO_3] **7**	1.67	–
[C_{12}im-PEG1000-C_{12}im]Cl_2 **8**	2.26	2.91

carbonate when used in a concentration range of 50–75 mol.% (Table 2, entry 2–3). A higher or lower amount led to lower performance (Table 2 entry 1 and 4), while only traces of product were found when using NaOAc or the organic base DBU instead. The addition of acetic acid as sometimes suggested in literature did not benefit the reaction. When investigating the impact of catalyst loading, we found that at least 5 mol.% of $Pd(OAc)_2$ (Table 2, entry 2 and 7) were necessary in order to obtain satisfactory results. Surprisingly a higher amount did not further improve the yield of octanoic acid (Table 2, entry 8). Concerning the effect of temperature on the reaction, the reaction performed poorly at room temperature or 50 °C, while an increased temperature of at least 80 °C was required to improve the results (Table 2, entry 10–12). Eventually, the highest yield was obtained when running the oxidation at 100 °C for 24 h using 5 mol.% $Pd(OAc)_2$ and 50 mol.% K_2CO_3, and up to 71% octanoic acid were formed (Table 2, entries 13–16). In order to compare surface-active ionic liquids with conventional surfactants, we also investigated the oxidation using 1-cetyltrimethylammonium bromide (CTAB) instead of [C_{12}mim]Cl

Table 2
Optimization of the reaction conditions for the oxidation of 1-octanol using 1 bar of O_2 as oxidizing agent.

Entry[a]	Temperature [°C]	Time [h]	$Pd(OAc)_2$ [mol.%]	K_2CO_3 [mol.%]	Yield[b] [%]
1	100	18	5	20	10
2	100	18	5	50	64
3	100	18	5	75	65
4	100	18	5	100	48
5	100	18	5	50[c]	<5
6	100	18	5	50[d]	<5
7	100	18	2	50	<5
8	100	18	10	50	56
9	100	18	2.5[e]	50	58
10	25	18	5	50	<5
11	50	18	5	50	<5
12	80	18	5	50	42
13	100	6	5	50	<5
14	100	12	5	50	48
15	100	24	5	50	71
16	100	48	5	50	64
17[f]	100	18	5	50	5

[a] Reactions performed using 0.4 mmol of 1-octanol in 2 ml of a 5 mM [C_{12}mim]Cl solution.
[b] Yield determined via GC analysis. Results are reported as average of two independent experiments.
[c] DBU used as base.
[d] NaOAc used as base.
[e] $[Pd(allyl)Cl]_2$ used as catalyst.
[f] Reactions performed with a 5 mM solution of CTAB instead of [C_{12}mim]Cl solution.

under the optimized conditions. It is important to highlight the superiority of surface active ionic liquids in micellar catalysis in comparison to conventional surfactants, in fact the use of CTAB afforded only 5% of the product (Table 2, entry 17). A similar effect has been observed by Cole-Hamilton et al. for hydroformylation reactions, were imidazolium-based surfactants outperformed ammonium- or pyridinium-based structures [40].

3.4. Impact of ionic liquid concentration

In order to gain a better understanding on the role of the ionic liquid in the system, different concentrations of ionic liquids [C_{12}mim]Cl **1** were evaluated under the previously optimized conditions using 1 bar of O_2 as oxidizing agent. As can be seen in the results reported in Fig. 4, a strong dependence of the yield of octanoic acid with regard to the surfactant concentration was found, which is in accordance with the concepts of micellar catalysis. Moreover, the presence of surface-active ionic liquids in the reaction mixture was essential, as only traces of the product could be identified in pure water as reaction media. As soon as the concentration of [C_{12}mim]Cl **1** reached 1 mM the yield of octanoic acid increased drastically to 50%. This suggests the formation of ionic liquid aggregates, although this concentration is below the CMC values for pure [C_{12}mim]Cl **1** (Table 1). However, it can be assumed that the presence of catalyst and base renders the CMC to a lower value, which is in accordance with literature data studying salt effects on the aggregation of imidazolium-based ionic liquids [41].

The best results were obtained with 5 mM [C_{12}mim]Cl **1** which allowed to obtain 64% of octanoic acid yield. The concentration profile shows a maximum at 5 mM and, as it is usual for micellar catalysis, the performance decreases again above 15 mM. Interestingly a different profile was obtained in the case of [$C_{12}m_2$im]Cl **2** which allowed to obtain good yields even at high concentrations. The slightly decrease in octanoic acid yield at 10 and 15 mM for [$C_{12}m_2$im]Cl **2** can be balanced by the additional formation of the ester octyloctanoate, these were the only conditions at which 5–10% ester formation was identified.

Further studies showed that the catalyst $Pd(OAc)_2$ is actually decomposing during the reaction, as we observed the formation

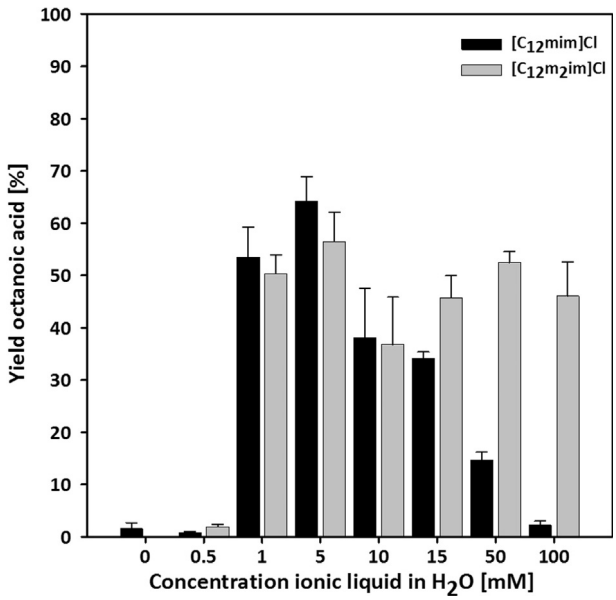

Fig. 4. Results for the oxidation of 1-octanol performed with [C_{12}mim]Cl (dark gray) and [$C_{12}m_2$im]Cl (light gray) at different concentrations. For reaction conditions see Table 2.

of heterogeneous Palladium aggregates forming during the oxidation (see ESI Fig. S1). This suggest a different catalytically active species compared to Han et al., who reported that structurally related 1,3-dialkylimidazolium compounds containing a quaternary ammonium moiety act as NHC-ligand in this oxidation.

However, the formation of Palladium-based nanoparticles is not uncommon in this reaction. Pioneering work on Palladium nanoparticle mediated oxidations was conducted by Moiseev et al., who reported that a Pd giant cluster was able to catalyze the oxidation of lower alcohols to a series of different products including aldehydes, esters, anhydrides, carboxylic acids and acetals, while benzyl alcohols were oxidized to aldehydes [42,43]. Different ligands have been used to stabilize Palladium nanoparticles. The previously mentioned neocuprine ligand was also found to stabilize nanoparticles that were catalytically active in the oxidation of 2-hexanol, but also of some steroidal alcohols [21,24]. Formation of Pd nanoparticles was mediated by the alcohol itself that acted as reducing agent in the presence of a co-solvent. Other stabilizing agents for Pd nanoparticles used in the oxidation of alcohols include polymers [44] such as polyethylenglycol [45,46]. Due to the high tendency of Palladium nanoparticles to aggregate several reports on supported nanoparticles emerged lately [47,48]. However their reactivity is mainly limited to allylic alcohols, while reports of their activity towards aliphatic alcohols is still scarce [15]. Different suggestions were made on the active species, as different species including Pd^0, Pd^+ and Pd^{2+} can be present on the surface of the nanoparticles at the same time, and the activity seems to be defined by the balance between PdO and metallic Pd [49].

In case of surface-active ionic liquid [C_{12}mim]Cl **1**, the catalytically active species seems to be dependent on the ionic liquid concentration. At high concentrations of [C_{12}mim]Cl **1** no decomposition of the pre-catalyst was observed and poor yields were obtained, indicating that the pre-catalyst was stabilized by the ionic liquid. At lower concentrations, the pre-catalyst decomposes into catalytically active Pd aggregates. When using [$C_{12}m_2$im]Cl **2** the decomposition seems to be independent from concentration of ionic liquid, as constant yields were obtained over the entire concentration range investigated. The different performance of the two ionic liquids at high concentration indicates that the co-existence of an homogenous and heterogeneous system, and it seems that the formation of a carbene on the imidazolium group plays a secondary role in the reaction mechanism. Moreover when the reaction mixture was warmed up in absence of the starting material 1-octanol no formation of Palladium aggregates but a light brown solution was obtained, suggesting that to initiate the catalytic cycle the alcohol is initially consumed to reduce Palladium.

3.5. Impact of ionic liquid structure

In order to improve the stabilization of the aggregates forming from the pre-catalyst decomposition, we expanded the range of surface-active ionic liquids to include dicationic and zwitterionic structures for the oxidation of 1-octanol to octanoic acid (Fig. 5).

In order to be able to compare the benefit of dicationic surface-active ionic liquids independently from the anion, [C_{12}mim]Br **3** was tested initially. Only 19% of octanoic acid were formed at a concentration of 1 mM, suggesting that [C_{12}mim]Br is less efficient compared to [C_{12}mim]Cl. Since dicationic surfactants usually present a lower CMC than the monocationic analogous [35], the dicationic structures [C_{12}im-C_1-C_{12}im]Br_2 **4** and [C_{12}im-C_5-C_{12}im]Br_2 **6** could improve the yield of octanoic acid to 27% and 24% respectively using a lower concentration of only 0.1 mM. The length of the spacer between the two imidazolium groups has however a strong influence: [C_{12}im-C_3-C_{12}im]Br_2 **5** only afforded traces of

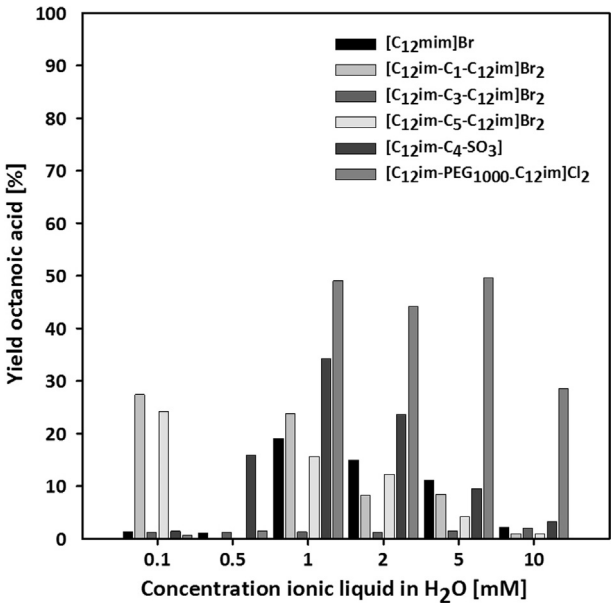

Fig. 5. Octainoic acid yield for the oxidation of 1-octanol with the aid of different dicationic and zwitterionic ionic liquids. For reaction conditions see Table 2.

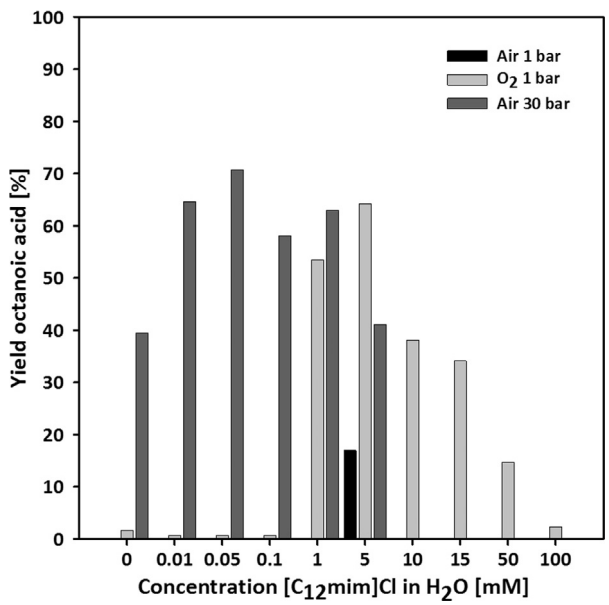

Fig. 6. Comparison of the oxidation of 1-octanol to octanoic acid with $[C_{12}mim]Cl$ at different concentrations with oxygen and air.

the product. Dicationic imidazolium based surfactants have already been reported for the stabilization of silver nanoparticles in water, and the length of the spacer between the imidazolium head groups was found to influence the shape and the size of the formed nanoparticles. In particular very short bridges such as an ethylene bridge favoured the formation of elongated nanoparticles that could have a less advantageous active surface/volume ratio for catalytic applications [37]. Best results were obtained when testing the PEG-modified zwitterionic ionic liquid $[C_{12}im\text{-}PEG1000\text{-}C_{12}im]Cl_2$ **8** with 50% yield of octanoic acid in a concentration range between 2 and 5 mM. Reports of PEG containing surfactants have shown that they are efficient stabilizer for Pd nanoparticles in water. Examples on the application for hydrogenation and even for the aerobic oxidation of alcohols exist; however, their application towards the oxidation of aliphatic primary alcohols in water is still scarce [50,45,32,51,52]. Eventually, the zwitterionic surface-active ionic liquid $[C_{12}im\text{-}C_4\text{-}SO_3]$ **7** performed better than the dicationic ones reaching a maximum yield of 35%. Similar surface-active ionic liquids were found to stabilize Palladium nanoparticles in water via the formation of a double layer, and applications in hydrogenations were reported [29]. In any case, it is important to realize that the key to efficient catalysis lies in the appropriate stabilization. If stabilization of the catalytically active species is too high, this would inhibit the reaction, making it challenging to identify intermediate reaction conditions.

3.6. From oxygen to air as oxidant

While pure oxygen was used for the initial screening experiments, the use of air is clearly more attractive and adds considerably to the safety of the process. As can be seen in Fig. 6 air could be used instead of oxygen, although a lower yield of 15% was obtained with 1 bar air. However, when increasing the pressure to 30 bar the yield could reach 40%. At this conditions the partial pressure of dioxygen is increased up to 6.2 bar. Further investigations on the optimization of the reaction conditions at higher pressure were made and confirmed conditions similar to those used at atmospheric pressure (see ESI Table S1). When comparing the influence of surface-active ionic liquid concentration with oxygen at atmospheric pressure and air at 30 bar it can be noticed that yields are shifted to lower concentration at high pressure compared to the ideal concentration range with oxygen at 1 bar (Fig. 6). This is advantageous for the oxidation, as the required amount of the surface-active ionic liquid can be significantly reduced while maintaining the good performance.

A similar behavior was found for the best-performing surface-active ionic liquid $[C_{12}im\text{-}PEG1000\text{-}C_{12}im]Cl_2$ **8** (Table 3). While yields remained low with air under atmospheric pressure, a strong improvement was obtained using 30 bar of air with 0.05 mM as concentration. Eventually, it was possible to isolate up to 75% of the product octanoic acid using only small amounts of surface-active ionic liquid in a 0.05 mM solution without further ligands.

Table 3
Comparison of the oxidation of 1-octanol to octanoic acid with oxygen and air.

Ionic liquid[a]	Concentration [mM]	Atmosphere	Pressure [bar]	Yield[b] [%]
$[C_{12}mim]Cl$	5	Oxygen	1	64
$[C_{12}mim]Cl$	5	Air	1	17
$[C_{12}mim]Cl$	5	Air	30	40
$[C_{12}mim]Cl$	0.05	Air	30	71 (63)[c]
$[C_{12}im\text{-}PEG1000\text{-}C_{12}im]Cl_2$	5	Oxygen	1	50
$[C_{12}im\text{-}PEG1000\text{-}C_{12}im]Cl_2$	5	Air	1	14
$[C_{12}im\text{-}PEG1000\text{-}C_{12}im]Cl_2$	0.05	Air	30	75 (75)[c]

[a] Reactions performed using 2 mmol of 1-octanol in 10 ml of ionic liquid solution.
[b] Yield determined via GC analysis.
[c] Isolated yield reported in brackets.

4. Conclusion

Herein we presented the synthesis and characterization of a series of new and known surface-active 1-dodecyl-3-methylimidazolium-based ionic liquids including dicationic and zwitterionic structures and investigated their aggregation behavior [9,36,35,37]. These surface-active ionic liquids were applied as sole additive in the aerobic palladium-catalyzed oxidation of 1-octanol to octanoic acid in water. Apart from pure oxygen, the system was also operating with air as a cheap, safe and benign oxidant which added considerable to the safety of the process. Among the tested surface-active ionic liquids the best results were obtained with the polyethylenglycol-based ionic liquid [C_{12}im-PEG1000-C_{12}im]Cl_2 in a 0.05 mM solution with a pressure of 30 bar air, and up to 75% yield of pure octanoic acid could be isolated. A strong influence on ionic liquid structure and concentration was found, suggesting that the surface-active ionic liquids play a dual role as surfactant and stabilizer for the catalytically active species as it has been also observed for Palladium-catalyzed cross-coupling in water [29]. Optimization of reaction parameters allowed to obtain octanoic acid in good yields, and a number of critical aspects offer advantages to currently available processes for the oxidation of non-activated alcohols in micellar media.

According to previously reported protocols and methods, the oxidation of alcohols in micellar catalysis still relies on the use of stoichiometric organic oxidants [46,53] or metal oxides as oxidant [54–56]. Moreover literature deals mainly with activated or short alkyl chain alcohols, which have a considerably higher solubility in water [1,57,58]. In our system even a small amount of imidazolium based surface-active ionic liquids was very effective in comparison to an ammonium-based surfactant, both in terms of surface activity and for the application in the oxidation of the scarcely reactive primary aliphatic alcohol 1-octanol to octanoic acid. Surface-active ionic liquids significantly improved the yield obtained with pure water, as they could not only overcome the limited solubility of octanol in water but were also able to stabilize the Pd-catalyst in such an extent that no additional ligands or support were required [48,24].

Our current research aims to elucidate the interplay between imidazolium-based surface-active ionic liquid and catalytically active species in this reaction. More studies concerning the concentration-dependent formation and stabilization of nanoparticles in surface-active ionic liquids for aqueous oxidations and cross coupling reactions are currently under way.

Acknowledgement

Financial support by the Austrian Science Fund (FWF): P25504-N28 is gratefully acknowledged.

Appendix A. Supplementary material

Supplementary data associated with this article can be found, in the online version, at http://dx.doi.org/10.1016/j.jcis.2016.12.063.

References

[1] B.H. Lipshutz, S. Ghorai, Transitioning organic synthesis from organic solvents to water. What's your E factor?, Green Chem 16 (2014) 3660–3679, http://dx.doi.org/10.1002/adsc.200390057.
[2] T. Dwars, E. Paetzold, G. Oehme, Reactions in micellar systems, Angew. Chem. Int. Ed. 44 (44) (2005) 7174–7199, http://dx.doi.org/10.1002/anie.200501365.
[3] G. La Sorella, G. Strukul, A. Scarso, Recent advances in catalysis in micellar media, Green Chem. 17 (2) (2015) 644–683, http://dx.doi.org/10.1039/C4GC01368A.
[4] J. Łuczak, J. Hupka, J. Thöming, C. Jungnickel, Self-organization of imidazolium ionic liquids in aqueous solution, Colloids Surf., A 329 (3) (2008) 125–133, http://dx.doi.org/10.1016/j.colsurfa.2008.07.012.
[5] C. Janiak, Ionic liquids for the synthesis and stabilization of metal nanoparticles, Z. Naturforsch. B Chem. Sci. 68(10). http://dx.doi.org/10.5560/znb.2013-3140.
[6] J. Łuczak, C. Jungnickel, M. Markiewicz, J. Hupka, Solubilization of benzene, toluene, and xylene (BTX) in aqueous micellar solutions of amphiphilic imidazolium ionic liquids, J. Phys. Chem. B 117 (18) (2013) 5653–5658, http://dx.doi.org/10.1021/jp3112205.
[7] A.K. Ressmann, R. Zirbs, M. Pressler, P. Gaertner, K. Bica, Surface-active ionic liquids for micellar extraction of piperine from black pepper, Z. Naturforsch. B Chem. Sci. 68b (2013) 1129–1137, http://dx.doi.org/10.5560/ZNB.2013-3196.
[8] K. Bica, P. Gärtner, P.J. Gritsch, A.K. Ressmann, C. Schröder, R. Zirbs, Micellar catalysis in aqueous-ionic liquid systems, Chem. Commun. 48 (41) (2012) 5013–5015, http://dx.doi.org/10.1039/c2cc31503c.
[9] A. Cognigni, P. Gaertner, R. Zirbs, H. Peterlik, K. Prochazka, C. Schröder, K. Bica, Surface-active ionic liquids in micellar catalysis: impact of anion selection on reaction rates in nucleophilic substitutions, Phys. Chem. Chem. Phys. 18 (19) (2016) 13375–13384, http://dx.doi.org/10.1039/C6CP00493H.
[10] J. Nowicki, J. Łuczak, D. Stańczyk, Dual functionality of amphiphilic 1-alkyl-3-methylimidazolium hydrogen sulfate ionic liquids: surfactants with catalytic function, RSC Adv. 6 (14) (2016) 11591–11601, http://dx.doi.org/10.1039/C5RA23415H.
[11] M. Cokoja, R.M. Reich, M.E. Wilhelm, M. Kaposi, J. Schäffer, D.S. Morris, C.J. Münchmeyer, M.H. Anthofer, I.I.E. Markovits, F.E. Kühn, W.A. Herrmann, A. Jess, J.B. Love, Olefin epoxidation in aqueous phase using ionic-liquid catalysts, ChemSusChem 9 (14) (2016) 1773–1776, http://dx.doi.org/10.1002/cssc.201600373.
[12] M. Hejazifar, M. Earle, K.R. Seddon, S. Weber, R. Zirbs, K. Bica, Ionic liquid-based microemulsions in catalysis, J. Org. Chem. 81 (24) (2016) 12332–12339, http://dx.doi.org/10.1021/acs.joc.6b02165.
[13] K. Alfonsi, J. Colberg, P.J. Dunn, T. Fevig, S. Jennings, T.A. Johnson, H.P. Kleine, C. Knight, M.A. Nagy, D.A. Perry, M. Stefaniak, Green chemistry tools to influence a medicinal chemistry and research chemistry based organisation, Green Chem. 10 (1) (2008) 31–36, http://dx.doi.org/10.1039/B711717E.
[14] C. Parmeggiani, F. Cardona, Transition metal based catalysts in the aerobic oxidation of alcohols, Green Chem. 14 (3) (2012) 547, http://dx.doi.org/10.1039/c2gc16344f.
[15] F. Cardona, C. Parmeggiani, Transition metal catalysis in aerobic alcohol oxidation, in: RSC Green Chemistry, Royal Society of Chemistry, 2014, pp. P001–P006.
[16] D.S. Bailie, G.M.A. Clendenning, L. McNamee, M.J. Muldoon, Anionic N,O-ligated Pd(II) complexes: highly active catalysts for alcohol oxidation, Chem. Commun. 46 (38) (2010) 7238, http://dx.doi.org/10.1039/c0cc01138j.
[17] L.M. Dornan, G.M.A. Clendenning, M.B. Pitak, S.J. Coles, M.J. Muldoon, N, O-ligated Pd(II) complexes for catalytic alcohol oxidation, Catal. Sci. Tech. 4 (8) (2014) 2526, http://dx.doi.org/10.1039/c4cy00296b.
[18] C. Melero, O.N. Shishilov, E. Álvarez, P. Palma, J. Cámpora, Well-defined alkylpalladium complexes with pyridine-carboxylate ligands as catalysts for the aerobic oxidation of alcohols, Dalton Trans. 41 (46) (2012) 14087, http://dx.doi.org/10.1039/c2dt31728a.
[19] G.-J. ten Brink, I.W.C.E. Arends, R.A. Sheldon, Green, catalytic oxidation of alcohols in water, Science 287 (5458) (2000) 1636–1639, http://dx.doi.org/10.1126/science.287.5458.1636.
[20] G.-J. ten Brink, I.W.C.E. Arends, M. Hoogenraad, G. Verspui, R.A. Sheldon, Catalytic conversions in water. Part 22: Electronic effects in the (diimine)palladium(II)-catalysed aerobic oxidation of alcohols, Adv. Synth. Catal. 345 (2003) 497–505, http://dx.doi.org/10.1002/adsc.200390057.
[21] R.A. Sheldon, Recent advances in green catalytic oxidations of alcohols in aqueous media, Catal. Today 247 (2015) 4–13, http://dx.doi.org/10.1016/j.cattod.2014.08.024.
[22] E. Levin, E. Ivry, C.E. Diesendruck, N.G. Lemcoff, Water in N-heterocyclic carbene-assisted catalysis, Chem. Rev. 115 (11) (2015) 4607–4692, http://dx.doi.org/10.1021/cr400640e.
[23] B.S. Cho, I.G. Jung, Y.K. Chung, J.W. Han, Palladium-catalyzed aerobic oxidation reaction of 1-heptanol in water using water-soluble N-heterocyclic carbene ligands, Bull. Korean Chem. Soc. 36 (2015) 451–452, http://dx.doi.org/10.1002/bkcs.10105.
[24] M. Mifsud, K.V. Parkhomenko, I.W. Arends, R.A. Sheldon, Pd nanoparticles as catalysts for green and sustainable oxidation of functionalized alcohols in aqueous media, Tetrahedron 66 (5) (2010) 1040–1044, http://dx.doi.org/10.1016/j.tet.2009.11.007.
[25] M. Vasiloiu, P. Gaertner, R. Zirbs, K. Bica, Coordinating chiral ionic liquids: design, synthesis, and application in asymmetric transfer hydrogenation under aqueous conditions, Eur. J. Org. Chem. 2015 (11) (2015) 2374–2381, http://dx.doi.org/10.1002/ejoc.201403555.
[26] M. Vasiloiu, D. Rainer, P. Gaertner, C. Reichel, C. Schröder, K. Bica, Basic chiral ionic liquids: a novel strategy for acid-free organocatalysis, Catal. Today 200 (2013) 80–86, http://dx.doi.org/10.1016/j.cattod.2012.07.002.
[27] R. Nissim, C. Batchelor-McAuley, R.G. Compton, Measuring oxygen solubility in micelles, ChemElectroChem 3 (1) (2016) 105–109, http://dx.doi.org/10.1002/celc.201500380.
[28] W. Zhu, Y. Yu, H. Yang, L. Hua, Y. Qiao, X. Zhao, Z. Hou, Cooperative effects in catalytic hydrogenation regulated by both the cation and anion of an ionic liquid, Chem. Eur. J. 19 (6) (2013) 2059–2066, http://dx.doi.org/10.1002/chem.201202707.

[29] B.S. Souza, E.C. Leopoldino, D.W. Tondo, J. Dupont, F. Nome, Imidazolium-based zwitterionic surfactant: a new amphiphilic Pd nanoparticle stabilizing agent, Langmuir 28 (1) (2012) 833–840, http://dx.doi.org/10.1021/la203501f.
[30] C. Pardin, L. Leclercq, A. Schmitzer, N, N′-methylenediimidazolium salts: from self-assembly to an efficient DNAse protection system, Chem. Eur. J. 16 (15) (2010) 4686–4692, http://dx.doi.org/10.1002/chem.200902794.
[31] H. Li, Y. Qiao, L. Hua, Z. Hou, B. Feng, Z. Pan, Y. Hu, X. Wang, X. Zhao, Y. Yu, Imidazolium polyoxometalate: an ionic liquid catalyst for esterification and oxidative esterification, ChemCatChem 2 (9) (2010) 1165–1170, http://dx.doi.org/10.1002/cctc.201000021.
[32] W. Zhu, H. Yang, Y. Yu, L. Hua, H. Li, B. Feng, Z. Hou, Amphiphilic ionic liquid stabilizing palladium nanoparticles for highly efficient catalytic hydrogenation, Phys. Chem. Chem. Phys. 13 (30) (2011) 13492–13500, http://dx.doi.org/10.1039/c1cp20255c.
[33] J.M. Grill, J.W. Ogle, S.A. Miller, An efficient and practical system for the catalytic oxidation of alcohols, aldehydes, and α,β-unsaturated carboxylic acids, J. Org. Chem. 71 (25) (2006) 9291–9296, http://dx.doi.org/10.1021/jo0612574.
[34] A.E. Bradley, C. Hardacre, J.D. Holbrey, S. Johnston, S.E.J. McMath, M. Nieuwenhuyzen, Small-angle X-ray scattering studies of liquid crystalline 1-alkyl-3-methylimidazolium salts, Chem. Mater. 14 (2) (2002) 629–635, http://dx.doi.org/10.1021/cm010542v.
[35] Q.Q. Baltazar, J. Chandawalla, K. Sawyer, J.L. Anderson, Interfacial and micellar properties of imidazolium-based monocationic and dicationic ionic liquids, Colloids Surf., A 302 (1) (2007) 150–156, http://dx.doi.org/10.1016/j.colsurfa.2007.02.012.
[36] M. Blesic, M.H. Marques, N.V. Plechkova, K.R. Seddon, L.P.N. Rebelo, A. Lopes, Self-aggregation of ionic liquids: micelle formation in aqueous solution, Green Chem. 9 (2007) 481–490, http://dx.doi.org/10.1039/B615406A.
[37] S. Datta, J. Biswas, S. Bhattacharya, How does spacer length of imidazolium gemini surfactants control the fabrication of 2D-langmuir films of silver-nanoparticles at the airwater interface?, J Colloid Interface Sci. 430 (2014) 85–92, http://dx.doi.org/10.1016/j.jcis.2014.05.018.
[38] C.-J. Cheng, G.-M. Qu, J.-J. Wei, T. Yu, W. Ding, Thermodynamics of micellization of sulfobetaine surfactants in aqueous solution, J. Surfact. Deterg. 15 (6) (2012) 757–763, http://dx.doi.org/10.1007/s11743-012-1374-8.
[39] C. Ren, F. Wang, Z. Zhang, H. Nie, N. Li, M. Cui, Synthesis, surface activity and aggregation behavior of gemini imidazolium surfactants 1,3-bis(3-alkylimidazolium-1-yl) propane bromide, Colloids Surf., A 467 (2015) 1–8, http://dx.doi.org/10.1016/j.colsurfa.2014.11.031.
[40] S.L. Desset, S.W. Reader, D.J. Cole-Hamilton, Aqueous-biphasic hydroformylation of alkenes promoted by weak surfactants, Green Chem. 11 (5) (2009) 630, http://dx.doi.org/10.1039/b822139a.
[41] J. Łuczak, M. Markiewicz, J. Thöming, J. Hupka, C. Jungnickel, Influence of the hofmeister anions on self-organization of 1-decyl-3-methylimidazolium chloride in aqueous solutions, J. Colloid Interface Sci. 362 (2) (2011) 415–422, http://dx.doi.org/10.1016/j.jcis.2011.06.058.
[42] M.K. Starchevsky, S.L. Hladiy, Y.A. Pazdersky, M.N. Vargaftik, I.I. Moiseev, Giant Pd-561 clusters: onset to new catalytic properties, J. Mol. Catal. A: Chem. 146 (1) (1999) 229–236, http://dx.doi.org/10.1016/S1381-1169(99)00086-2.
[43] G. Kovtun, T. Kameneva, S. Hladyi, M. Starchevsky, Y. Pazdersky, I. Stolarov, M. Vargaftik, I. Moiseev, Oxidation, redox disproportionation and chain termination reactions catalysed by the Pd-561 giant cluster, Adv. Synth. Catal 344 (2002) 957–964, http://dx.doi.org/10.1002/1615-4169(200210)344:9<957::AID-ADSC957>3.0.CO;2-V.
[44] A. Ohtaka, R. Kuroki, T. Teratani, T. Shinagawa, G. Hamasaka, Y. Uozumi, O. Shimomura, R. Nomura, Recovery of in situ-generated Pd nanoparticles with linear polystyrene, Green Sust. Chem. 01 (2) (2011) 19–25, http://dx.doi.org/10.4236/gsc.2011.12004.
[45] G. Giachi, W. Oberhauser, M. Frediani, E. Passaglia, L. Capozzoli, L. Rosi, Pd-nanoparticles stabilized by pyridine-functionalized poly(ethylene glycol) as catalyst for the aerobic oxidation of α,β-unsaturated alcohols in water, J. Polym. Sci., Part A: Polym. Chem. 51 (11) (2013) 2518–2526, http://dx.doi.org/10.1002/pola.26645.
[46] C. Zhu, Y. Wei, L. Ji, Catalytic oxidation of alcohols to corresponding aldehydes or ketones with TEMPO-mediated iodosobenzene in water in the presence of a surfactant, Synth. Commun. 40 (14) (2010) 2057–2066, http://dx.doi.org/10.1080/00397910903219427.
[47] S.E. Davis, M.S. Ide, R.J. Davis, Selective oxidation of alcohols and aldehydes over supported metal nanoparticles, Green Chem. 15 (1) (2013) 17–45, http://dx.doi.org/10.1039/C2GC36441G.
[48] S. Rostamnia, E. Doustkhah, Z. Karimi, S. Amini, R. Luque, Surfactant-exfoliated highly dispersive pd-supported graphene oxide nanocomposite as a catalyst for aerobic aqueous oxidations of alcohols, ChemCatChem 7 (11) (2015) 1678–1683, http://dx.doi.org/10.1002/cctc.201500126.
[49] C.V. Gaskell, C.M.A. Parlett, M.A. Newton, K. Wilson, A.F. Lee, Redox-controlled crotyl alcohol selective oxidation: in situ oxidation and reduction dynamics of catalytic Pd nanoparticles via synchronous XANES/MS, ACS Catal. 2 (11) (2012) 2242–2246, http://dx.doi.org/10.1021/cs300445y.
[50] B. Feng, Z. Hou, H. Yang, X. Wang, Y. Hu, H. Li, Y. Qiao, X. Zhao, Q. Huang, Functionalized poly(ethylene glycol)-stabilized water-soluble palladium nanoparticles: property/activity relationship for the aerobic alcohol oxidation in water, Langmuir 26 (4) (2010) 2505–2513, http://dx.doi.org/10.1021/la9027755.
[51] E. Drinkel, F.D. Souza, H.D. Fiedler, F. Nome, The chameleon effect in zwitterionic micelles: Binding of anions and cations and use as nanoparticle stabilizing agents, Curr. Opin. Colloid Interface Sci. 18 (1) (2013) 26–34, http://dx.doi.org/10.1016/j.cocis.2013.01.001.
[52] D.W. Tondo, E.C. Leopoldino, B.S. Souza, G.A. Micke, A.C.O. Costa, H.D. Fiedler, C.A. Bunton, F. Nome, Synthesis of a new zwitterionic surfactant containing an imidazolium ring. Evaluating the chameleon-like behavior of zwitterionic micelles, Langmuir 26 (20) (2010) 15754–15760, http://dx.doi.org/10.1021/la102391e.
[53] S. Pandey, S.K. Upadhyay, Effect of cationic micellar aggregates on the kinetics of oxidation of aminoalcohols by n-bromosuccinimide in alkaline medium, J. Colloid Interf. Sc. 285 (2) (2005) 789–794, http://dx.doi.org/10.1016/j.jcis.2004.01.085.
[54] P. Sar, A. Ghosh, S. Malik, D. Ray, B. Das, B. Saha, Selective heteroaromatic nitrogen base promoted chromium(VI) oxidation of isomeric pentanols in aqueous micellar media at room temperature, J. Ind. Eng. Chem. 42 (2016) 53–62, http://dx.doi.org/10.1016/j.jiec.2016.07.028.
[55] P. Bhattacharyya, A. Ghosh, B. Saha, Room temperature micellar catalysis on permanganate oxidation of butanol to butanal in aqueous medium at atmospheric pressure, Tenside Surfact. Deterg. 52 (1) (2015) 36–40, http://dx.doi.org/10.3139/113.110346.
[56] A. Ghosh, R. Saha, B. Saha, Effect of CHAPS and CPC micelles on Ir(III) catalyzed Ce(IV) oxidation of aliphatic alcohols at room temperature and pressure, J. Mol. Liq. 196 (2014) 223–237, http://dx.doi.org/10.1016/j.molliq.2014.03.037.
[57] B.-T. Chen, K.V. Bukhryakov, R. Sougrat, V.O. Rodionov, Enzyme-inspired functional surfactant for aerobic oxidation of activated alcohols to aldehydes in water, ACS Catal. 5 (2) (2015) 1313–1317, http://dx.doi.org/10.1021/cs5020018.
[58] M. Bettoni, L. Brinchi, T. Del Giacco, R. Germani, S. Meniconi, C. Rol, G.V. Sebastiani, Surfactant effect on titanium dioxide photosensitized oxidation of 4-dodecyloxybenzyl alcohol, J. Photochem. Photobiol. A Chem. 229 (1) (2012) 53–59, http://dx.doi.org/10.1016/j.jphotochem.2011.12.003.

RSC Advances

PAPER

Check for updates

Cite this: *RSC Adv.*, 2017, **7**, 41144

Surface-active ionic liquids for palladium-catalysed cross coupling in water: effect of ionic liquid concentration on the catalytically active species†

Meltem Taskin,‡[a] Alice Cognigni,‡[a] Ronald Zirbs,[b] Erik Reimhult[b] and Katharina Bica*[a]

Received 14th July 2017
Accepted 10th August 2017

DOI: 10.1039/c7ra07757b

rsc.li/rsc-advances

We report the design and synthesis of surface-active ionic liquids for application in palladium-catalyzed cross coupling reactions. A series of dodecylimidazolium-based ionic liquids were applied as additives in the Heck reaction of ethyl acrylate and iodobenzene, and high yields of >90% could be obtained in water without the addition of further ligands. Our results indicate that the ionic liquid concentration in water is the key factor affecting the formation of the catalytically active species and hence the yield. Moreover, imidazolium-based ionic liquids that are able to form a carbene species differ significantly from conventional cationic surfactants, as a concentration dependent formation of the N-heterocyclic carbene complex was observed.

Introduction

With the recent focus on sustainable chemistry, considerable effort has been spent on the search for novel reaction media, *e.g.* ionic liquids for improved performance, catalyst recycling and product separation. In a seminal paper in 1999, Carmichael *et al.* demonstrated the potential of ionic liquids in multiphase Heck reactions and opened the field for palladium-catalysed cross-coupling in ionic liquids.[1] A number of benefits in terms of catalyst reuse and facilitated product separation based on the distinctive phase behaviour exist in ionic liquids.[2] Moreover, changes in reactivity compared to traditional molecular solvents were observed based on the ionic nature of the reaction media.[3] In fact, it is now well recognized that ionic liquids are far from innocent when used as solvents in transition metal chemistry and can actively participate in catalysis.[4] This is particularly true for 1,3-dialkylimidazolium-based ionic liquids that are likely to take an active part in a reaction,[5,6] for example *via* the formation of a N-heterocyclic carbene complex with a number of transition metals,[7,8] substrates[9] or gases such as CO_2.[10]

In parallel to the developments in the area of ionic liquids, research has focused on the use of water as the most abundant and non-toxic solvent for transition metal catalysis.[11] Aqueous organic solvents, *e.g.* H_2O–dimethylformamide, but also aqueous organic biphasic systems in combination with water-soluble ligands were successfully applied in palladium catalysis under aqueous conditions, although the nature of the active catalyst in water is not always completely understood.[12] The limited solubility of many organic starting materials can be overcome by the addition of surfactants, and ground-breaking contributions by Lipshutz and co-workers revealed the potential of aqueous-micellar systems for palladium-catalysed cross-coupling.[13] The development of designer surfactants based on nature-derived tocopherol cores resulted in outstanding catalytic activity for a number of transition-metal catalysed processes and a revival of interest in micellar catalysis.[14]

The scope of ionic liquids as alternative solvents has only been recently expanded to include their well-defined mixtures with water.[15] While the typical properties of ionic liquids continue to exist at low to moderate water content, electrostatic screening is progressively attenuated with higher dilution. For short chain imidazolium-based ionic liquids, the interaction with water is mediated by the anions as they are capable of forming hydrogen bonds with water.[16] However, these aqueous ionic liquid mixtures seem to resemble polar mixtures rather than behave as normal electrolytes.[17] Increasing the alkyl chain length of the imidazolium cations leads to aggregation and consequently to the formation of micelles.[18] This provides a dual beneficial approach for synthesis and catalysis, as surface-active ionic liquids in water cannot only overcome the price or viscosity issues of pure ionic liquids as solvents, but form nanoreactors that can easily be tuned and modified to fit the reaction requirements.[19]

[a]*Institute of Applied Synthetic Chemistry, Vienna University of Technology, Getreidemarkt 9/163, 1060 Vienna, Austria. E-mail: katharina.schroeder@tuwien.ac.at; Fax: +43 1 58801 16360; Tel: +43 1 58801 163601*

[b]*Institute for Biologically Inspired Materials, Department of Nanobiotechnology, University of Natural Resources and Life Sciences, Vienna, Muthgasse 11-II, A-1190 Vienna, Austria*

† Electronic supplementary information (ESI) available. See DOI: 10.1039/c7ra07757b

‡ These authors contributed equally to this work.

This journal is © The Royal Society of Chemistry 2017

Consequently, the aggregation behaviour of ionic liquids with an alkyl chain longer than eight carbon atoms in water has been increasingly investigated in the past years, particularly for imidazolium based derivatives.[20–23] Micellar aggregates of surface-active imidazolium-based ionic liquids can increase the solubility of organic compounds in water,[24] which renders them ideally suited for the extraction of natural compounds from biomass.[25–28] Moreover, the high tunability of surface-active ionic liquids provides a powerful tool for synthesis and catalysis in water. A strong impact on activity and selectivity through specific interactions between micelle, substrates and catalysts has been observed by a number of authors.[29–34]

In our previous work, we demonstrated that the self-organization of surface-active 1-alkyl-3-methylimidazolium salts [$C_n$mim]X can considerably increase the rate constants of organic and transition metal catalyzed reactions compared to neat water and can affect the outcome of the reactions.[35,36] Here, we explore their application towards palladium-catalysed cross coupling and present a striking influence of ionic liquid concentration on the catalytic performance.

Results and discussion

The choice of ionic liquid type can be crucial for the success or failure of any organic reaction. We selected a set of surface-active imidazolium-based ionic liquids **1–8** that are composed of a hydrophilic imidazolium head group and a hydrophobic dodecyl chain (Fig. 1). Consequently, they exhibit amphiphilic behaviour, forming micelles in aqueous solution. Critical micelle concentrations (CMC) typically between 5 and 15 mM have been reported by a number of authors (see ESI Table S1†).[20,37–40] We were particularly interested in surface-active ionic liquids with imidazolium cores and optional side-chain functionalization, as they offer the possibility for N-heterocyclic carbene (NHC) formation.[41,42] Carbene formation in imidazolium salts typically occurs by deprotonation of the acidic proton in position 2, although carbenes on position 4 and 5 have been described as well.[10] However, these so-called normal carbenes are typically less stable and hardly observed in an aqueous environment.[42] For comparison, we have also included the 1,2-dimethylimidazolium-based ionic liquid [$C_{12}m_2$im]Cl in our selection.

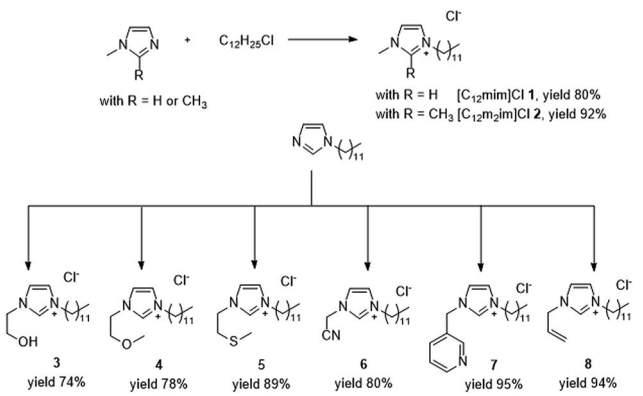

Fig. 1 Selection and synthesis of amphiphilic imidazolium chlorides **1–8** for palladium-catalysed cross coupling in aqueous solution. CMC: critical micelle concentration determined *via* surface tension measurements at 25 °C. See ESI Table S1† for more information.

Unfunctionalized surface-active ionic liquids [C_{12}mim]Cl **1** and [$C_{12}m_2$im]Cl **2** were prepared *via* the direct alkylation of 1-methylimidazole or 1,2-dimethylimidazole with dodecyl chloride. For the functionalized ionic liquids **3–8** we relied on a two-step procedure *via* the pre-formation of *N*-dodecylimidazolium which was then further reacted with the appropriate halides. This gave straight forward access to the desired functionalized surface-active ionic liquids. In any case, the surface-active ionic liquids were obtained as colourless crystals in excellent yields after recrystallization from suitable solvents.

Initial experiments on the Heck reaction were performed in 100 mM solutions of surface-active ionic liquids **1–8** in water, as this concentration is well above the critical micelle concentrations of the respective surface-active ionic liquids (Fig. 2). The reaction of ethyl acrylate and iodobenzene using $Pd_2(allyl)_2Cl_2$ as the metal source was performed at 80 °C and revealed a surprising behaviour (Table 1). While high yields at 100 mM concentration could be obtained with the ionic liquid [$C_{12}m_2$im]Cl **2**, all other ionic liquids (**1** and **3–8**) that have a proton available at C-2 failed as reaction media and were outperformed even by pure water. In contrast, a completely different behaviour was observed when lowering the concentration to 10 mM. In the case of the surface-active ionic liquid [C_{12}mim]Cl **1** the yield increased to 51%. This increase of yield at a lower surfactant concentration was observed for all side-chain functionalized ionic liquids with the exception of the pyridine derivative **7**, and the best yields were obtained with the nitrile-functionalized imidazolium chloride **6**. In contrast, the yield of ethyl cinnamate **11** was reduced to 25% when lowering the concentration of [$C_{12}m_2$im]Cl **2** to 10 mM.

Further investigation revealed a striking influence of the concentration of the surface-active ionic liquids and a fundamentally different behaviour between the C-2 protonated and methylated ionic liquids (Fig. 3). In the case of [C_{12}mim]Cl **1**, a decrease of the concentration in water resulted in a sudden increase in catalytic activity at 10 mM. A maximum yield of 51% was found at 10 mM, whereas yields gradually dropped with a further decrease of the concentration to eventually reach the values that were obtained with pure water. This rather unique behaviour is entirely different to the concentration effect observed in the C-2 methylated ionic liquid [$C_{12}m_2$im]Cl **2**, for which high yields of up to 92% were observed that gradually decreased over the entire concentration range, as would be expected in the presence of a commonly used surfactant in water.

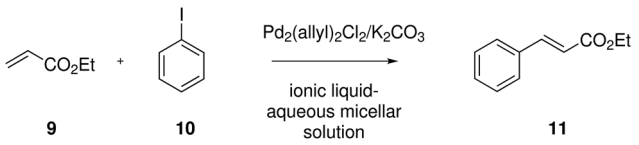

Fig. 2 Palladium-catalysed Heck reaction of ethyl acrylate **9** and iodobenzene **10** in ionic liquid-aqueous micellar solutions.

Table 1 Impact of surface-active ionic liquid concentration in the palladium-catalyzed Heck reaction of ethyl acrylate **9** and iodobenzene **10**

Entry[a]	Surfactant	Conc. (mM)	Yield[b] (%)
1	$[C_{12}mim]Cl$ **1**	100	<1
2	$[C_{12}m_2im]Cl$ **2**	100	92
3	**3**	100	<1
4	**4**	100	<1
5	**5**	100	<1
6	**6**	100	<1
7	**7**	100	<1
8	**8**	100	<1
9	CTAB	100	52
10	$[C_{12}mim]Cl$ **1**	10	51
11	$[C_{12}m_2im]Cl$ **2**	10	25
12	**3**	10	51
13	**4**	10	16
14	**5**	10	12
15	**6**	10	68
16	**7**	10	<1
17	**8**	10	11
18	CTAB	10	20
19	Pure H_2O	—	3

[a] Reactions were carried out with 1 mmol ArI, 1.5 mmol ethyl acrylate and 1.5 mmol K_2CO_3 in 5 mL of aqueous ionic liquid solution at 80 °C under air for 180 min. [b] Yield determined *via* HPLC using phenol as internal standard.

In fact, when comparing $[C_{12}m_2im]Cl$ **2** with the conventional cationic surfactant cetyltrimethylammonium bromide (CTAB), a similar trend was observed, although the ionic liquid performed significantly better and gave almost twice the yield. This outstanding performance of imidazolium-based surface-active ionic liquids compared to conventional ammonium-based surfactants is in accordance with our previous observations in micellar catalysis and might be a result of the different interplay of headgroup hydration and counterion binding in imidazolium-based surfactants.[43]

As can be easily observed from the appearance of the reaction mixture, this striking concentration effect in the case of surface-active ionic liquid **1** is caused by the presence of different catalytically active palladium species in the aqueous reaction media. At a concentration of 10 mM and below, the black appearance of the reaction mixture indicated the formation of catalytically-active Pd(0) aggregates. This might also explain why the highest yield was obtained with the nitrile-functionalized surface-active ionic liquid: it has been reported that imidazolium-based ionic liquids with CN groups in the side chain can simultaneously act as a solvent and efficiently stabilize palladium nanoparticles, although these observations refer to pure ionic liquids rather than to their aqueous solutions.[44] At higher concentration a soluble palladium species is present, presumably the NHC complex immobilized on the micellar surface (Fig. 4). This switch between the soluble carbene complex and Pd(0) particles between approx. 10 and 15 mM seems to correlate roughly with the critical micelle concentration (CMC) of the involved ionic liquids that vary between 2 and 13 mM. However, it should be noted that the CMC values are

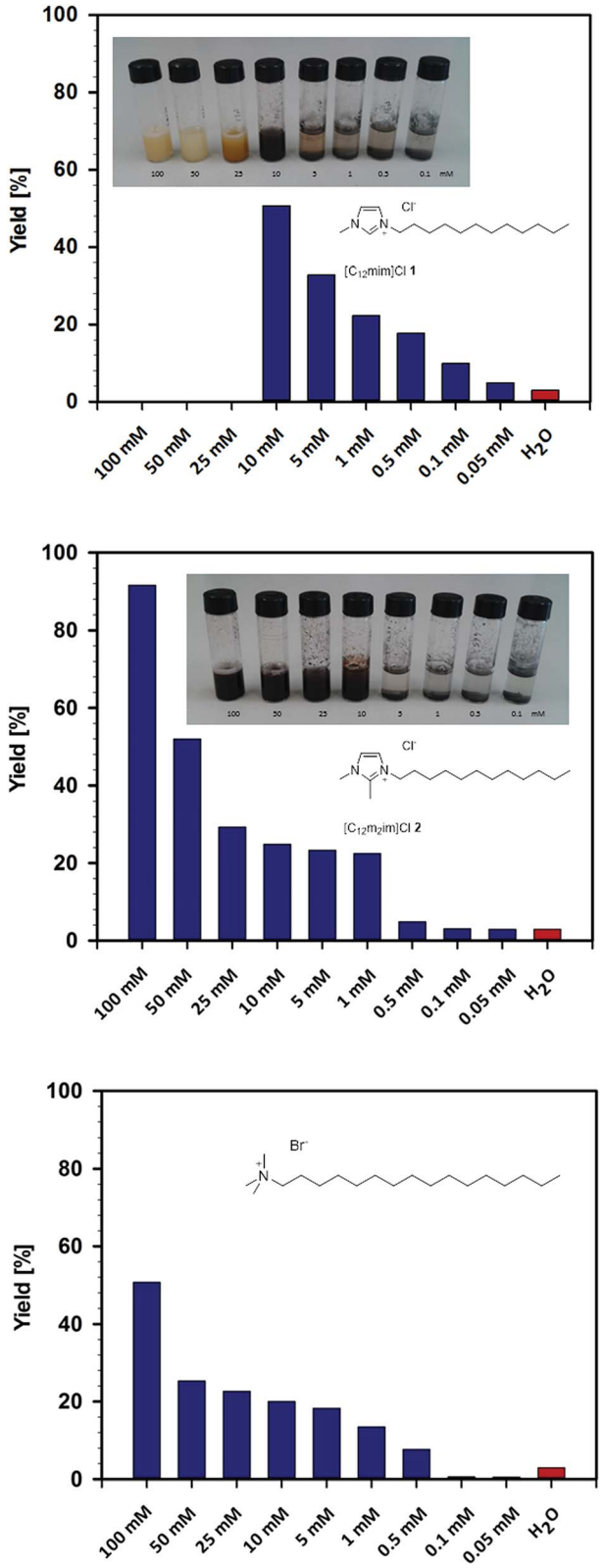

Fig. 3 Concentration dependence of the Heck reaction of ethyl acrylate **9** and iodobenzene **10** in aqueous solutions of ionic liquids $[C_{12}mim]Cl$ **1** (top) and $[C_{12}m_2im]Cl$ **2** (middle) and the conventional surfactant CTAB (bottom).

 This journal is © The Royal Society of Chemistry 2017

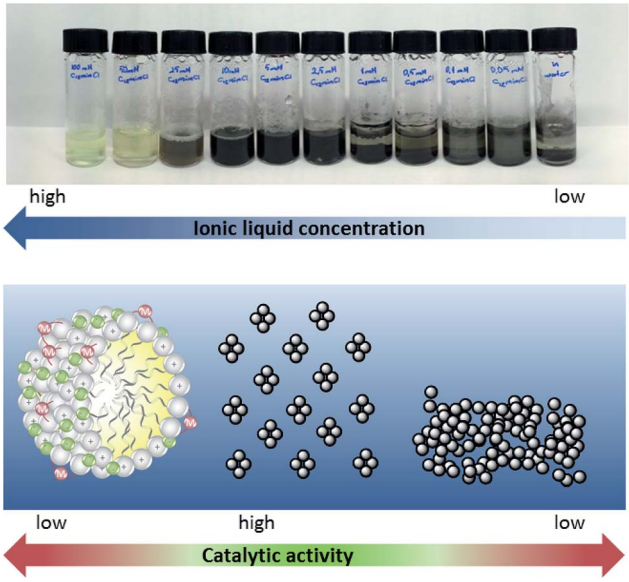

Fig. 4 Concentration dependence of palladium-metallomicelles and Pd nanoparticles in aqueous-ionic liquid micellar solution. Conditions: 2 mL [C_{12}mimCl] **1** solution, 0.02 mmol $Pd_2(allyl)_2Cl_2$ and 0.02 mmol K_2CO_3; 60 min at 80 °C under air.

determined for pure aqueous solutions at 25 °C, whereas reactions were run at 80 °C in the presence of salts and reagents, and a certain deviation has to be expected. Additionally, the formed Pd(0) aggregates seem well stabilized in a 10 mM [C_{12}mim]Cl **1** solution; however, when the concentration of surfactant further decreases the surfactant tends to agglomerate and form catalytically inactive bulk palladium; hence the yield of ethyl cinnamate gradually decreases below 5 mM.

The consecutive evaluation of reaction conditions showed that a switch to organic bases, *e.g.* diisopropylethylamine (DIPEA) could further improve conversion towards the Heck product, while the extraordinary concentration dependence of [C_{12}mim]Cl **1** was retained (see ESI Fig. S1†). A further increase in reaction time to 6 h gave complete conversion of iodobenzene. Under the optimized conditions we were able to isolate ethyl cinnamate in 92% yield using a 10 mM solution of [C_{12}mim]Cl **1** in water (Table 2). This provides an efficient protocol for aqueous Heck reaction under aerobic conditions, using only small amounts of surface-active ionic liquid in water without further ligands. To complement this, the reaction could also be optimized for the surface-active ionic liquid [$C_{12}m_2$im]Cl **2**; here a higher ionic liquid concentration of 100 mM under otherwise similar reaction conditions was found as the optimum and ethyl cinnamate could be isolated in 93% yield. To evaluate the potential catalytic activity, we switched from iodobenzene to bromobenzene and chlorobenzene; however, yields remained low for bromobenzene whereas no conversion was observed for chlorobenzene independent of the ionic liquid used. Although few highly-active water-soluble palladium complexes have been reported for this purpose, the coupling of aryl halides other than iodobenzene clearly remains a challenge, particularly when using ligand-free systems. Moreover,

Table 2 Screening of reaction conditions for surface-active ionic liquids

Entry[a]	Ionic liquid	Conc. (mM)	Base	Time (min)	Yield[b,c] (%)
1	[C_{12}mim]Cl **1**	10	K_2CO_3	180	52
2	[C_{12}mim]Cl **1**	10	Na_2CO_3	180	46
3	[C_{12}mim]Cl **1**	10	NaOH	180	11
4	[C_{12}mim]Cl **1**	10	NaOAc	180	48
5	[C_{12}mim]Cl **1**	10	Et_3N	180	71
6	[C_{12}mim]Cl **1**	10	DIPEA	180	90
7	[C_{12}mim]Cl **1**	10	DIPEA	360	>99 (92)
8	[$C_{12}m_2$im]Cl **2**	100	DIPEA	360	99 (93)
9	Pure H_2O	—	DIPEA	360	1

[a] Reactions were carried out with 1 mmol ArI, 1.5 mmol ethyl acrylate and 1.5 mmol base in 5 mL of aqueous ionic liquid solution at 80 °C under air. [b] Yield determined *via* HPLC using phenol as internal standard. [c] Isolated yield after column chromatography.

the reduction of the palladium source to lower amounts < 1 mol% resulted in drastically lower yields, thereby clearly showing the limitations of this approach.

Further investigations towards the formation of the catalytically active species were performed in solutions of [C_{12}mim]Cl **1** in the presence of K_2CO_3 and $Pd_2(allyl)_2Cl_2$ without the addition of the starting materials. A rapid and temperature-induced formation of Pd(0) was again observed for ionic liquid concentrations below 25 mM when the sample was heated for 60 min at 80 °C under aerobic conditions. At higher concentrations, a soluble palladium species was present (Fig. 4). This was also supported *via* UV-vis spectroscopy, as a disappearance of the band at 305 nm was observed within 60 min at 80 °C for a 5 mM solution, indicating the formation of palladium nanoparticles.[45] In contrast, no change of the spectrum was observed for a 50 mM solution. ^{13}C NMR spectroscopy in D_2O gave clear evidence for the presence of a NHC–carbene complex in [C_{12}mim]Cl **1** at high concentrations, as the typical signal of C-2 emerged at 177 ppm (see ESI Fig. S2†). This concentration-dependent change between the palladium species is different to other literature protocols showing the formation of palladium nanoparticles in aqueous solutions of surface-active ionic liquids. For example Zhu *et al.* reported the formation of well-dispersed palladium colloids in amphiphilic imidazolium-based ionic liquids that acted simultaneously as stabilizers for the nanoparticles and as surfactants generating an emulsion for the hydrophobic substrates.[46] Palladium nanoparticles were prepared in aqueous solution *via* hydrogenation, and are formed independent of the concentration range of the ionic liquid. When assessing the impact of ionic liquid concentration on the catalytic activity, the authors observed a constant increase in turn-over frequency (TOF) that continued distinctly above the CMC of the respective ionic liquid, and only decreases slowly at very high concentrations.

The switch between the soluble palladium carbene complex and Pd(0) was further confirmed *via* transmission electron microscopy (TEM) (Fig. 5). In the case of ionic liquid [C_{12}mim]Cl **1**, small, spherical Pd(0) nanoparticles are formed at ionic liquid concentrations < 25 mM that aggregate into well-

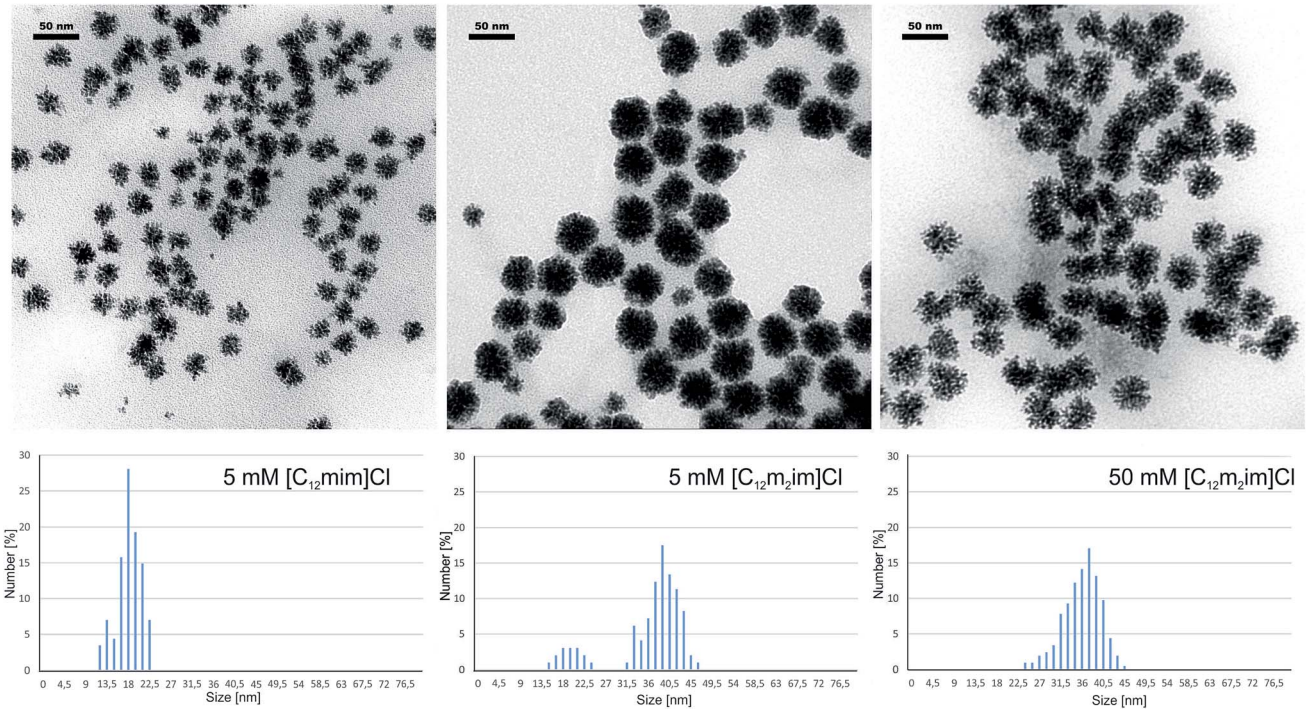

Fig. 5 Transmission electron microscopy (TEM) analysis of Pd aggregates and their corresponding size distribution. Left: 5 mM [C_{12}mim]Cl **1**, middle: 5 mM [$C_{12}m_2$im]Cl **2**, right: 50 mM [$C_{12}m_2$im]Cl **2**; conditions: 2 mL ionic liquid solution, 0.02 mmol $Pd_2(allyl)_2Cl_2$ and 0.02 mmol K_2CO_3; 60 min at 80 °C under air.

dispersed star-shaped clusters of approx. 20 nm diameter. The unique concentration dependence of the soluble palladium complex and nanoparticles was not found for the C-2 methylated ionic liquid [$C_{12}m_2$im]Cl **2**. We observed the formation of Pd(0) aggregates over the entire concentration range; however, when comparing the size distribution in a 5 mM [$C_{12}m_2$im]Cl **2** solution, larger aggregates with approx. 40 nm diameter were formed.

Conclusion

We presented the application of surface-active imidazolium-based ionic liquids in water as reaction media for Pd-catalyzed cross coupling and found a surprising concentration effect. Our results indicate that the ionic liquid concentration is the key factor affecting the morphology and chemical state of the palladium species and thus for controlling the catalytic activity in Heck-coupling. While an N-heterocyclic carbene complex is formed at higher concentrations, these metallomicelles rapidly decompose into catalytically active Pd(0) nanoclusters at lower surfactant concentrations. This unique behaviour was only observed for amphiphilic ionic liquids that are able to form a carbene species in water and differs significantly from dimethylimidazolium-based ionic liquids or from conventional surfactants. We envision that imidazolium based surfactants can therefore simultaneously act as templates for nanoparticle formation *via* NHC carbene complex formation, but also as stabilizers and surfactants for a consecutive reaction, and more investigations in this regard are currently ongoing in our lab.

Experimental

General

Commercially available reagents and solvents were used as received from Sigma Aldrich unless otherwise specified. *N*-Methylimidazole was distilled before use. All ionic liquids were dried for at least 48 h at room temperature and 0.01 mbar before use and were stored under an argon atmosphere. Doubly-distilled deionized water was obtained from a Millipore Milli-Q water purification system (Millipore, USA).

^{1}H and ^{13}C NMR spectra were recorded on a Bruker Advance UltraShield 400 (400 MHz) spectrometer, using the solvent peak as reference. Elemental analysis was performed at the University of Vienna, Department of Physicochemistry Laboratory for Microanalysis, Währingerstrasse 42, A-1090 Vienna. The FT-IR spectrometer was equipped with a specac MK II Golden Gate Single Reflection ATR unit. TEM studies were performed on a FEI Tecnai G2 20 transmission electron microscope operating at 160 kV. A drop of the dispersion was added on a 300-mesh carbon-coated copper grid and the solvent was subsequently evaporated in air.

HPLC analysis was performed on a Jasco HPLC unit equipped with a PDA detector under reverse-phase conditions. A Maisch ReproSil 100 C18 250 × 4.6, 5 μm was used with MeOH : H_2O (70 : 30; 0.1% trifluoroethanoic acid) as solvent and a flow of 0.8 cm^3 min^{-1}; detection was at 210 nm, at 30 °C column oven temperature. Calibration curves were prepared in the range from 2.0–0.01 mg mL^{-1} for starting materials and products using phenol as internal standard.

 This journal is © The Royal Society of Chemistry 2017

For the determination of the critical micelle concentrations (CMCs) of the surface-active ionic liquids a similar protocol to our previous work was followed.[36] Solutions at various concentrations of the ionic liquids were prepared with doubly-distilled Millipore Milli-Q water and left under shaking at 360 min^{-1} for 24 h at room temperature (RT) to equilibrate. For conductivity measurements, samples were previously equilibrated at 25 ± 0.1 °C in a HAAKE K15 thermostat. Conductivity measurements were performed on a Mettler Toledo Seven Excellence system, equipped with an InLAB 741-ISM electrode (cell constant κ = 0.105). The conductometer was calibrated with a standard KCl solution and two independent measurements were performed. The CMC was calculated as the intersection point of the two linear regimes in the conductivity/concentration graph. Surface tension was determined with the Du Noüy ring method on a Krüss manual tensiometer K6 at room temperature. Each measurement was repeated 5 times.

Synthesis of ionic liquids

Unfunctionalized imidazolium salts [C_{12}mim]Cl **1** and [$C_{12}m_2$im]Cl **2** were synthesized according to standard methodologies, which include the alkylation of *N*-methylimidazole or dimethylimidazole with the appropriate dodecyl chloride to afford the corresponding imidazolium halide. The imidazolium salts were repeatedly crystallized in order to obtain colorless solids. All ionic liquids were dried for at least 48 h at room temperature and 0.01 mbar before use and were stored under an argon atmosphere.

1-Dodecyl-3-methylimidazolium chloride (1). After following the general procedure the product was repeatedly recrystallized from THF and obtained in 80% yield. ^{1}H NMR (400 MHz; $CDCl_3$; 22 °C): δ (ppm) = 10.57 (1H, s, H(2)-im), 7.54 (1H, s, H(5)-im), 7.35 (1H, s, H(4)-im), 4.27 (2H, t, NCH_2, J = 14.83 Hz), 4.09 (3H, s, NCH_3), 1.86 (2H, m, $NCH_2\mathit{CH_2}$), 1.20 (18H, m, $\mathit{C_9H_{18}}CH_3$), 0.83 (3H, t, $NC_{11}H_{22}\mathit{CH_3}$, J = 6.36 Hz). ^{13}C NMR (100 MHz; $CDCl_3$; 22 °C): δ (ppm) = 137.35 (d, C(2)-im), 123.76 (d, C(5)-im), 121.83 (d, C(4)-im), 49.83 (t, NCH_2), 36.38 (q, NCH_3), 26.09–31.72 (t, $C_8H_{16}CH_2CH_3$), 22.48 (t, NCH_2CH_2), 13.93 (q, CH_3). The data was in accordance with the literature.[33]

1-Dodecyl-2,3-dimethylimidazolium chloride (2). After following the general procedure the product was repeatedly recrystallized from THF and obtained in 92% yield. ^{1}H NMR (400 MHz; $CDCl_3$; 22 °C): δ (ppm) = 7.78 (1H, d, H(5)-im, J = 2.08 Hz), 7.44 (1H, d, H(4)-im, J = 2.04 Hz), 4.10 (2H, t, NCH_2, J = 14.88 Hz), 3.93 (3H, s, NCH_3), 2.70 (3H, s, –CCH_3), 1.67 (2H, m, $NCH_2\mathit{CH_2}$), 1.11 (18H, m, $CH_2\mathit{C_9H_{18}}CH_3$), 0.74 (3H, t, $NC_{11}H_{22}\mathit{CH_3}$, J = 6.86 Hz). ^{13}C NMR (100 MHz; $CDCl_3$; 22 °C): δ (ppm) = 143.44 (d, C(2)-im), 123.31 (d, C(5)-im), 121.15 (d, C(4)-im), 49.84 (t, NCH_2), 35.88 (q, NCH_3), 31.76–26.42 (t, $C_8H_{16}CH_2CH_3$), 22.55 (t, NCH_2CH_2), 14.00 (q, CH_3), 10.47 (q, CH_3). The data was in accordance with the literature.[33]

Functionalized imidazolium salts **3–8** were synthesized through a two step procedure involving the alkylation of 1-dodecylimidazole which was previously synthesized following a procedure reported in the literature and distilled before use with the appropriate halide.[47]

1-Dodecyl-3-(2-hydroxyethyl)-imidazolium chloride (3). *N*-Dodecylimidazole (5.00 g, 21.2 mmol) was mixed with 2-chloroethanol (2.90 g, 36.0 mmol). The mixture was heated to 50 °C for 76 h. After evaporation of the remaining volatile materials, the crude product was twice crystallized from anhydrous THF to yield 1-dodecyl-2-(2-hydroxyethyl)-imidazolium chloride (**3**) as a colourless solid in 74% yield. ^{1}H NMR (400 MHz, $CDCl_3$; 22 °C): δ (ppm) = 9.72 (1H, s, H(2)-im), 7.68 (1H, s, H(5)-im), 7.32 (1H, s, H(4)-im), 5.13 (1H, m, OH), 4.53 (2H, t, $HOCH_2\mathit{CH_2}N$, J = 4.31 Hz), 4.41 (2H, t, NCH_2, J = 7.21 Hz), 3.83 (2H, t, $HO\mathit{CH_2}$-CH_2N, J = 4.13 Hz), 1.77 (2H, m, $NCH_2\mathit{CH_2}$), 1.13 (18H, m, $\mathit{C_9H_{18}}CH_3$), 0.75 (3H, t, $NC_{11}H_{22}\mathit{CH_3}$, J = 7.13 Hz). ^{13}C NMR (100 MHz; $CDCl_3$; 22 °C): δ (ppm) = 138.10 (d, C(2)-im), 124.12 (d, C(5)-im), 121.72 (d, C(4)-im), 62.69 (t, $HO\mathit{CH_2}CH_2N$), 52.00 (t, $HOCH_2\mathit{CH_2}N$), 50.13 (t, NCH_2), 30.11–26.74 (t, $C_8H_{16}CH_2CH_3$), 22.48 (t, $NCH_2\mathit{CH_2}$), 13.93 (q, CH_3). The data was in accordance with the literature.[40]

1-Dodecyl-3-(2-methoxyethyl)-imidazolium chloride (4). *N*-Dodecylimidazole (5.00 g, 21.2 mmol) was mixed with 1-chloro-2-methoxyethane (3.60 g, 38.1 mmol). The mixture was heated to 80 °C for 76 h. After evaporation of the remaining volatile materials, the crude product was twice crystallized from anhydrous THF to yield 1-dodecyl-3-(2-methoxyethyl)-imidazolium chloride (**4**) as a colourless solid in 78% yield. ^{1}H NMR (400 MHz, $CDCl_3$; 22 °C): δ (ppm) = 10.67 (1H, s, H(2)-im), 7.49 (1H, s, H(5)-im), 7.24 (1H, s, H(4)-im), 4.63 (2H, t, CH_3OCH_2-$\mathit{CH_2}N$, J = 4.66 Hz), 4.27 (2H, t, NCH_2, J = 7.45 Hz), 3.75 (2H, t, $CH_3O\mathit{CH_2}CH_2N$, J = 4.65 Hz), 3.35 (3H, s, OCH_3), 1.88 (2H, m, $NCH_2\mathit{CH_2}$), 1.22 (18H, m, $\mathit{C_9H_{18}}CH_3$), 0.84 (3H, t, $NC_{11}H_{22}\mathit{CH_3}$, J = 7.21 Hz). ^{13}C NMR (100 MHz; $CDCl_3$; 22 °C): δ (ppm) = 136.97 (d, C(2)-im), 123.23 (d, C(5)-im), 121.58 (d, C(4)-im), 70.36 (t, $CH_3O\mathit{C_2}CH_2N$), 58.85 (q, OCH_3), 49.49 (t, NCH_2), 31.70 (t, $CH_3OCH_2\mathit{CH_2}N$), 30.22–26.34 (t, $\mathit{C_8H_{16}}CH_2CH_3$), 22.60 (t, $NCH_2\mathit{CH_2}$), 13.91 (q, CH_3). ATR-IR (neat): λ = 3394, 2922, 2853, 1563, 1465, 1166, 1120 cm^{-1}. $C_{18}H_{35}ClN_2O$: calcd C 65.33, H 10.66, N 8.46; found C 65.36, H 11.16, N 8.34.

1-Dodecyl-3-(2-(methylthio)ethyl)-imidazolium chloride (5). Dodecylimidazole (5.00 g, 21.2 mmol) was mixed with (2-chloroethyl)(methyl)sulfane (2.46 g, 22.2 mmol). The mixture was heated to 80 °C for 76 h. After evaporation of the remaining volatile materials, the crude product was twice crystallized from anhydrous THF to yield 1-dodecyl-3-(2-(methylthio)ethyl)-imidazolium chloride (**5**) as a colourless solid in 89% yield. ^{1}H NMR (400 MHz, $CDCl_3$; 22 °C): δ (ppm) = 10.52 (1H, s, H(2)-im), 7.80 (1H, s, H(5)-im), 7.37 (1H, s, H(4)-im), 4.56 (2H, t, NCH_2, J = 6.63 Hz), 4.18 (2H, t, $CH_3SCH_2\mathit{CH_2}N$, J = 7.58 Hz), 2.95 (2H, t, $CH_3S\mathit{CH_2}CH_2N$, J = 4.7.56 Hz), 2.08 (3H, s, SCH_3), 1.80 (2H, m, $NCH_2\mathit{CH_2}$), 1.12 (18H, m, $\mathit{C_9H_{18}}CH_3$), 0.75 (3H, t, $NC_{11}H_{22}\mathit{CH_3}$, J = 7.09 Hz). ^{13}C NMR (100 MHz; $CDCl_3$; 22 °C): δ (ppm) = 138.00 (d, C(2)-im), 123.07 (d, C(5)-im), 121.61 (d, C(4)-im), 50.05 (t, $CH_3SCH_2\mathit{CH_2}N$), 48.59 (t, NCH_2), 31.76 (t, $CH_3S\mathit{CH_2}CH_2N$), 30.44–26.34 (t, $\mathit{C_8H_{16}}CH_2CH_3$), 22.53 (t, $NCH_2\mathit{CH_2}$), 15.51 (q, SCH_3), 14.05 (q, CH_3). ATR-IR (neat): λ = 3378, 2916, 2847, 1573, 1560, 1467, 1173 cm^{-1}. $C_{18}H_{35}ClN_2S$: calcd C 62.30, H 10.17, N 8.07; found C 62.14, H 10.41, N 8.06.

1-Cyanomethyl-3-dodecyl-imidazolium chloride (6). Dodecylimidazole (5.00 g, 21.2 mmol) was mixed with 2-chloroacetinitril (1.59 g, 21.2 mmol). The mixture was heated to 80 °C for 30 min. After evaporation of the remaining volatile materials, the crude product was crystallized from anhydrous THF to yield 1-cyanomethyl-3-dodecyl-imidazolium chloride (**6**) as a colourless solid in 80% yield. ^{1}H NMR (400 MHz, $CDCl_3$; 22 °C): δ (ppm) = 10.55 (1H, s, H(2)-im), 8.25 (1H, s, H(5)-im), 7.44 (1H, s, H(4)-im), 6.26 (s, 2H, NCH_2CN), 4.24 (2H, t, NCH_2, J = 7.50 Hz), 1.85 (2H, m, NCH_2CH_2), 1.12 (18H, m, $C_9H_{18}CH_3$), 0.85 (3H, t, $NC_{11}H_{22}CH_3$, J = 6.50 Hz). ^{13}C NMR (100 MHz; $CDCl_3$; 22 °C): δ (ppm) = 135.67 (d, C(2)-im), 121.95 (d, C(5)-im), 120.59 (d, C(4)-im), 112.35 (s, CN), 48.73 (t, NCH_2), 35.85 (t, NCH_2CN), 30.02–24.43 (t, $C_8H_{16}CH_2CH_3$), 20.79 (t, NCH_2CH_2), 12.12 (q, CH_3). ATR-IR (neat): λ = 3114, 3079, 2918, 2852, 2254, 1549, 1151 cm^{-1}. $C_{17}H_{30}ClN_3$: calcd C 65.47, H 9.70, N 13.47; found C 65.05, H 9.81, N 13.57.

1-Dodecyl-3-(2-pyridylmethyl)imidazolium chloride (7). 2-(Chloromethyl)pyridine hydrochloride (4.92 g, 30 mmol) was dissolved in water (165 mL). Solid $NaHCO_3$ was added (5.02 g, 60 mmol) under magnetic stirring, and the mixture was repeatedly extracted with dichloromethane. The combined organic layers were washed with brine, dried over Na_2SO_4 and the solvent was removed under reduced pressure. 2-(Chloromethyl)pyridine was obtained as a light brown liquid in 97% yield and directly subjected to the next step. 2-(Chloromethyl) pyridine (3.87 g, 25 mmol) and freshly distilled 1-dodecylimidazol (5.91 g, 25 mmol) were heated with an oil bath at 80 °C in a three-neck round-bottomed flask equipped with a stirrer bar and reflux condenser under a dry argon atmosphere for 48 h until NMR indicated complete conversion. The crude product was repeatedly washed with anhydrous ethyl acetate. Remaining solvent traces were removed under reduced pressure (10^{-2} mbar) to yield 1-dodecyl-3-(2-pyridylmethyl)imidazolium chloride (7) as a light brown viscous liquid in 95% yield. ^{1}H NMR (400 MHz, $CDCl_3$; 22 °C): δ (ppm) = 10.68 (1H, s, H(2)-im), 8.40 (1H, s, H(5)-im), 7.78 (1H, s, H(4)-im), 7.70 (1H, s), 7.63 (1H, m), 7.27 (1H, m), 7.21 (1H, m), 5.7 (2H, s, NCH_2), 4.23 (2H, t, NCH_2CH$_2$, J = 7.5 Hz), 1.86 (2H, m, NCH_2CH_2), 1.10 (18H, m, $C_9H_{18}CH_3$), 0.80 (3H, t, $NC_{11}H_{22}CH_3$, J = 6.36 Hz). ^{13}C NMR (100 MHz, $CDCl_3$; 22 °C): δ (ppm) = 152.09 (s), 149.76 (d, C(2)-im), 137.02 (2d, C(5)-im, C(4)-im), 124.30 (d), 122.74 (2d), 121.46 (d), 54.05 (t, NCH_2), 50.21 (t, NCH_2CH_2), 31.77 (q, NCH_3), 30.29–26.31 (t, $C_8H_{16}CH_2CH_3$), 22.60 (t, NCH_2CH_2), 14.06 (q, CH_3). $C_{21}H_{34}ClN_3$: calcd C 69.30, H 9.42, N 11.55; $C_{21}H_{34}ClN_3 \cdot 0.6H_2O$: calcd C 67.30, H 9.47, N 11.21; found C 67.29, H 9.72, N 11.22.

1-Allyl-3-dodecyl-imidazolium chloride (8). Dodecylimidazole (5.00 g, 21.2 mmol) was mixed with allyl chloride (4.05 g, 52.9 mmol). The mixture was heated to 50 °C for 24 h. After evaporation of the remaining volatile materials, the crude product was crystallized from anhydrous THF to yield 1-allyl-3-dodecyl-imidazolium chloride (**8**) as a colourless solid in 94% yield. ^{1}H NMR (400 MHz, $CDCl_3$; 22 °C): δ (ppm) = 10.75 (1H, s, H(2)-im), 7.45 (1H, s, H(5)-im), 7.42 (1H, s, H(4)-im), 5.69 (m, 1H, allyl-CH), 5.40 (2H, t, NCH_2, J = 7.50 Hz), 5.01 (2H, d, NCH_2CHCH$_2$, J = 6.60 Hz), 4.28 (m, 2H, allyl-CH_2), 1.85 (2H, m, NCH_2CH_2), 1.12 (18H, m, $C_9H_{18}CH_3$), 0.82 (3H, t, $NC_{11}H_{22}CH_3$, J = 6.60 Hz). ^{13}C NMR (100 MHz; $CDCl_3$; 22 °C): δ (ppm) = 137.10 (d, C(2)-im), 130.08 (d, allyl-CH), 122.31 (d, C(5)-im), 122.15 (d, C(4)-im), 122.10 (t, allyl-CH_2) 51.71 (t, NCH_2), 49.94 (t, NCH_2CHCH$_2$), 31.69 (t, $CH_3SCH_2CH_2N$), 30.17–26.10 (t, $C_8H_{16}CH_2CH_3$), 22.47 (t, NCH_2CH_2), 13.94 (q, CH_3). ATR-IR (neat): λ = 3382, 2922, 2852, 1645, 1560, 1465, 992, 940 cm^{-1}. $C_{18}H_{33}ClN_2$: calcd C 69.09, H 10.63, N 8.95; $C_{18}H_{33}ClN_2 \cdot 0.65H_2O$: calcd C 66.60, H 10.65, N 8.63; found C 66.68, H 10.49, N 8.30.

Application of surface-active ionic liquids in the Heck reaction. The representative procedure for the Heck reaction of ethyl acrylate **9** and iodobenzene **10** in aqueous solution of ionic liquids for Heck cross-coupling is as follows: a screw-cap vial with a Teflon seal was charged with 0.02 mmol $Pd_2(allyl)_2Cl_2$, 1.5 mmol K_2CO_3 and a magnetic stirring bar. Aqueous-ionic liquid micellar solution (5.0 mL) was added and the reaction mixture was stirred at 80 °C for 15 minutes. Freshly distilled ethyl acrylate (1.5 mmol) and iodobenzene (1.0 mmol) were added and the mixture was reacted at 80 °C until completion. The reaction mixture was extracted with light petrol (fraction 40–60 °C) three times. The combined organic phases were once extracted with 2 N HCl and filtered over a batch of silica. The solvent was removed under reduced pressure (40 °C, 50 mbar) to yield ethyl cinnamate in 93% yield. ^{1}H NMR (400 MHz, $CDCl_3$; 22 °C): δ (ppm) = 7.86 (1H, d, J = 16.04 Hz), 7.53 (2H, m), 7.38 (3H, m), 6.37 (1H, d, J = 16.09 Hz), 4.27 (2H, q, J = 7.02 Hz), 1.34 (3H, t, J = 7.10 Hz). The data was in accordance with the literature.[48]

Conflicts of interest

There are no conflicts to declare.

Acknowledgements

Financial support by the Austrian Science Fund (FWF project P25504-N28) is gratefully acknowledged.

References

1 A. J. Carmichael, M. J. Earle, J. D. Holbrey, P. B. McCormac and K. R. Seddon, *Org. Lett.*, 1999, **1**, 997–1000.
2 V. I. Pârvulescu and C. Hardacre, *Chem. Rev.*, 2007, **107**, 2615–2665.
3 J. Dupont, R. F. de Souza and P. A. Z. Suarez, *Chem. Rev.*, 2002, **102**, 3667–3692.
4 T. Welton, *Coord. Chem. Rev.*, 2004, **248**, 2459–2477.
5 O. Holloczki, D. Gerhard, K. Massone, L. Szarvas, B. Nemeth, T. Veszpremi and L. Nyulaszi, *New J. Chem.*, 2010, **34**, 3004–3009.
6 O. Holloczki and L. Nyulaszi, *Org. Biomol. Chem.*, 2011, **9**, 2634–2640.
7 L. Xu, W. Chen and J. Xiao, *Organometallics*, 2000, **19**, 1123–1127.
8 W. A. Herrmann, *Angew. Chem., Int. Ed.*, 2002, **41**, 1290–1309.

 This journal is © The Royal Society of Chemistry 2017

9 M. Fèvre, P. Coupillaud, K. Miqueu, J.-M. Sotiropoulos, J. Vignolle and D. Taton, *J. Org. Chem.*, 2012, **77**, 10135–10144.
10 Z. Kelemen, B. Péter-Szabó, E. Székely, O. Hollóczki, D. S. Firaha, B. Kirchner, J. Nagy and L. Nyulászi, *Chem.–Eur. J.*, 2014, **20**, 13002–13008.
11 M.-O. Simon and C.-J. Li, *Chem. Soc. Rev.*, 2012, **41**, 1415–1427.
12 M. T. Reetz and J. G. de Vries, *Chem. Commun.*, 2004, 1559–1563.
13 B. H. Lipshutz and B. R. Taft, *Org. Lett.*, 2008, **10**, 1329–1332.
14 B. H. Lipshutz, N. A. Isley, J. C. Fennewald and E. D. Slack, *Angew. Chem., Int. Ed.*, 2013, **52**, 10952–10958.
15 Y. Kohno and H. Ohno, *Chem. Commun.*, 2012, **48**, 7119–7130.
16 C. Schröder, T. Rudas, G. Neumayr, S. Benkner and O. Steinhauser, *J. Chem. Phys.*, 2007, **127**, 234503.
17 C. Schröder, J. Hunger, A. Stoppa, R. Buchner and O. Steinhauser, *J. Chem. Phys.*, 2008, **129**, 184501.
18 R. Hayes, G. G. Warr and R. Atkin, *Chem. Rev.*, 2015, **115**, 6357–6426.
19 G. La Sorella, G. Strukul and A. Scarso, *Green Chem.*, 2015, **17**, 644–683.
20 M. Blesic, M. H. Marques, N. V. Plechkova, K. R. Seddon, L. P. N. Rebelo and A. Lopes, *Green Chem.*, 2007, **9**, 481–490.
21 J. Łuczak, M. Markiewicz, J. Thöming, J. Hupka and C. Jungnickel, *J. Colloid Interface Sci.*, 2011, **362**, 415–422.
22 G. Singh, G. Singh and T. S. Kang, *J. Phys. Chem. B*, 2016, **120**, 1092–1105.
23 B. Šarac, Ž. Medoš, A. Cognigni, K. Bica, L.-J. Chen and M. Bešter-Rogač, *Colloids Surf., A*, 2017, DOI: 10.1016/j.colsurfa.2017.01.062.
24 J. Łuczak, C. Jungnickel, M. Markiewicz and J. Hupka, *J. Phys. Chem. B*, 2013, **117**, 5653–5658.
25 A. K. Ressmann, R. Zirbs, M. Pressler, P. Gaertner and K. Bica, *Z. Naturforsch. B Chem. Sci.*, 2013, **68**, 1129–1137.
26 I. Svinyarov and M. G. Bogdanov, *Sep. Sci. Technol.*, 2017, DOI: 10.1080/01496395.2017.1295995.
27 E. L. P. de Faria, S. V. Shabudin, A. F. M. Cláudio, M. Valega, F. M. Domingues, C. S. R. Freire, A. J. Silvestre and M. G. Freire, *ACS Sustainable Chem. Eng.*, 2017, **5**(8), 7344–7351.
28 F. A. Vieira, R. J. Guilherme, M. C. Neves, A. Rego, M. H. Abreu, J. A. Coutinho and S. P. Ventura, *Sep. Purif. Technol.*, 2017, DOI: 10.1016/j.seppur.2017.05.006.
29 M. Vasiloiu, D. Rainer, P. Gaertner, C. Reichel, C. Schröder and K. Bica, *Catal. Today*, 2013, **200**, 80–86.
30 M. Vasiloiu, P. Gaertner, R. Zirbs and K. Bica, *Eur. J. Org. Chem.*, 2015, **2015**, 2374–2381.
31 J. Nowicki, J. Łuczak and D. Stańczyk, *RSC Adv.*, 2016, **6**, 11591–11601.
32 M. Cokoja, R. M. Reich, M. E. Wilhelm, M. Kaposi, J. Schäffer, D. S. Morris, C. J. Münchmeyer, M. H. Anthofer, I. I. E. Markovits, F. E. Kühn, W. A. Herrmann, A. Jess and J. B. Love, *ChemSusChem*, 2016, **9**, 1773–1776.
33 M. Hejazifar, M. Earle, K. R. Seddon, S. Weber, R. Zirbs and K. Bica, *J. Org. Chem.*, 2016, **81**, 12332–12339.
34 R. Sharma, B. Gupta, T. Yadav, S. Sinha, A. K. Sahu, Y. Karpichev, N. Gathergood, J. Marek, K. Kuca and K. K. Ghosh, *ACS Sustainable Chem. Eng.*, 2016, **4**, 6962–6973.
35 K. Bica, P. Gärtner, P. J. Gritsch, A. K. Ressmann, C. Schröder and R. Zirbs, *Chem. Commun.*, 2012, **48**, 5013–5015.
36 A. Cognigni, P. Gaertner, R. Zirbs, H. Peterlik, K. Prochazka, C. Schröder and K. Bica, *Phys. Chem. Chem. Phys.*, 2016, **18**, 13375–13384.
37 O. A. El Seoud, P. A. R. Pires, T. Abdel-Moghny and E. L. Bastos, *J. Colloid Interface Sci.*, 2007, **313**, 296.
38 J. Łuczak, J. Hupka, J. Thöming and C. Jungnickel, *Colloids Surf., A*, 2008, **329**, 125–133.
39 A. Cognigni, S. Kampichler and K. Bica, *J. Colloid Interface Sci.*, 2017, **492**, 136–145.
40 X.-F. Liu, L.-L. Dong and Y. Fang, *J. Surfactants Deterg.*, 2011, **14**, 203–210.
41 O. Schuster, L. Yang, H. G. Raubenheimer and M. Albrecht, *Chem. Rev.*, 2009, **109**, 3445–3478.
42 E. Levin, E. Ivry, C. E. Diesendruck and N. G. Lemcoff, *Chem. Rev.*, 2015, **115**, 4607–4692.
43 S. Friesen, T. Buchecker, A. Cognigni, K. Bica and R. Buchner, *Langmuir*, 2017, DOI: 10.1021/acs.langmuir.7b02201.
44 D. Zhao, Z. Fei, T. J. Geldbach, R. Scopelliti and P. J. Dyson, *J. Am. Chem. Soc.*, 2004, **126**, 15876–15882.
45 P. A. Namini, A. A. Babaluo and B. Bayati, *Int. J. Nanosci. Nanotechnol.*, 2007, **3**, 37–44.
46 W. Zhu, H. Yang, Y. Yu, L. Hua, H. Li, B. Feng and Z. Hou, *Phys. Chem. Chem. Phys.*, 2011, **13**, 13492–13500.
47 B. S. Souza, E. C. Leopoldino, D. W. Tondo, J. Dupont and F. Nome, *Langmuir*, 2012, **28**, 833–840.
48 S. Omar and R. Abu-Reziq, *J. Phys. Chem. C*, 2014, **118**(51), 30045–30056.

This journal is © The Royal Society of Chemistry 2017

Chapter 5

Surface-active ionic liquids for sustainable energy production

In this chapter the application of surface-active ionic liquids is expanded towards sustainable energy production via catalytic water splitting. A set of iridium containing catalysts was synthesized using different imidazolium based surface-active ionic liquids as ligand precursor, including dicationic species. The catalysts were then tested in the water oxidation reaction with cerium ammonium nitrate to produce molecular oxygen. The ionic liquids can act both as ligand and as additive, delivering excellent catalytic activity and increased initial reaction rates.

The following manuscripts will be presented in this chapter:

- Cognigni, Alice; Schröder,Christian; Peterlik, Herwig; Muellner, Alexander; Zirbs, Ronald; Weil, Matthias and Bica, Katharina **Surface-active ionic liquids in catalytic water splitting** submitted to *Dalton Trans.* **2017**.

As first author I planned and performed a major part of the experimental work, including the synthesis of surface-active ionic liquids and iridium catalysts as well as studies on the catalytic activity in water oxidation reactions. Furthermore I wrote the manuscript.

Supporting information for the manuscript can be found in Appendix C.

Journal Name

ARTICLE TYPE

Cite this: DOI: 10.1039/xxxxxxxxxx

Surface-active ionic liquids in catalytic water splitting †

Alice Cognigni,[a] Christian Schröder,[b] Herwig Peterlik,[c] Alexander R. M. Müllner,[c] Ronald Zirbs,[d] Matthias Weil[e] and Katharina Bica*[a]

Received Date
Accepted Date

DOI: 10.1039/xxxxxxxxxx

www.rsc.org/journalname

We report the application of surface-active ionic liquids as ligands and optional reaction media in iridium-catalyzed water oxidations. Three novel catalysts with *N,N*-dialkylimidazolidin-2-ylidene ligands based on amphiphilic imidazolium ionic liquids were synthesized and characterized. Excellent turn-over frequencies (TOF) of up to 0.92 s^{-1} were obtained in catalytic water splitting, and activity was maintained for five consecutive catalytic cycles with an overall turn-over number (TON) of 8967. The addition of external surface-active ionic liquid showed an unexpected behaviour, because strongly enhanced initial reaction rates were observed.

1 Introduction

Based on the constantly increasing global energy demand, attention for a hydrogen-based economy has spiked since the turn of the millennium. Molecular hydrogen produced through photo catalytic water splitting offers a convenient and sustainable source to satisfy energy and fuel demands in the future. The overall process of photo-catalytic water splitting (1) involves two semi-reactions for the production of molecular hydrogen (2) and molecular oxygen (3).

$$2H_2O + h\nu \rightarrow O_2 + 2H_2 \quad (1)$$

$$4H^+ + 4e^- \rightarrow 2H_2 \quad (2)$$

$$2H_2O \rightarrow O_2 + 4H^+ + 4e^- \quad (3)$$

The latter reaction (3) is considered as the bottle-neck in the development of devices for artificial photosynthesis. The oxidation of water to molecular oxygen requires the transfer of four electrons and the rearrangement of multiple bonds; a catalyst able to sustain high oxidation states is therefore required.[1]

Several well-defined molecular catalysts for these reactions have been reported based on different metal and ligand systems. While ruthenium-based catalysts were the first and are still one of the most studied systems, cheaper metals such as iron and cobalt have also been reported although they suffer from low stability.[1,2]

Recently iridium based complexes have received much attention as good and robust catalysts. After Bernhard *et al.* initially reported the iridium-based catalyst $[Ir(ppy)_2(OH_2)_2]^+$] (ppy = 2-phenylpyridine), fine-tuning of the ligand structure soon revealed the importance of the pentamethyl-cyclopentadienyl ring (Cp*) which became a very common structural motif for iridium-based water oxidation catalysts.[3] Simple compounds such as $[Ir^*Cp(H_2O)_3]^{2+}$ have been reported as effective catalysts, reaching a turn-over frequency (TOF) of 0.092 s^{-1}.[4,5] The incorporation of *N*-heterocyclic carbene (NHC) ligands was a further milestone in the development of highly active, stable and robust water oxidation catalysts based on iridium.[6–8] This can be rationalized by the electron-rich and donating nature of these ligands that are able to stabilize the catalyst at high oxidation states, which occur during the catalytic cycle.[9] In particular, Hetterscheid and Reek reported a dichlorido iridium complex $[C_1mim\text{-}Ir^*CpCl_2]$ based on the *N*-dimethylimidazolidin-2-ylidene ligand, which resulted in excellent activity and robustness.[6] Further studies on the catalytic activity of this catalyst via in situ surface-enhanced Raman spectroscopy showed that the catalyst undergoes a bis-μ-oxido iridium dimer formation in its catalytic cycle in order to form the O-O bond.[6,10] Corresponding dicarbene ligands have been developed showing comparable activity to previously reported iridium water oxidation catalysts.[11] Eventually, recent finding by Albrecht *et al.* who reported on a series of pyridine-carbene ligands based on triazolylidene revealed that the catalytic activity could be substantially improved by adding a long alkyl chain on the tri-

[a] *Institute of Applied Synthetic Chemistry, Vienna University of Technology, Getreidemarkt 9/163, 1060 Vienna (Austria), Fax: +43 1 58801 16360; Tel: +43 1 58801 163601. E-mail: katharina.bica@tuwien.ac.at or katharina.schroeder@tuwien.ac.at*
[b] *Institute of Computational Biological Chemistry, Faculty of Chemistry, University of Vienna, Währingerstrasse 17, 1090 Vienna, Austria*
[c] *Faculty of Physics, University of Vienna, Boltzmanngasse 5, 1090 Vienna, Austria.*
[d] *Institute for Biologically inspired materials, Department of Nanobiotechnology, University of Natural Resources and Life Sciences, Vienna, Muthgasse 11-II, A-1190 Vienna, Austria.*
[e] *Institute for Chemical Technologies and Analytics, Vienna University of Technology, Getreidemarkt 9/164, 1060 Vienna, Austria*

† Electronic Supplementary Information (ESI) available: [Additional graphs and analytical data]. See DOI: 10.1039/b000000x/

azolydiene moiety, indicating that an amphiphilic character of the catalyst is beneficial.[12]

Apart from their use as *N*-heterocyclic carbene precursors, imidazolium salts are also typical constituents of ionic liquids. 1-Alkyl-3-methylimidazolium cations with variable anions are among the most popular and investigated class of ionic liquids. Due to the presence of hydrophobic and hydrophilic domains they posses a well-organized nano-structured network which is responsible for many of their peculiar properties.[13–16] This organization can be maintained when they are mixed with water, particularly when 1-alkyl-3-methylimidazolium salts are used that bear a long alkyl group with more than eight carbon atoms.[17] As a result of the charged hydrophilic head group and the hydrophobic tail, the ionic liquid has amphiphilic character and can behave like a surfactant, forming aggregates such as micelles when dissolved in water.[18,19]

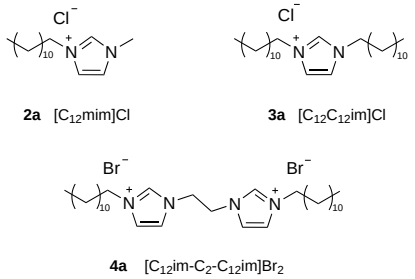

Fig. 1 Surface-active ionic liquids used in this study

In recent years this type of surface-active ionic liquids has received much attention because of their favourable properties compared to conventional ammonium-based surfactants. Due to the less polar head groups with good charge delocalization of imidazolium-based surface-active ionic liquids, they usually show a higher surface activity compared to conventional ammonium surfactants with similar alkyl chain length, showing both higher adsorption efficiency at the air-water interface, higher water surface tension decrease and a difference in hydration and counterion binding to the headgroup.[20–22] In addition, their tunable structures renders them ideally suited for multiple applications in synthesis and catalysis.[23,24] A number of authors demonstrated that surface-active ionic liquids led to improved reaction rates and selectivities through targeted interactions between surfactant, catalyst and substrates.[25–29] Moreover, their ability to form carbene intermediates has a strong influence on the outcome of reactions performed in aqueous solutions of surface-active ionic liquids performance.[30,31]

Based on recent developments in the design of *N*-heterocyclic carbene complexes as water oxidation catalysts with amphiphilic structures, we were interested in expanding our recent research on the application of surface-active ionic liquids in catalysis towards their use in water oxidations. In here, we present the use of surface-active imidazolium-based ionic liquids as ligands and reaction media for iridium-catalyzed water oxidations, envisioning that their ability for forming aggregates in water should also facilitate the formation of the catalyst dimer assumed to be a key step in the oxygen-oxygen bond formation.

2 Results and discussion

2.1 Synthesis of the catalysts

Based on our previous experience in the field of micellar catalysis with surface-active ionic liquids, we selected three surface-active 1-dodecyl-3-alkylimidazolium-based ionic liquids **2a** - **4a**, including a dicationic species, for the simultaneous use as ligand and surfactant in the water oxidation reaction.[25,29,30] For the purpose of comparison, dimethylimidazolium bromide which does not possess any surface-active behaviour, was also included as it has already been used as a precursor for iridium-based water oxidation catalysts. Starting with the structures shown in 1 iridium-based catalysts were synthesized through a two step pathway as shown in figure 2. The synthesis involves the initial formation of a silver carbene species from the corresponding surface-active imidazolium salts with a small excess of silver oxide. The silver carbene was obtained via filtration and used in situ for a transmetallation with $[Cp^*IrCl_2]_2$ to afford the desired complexes **1** - **4**. In case of the dicationic surface-active ionic liquid (**4a**) the corresponding silver carbene complex showed poor solubility in dichloromethane; therefore no intermediate filtration could be performed. Hence the iridium precursor was directly added to the crude mixture, and unsoluble by-products were separated via precipitation in acetonitrile. With the exception of the dicationic species **4**, high yields of the iridium-based catalysts could be obtained, and structures could be verified by ^{1}H NMR, ^{13}C NMR and mass spectroscopy. In all cases the ^{1}H NMR spectra showed the absence of the typical signal at 9-12 ppm for the acidic proton of the imidazolium moiety. In ^{13}C NMR spectroscopy the typical new peaks at around 155 ppm for catalysts **2** and **3**, and at 145 ppm for catalyst **4** confirmed carbene formation.

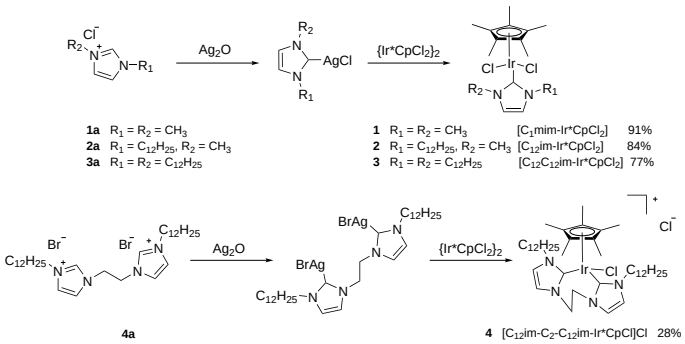

Fig. 2 Synthesis of surface-ionic liquids derived water oxidation catalysts

The molecular structure of complex **3** is depicted in figure 3. The complete molecule exhibits point group symmetry *m*, with the Ir atom, the C1 atom of the imidazole moiety and the C17 and C20 atoms of the Cp* ring located on the mirror plane. This symmetry restriction requires the H atoms of the methyl group C20 to be equally disordered over two sets of sites. The five Ir-C(Cp*) bonds (average 2.17(4) Å) are in the usual range and are significantly longer than the Ir-C(carbene) bond of 2.051(4) Å).[32] Under consideration of the Cp* ring system as a single coordination partner (Ir-Cp*(centroid) distance 1.803 Å), the overall coordination environment of the Ir atom is distorted tetrahedral,

This journal is © The Royal Society of Chemistry [year]

with the Cp*(centroid)-Ir-Cl and Cp*(centroid)-Ir-C(carbene) angles of 123.55° and 127.89° greater than the Cl-Ir-C(carbene) and Cl-Ir-Cl' (' denotes the symmetry-related counterpart) angles of 92.09° and 86.32°.

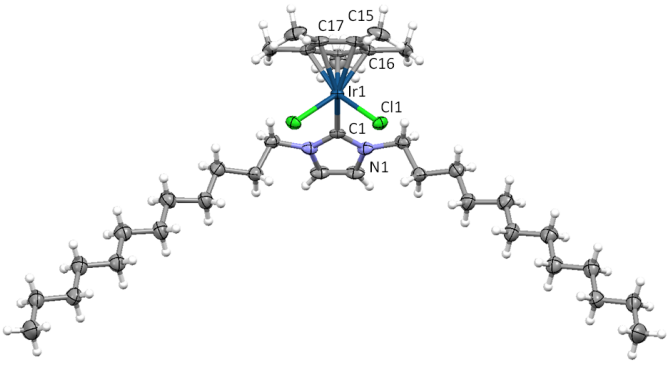

Fig. 3 Molecular structure of $[C_{12}C_{12}im\text{-}^*CpIrCl_2]$ with selected atom labelling and displacement ellipsoids drawn at the 80% probability level. H atoms are given as spheres of arbitrary size.

2.2 Catalytic water oxidation

In order to compare the performance of various catalysts for water oxidation, catalysts are typically evaluated using a sacrificial oxidant, which allows a fast and simple variation of conditions and screening of compounds. A commercially available and commonly utilized sacrificial oxidant is CAN (Cerium Ammonium Nitrate, $(NH_4)_2Ce(NO_3)_6$). It is a powerful one-electron oxidant, and as an additional advantage it has a strong absorption band in the UV region, which can be used to monitor its consumption during the catalytic reaction. However, it needs to operate at pH below 3.0 to avoid the formation of insoluble oxide species, and it is therefore usually tested in an HNO_3 0.1 M solution.[33]

$$4Ce^{4+} + 2H_2O \rightarrow 4Ce^{3+} + 4H^+ + O_2$$

The performance of the catalysts **1** - **4** for the water oxidation reaction using Ce^{4+} as sacrificial oxidant was initially investigated without additional surface-active ionic liquid. The depletion of Ce^{4+} was followed by UV-Vis spectroscopy at 360 nm until its consumption was quantitative, or, if no complete conversion was observed for at least four half-lives. The respective absorbance curves can be fitted by

$$[Ce^{4+}](t) \propto a_1 e^{-k_1 t} + \frac{a_2}{1 + e^{k_2(t-t_0)}} \quad (1)$$

which corresponds to a first order reaction with a rate constant of k_1 and in parallel an autocatalyzed reaction described via a logistic function. Here, k_2 is a rate constant and t_0 the time when half of this process has finished. The amplitudes a_1 and a_2 characterize the relative importance of the process for the overall depletion of Ce^{4+}.

In literature, the time-dependent turn-over frequency

$$TOF(t) = \frac{-\frac{d}{dt}[Ce^{4+}](t)}{[cat]} \quad (2)$$

is used for the characterization of catalytic efficiency. However, the maximum value TOF_{max} that is often reported is not a good measure for the efficiency as a very fast process with low partial amplitude a may adulterate the value significantly (see Eq. (2)). Consequently, we report the turn-over-frequency $TOF_{\langle t \rangle}$ at the mean reaction time $\langle t \rangle$ which is defined by

$$\langle t \rangle = \int_0^\infty \frac{[Ce^{4+}](t)}{[Ce^{4+}](0)} dt. \quad (3)$$

but also give the TOF_{max} to compare with literature. Further details are given in the supplementary material.

Initially the iridium complex **2** was evaluated as water oxidation catalyst in the presence of different CAN concentrations. As to be expected from literature data, a higher excess of CAN improved the catalyst performance, and a six-fold increase in $TOF_{\langle t \rangle}$ was obtained by increasing the CAN concentration from 0.5 mM to 3 mM (Table 1, entry 1-3).[34] A similar trend was observed also for catalyst **1** (Table 1, entry 4 - 5) which showed a $TOF_{\langle t \rangle}$ of 0.37 and 0.69 s^{-1} when using CAN 1.5 and 3 mM respectively.[35] When comparing the two catalysts under a similar experimental set-up, the effect of the long alkyl chain becomes readily apparent. At both CAN concentrations, catalyst **2** with the dodecyl chain as structural motif performs better than the corresponding dimethyl-based species **1**, although the effect is less explicit than reported for amphiphilic triazolydiene ligands.[12]

Table 1 CAN concentration effect for catalysts **1** and **2**

Entry‡	CAN [mM]	Catalyst	$[C_{12}mim]Cl$ [mM]	$TOF_{\langle t \rangle}$ § [s^{-1}]
1	0.5	**2**	0	0.14±0.002
2	1.5	**2**	0	0.44±0.05
3	3	**2**	0	0.90±0.09
4	1.5	**1**	0	0.37±0.05
5	3	**1**	0	0.69±0.03
6	1.5	**2**	1	0.24±0.02
7	3	**2**	1	0.08±0.02

‡Reactions performed with a catalyst concentration of 2 μM in HNO_3 0.1 M. §Results are reported as average from at least 4 runs.

After initial optimization of the CAN concentration, the three surface-active ionic liquid derived iridium catalysts were compared over a broader concentration range, and a strong dependence of efficiency on the concentration was observed as shown in figure 4. While catalyst **2** was evaluated from 0.3 μM to 100 μM, a smaller range was investigated for catalysts **3** and **4** due to solubility restrictions when preparing the homogeneous stock solution. Although the absolute reaction rate was expectedly faster with a higher catalyst concentration, the catalyst efficiency showed a maximum and decreased at lower or higher concentrations. For compounds **2** and **3**, the maximum was ob-

served at around 2-5 μM, whereas the concentration dependency is less explicit for catalyst **4**. Independent of the concentration, the best results were obtained for the catalyst[C_{12}mim-Ir*$CpCl_2$], which reached a $TOF_{\langle t \rangle}$ of 0.92 s^{-1} under optimum conditions. All four catalysts showed an induction time, the longest being for the bidentately-bound catalyst **4**. It is interesting to note that although catalysts **2** and **3** show the same initial behaviour, a stronger rate enhancement takes place for catalyst **2** (see figure S1).

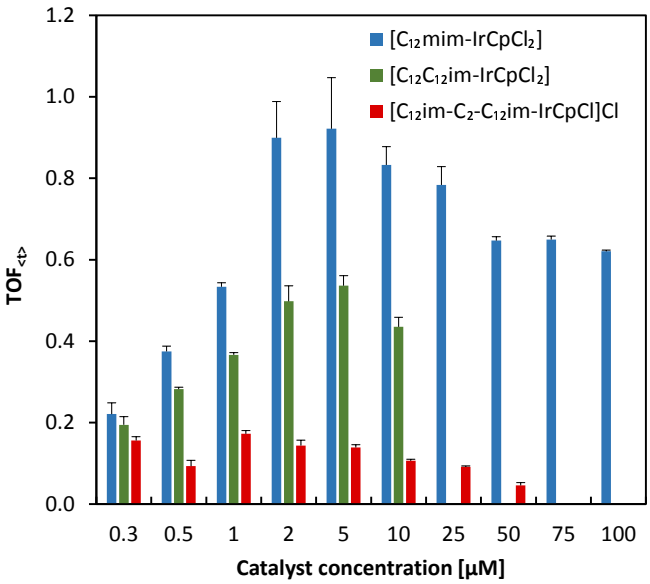

Fig. 4 Concentration effect of the reported catalysts (reactions performed with 3 mM CAN in HNO_3 0.1 M)

Dynamic light scattering (DLS) analysis after the reaction showed the absence of nanoparticles formation (Table 2, entry 2) suggesting that a homogeneous process is taking place.[1,11,36] The considerably better performance of catalyst **2** compared to **3** and **4** might give information on the catalytically active species. Diaz-Morales *et al.* reported for catalyst **1** [C_1mim-Ir*$CpCl_2$] that the carbene as well as the Cp* ligand are not lost during the activation process of the complex. The catalytically active form for the water oxidation reaction is a bis-μ-oxido di-iridium(IV) compound.[10] While in the case of catalyst **2** the dimer formation can still be favoured, for catalyst **3** it might be hindered from the higher steric demand of two dodecycl chains, resulting in a lower activity than the corresponding 1-dodecyl-3-methylimidazolidine derivative. Similarly, catalyst **4** that is based on the dicationic surface-active ionic liquids lacks an additional free coordination site which would be necessary to form the dimer. In fact, for other bidentate ligands it has been reported that the Cp* ring is lost during the catalytic cycle. This might not only explain the comparably poor performance of the bidentate ligand, but could also explain the longer incubation time at the beginning, since two steps are involved in the activation process of the catalyst.[35,37]

Multiple run kinetic experiments were also conducted by adding an equivalent aliquot of CAN after Ce^{4+} was consumed.

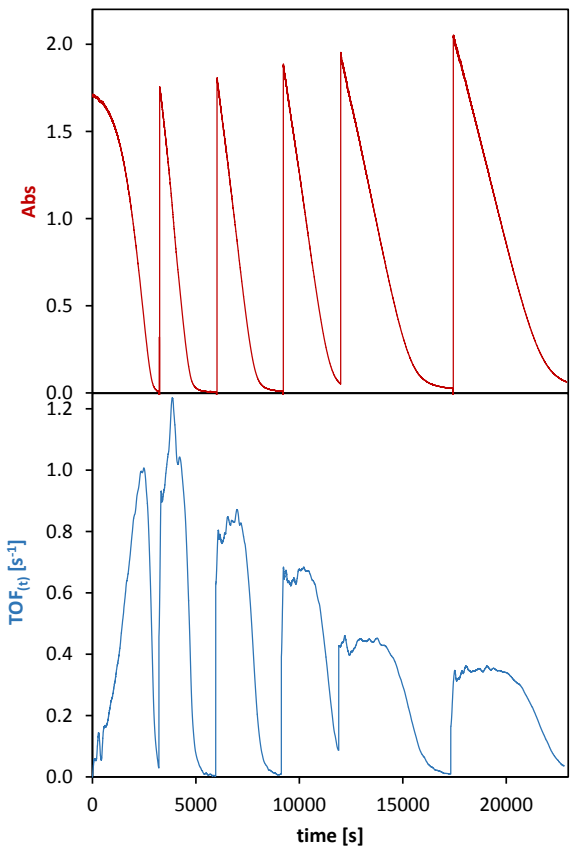

Fig. 5 Multiple run kinetics (reaction performed with catalyst **2** 2μM, CAN 3 mM in each run, in HNO_3 0.1 M).

The system remained active for at least five times as can be seen in figure 5. The required induction period for the catalyst is visible only in the first run; moreover, during the second run a further increase of the $TOF_{(t)}$ was observed reaching a maximum of almost 1.2 s^{-1}. In the following runs the $TOF_{(t)}$ progressively decreased, but losses remained rather constant with every run. Overall, a high overall turn-over number (TON) of 8967 was calculated. In comparison, this value is between the values reported for the dimethylimidazolium derivative (120) and those reported for triazolium-derived ligands (8000-22800).[6,7,38]

The reason for the decrease in performance may be the progressive degradation of the catalyst under the harsh acidic conditions required by the sacrificial oxidant. Degradation of the Cp*-moiety to acetic acid and eventually CO_2 after multiple catalytic cycles has been reported with CAN. However, no blue colour, indicating the formation of iridium nanoparticles was observed in our systems.[8,11,36]

Eventually, the impact of additional surface-active ionic liquid on the catalytic performance was also investigated and revealed an unexpected behaviour. A strong increase in the initial reaction rate was observed when performing water oxidation in solution of [C_{12}mim]Cl varying from 0.1 - 50 mM. However, the reaction rate decreased rapidly, indicating an inhibition of the catalytically active system.

This journal is © The Royal Society of Chemistry [year]

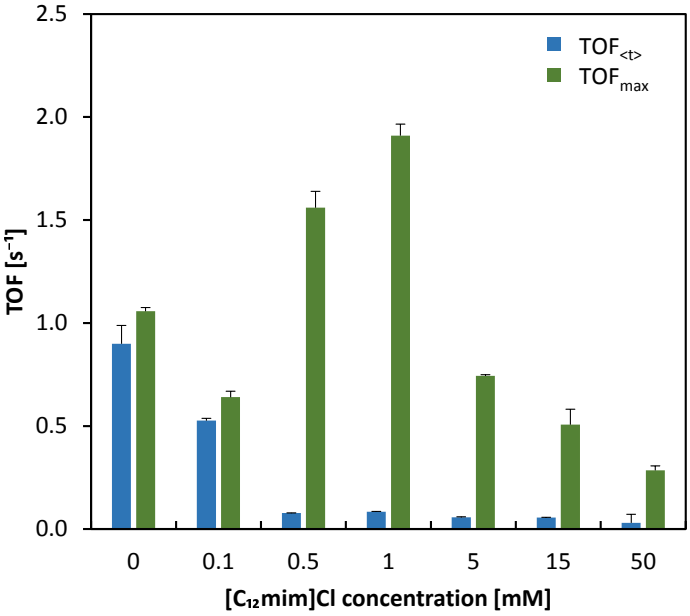

Fig. 6 Effect of the external surface-active ionic liquid (reactions performed with [C_{12}mim-Ir*CpCl$_2$] and 3 mM CAN in HNO_3 0.1 M)

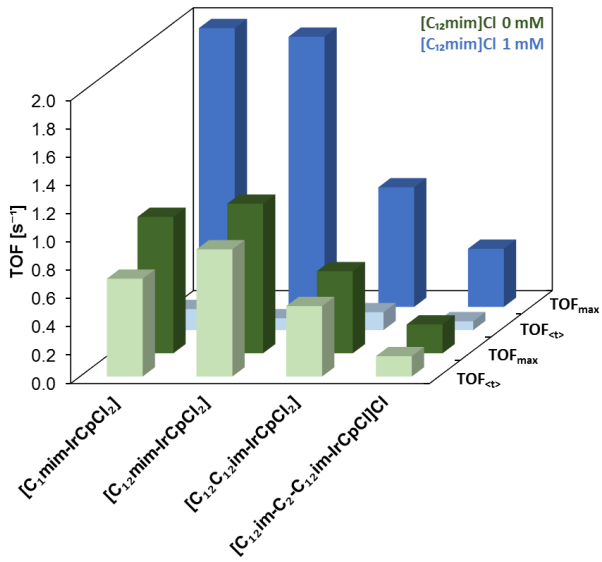

Fig. 7 Comparison of $TOF_{\langle t \rangle}$ and $TOF_{\max}$ at different external [C_{12}mim]Cl concentrations (reactions performed with 2 μM catalyst and 3 mM CAN)

The dependency of TOF on the ionic liquid concentration is reported in figure 6; for a better visualization both $TOF_{\langle t \rangle}$, calculated at the mean reaction time, and the maximum TOF ($TOF_{\max}$) obtained in the initial part of the reaction are shown. While there is no appreciable difference between the two values when the catalyst is used without addition of [C_{12}mim]Cl, a significant difference between the two values is observed through addition of surface-active ionic liquid. The $TOF_{\langle t \rangle}$ value steadily decreases with increasing [C_{12}mim]Cl concentration, but at the same time the $TOF_{\max}$ significantly increases, reaching a maximum of 1.91 s^{-1} in the presence of 1 mM ionic liquid [C_{12}mim]Cl.

From the experimental curves (see ESI Fig. S2) it can be seen that the reaction starts with a higher reaction rate without an induction period. However, the reaction is inhibited over time, and no full consumption of Ce^{4+} is observed for ionic liquid concentrations of 0.5 mM or higher. Similar results are also obtained when less CAN 1.5 mM is used (see ESI Fig. S3 and S4); however a slower inhibition and decrease of $TOF_{\langle t \rangle}$ is observed. As reported in Table 1 (entry 6-7) the presence of 1 mM surface-active ionic liquid [C_{12}mim]Cl can even reverse the dependency of $TOF_{\langle t \rangle}$ on the CAN concentration, resulting in a higher $TOF_{\langle t \rangle}$ with lower CAN concentration. As can be seen from figure 7, a similar behaviour was found for the water oxidation with catalysts **1**, **3** and **4** in the presence of 1 mM surface-active ionic liquid [C_{12}mim]Cl. In any case, a minor difference between $TOF_{\langle t \rangle}$ and $TOF_{\max}$ is observed when no external ionic liquid is added, while an initial rate enhancement as visualized by $TOF_{\max}$ and a drastic decrease in $TOF_{\langle t \rangle}$ was observed in the presence of [C_{12}mim]Cl 1 mM.

Further investigations on the aggregation behaviour after addition of 50 mM [C_{12}mim]Cl were conducted with SAXS and DLS. The presence of micellar aggregates of the surface-active ionic liquids during the reaction (Table 2, entry 2) was confirmed by both techniques. The aggregate size of DLS and SAXS is in good coincidence (2.6 nm in DLS and 2.8 nm in SAXS). In comparison to a pure 50 mM solution of [C_{12}mim]Cl in water, the addition of CAN and catalyst results in the formation of aggregates with increased size (Table 2, entry 1 and 2). In particular, in the evaluation of SAXS data, the size of the shell increases significantly, whereas the core radius is slightly smaller, probably induced by the high electron density of Ir atoms of the catalyst in the corer of the micelle. This is also supported by the low value of the scaled medium contrast γ, which indicate that scattering arises mainly from the core and the density of the shell is similar to the density of the surrounding solution.[39] A larger size of the aggregates can be induced by the ability of salts to screen charges in the micelles.[40] In contrast, we were not able to conduct any measurements on the catalyst alone without the presence of additional ionic liquid [C_{12}mim]Cl due to its low concentration under reaction conditions. According to SAXS findings and the surface-active character of the catalyst **2** it can be assumed that it will be embedded in the micelles as well, in close proximity with CAN adsorbed at the micellar interface. This would allow for a fast and efficient reactivity, corresponding to the high initial reaction rates that we have observed. The reduced CAN might diffuse only slowly due to strong salt-micelle interactions, which might explain the drastically reduced reaction rates over time. It should be however noted that the exact speciation of CAN is not know, as the literature reports a partial displacement of the coordinating nitrate by aqua ligands.[41]

3 Conclusion

In here, we demonstrated the application of imidazolium-based surface-active ionic liquids as ligands and additives for a water oxidation catalyst. The performance of ionic liquid derived catalyst **2** compares well with similar reported iridium catalysts, while

Table 2 Aggregate size measured by SAXS and DLS

Entry	Solution	DLS radius [nm]	SAXS core radius [nm]	SAXS shell thickness [nm]	γ
1	$[C_{12}mim]Cl$ 50 mM	n.a.	1.2[25]	0.9[25]	0.06[25]
2	Reaction mixture[‡]	2.6±1.0	0.8	2.1	0.035

[a] Mixture containing catalyst **2** 50 μM, $[C_{12}mim]Cl$ 50 mM, CAN 3 mM, HNO_3 0.1 M.

more sterically demanding catalysts **3** and **4** lead to reduced reaction rates.[35] The catalyst **2** was active over multiple kinetic runs, showing even an increase in activity in the second cycle where a maximum TOF_{max} of almost 1.2 s^{-1} was reached, and at the end of the 5 cycles an overall TON of 8967 could be obtained. Moreover, the addition of surface-active ionic liquid as reaction media resulted in the formation of micellar aggregates. A strong increase of the initial rates and a TOF_{max} of 1.91 s^{-1} could be obtained for catalyst $[C_{12}mim\text{-}Ir^*CpCl_2]$. As a conclusion, iridium complexes derived from surface-active ionic liquids display high potential as a new class of ligands for water oxidation catalysts, while their use as additives in this reaction shows a controversial behaviour that will require further investigations.

Conflict of interest

There are no conflicts to declare.

Acknowledgement

Financial support by the Austrian Science Fund (FWF project P25504-N28) is gratefully acknowledged.

Experimental

3.1 General

Commercially available reagents and solvents were used as received from Sigma Aldrich unless otherwise specified. Doubly distilled deionized water was obtained from a Millipore Milli-Q water purification system (Millipore, USA). All ionic liquids were dried for at least 48 h at room temperature and 0.01 mbar before use and were stored under an argon atmosphere. All synthetic procedure were carried out by using standard Schlenk techniques under dry argon. ^1H and ^{13}C NMR spectra were recorded on a Bruker AC 400 MHz, using the solvent peak as reference. HR-Mass Spectrometry analysis was carried out using on an Agilent 1100/1200 HPLC equipped with an Agilent 6230 AJS ESI-TOF mass spectrometer.

3.2 Synthesis of catalysts

Catalyst precursor 1-dodecyl-3-methylimidazolium chloride (**2a**) was synthesized according to a known protocol.[25] A procedure reported in literature was used for the synthesis of catalyst **1** and adapted for the surface-active ionic liquid based catalysts, details are reported in the following section.[32]

3.2.1 Synthesis of catalyst $[C_{12}mim\text{-}Ir^*CpCl_2]$ (**2**)

1-Dodecyl-3-methylimidazolium chloride (43.2 mg, 0.15 mmol, 1 eq) and silver oxide (20.8 mg, 0.09 mmol, 1.2 eq) were placed in a schlenk flask under inert atmosphere. 5 ml of dry and degassed dichloromethane were subsequently added and the reaction was left stirring in the dark for 4 hours at room temperature. The solution was then filtered over celite under inert atmosphere and $[Cp^*IrCl_2]_2$ (59.7 mg, 0.075 mmol, 0.5 eq) was added; the mixture was stirred for 15 h at room temperature and filtered. The solvent was removed under reduced pressure, the solid residue washed trice with diethyl ether and dried under high vacuum. Catalyst **2** was obtained as an orange solid in 84% yield. ^1H NMR (400 Hz, $CDCl_3$): δ (ppm) = 0.81 (3 H, t, J = 6.82 Hz, -$C_{11}H_{22}$-CH_3), 1.19 (19 H, br, -C_2H_4-C_9H_{18}-CH_3), 1.55 (15 H, m, Cp-CH_3), 1.95 (1 H, br, -N-CH_2-CH_2-$C_{10}H_{21}$), 3.77 (1 H, td, J =12.18, 4.62 Hz, -N-HCH-$C_{11}H_{23}$), 3.89 (3 H, s, -N-CH_3), 4.53 (1 H, td, J = 12.22, 5.04 Hz, -N-HCH-$C_{11}H_{23}$), 6.85 (2 H, d, J =2.00 Hz, -N-CH=CH), 6.91 (2 H, d, J =2.04 Hz, -N-CH=CH). ^{13}C NMR (100 Hz, $CDCl_3$): δ (ppm) = 9.12, 14.13, 22.70, 26.93, 29.36, 29.49, 29.56, 29.62, 29.64, 29.66, 31.86, 31.93, 38.56, 50.93, 88.55, 120.95, 123.25, 156.10. HRMS Calc. for $[C_{12}mim\text{-}IrCpCl]^+$ $(M\text{-}Cl)^+$: 613.2901 Found 613.2906.

3.2.2 Synthesis of 1,3-didodecylimidazolium chloride (**3a**)

N-dodecylimidazole was synhtesized according to a reported procedure and distilled prior to use.[42] Dodecylchloride (4 ml, 16.4 mmol, 2.4 eq) was added dropwise at RT in a 5 ml solution of dodecylimidazole (1.6 g, 6.8 mmol, 1 eq) in THF in a pressure-tight MW vial. The mixture was then stirred for 3 weeks at 80°C. The product was recrystallized from THF four times and dried at high vacuum overnight. 1,3-decylimidazoliumchloride was obtained as a white powder in 55% yield. ^1H NMR (400 Hz, $CDCl_3$): δ (ppm) = 0.87 (6 H, t, J = 6.04 Hz, -$C_{11}H_{22}$-CH_3), 1.24 (36 H, br,-C_2H_4-C_9H_{18}-CH_3),1.91 (4 H, br, -CH_2-CH_2-$C_{10}H_{21}$), 4.35 (4 H, t, J = 6.92 Hz, -N-CH_2-$C_{11}H_{23}$), 7.37 (2 H, br, -N-CH=CH), 10.87 (1 H, s, -N-CH-N-). ^{13}C NMR (100 Hz, $CDCl_3$): δ (ppm) = 138.08, 121.59, 50.10, 31.88, 30.33, 29.57, 29.48, 29.37, 29.30, 29.00, 26.26, 22.66, 14.09. Spectroscopic data were in accordance with literature.[43]

3.2.3 Synthesis of catalyst $[C_{12}C_{12}im\text{-}Ir^*CpCl_2]$ (**3**)

1,3-Didodecylimidazolium chloride (**3a**) (66.2 mg, 0.15 mmol, 1 eq) and silver oxide (20.8 mg, 0.09 mmol, 1.2 eq) were placed in a schlenk flask under inert atmosphere. 5 ml of dry and degassed dichloromethane were subsequently added and the reaction was left stirring in the dark for 15 h at room temperature. The solution was then filtered over celite under inert atmosphere and $[Cp^*IrCl_2]_2$ (59.7 mg, 0.075 mmol, 0.5 eq) was added; the mixture was stirred for 24 h at room temperature and filtered. The solvent was removed under reduced pressure, the solid residue washed three times with diethyl ether and dried under high vacuum. Catalyst **3** was obtained as an orange solid in 77% yield. Crystals suitable for X-ray diffraction were grown from slow diffusion of petrol ether to a concentrated solution of catalyst in

This journal is © The Royal Society of Chemistry [year]

chloroform. ^{1}H NMR (400 Hz, $CDCl_3$): δ (ppm) = 0.81 (7 H, t, J = 13.72 Hz, -$C_{11}H_{22}$-CH_3), 1.19 (36 H, br, -C_2H_4-C_9H_{18}-CH_3), 1.53 (15 H, m, Cp-CH_3), 1.62, 1.85 (1.5 H, m, -N-CH_2-CH_2-$C_{10}H_{21}$), 3.76 (2 H, td, J = 12.20, 5.08 Hz, -HCH-$C_{11}H_{23}$), 4.53 (2 H, td, J = 12.24, 5.00 Hz, -HCH-$C_{11}H_{23}$) 6.92 (2 H, s, -N-CH=CH). ^{13}C NMR (100 Hz, $CDCl_3$): δ (ppm) = 8.06, 8.32, 13.11, 21.68, 25.94, 28.34, 28.49, 28.53, 28.62, 28.64, 30.82, 30.90, 49.84, 87.48, 120.08, 154.77. HRMS Calc. for [$C_{12}C_{12}$im-IrCpCl]$^+$ (M-Cl)$^+$: 767.4622 Found 767.4700.

3.2.4 Synthesis of 1,3-Bis(3-dodecanimidazolium-1yl) ethane dibromide [C_{12}im-C_2-C_{12}im]Br_2 (4a)

N-dodecylimidazole was syntehsized according to a reported procedure and distilled prior to use.[42] 1,2-Dibromoethan (130 μl, 1.5 mmol, 1 eq) was added at RT in a 3.5 ml solution of dodecylimidazole (745 mg, 3.18 mmol, 2.1 eq) in THF in a pressure-tight microwave vial with Teflon seal. The mixture was then stirred for one week at 80°C. The product was recrystallized from THF twice and dried at high vacuum overnight. 1,3-Bis(3-dodecanimidazolium-1yl) ethane dibromide was obtained as a white powder in 76% yield. ^{1}H NMR (400 Hz, $CDCl_3$): δ (ppm) = 0.81 (6 H, t, J = 6.82 Hz, -$C_{11}H_{22}$-CH_3), 1.19 (36 H, br,-C_2H_4-C_9H_{18}-CH_3), 1.85 (4 H, m, -CH_2-CH_2-$C_{10}H_{21}$), 4.11 (4 H, t, J = 7.58 Hz, -N-CH_2-$C_{11}H_{23}$), 5.24 (4 H, s, -N-CH_2-CH_2-N-), 7.20 (2 H, s, -N-CH=CH-), 8.72 (2 H, s, -N-CH=CH-), 10.25 (2 H, s, -N-CH-N-). ^{13}C NMR (100 Hz, $CDCl_3$): δ (ppm) = 14.11, 22.67, 26.28, 28.88, 29.31, 29.44, 29.55, 29.57, 30.06, 31.88, 48.01, 50.56, 121.24, 124.96, 136.65. 250.2409. HRMS Calc. for [C_{12}im-C_2-C_{12}im]$^{2+}$ (M)$^{2+}$: 250.2409 Found 250.2433

3.2.5 Synthesis of catalyst [C_{12}im-C_2-C_{12}im-Ir*CpCl] (4)

[C_{12}im-C_2-C_{12}im]Br_2 (**4a**) (112.3 mg, 0.17 mmol, 1 eq) and silver oxide (41.4 mg, 0.178 mmol, 1.05 eq) were placed in a schlenk flask under inert atmosphere. 10 ml of dry and degassed dichloromethane were subsequently added and the reaction was left stirring in the dark for 15 hours at room temperature. Then [Cp*$IrCl_2$]$_2$ (67.7 mg, 0.085 mmol, 0.5 eq) was added; the mixture was stirred for 24 h at room temperature in the dark and filtered through celite. The solvent was removed and the product was refluxed for 2 h in ACN, afterwards a solid precipitate was separated via centrifugation. The top phase was collected and the solvent dried under reduce pressure, the solid residue washed three times with diethylether. The product was obtained as a yellow glassy solid in 28% yield. ^{1}H NMR (400 Hz, CD_2Cl_2): δ (ppm) = 0.80 (6 H, t, J = 6.80 Hz, -$C_{11}H_{22}$-CH_3), 1.19 (36 H, br,-C_2H_4-C_9H_{18}-CH_3), 1.53 (15 H, s, Cp-CH_3), 1.73 (4 H, m, -N-CH_2-CH_2-$C_{10}H_{21}$), 3.58 (2 H, m, CH_2), 4.31 (2 H, m, CH_2), 4.58 (2 H, m, CH_2), 4.72 (2 H, m, CH_2), 7.04 (2 H, s, -N-CH=CH-), 7.35 (2 H, s, -N-CH=CH-). ^{13}C NMR (100 Hz, CD_2Cl_2): δ (ppm) = 9.13, 13.87, 22.68, 26.79, 29.63, 31.91, 49.60, 50.97, 92.99, 122.16, 124.20, 145.30. HRMS Calc. for [C_{12}im-C_2-C_{12}im-IrCpCl]$^+$ (M)$^+$: 861.5153 Found 861.5217.

3.3 Kinetic measurements

Kinetics experiments were performed by UV-Visible spectroscopy on a Shimadzu UV1800 spectrometer equipped with a CPS-240A cell positioner and a thermostat at 25°C. In a typical experiment 20 μl of a stock solution in acetonitrile of the catalyst were added to 2 ml of a HNO_3 0.1 M Milli-Q water solution in the cuvette, afterwards 1 ml of a freshly prepared cerium ammonium nitrate stock solution in HNO_3 0.1 M in Milli-Q water was added into the cuvette, the mixture was quickly mixed and the experiment started. The consumption of Ce^{4+} was followed at 360 nm until complete consumption. 4 runs could be preformed in parallel, and the given TOF are an average thereof. The TOF was computed via Eq. (2). $TOF_{\max}$ is the maximum turn-over-frequency during the reaction and $TOF_{\langle t \rangle}$ the turn-over-frequency at the mean reaction time $\langle t \rangle$ (see Eq. (3)).

For recycling experiments a first run such as the previously reported kinetic experiments for catalyst **2** 2 μM and CAN 3 mM was performed, and when all CAN was consumed a new neat aliquot of solid salt was added to the cuvette. The addition was repeated 5 times. The calculated TON is defined as moles of converted CAN per mole of catalyst n_{CAN}/n_{cat}.

3.4 Single crystal diffraction

Single crystals of (**3**) were embedded in perfluorinated polyether and mounted on MiTeGen MicroLoops®. X-ray diffraction data were collected on a Bruker Kappa APEX-II CCD diffractometer working with graphite-monochromated Mo-Kα radiation (λ = 0.71073 Å), using narrow φ- and ω-scan frames. Corrections for absorption were applied with the multi-scan technique using SADABS.[44] The structure was solved with SHELXT and refined on F^2 with SHELXL-2016.[45,46] All non-hydrogen atoms were refined with anisotropic displacement parameters. H atoms were placed in calculated positions and thereafter treated as riding. Crystallographic data of (**3**): $C_{37}H_{67}Cl_2IrN_2$, M_r = 803.02, yellow plate, 0.12 × 0.10 × 0.2 mm^3, monoclinic, space group $P2_1/m$, a = 7.1353(9) Å, b = 33.613(4) Å, c = 8.1947(10) Å, β = 104.648(2)°, V = 1901.5(4) Å, Z = 2, d_x = 1.402 g/cm^3, T = 100 K. 34587 reflections collected (Θ_{max} = 31.54°) and merged to 6441 independent data with $I > 2\sigma(I)$ (R_{int} = 0.067); final R indices (all data) R_1 = 0.0431, wR_2 = 0.0791, GooF = 1.177, 200 parameter. Deposition number CCDC 1569509 for (**3**) contains the supplementary crystallographic data for this paper in CIF format. These data can be obtained free of charge from The Cambridge Crystallographic Data Centre via http://www.ccdc.cam.ac.uk/data_request/cif.

References

1 M. D. Kärkäs, O. Verho, E. V. Johnston and B. Åkermark, *Chem. Rev.*, 2014, **114**, 11863–12001.

2 J. D. Blakemore, R. H. Crabtree and G. W. Brudvig, *Chem. Rev.*, 2015, **115**, 12974–13005.

3 N. D. McDaniel, F. J. Coughlin, L. L. Tinker and S. Bernhard, *J. Am. Chem. Soc.*, 2008, **130**, 210–217.

4 J. D. Blakemore, N. D. Schley, D. Balcells, J. F. Hull, G. W. Olack, C. D. Incarvito, O. Eisenstein, G. W. Brudvig and R. H. Crabtree, *J. Am. Chem. Soc.*, 2010, **132**, 16017–16029.

5 J. F. Hull, D. Balcells, J. D. Blakemore, C. D. Incarvito,

O. Eisenstein, G. W. Brudvig and R. H. Crabtree, *J. Am. Chem. Soc.*, 2009, **131**, 8730–8731.
6 D. G. H. Hetterscheid and J. N. H. Reek, *Chem. Commun.*, 2011, **47**, 2712.
7 A. Petronilho, M. Rahman, J. A. Woods, H. Al-Sayyed, H. Müller-Bunz, J. M. Don MacElroy, S. Bernhard and M. Albrecht, *Dalton Trans.*, 2012, **41**, 13074.
8 J. A. Woods, R. Lalrempuia, A. Petronilho, N. D. McDaniel, H. Müller-Bunz, M. Albrecht and S. Bernhard, *Energy Environ. Sci.*, 2014, **7**, 2316–2328.
9 T. P. Brewster, J. D. Blakemore, N. D. Schley, C. D. Incarvito, N. Hazari, G. W. Brudvig and R. H. Crabtree, *Organometallics*, 2011, **30**, 965–973.
10 O. Diaz-Morales, T. J. P. Hersbach, D. G. H. Hetterscheid, J. N. H. Reek and M. T. M. Koper, *J. Am. Chem. Soc.*, 2014, **136**, 10432–10439.
11 A. Volpe, A. Sartorel, C. Tubaro, L. Meneghini, M. Di Valentin, C. Graiff and M. Bonchio, *Eur. J. Inorg. Chem.*, 2014, **2014**, 665–675.
12 I. Corbucci, A. Petronilho, H. Müller-Bunz, L. Rocchigiani, M. Albrecht and A. Macchioni, *ACS Catal.*, 2015, **5**, 2714–2718.
13 S. Chen, S. Zhang, X. Liu, J. Wang, J. Wang, K. Dong, J. Sun and B. Xu, *Phys. Chem. Chem. Phys.*, 2014, **16**, 5893–5906.
14 R. Hayes, G. G. Warr and R. Atkin, *Chem. Rev.*, 2015, **115**, 6357–6426.
15 J. Bowers, C. P. Butts, P. J. Martin, M. C. Vergara-Gutierrez and R. K. Heenan, *Langmuir*, 2004, **20**, 2191–2198.
16 Y. Kohno and H. Ohno, *Chem. Commun.*, 2012, **48**, 7119.
17 J. Łuczak, J. Hupka, J. Thòming and C. Jungnickel, *Colloids Surf. A : Physicochem. Eng. Aspects*, 2014, **329**, 125–133.
18 C. Jungnickel, J. Łuczak, J. Ranke, J. F. Fernández, A. Müller and J. Thöming, *Colloids Surf. A: Physicochem Eng. Aspects*, 2008, **316**, 278–284.
19 M. Blesic, M. H. Marques, N. V. Plechkova, K. R. Seddon, L. P. N. Rebelo and A. Lopes, *Green Chem.*, 2007, **9**, 481.
20 S. Friesen, T. Buchecker, A. Cognigni, K. Bica and R. Buchner, *Langmuir*, DOI: 10.1021/acs.langmuir.7b02201.
21 T. Inoue, H. Ebina, B. Dong and L. Zheng, *J. Colloid Interface Sci.*, 2007, **314**, 236–241.
22 B. Šarac, Žiga Medoš, A. Cognigni, K. Bica, L.-J. Chen and M. Bešter-Rogač, *Colloids Surf., A*, 2017, DOI: 10.1016/j.colsurfa.2017.01.062.
23 J. P. Hallett and T. Welton, *Chem. Rev.*, 2011, **111**, 3508–3576.
24 *Ionic liquid-based surfactant science: formulation, characterization, and applications*, ed. B. K. Paul and S. P. Moulik, Wiley, 2015.
25 A. Cognigni, P. Gaertner, R. Zirbs, H. Peterlik, K. Prochazka, C. Schröder and K. Bica, *Phys. Chem. Chem. Phys.*, 2016, **18**, 13375–13384.
26 M. Cokoja, R. M. Reich, M. E. Wilhelm, M. Kaposi, J. Schäffer, D. S. Morris, C. J. Münchmeyer, M. H. Anthofer, I. I. E. Markovits, F. E. Kühn, W. A. Herrmann, A. Jess and J. B. Love, *ChemSusChem*, 2016, **9**, 1773–1776.
27 R. Sharma, B. Gupta, T. Yadav, S. Sinha, A. K. Sahu, Y. Karpichev, N. Gathergood, J. Marek, K. Kuca and K. K. Ghosh, *ACS Sustainable Chem. Eng.*, 2016, **4**, 6962–6973.
28 J. Nowicki, J. Łuczak and D. Stańczyk, *RSC Adv.*, 2016, **6**, 11591–11601.
29 K. Bica, P. Gärtner, P. J. Gritsch, A. K. Ressmann, C. Schröder and R. Zirbs, *Chem. Commun.*, 2012, **48**, 5013–5015.
30 A. Cognigni, S. Kampichler and K. Bica, *J. Colloid Interface Sci.*, 2017, **492**, 136–145.
31 M. Taskin, A. Cognigni, R. Zirbs, E. Reimhult and K. Bica, *RSC Adv.*, 2017, **7**, 41144–41151.
32 X.-Q. Xiao and G.-X. Jin, *J. Organomet. Chem.*, 2008, **693**, 3363–3368.
33 A. R. Parent, R. H. Crabtree and G. W. Brudvig, *Chem. Soc. Rev.*, 2013, **42**, 2247–2252.
34 Z. Codolà, J. a. M.S. Cardoso, B. Royo, M. Costas and J. Lloret-Fillol, *Chem. Eur. J.*, 2013, **19**, 7203–7213.
35 J. M. Koelewijn, M. Lutz, W. I. Dzik, R. J. Detz and J. N. H. Reek, *ACS Catal.*, 2016, **6**, 3418–3427.
36 A. Savini, P. Belanzoni, G. Bellachioma, C. Zuccaccia, D. Zuccaccia and A. Macchioni, *Green Chem.*, 2011, **13**, 3360.
37 U. Hintermair, S. W. Sheehan, A. R. Parent, D. H. Ess, D. T. Richens, P. H. Vaccaro, G. W. Brudvig and R. H. Crabtree, *J. Am. Chem. Soc.*, 2013, **135**, 10837–10851.
38 R. Lalrempuia, N. D. McDaniel, H. Müller-Bunz, S. Bernhard and M. Albrecht, *Angew. Chem. Int. Ed.*, 2010, **49**, 9765–9768.
39 P. Bartlett and R. H. Ottewill, *J. Chem. Phys.*, 1992, **96**, 3306–3318.
40 J. Łuczak, M. Markiewicz, J. Thöming, J. Hupka and C. Jungnickel, *J. Colloid Interface Sci.*, 2011, **362**, 415–422.
41 D. J. Wasylenko, C. Ganesamoorthy, M. A. Henderson and C. P. Berlinguette, *Inorg. Chem.*, 2011, **50**, 3662–3672.
42 B. S. Souza, E. C. Leopoldino, D. W. Tondo, J. Dupont and F. Nome, *Langmuir*, 2012, **28**, 833–840.
43 X. Wang, F. W. Heinemann, M. Yang, B. U. Melcher, M. Fekete, A.-V. Mudring, P. Wasserscheid and K. Meyer, *Chem. Commun.*, 2009, 7405–7407.
44 L. Krause, R. Herbst-Irmer, G. M. Sheldrick and D. Stalke, *J. Appl. Crystallogr.*, 2015, **48**, 3–10.
45 G. M. Sheldrick, *Acta Crystallogr., Sect. A: Found. Crystallogr.*, 2015, **71**, 3–8.
46 G. M. Sheldrick, *Acta Crystallogr., Sect. C: Cryst. Struct. Commun.*, 2015, **71**, 3–8.

This journal is © The Royal Society of Chemistry [year]

Chapter 6

Conclusions

This thesis focused on the design and synthesis of imidazolium based surface-active ionic liquids and their consecutive application in synthesis and catalysis.

A series of 1-alkyl-3-dodecylimidazolium based ionic liquids with different anions such as halides and alkylsulfates, and variable core structures, including dicationic and zwitterionic ones, was synthesized. From studies on their aggregation behaviour in water a correlation between the CMC and the structure of the ionic liquids was identified. In general, a lower CMC was observed for more hydrophobic compounds, either arising from the low hydrated anion or resulting from multiple long alkyl chains in case of dicationic structures.

These characteristics reflected also their application in micellar catalysis. A first investigation on the role of the anion was conducted with the nucleophilic substitution for the degradation of an organophosphorus compound in water. Interestingly a strong correlation between the CMC and the reaction performance was observed: for all tested ionic liquids the highest reaction rate enhancement occurred at the corresponding CMC. Moreover, better performance was obtained with less hydrated counter-anions which do not reside on the micellar surface, and therefore provide access for the nucleophile to the active reaction site. These results were also further supported by thermodynamic and dielectric spectroscopy studies, which proved the different degree of hydration in various surface-active ionic liquids.
Subsequently surface-active ionic liquids could be successfully applied in Palladium catalysed reactions. Two examples relevant in organic synthesis were selected: the aerobic oxidation of 1-octanol to octanoic acid and the Heck cross-coupling reaction between ethyl acrylate and iodobenzene. In both cases the catalyst decomposed into catalytically active nanoparticles that could be effectively stabilized by the surface-active ionic liquid even at concentrations below their CMC. Interestingly a strong influence on the capability of the ionic liquids to form a *N*-heterocyclic carbene species was observed: when a carbene formation was possible a high ionic liquid concentration would stabilize the pre-catalyst and hamper the reaction outcome, making a lower amount of surface-active ionic liquids more effective. Moreover, it could be shown that surface-active ionic liquids can have a superior performance over conventional ammonium surfactants.
Finally surface-active ionic liquids could be used as precursors of ligands for Iridium based catalyst and applied in the water oxidation reaction for sustainable energy production. Excellent performance of the surface-active catalyst was observed, and the addition of external surface-active ionic liquids resulted in increased initial reaction rates.

In all examples it was shown that surface-active ionic liquids can effectively improve reaction performance in water even if used in very small amounts, and therefore contribute to the reduction of overall costs, risk and environmental impact of the process. Moreover, their

properties can be modified and tuned to suit a wide range of reactions varying from organic to transition metal catalysed reactions and play different roles such as catalyst, stabilizer or ligand. In all cases a strong dependence on the ionic liquid concentration and structure was observed, which is in accordance with the concepts of micellar catalysis. Optimum conditions for each reaction system could be identified, and the use of ionic liquids strongly improved the reaction performance compared to pure water.
As a conclusion, surface-active ionic liquids are a powerful tool for the application in micellar catalysis as they can benefit the reaction performance from several points of view. However, their structural design is a key aspect in the process optimization, and therefore a careful selection should be conducted according to the specific reaction requirements.

Appendix A

Supporting information:

Surface-active ionic liquids in micellar catalysis

Electronic Supplementary Material (ESI) for Physical Chemistry Chemical Physics.
This journal is © the Owner Societies 2016

Supporting informations

Surface-active ionic liquids in micellar catalysis: Impact of anion selection on reaction rates in nucleophilic substitutions

Alice Cognigni,[a] Peter Gaertner,[a] Ronald Zirbs,[b] Herwig Peterlik,[c] Katharina Prochazka,[c] Christian Schröder,[d] and Katharina Bica*,[a]

[a]Institute of Applied Synthetic Chemistry, Vienna University of Technology, Getreidemarkt 9/163, 1060 Vienna, Austria.

[b]Group for Biologically Inspired Materials, Institute of Nanobiotechnology (DNBT), University of Natural Resources and Life Sciences, Muthgasse 11, 1190 Vienna, Austria.

[c]Dynamics of Condensed Systems, University of Vienna, Boltzmanngasse 5, 1090 Vienna, Austria.

[d]Institute of Computational Biological Chemistry, University of Vienna, Währingerstrasse 17, 1090 Vienna, Austria

*Corresponding author Katharina Schröder (née Katharina Bica). Email: katharina.schroeder@tuwien.ac.at

Table of contents

1. Thermodynamic properties calculation 2

2. Kinetic constants fitting 3

3. Additional SAXS data 5

4. ^{1}H and ^{13}C NMR spectra of the surface active ILs 7

1. CMC determination and aggregation parameters calculation

For all the techniques implied the CMC was determined at the break point, i.e. the intersection of the two linear fittings of data points.

Surface tension

Π_{CMC} is the effectiveness of the surface tension reduction, it is defined according to the following equation[1] (1):

$$\Pi_{CMC} = \gamma_0 - \gamma_{CMC,} \quad (1)$$

where γ_0 is the surface tension of water, and γ_{CMC} is the surface tension of the solution at the CMC.

The Gibbs adsorption isotherm equation can be used to estimate the average area per molecule residing at the surface (A_{min}), assuming that the structure pattern corresponds to a monolayer, it is defined according to the following equations[2] (2-3):

$$A_{min}=10^{21}/N\Gamma \text{ [nm}^2\text{]} \quad (2)$$

where N= Avogadro's number, and Γ=surface excess concentration [mol/1000 m^2]

$$\Gamma = -\frac{1}{4.606\,RT}\left(\frac{d\gamma}{d\,log\,C_1}\right)_T \quad (3)$$

where $\frac{d\gamma}{d\,log\,C_1}$ is the slope of the curve surface tension vs logC before the CMC, and the concentration is expressed in mol/L, and R=8.31 J /mol K.

The packing parameter[3] (P) which includes the volume (v) of the hydrocarbon chain imbedded in the hydrocarbon core of the aggregate and the maximum effective length (l_c) that the chain can assume, calculated according to Tanford equation (6-7)[37]:

$$v = (27.4+26.9 * n)*10^{-3}\ \text{nm}^3 \quad (6)$$
$$l_c = (0.154 + 0.1265 * n)\ \text{nm} \quad (7)$$

n equals the actual number of atom in the hydrophobic core of the micelle, so generally one is left out.
The packing parameter is then defined as $P=v/a_0 l_c$, where a_0 is the cross-sectional area occupied by the hydrophilic group at the micelle-solution interface, it is in our case approximated with A_{min}. A value of P < 0.33 corresponds to spherical micelles, and intermediate value 0.33<P<0.5 corresponds

[1]Blesic, M.; Swadźba-Kwaśny, M.; Holbrey, J. D.; Canongia Lopes, J. N.; Seddon, K. R.; Rebelo, L. P. N. *Physical Chemistry Chemical Physics* 2009, **11**, 4260.
[2] Milton J. Rosen and Joy T. Kunjappu, *Surfactants and interfacial phenomena*, John Wiley & Sons, 4th end., 2012.
[3] J. N. Israelachvili, in *Intermolecular and Surface Forces*, Elsevier, 2011, pp. 535–576.

to non-spherical, ellipsoidal micelles, while higher values correspond to rod-like micelles and various interconnected structures.[36]

Conductivity

The degree of counterion binding (β) can be estimated from the conductivity data, based on the ratio of the slopes above (S_2) and below (S_1) the cmc[4] (4):

$$\beta = (1 - S_2/S_1) \quad (4)$$

The Gibbs energy of micellization (ΔG^0_{mic}) was calculated form the conductivity data according to the following equation[5] (5):

$$\Delta G^0_{mic} = (1+ \beta)\ RT \ln (CMC/W) \quad (5)$$

Where the argument of the logarithms is the molar fraction of the surfactant, and water concentration is taken as W=55.4 mol/L.

[4] Ao, M.; Kim, D. *Journal of Chemical & Engineering Data* 2013, **58**, 1529.
[5] R. Zana, *Langmuir*, 1996, **12**, 1208.

2. Kinetic constants fitting

The investigated reaction between 4-nitrophenyl diphenyl phosphate (**PNPDPP**) and acetaldoxime follows a follows a $S_N2(P)$ mechanism via in the attack of the nucleophile acetaldoxime at the phosphorous centre. Two leaving groups are possible, either the favoured *p*-nitrophenolate (**NP**), whose formation can be followed at 402.5 nm or phenolate (**P**) as a by-product.

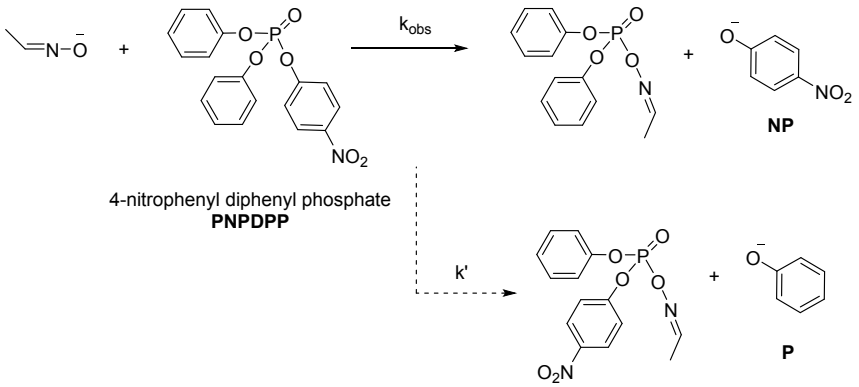

For the determination of the rate constants for both, the desired reaction (k_{obs}) and the by-product formation (k'), a competitive reaction scheme (see figure above) is assumed which leads to a system of coupled differential equations:

$$\frac{d\vec{c}(t)}{dt} = \boldsymbol{R} \cdot \vec{c}(t) \tag{1}$$

where the vector $\vec{c}$(t) represents the concentration of PNPDPP, NP and P at time t

$$\vec{c}(t) = \begin{pmatrix} [\mathrm{PNPDPP}](t) \\ [\mathrm{NP}](t) \\ [\mathrm{P}](t) \end{pmatrix} \tag{2}$$

and the reaction matrix **R** looks like

$$\boldsymbol{R} = \begin{pmatrix} -k_{obs} - k' & 0 & 0 \\ k_{obs} & 0 & 0 \\ k' & 0 & 0 \end{pmatrix} \tag{3}$$

The general solution of the coupled differential equations in Eq. (1) depends on the Eigenvalues λ_1=0, λ_2=0 and λ_3=-(k_{obs} +k') and the corresponding Eigenvectors

$$\vec{e}_1 = \begin{pmatrix} 0 \\ 0 \\ 1 \end{pmatrix} \qquad \vec{e}_2 = \begin{pmatrix} 0 \\ 1 \\ 0 \end{pmatrix} \qquad \vec{e}_3 = \frac{1}{k'} \begin{pmatrix} -(k_{obs} + k') \\ k_{obs} \\ k' \end{pmatrix}$$

of the reaction matrix **R**:

$$\vec{c}(t) = \sum_{i=1}^{3} \alpha_i \vec{e}_i e^{\lambda_i t} \tag{4}$$

At time t=0, $\vec{c}$(0) = ([PNPDPP]$_0$, 0, 0) since only the reactant is present. Using this initial condition, the α-coefficients can be determined:

$$\alpha_3 = -[\mathrm{PNPDPP}]_0 \frac{k'}{k_{obs} + k'}$$

$$\alpha_2 = [\mathrm{PNPDPP}]_0 \frac{k_{obs}}{k_{obs} + k'}$$

$$\alpha_1 = [\mathrm{PNPDPP}]_0 \frac{k'}{k_{obs} + k'} = -\alpha_3$$

As a result, the time-dependent concentration of NP yields

$$[\mathrm{NP}](t) = [\mathrm{PNPDPP}]_0 \quad \frac{k_{obs}}{k_{obs} + k'} \left(1 - e^{-(k_{\mathrm{obs}} + k')t}\right) \tag{5}$$

In a least-square fit of the spectroscopic data to Eq. (5) using gnuplot, the sum of the two rate constants k_{obs} + k' can be determined. The individual values of k_{obs} and k' are evaluated from the ratio of the initial concentration of the reactant $[PNPDPP]_0$ and the final concentration of the product NP which also equals k_{obs} / (k_{obs}+k').

3. Additional SAXS data

The scaled medium contrast is obtained by the ratio of the electron densities (ref. 35 of the paper, P. Bartlett and R.H. Ottewill, *J. Chem. Phys.*, 1992, **96**, 3306)

$$\gamma = \frac{\rho_m - \rho_s}{\rho_c - \rho_s}$$

where the subscript denotes (surrounding) **m**atrix, **s**hell and **c**ore, respectively. $\gamma = 0$ means that density of core and medium are identical, $\rho_m = \rho_s$, and only the core scatters. For $\gamma = 1$, $\rho_m = \rho_c$ and only the shell contributes to scattering.

The following Figures S1a to S1c show the shift towards a more uniform distribution of the radius of the core for higher concentrations. It may be not the case for Cl (as these data are difficult to evaluate due to the weakly pronounced maximum in the scattering intensities), but clearly visible for Br and OTS.

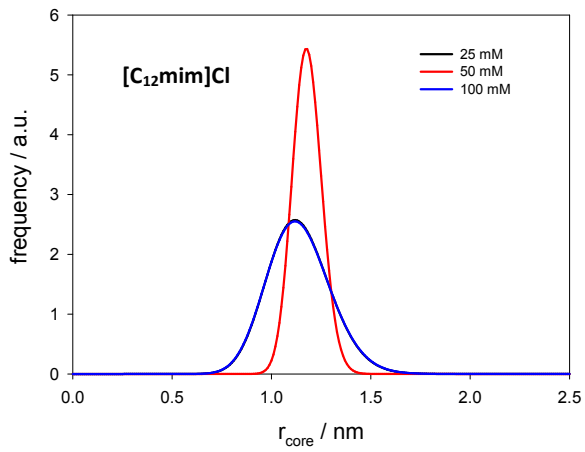

Fig. S1a: Size distribution of core radius for different concentrations of $[C_{12}mim]Cl$.

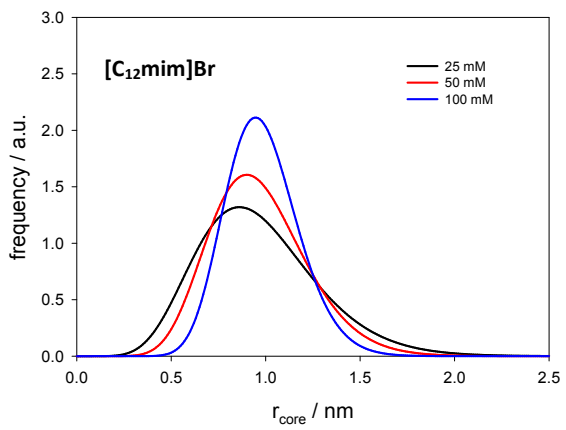

Fig. S1b: Size distribution of core radius for different concentrations of $[C_{12}mim]Br$.

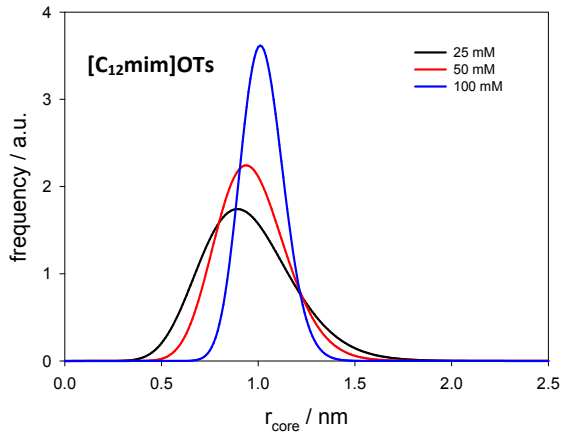

Fig. S1c: Size distribution of core radius for different concentrations of $[C_{12}mim]OTs$.

4. ^{1}H and ^{13}C NMR spectra of the surface active ILs

[C_{12}mim]Cl

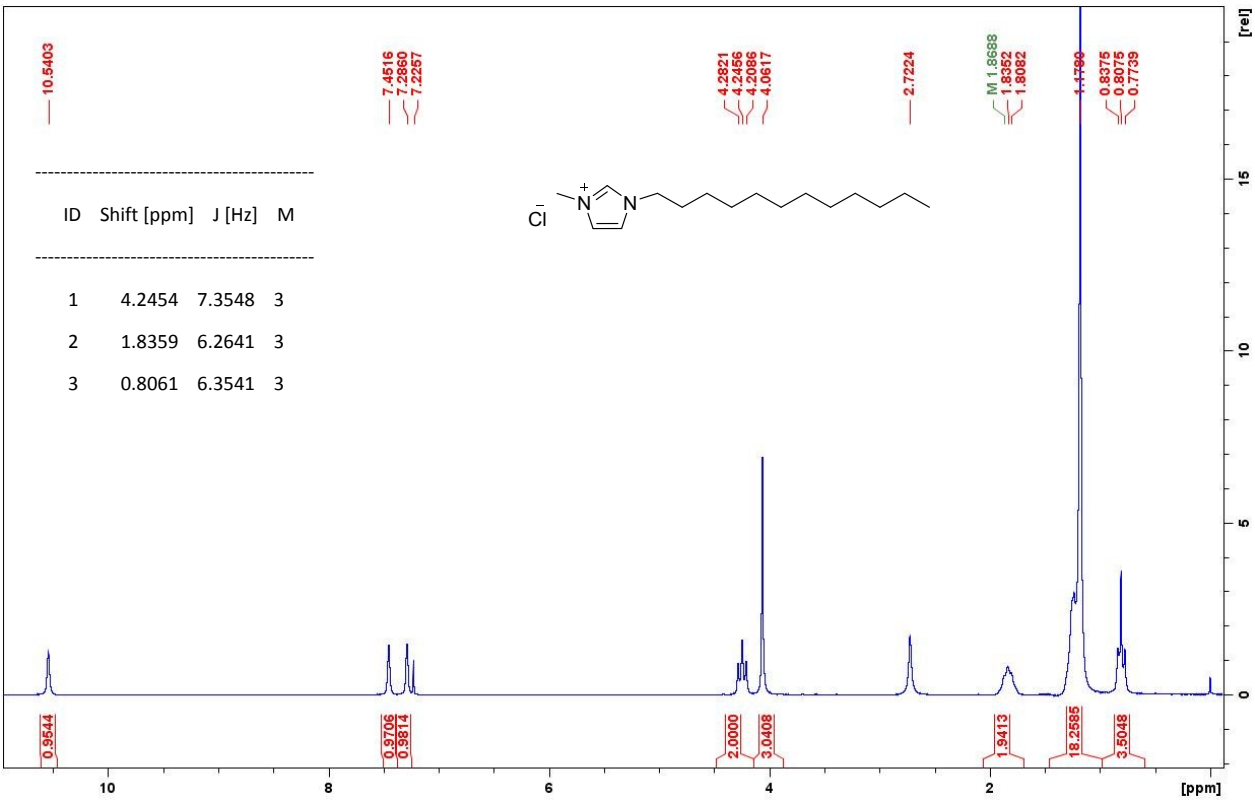

ID	Shift [ppm]	J [Hz]	M
1	4.2454	7.3548	3
2	1.8359	6.2641	3
3	0.8061	6.3541	3

[C_{12}mim]Br

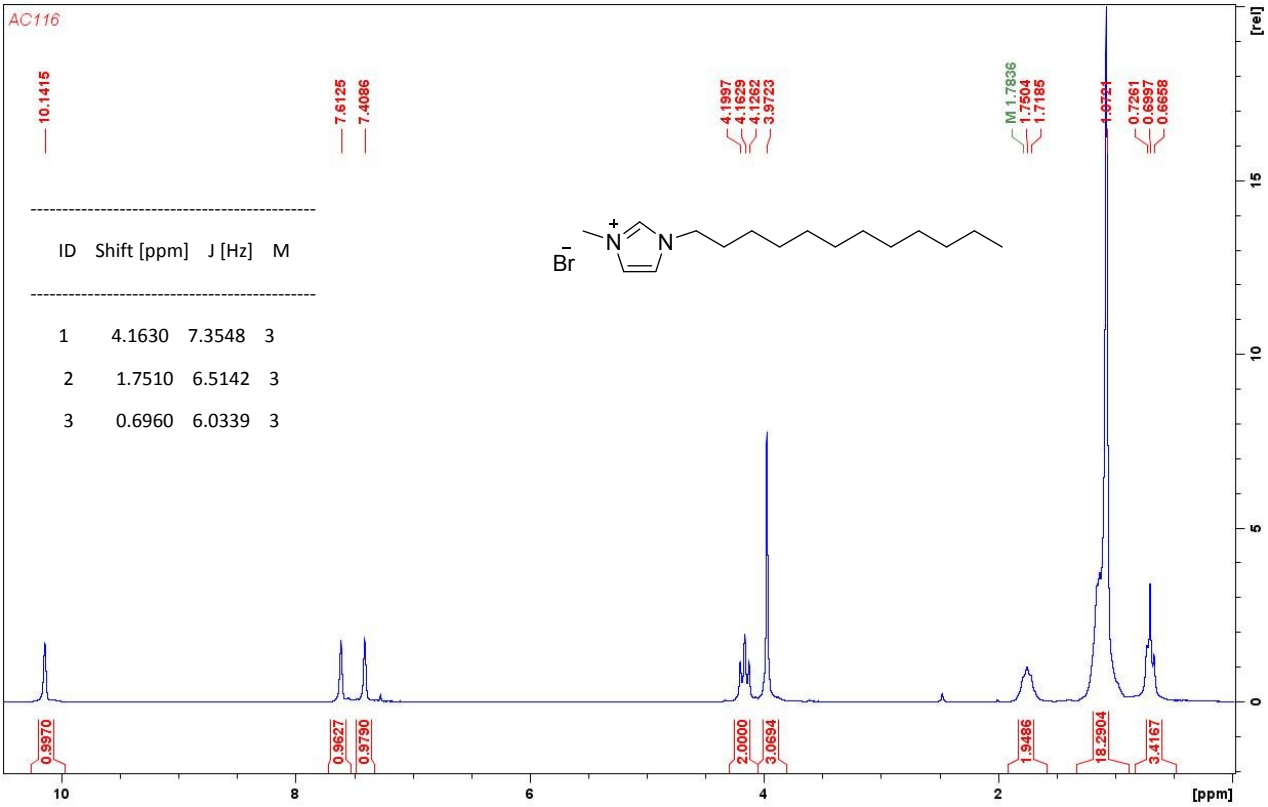

ID	Shift [ppm]	J [Hz]	M
1	4.1630	7.3548	3
2	1.7510	6.5142	3
3	0.6960	6.0339	3

S9

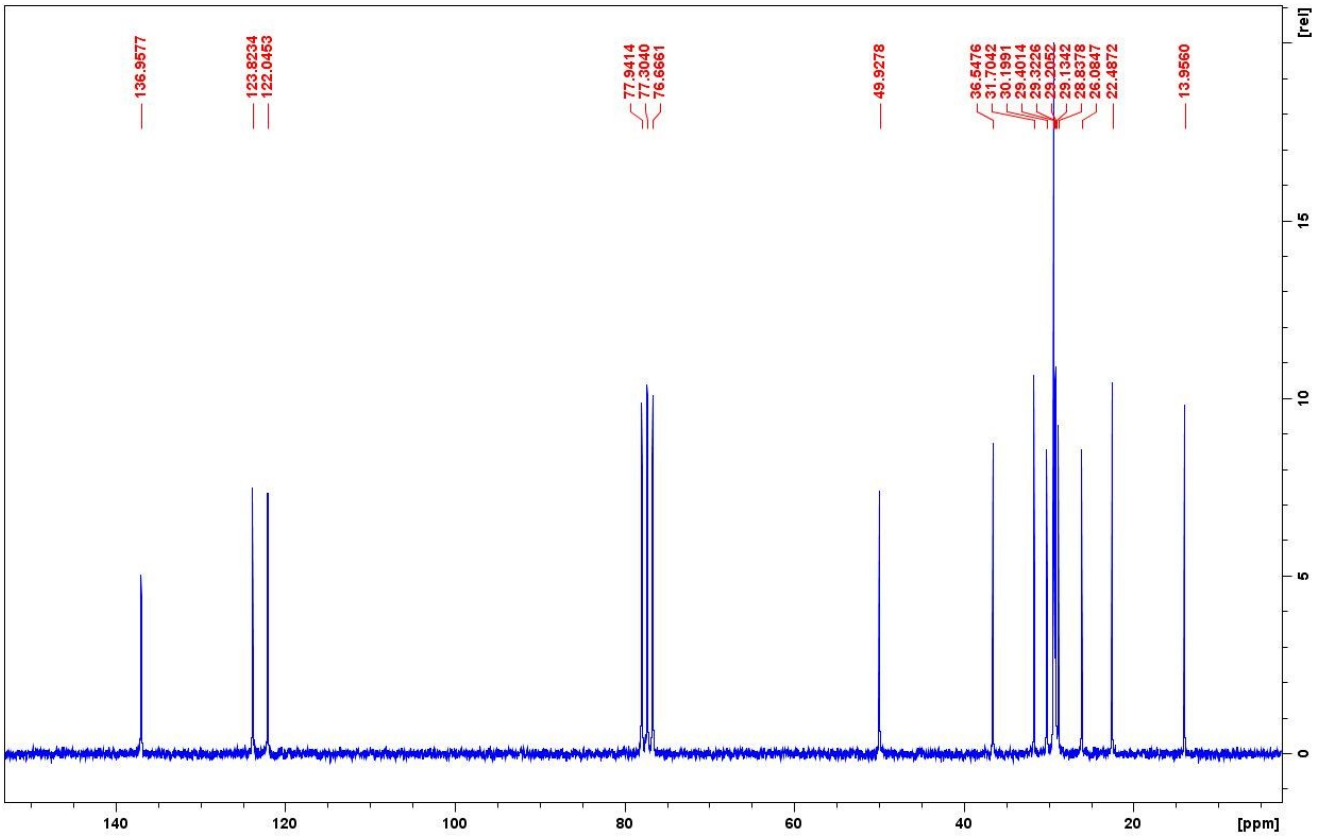
136.9577
123.8234
122.0453
77.9414
77.3040
76.6661
49.9278
36.5476
31.7042
30.1991
29.4014
29.3226
29.2052
29.1342
28.8378
26.0847
22.4872
13.9560
[rel]
0
5
10
15
140
120
100
80
60
40
20
[ppm]

S10

[C_{12}mim]I

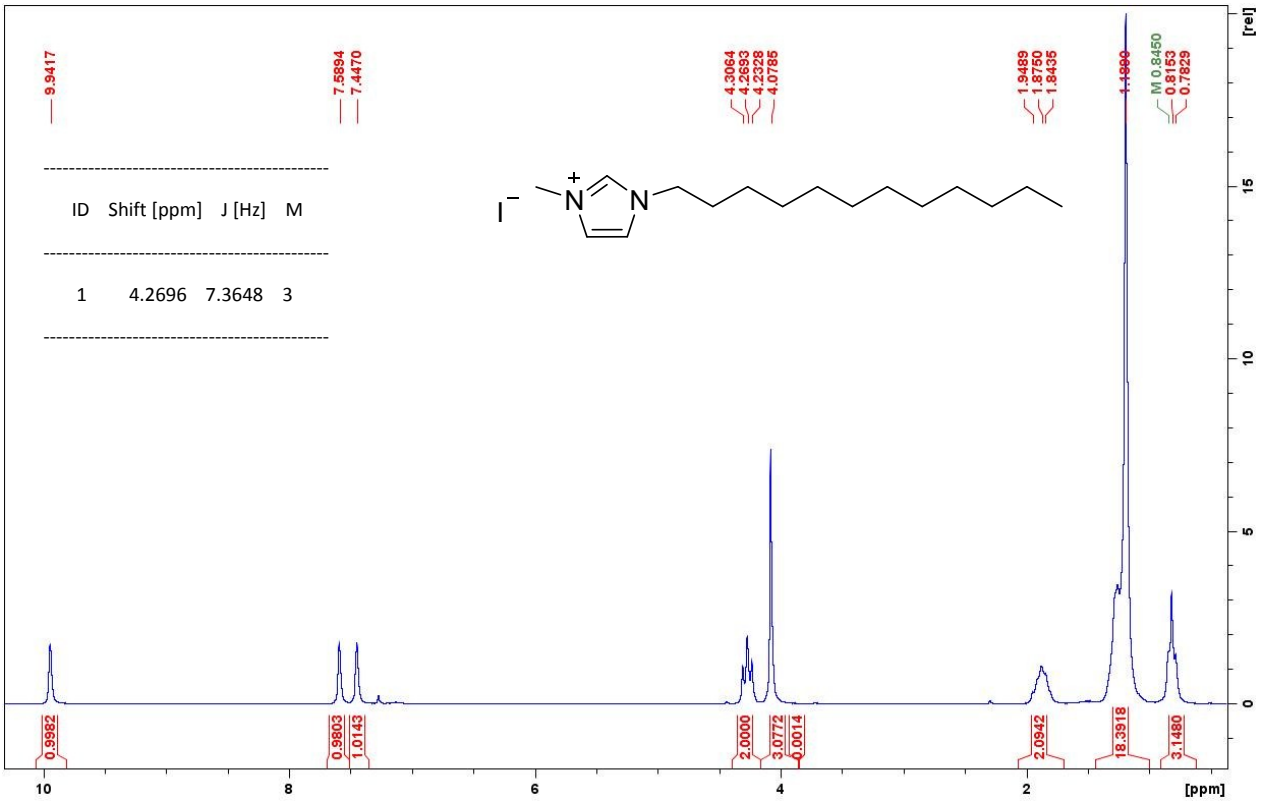

ID	Shift [ppm]	J [Hz]	M
1	4.2696	7.3648	3

S11

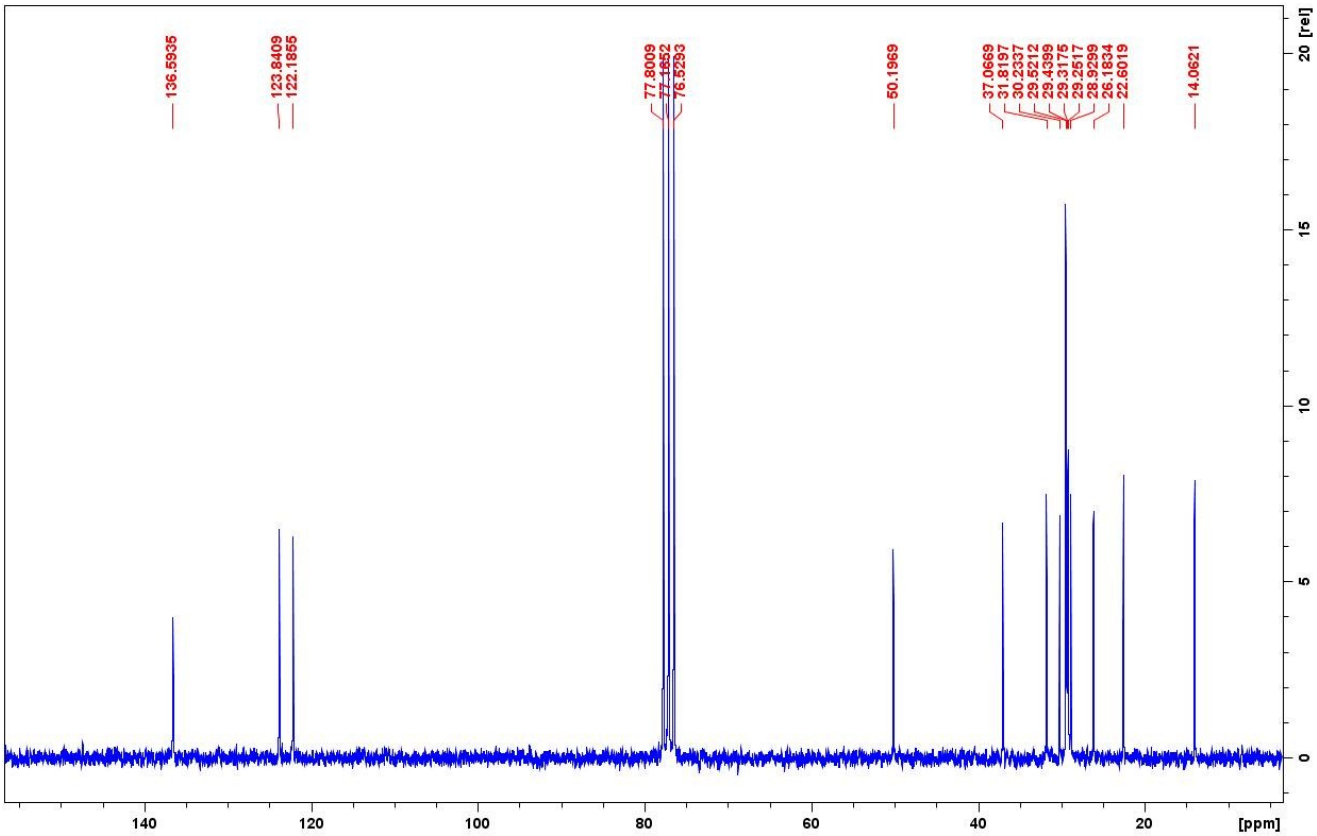
136.5935
123.8409
122.1855
77.8009
77.1652
76.5293
50.1969
37.0669
31.8197
30.2337
29.5212
29.4399
29.3175
29.2517
28.9299
26.1834
22.6019
14.0621
20 [rel]
15
10
5
0
140
120
100
80
60
40
20
[ppm]

S12

[C_{12}mim]OMs

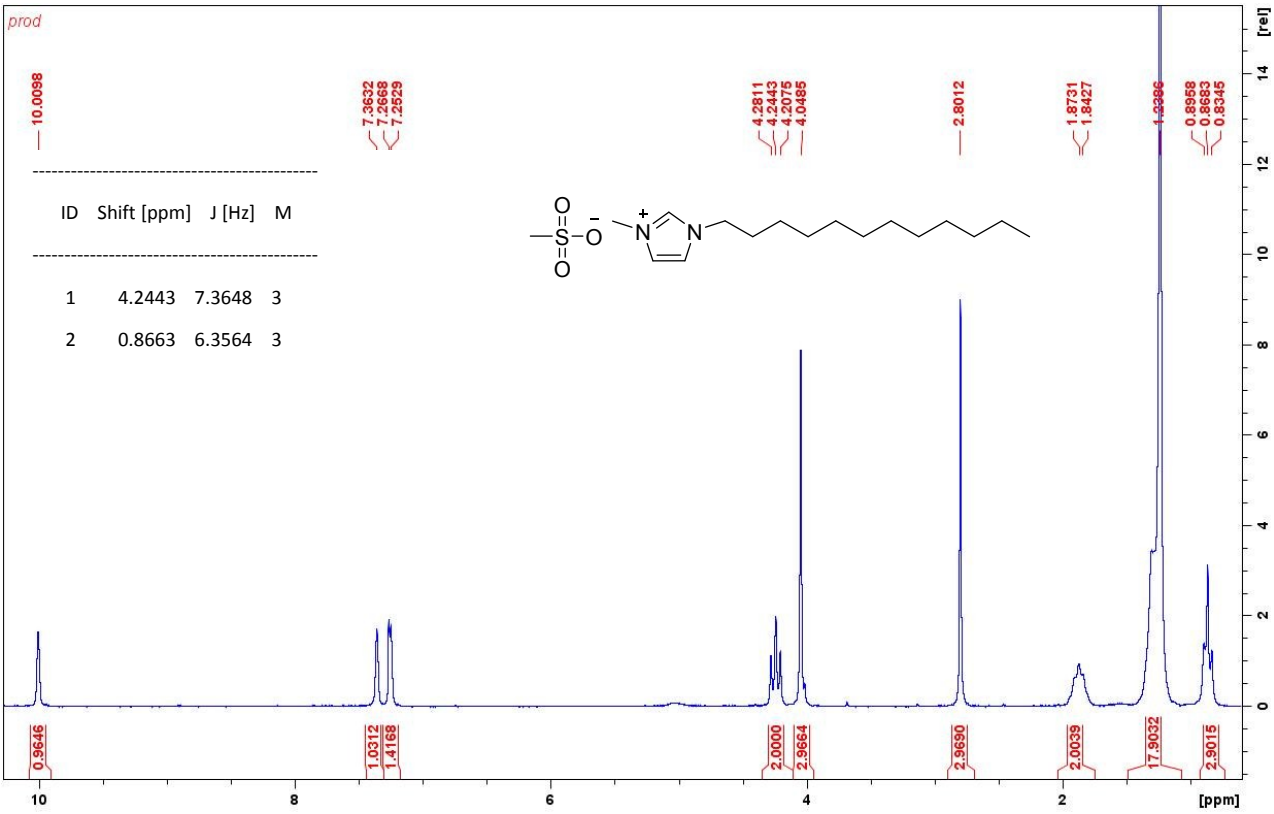
prod
10.0098
7.3632
7.2668
7.2529
4.2811
4.2443
4.2075
4.0485
2.8012
1.8731
1.8427
1.0386
0.8958
0.8683
0.8345
ID Shift [ppm] J [Hz] M
1 4.2443 7.3648 3
2 0.8663 6.3564 3
0.9646
1.0312
1.4168
2.0000
2.9664
2.9690
2.0039
17.9032
2.9015
[ppm]
[rel]

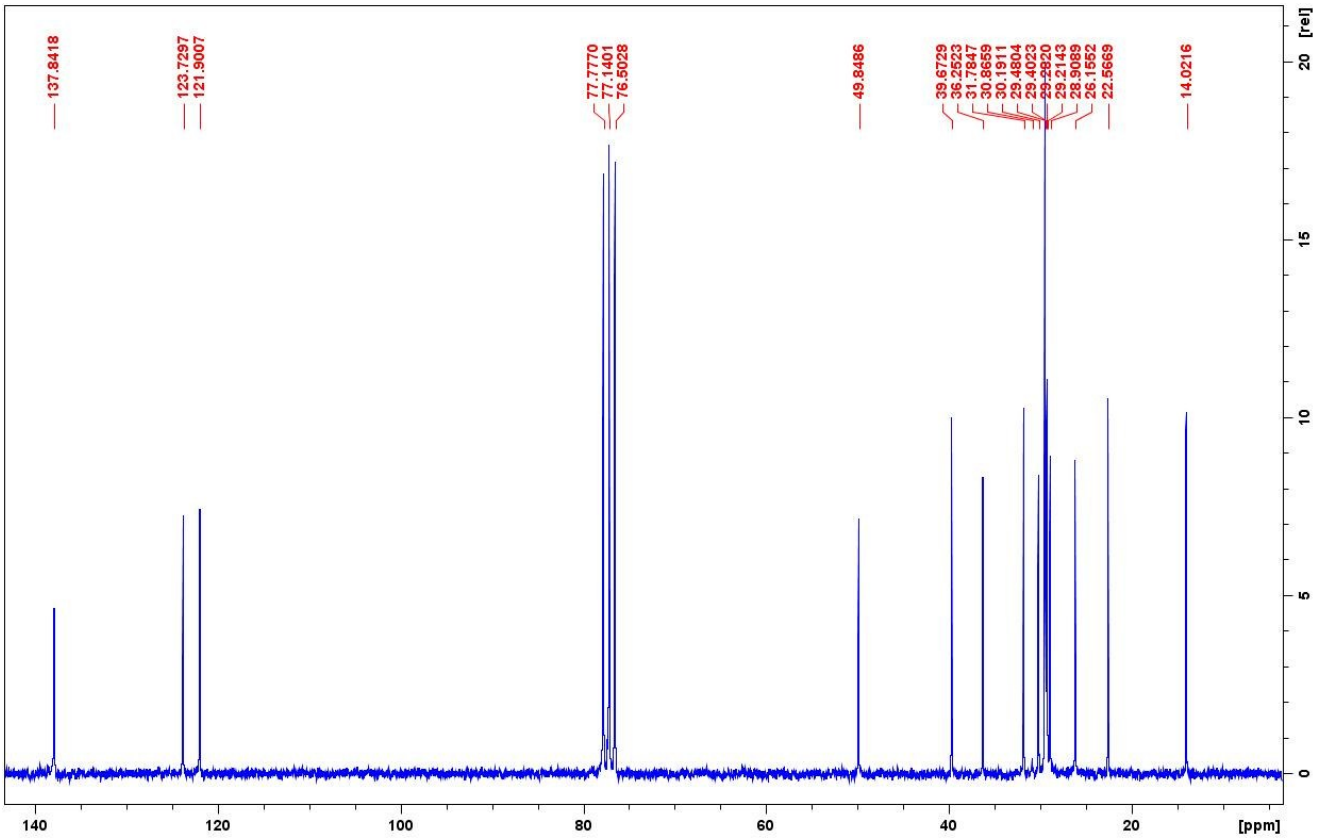
137.8418
123.7297
121.9007
77.7770
77.1401
76.5028
49.8486
39.6729
36.2523
31.7847
30.8659
30.1911
29.4804
29.4023
29.2820
29.2143
28.9089
26.1552
22.5669
14.0216
[rel]
[ppm]

S14

[C_{12}mim]OTs

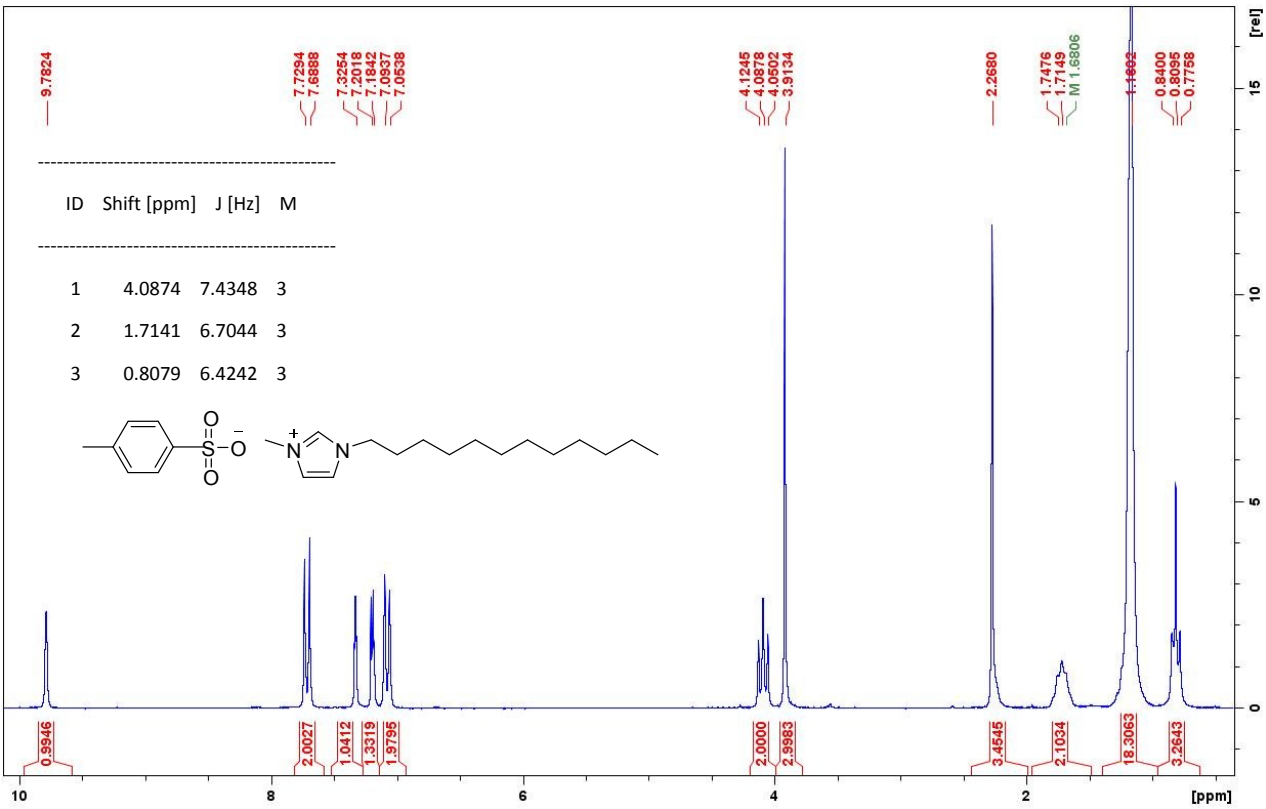

S15

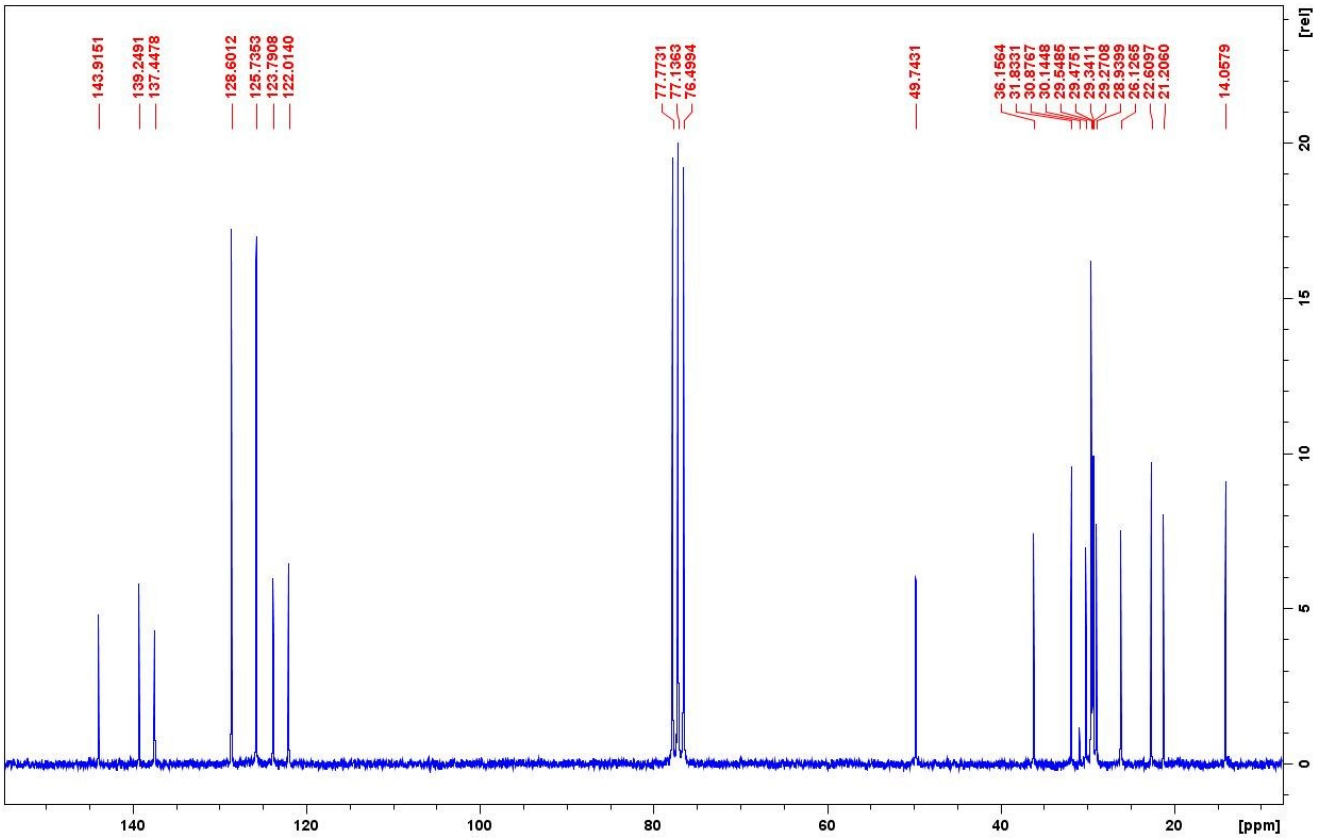
143.9151
139.2491
137.4478
128.6012
125.7353
123.7908
122.0140
77.7731
77.1363
76.4994
49.7431
36.1564
31.8331
30.8767
30.1448
29.5485
29.4751
29.3411
29.2708
28.9399
26.1265
22.6097
21.2060
14.0579
[rel]
[ppm]

S16

[C_{12}mim]OTf

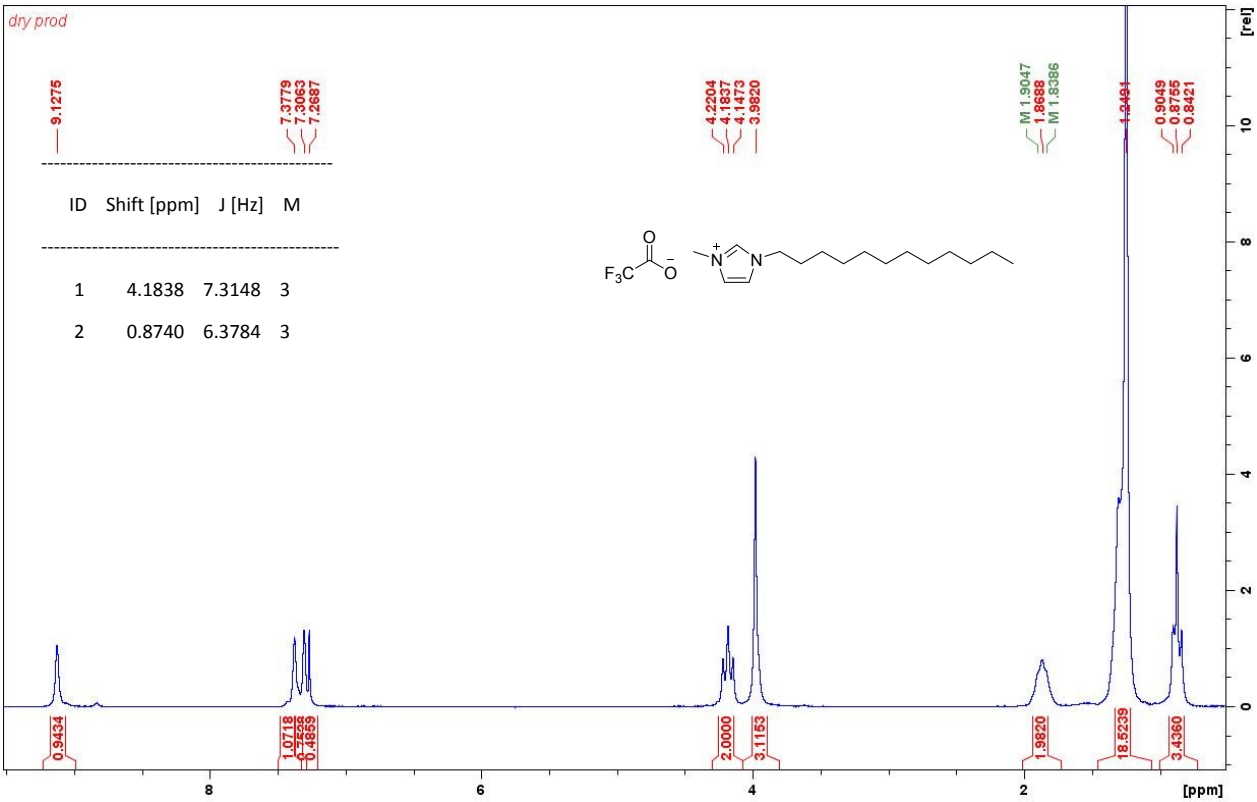

S17

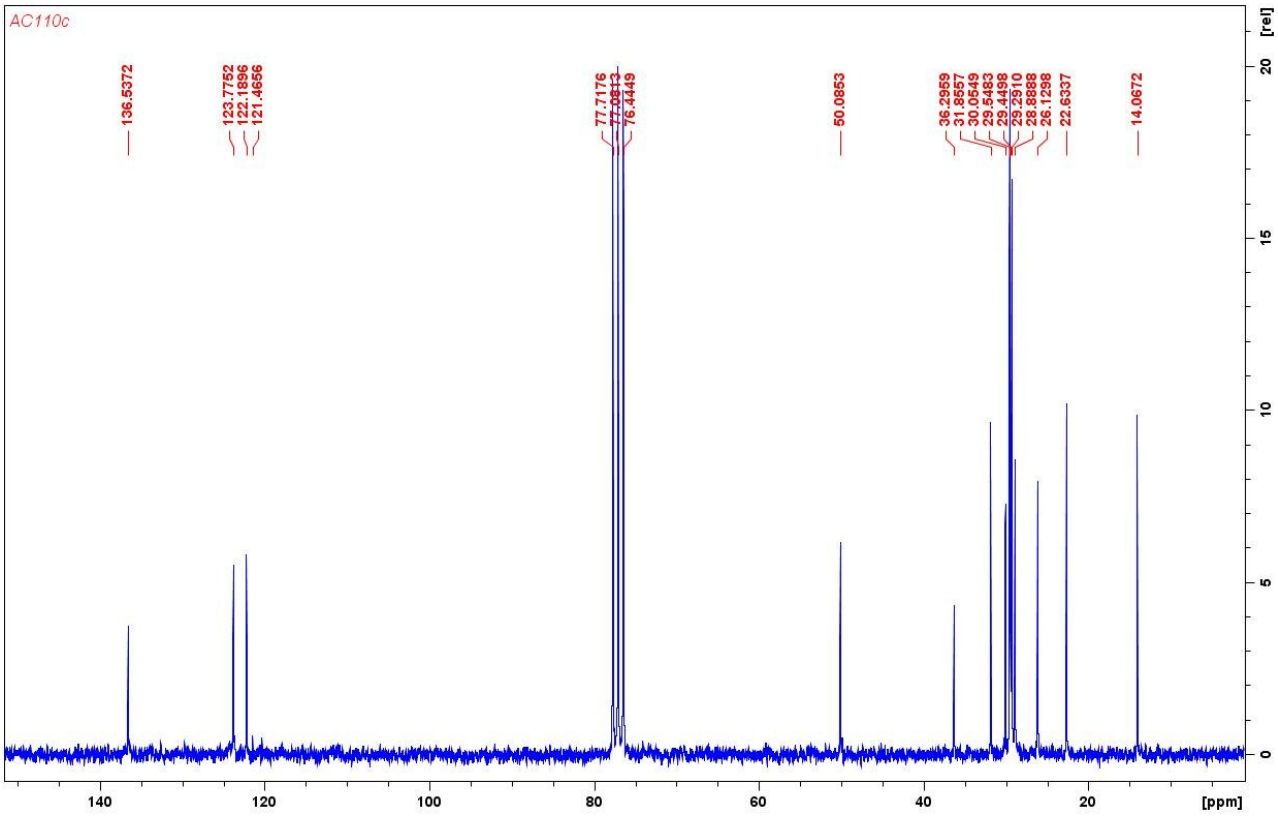
AC110c
136.5372
123.7752
122.1896
121.4656
77.7176
77.0813
76.4449
50.0853
36.2959
31.8557
30.0549
29.5483
29.4498
29.2910
28.8888
26.1298
22.6337
14.0672
[rel]
[ppm]

S18

Thermodynamic Study for Micellization of Imidazolium Based Surface Active Ionic Liquids in Water: Effect of Alkyl Chain Length and Anions

Bojan Šarac[a], Žiga Medoš[a], Alice Cognigni[b], Katharina Bica[b,*], Li-Jen Chen[c], Marija Bešter-Rogač[a,*]

[a]Faculty of Chemistry and Chemical Technology, University of Ljubljana, Večna pot 113, SI-1000 Ljubljana, Slovenia

[b]Institute of Applied Synthetic Chemistry, Vienna University of Technology Getreidemarkt 9/163, A-1060 Vienna, Austria

[c]Department of Chemical Engineering, National Taiwan University, Taipei 10617, Taiwan

*Corresponding authors:

Katharina Bica

Institute of Applied Synthetic Chemistry, Vienna University of Technology Getreidemarkt 9/163

A-1060 Vienna, Austria

katharina.schroeder@tuwien.ac.at

Marija Bešter-Rogač

Faculty of Chemistry and Chemical Technology, Večna pot 113, University of Ljubljana, SI-1000 Ljubljana, Slovenia

marija.bester@fkkt.uni-lj.si

Supplementary Material

Content of Supplementary Material

Thermodynamic analysis

Fig. S1. Temperature dependent enthalpograms for investigated SAILs in water. Solid lines represent the global fits according to the Eqs. (m-t).

Fig. S2. Temperature dependence of cmc for investigated SAILs in water. Solid lines represent the corresponding polynomial fits, cmc=A+BT+CT^2. Coefficients are given in Table S2 in Supporting Information.

Fig. S3. Temperature dependence of the standard enthalpy of micellization, $\Delta_M H^0$, for investigated SAILs in water. Solid lines represent the corresponding linear fits,

Fig. S4. Enthalpy-entropy compensation plots for the micellization process of investigated SAILs in water. Solid lines represent linear fits (Eq. (11) in main manuscript).

Fig. S5. Correlation between $\Delta_M c_p^0$ and β for the micellization process of investigated [C_{12}mim]X SAILs in water.

Fig. S6. Viscosities of aqueous solutions of investigated [C_{12}mim]X SAILs at 298.15 K.

Table S1: Thermodynamic parameters of micellization for investigated SAILs in water at all the investigated temperatures: critical micelle concentration, cmc, degree of micelle ionization, β, standard enthalpy, $\Delta_M H^0$, Gibbs free energy, $\Delta_M G^0$, and entropy contributions, $T\Delta_M S^0$, for micellization for investigated systems in water as obtained by the fitting procedure.

Table S2. Coefficients of polynomials cmc =A+ BT + CT^{2a}.

Thermodynamic analysis

a) Model description. According to the mass-action model [1-4] the micellization process of a cationic surfactant at constant temperature, T, and pressure, p, may be described as

$$n\mathrm{S}^{+} + (n-z)\mathrm{C}^{-} \text{ Ä } \mathrm{M}^{z} \qquad \text{(a)}$$

where S^+ represents the monomeric state of surfactant, C^- corresponding counterions and M^{p+} the micellar aggregate of n surfactant monomers with an effective charge of z. The equilibrium between species can be expressed by equilibrium constant, K, as

$$K = \frac{a_{\mathrm{M}}}{a_{\mathrm{S}}^{n}\, a_{\mathrm{C}}^{n-z}} = \frac{m_{\mathrm{M}} / m^{0}}{(m_{\mathrm{S}} / m^{0})^{n} (m_{\mathrm{C}} / m^{0})^{n-z}} \cdot \frac{\gamma_{\mathrm{M}}}{\gamma_{\mathrm{S}}^{n}\, \gamma_{\mathrm{C}}^{n-z}} = K_{\mathrm{M}} \cdot K_{\gamma} \qquad \text{(b)}$$

where a_S, a_C and a_M are the activities of the surfactant ions in monomeric form, counterions and micelles, respectively; m_S, m_C and m_M are the corresponding molalities; γ_S, γ_C and γ_M the corresponding activity coefficients and m^0 standard molality, 1 mol kg^{-1}.

At low concentrations of surfactant it can be assumed that $K_\gamma \approx 1$, and the apparent equilibrium constant, K_M, usually is written in a simplified form as

$$K_{\mathrm{M}} = \frac{m_{\mathrm{M}}}{m_{\mathrm{S}}^{n}\, m_{\mathrm{C}}^{n-z}} \qquad \text{(c)}$$

Surfactant solution with concentration greater than cmc can be considered as a mixed electrolyte solution with the total surfactant molality, m,

$$m = m_{\mathrm{S}} + n \cdot m_{\mathrm{M}} \qquad \text{(d)}$$

and the degree of micellization $\alpha_{\mathrm{M}} = n \cdot m_{\mathrm{M}} / m$. The total molality of counterions, m_C, is given as

$$m_{\mathrm{C}} = m - (n-z)\, m_{\mathrm{M}} \qquad \text{(e)}$$

From the above equations it follows that the standard Gibbs free energy for micellization, $\Delta_{\mathrm{M}} G^{0}$, of ionic surfactant can be expressed as

$$\Delta_{\mathrm{M}} G^{0} = -\frac{RT}{n} \ln K_{\mathrm{M}} = -\frac{RT}{n} \ln \left(\frac{\alpha_{\mathrm{M}}\, m^{1-n}}{n (1-\alpha_{\mathrm{M}})^{n} \left(m \left(1 - \alpha_{\mathrm{M}} (1-\beta) \right) \right)^{n-z}} \right). \qquad \text{(f)}$$

where β is degree of micelle ionization (=z/n, where z is the effective charge of the micelles and n is the number of surfactant monomer in the micellar aggregate).

b) Connection of model to experiment. The equilibrium between monomeric surfactant ions, their micelles and corresponding simple counterions can be also described in terms of the composition variables n_1 (the number of moles of solvent), n_S (the number of moles of surfactant ions in monomeric form), n_C (the number of moles of free counterions), and n_M (the number of moles of surfactant ions in micellar form) and the corresponding partial molar enthalpies $\bar{H}_1$, $\bar{H}_S$, $\bar{H}_C$, and $\bar{H}_M$. The enthalpy of solution in the titration cell obtained after i-th injection, H_i, can be thus expressed as

$$H_i = n_1\bar{H}_1 + n_2\bar{H}_2 = n_1\bar{H}_1 + n_S\bar{H}_S + n_C\bar{H}_C + n_M\bar{H}_M . \tag{g}$$

By taking into account the total number of moles of surfactant, $n_2 = n_S + n_M$, and counterions, $n_C = n_S + (z/n)n_M$, Eq. (g) becomes

$$H_i = n_1\bar{H}_1 + n_2\left(\bar{H}_S + \bar{H}_C\right) + n_M\Delta_M H \tag{h}$$

where the enthalpy of micelle formation, $\Delta_M H$, is defined as

$$\Delta_M H = \left(\bar{H}_M - \bar{H}_S - (1 - z/n)\bar{H}_C\right). \tag{i}$$

By taking the partial derivative of enthalpy, H_i, with respect to n_2 at constant p, T, and n_1 and using the Gibbs-Duhem equation ($\sum_i n_i \, d\bar{H}_i = 0$, p,T = const.) we obtain

$$\begin{aligned} \bar{H}_2 &= \left(\frac{\partial H_i}{\partial n_2}\right)_{p,T,n_1} = \\ &= \frac{\partial n_1}{\partial n_2}\bar{H}_1 + n_1\frac{\partial \bar{H}_1}{\partial n_2} + \frac{\partial n_2}{\partial n_2}\left(\bar{H}_S + \bar{H}_C\right) + n_2\frac{\partial\left(\bar{H}_S + \bar{H}_C\right)}{\partial n_2} + \frac{\partial n_M}{\partial n_2}\Delta_M H + n_M\frac{\partial \Delta_M H}{\partial n_2} \end{aligned} \tag{j}$$

which gives us the relation below

$$\bar{H}_2 = \left(\bar{H}_S + \bar{H}_C\right) + \Delta_M H\left(\frac{\partial n_M}{\partial n_2}\right)_{n_1,p,T} . \tag{k}$$

In the ITC experiment (constant *p, T*), the measured property reflects heat effect, q_{i}, that results from each (i-th) injection of the titrant solution into the titration cell. The measured heat effect is thus usually given as the enthalpy change, ΔH, expressed per mole of added titrant (solute)

$$\Delta H = \frac{q_{\mathrm{i}}}{\Delta n_2} = \frac{\left(H_{\mathrm{i}} - H_{\mathrm{i-1}}\right)}{\Delta n_2} - \frac{H_{\mathrm{a}}}{\Delta n_2} \tag{l}$$

where H_{i} and $H_{\mathrm{i-1}}$ represent the enthalpies of solution in measuring cell after i-th and (i–1)-th injection, respectively. H_{a} is the enthalpy of injected aliquot of titrant solution and Δn_2 is the amount of solute in that aliquot. As during the titration procedure the aliquots are constant and very small ($\Delta n_2 << n_1 =$ amount of solvent in the titration cell), the Eq. (l) simplifies into

$$\Delta H = \left(\frac{\partial H}{\partial n_2}\right)_{n_1,p,T} - \text{const} = \bar{H}_2 - \text{const}. \tag{m}$$

The combination of Eqs. (k) and (m) leads to the measured relative molar enthalpy, ΔH, containing the enthalpy of micellization which is assumed to be concentration independent and thus equal to its value in the standard state ($\Delta_{\mathrm{M}} H = \Delta_{\mathrm{M}} H^0$).

$$\Delta H = \left(\bar{H}_{\mathrm{S}} + \bar{H}_{\mathrm{C}} - \text{const}\right) + \Delta_{\mathrm{M}} H^0 \left(\frac{\partial n_{\mathrm{M}}}{\partial n_2}\right)_{n_1,p,T}. \tag{n}$$

Using the Gibbs-Helmholtz relation and the Guggenheim approximation for surfactant mean activity coefficient[3,5]

$$-\log\gamma_{\pm} = \frac{A_{(T)}\sqrt{m}}{1+\sqrt{m}} + B_{(T)} m \tag{o}$$

below the cmc $(\bar{H}_{\mathrm{S}} + \bar{H}_{\mathrm{C}})$ contribution can be expressed as

$$\bar{H}_{\mathrm{C}} + \bar{H}_{\mathrm{S}} = \bar{H}_2^0 + 2 \cdot RT^2 \left(\frac{A'_{(T)}\sqrt{m}}{1+\sqrt{m}} + B'_{(T)}\, m\right) \tag{p}$$

where $\bar{H}_2^0$ represents the partial molar enthalpy of surfactant in its standard state. The coefficients $A'_{(T)}$ and $B'_{(T)}$ are temperature derivatives of the constants $A_{(T)}$ and $B_{(T)}$, that reflect solvent properties and ion-ion interactions, respectively [5].

Above the cmc, $(\overline{H}_{\mathrm{S}}+\overline{H}_{\mathrm{C}})$ contribution is assumed to remain constant and equal to its value at the cmc due to the small changes in concentrations of S^+ and C^- ions.

The $\left(\partial n_{\mathrm{M}}/\partial n_2\right)_{n_1,p,T}$ derivative in the Eq. (n) represents the fraction of surfactant molecules in micellar state M and can be derived from the apparent equilibrium constant, K_{M}, (Eqs. (c) and (f)) as

$$\left(\frac{\partial n_{\mathrm{M}}}{\partial n_2}\right)_{n_1,p,T}=\frac{n\left[u+g\right]}{1+n\left[u+\left(1-\beta\right)g\right]} \tag{q}$$

where the parameters u and g are functions of the degree of micellization (α_{M}) and the degree of micelle ionization (β)

$$u=\frac{\alpha_{\mathrm{M}}}{1-\alpha_{\mathrm{M}}}\ ,\qquad g=\frac{\left(1-z/n\right)\alpha_{\mathrm{M}}}{1-\left(1-z/n\right)\alpha_{\mathrm{M}}+m_x/m}. \tag{r}$$

c) Fitting procedure. In the global analysis (fitting of experimental curves at all temperatures simultaneously) of ITC data we used the Kirchhoff's law

$$\Delta_{\mathrm{M}}H^0(T)=\Delta_{\mathrm{M}}H^0(T_{\mathrm{r}})+\Delta_{\mathrm{M}}c_p^0\left(T-T_{\mathrm{r}}\right) \tag{s}$$

and the integrated Gibbs-Helmholtz equation

$$\Delta_{\mathrm{M}}G^0(T)=T\left(\Delta_{\mathrm{M}}G^0(T_{\mathrm{r}})/T_{\mathrm{r}}+\Delta_{\mathrm{M}}H^0(T_{\mathrm{r}})\left[1/T-1/T_{\mathrm{r}}\right]+\Delta_{\mathrm{M}}c_p^0\left[1-T_{\mathrm{r}}/T-\ln\left(T/T_{\mathrm{r}}\right)\right]\right) \tag{t}$$

where $\Delta_{\mathrm{M}}H^0(T_{\mathrm{r}})$ and $\Delta_{\mathrm{M}}G^0(T_{\mathrm{r}})$ are the standard enthalpy and the standard Gibbs free energy of micellization at some reference temperature T_{r}. Therefore, it follows from the Eq. (f) and Eqs. (o-t), that the ITC model equation (Eq. (n)) may be described in terms of n, $\Delta_{\mathrm{M}}H^0$, $\Delta_{\mathrm{M}}G^0$, $\Delta_{\mathrm{M}}c_p^0$, and the coefficients $A'_{(T)}$ and $B'_{(T)}$ at any surfactant concentration and temperature, T. All these values were obtained by fitting of the model equation to the experimental data points in the following manner. The model equation was compared to the experimental curves via the χ^2 function defined as

$$\chi^2 = \sum_i \left(\frac{\Delta H_\mathrm{i} - \Delta H_\mathrm{i}^\mathrm{mod}}{\Delta\left(\Delta H_\mathrm{i}\right)} \right)^2 \qquad \text{(u)}$$

where ΔH_i and $\Delta H_\mathrm{i}^\mathrm{mod}$ represent the experimental and the model enthalpy, whereas $\Delta\left(\Delta H_\mathrm{i}\right)$ represents the absolute error in measured enthalpy, ΔH_i . By minimization of χ^2 function best-fit values of the above-mentioned parameters were calculated using the Levenberg-Marquardt nonlinear regression algorithm [6]. Their values were further used to calculate corresponding $\Delta_\mathrm{M} H^0$, $\Delta_\mathrm{M} G^0$, and $T\Delta_\mathrm{M} S^0$ at some other temperature. The entropy change, $\Delta_\mathrm{M} S^0$, associated with the examined process was obtained from the Gibbs-Helmholtz equation

$$\Delta_\mathrm{M} S^0 = \frac{\Delta_\mathrm{M} H^0 - \Delta_\mathrm{M} G^0}{T} \qquad \text{(v)}$$

and the molar heat capacity change of micelle formation, $\Delta_\mathrm{M} c_p^0$, was given from the temperature dependence of $\Delta_\mathrm{M} H^0$.

d) Fitting algorithm. Modeling algorithm of fitting of model function (Eq. (n)) to the corresponding experimental data (Fig. 1 in the main manuscript and S1 in Supplementary material) was following:

1. At a given T_r (usually 298.15 K) reasonable initial values of adjustable parameters n, $\Delta_\mathrm{M} H^0(T_\mathrm{r})$, $\Delta_\mathrm{M} G^0(T_\mathrm{r})$, $\Delta_\mathrm{M} c_p^0$, and the coefficients $A'_{(T)}$ and $B'_{(T)}$ are chosen.

2. For a given $\Delta_\mathrm{M} G^0(T_\mathrm{r})$ value α_M can be determined at any concentration m iteratively from Eq.(f) together with the corresponding derivative , $(\partial n_\mathrm{M}/\partial n_2)_{n1,\,p,\,T}$ (Eq. (q)).

3. The value of the model function (Eq. (n)) at a given titration point (m) is calculated for the selected set of adjustable parameters.

4. Using Kirchhoff's law and the integrated Gibbs-Helmholtz (Eqs. (s) and (t)) the $\Delta_M G^0$ and $\Delta_M H^0$ are calculated for other temperatures.

5. Steps 2, 3 are repeated for every experimental point (each successive *m*) to calculate the corresponding model functions (Eq.(n)).

6. The model functions (Eq. (n)) are compared to the corresponding experimental curves via the χ^2 function defined as:

$$\chi^2 = \sum_i \left(\frac{\Delta H_i - \Delta H_i^{mod}}{\Delta(\Delta H_i)} \right)^2 \qquad (z)$$

where ΔH_i is the experimental ΔH at given titration point (*m*), ΔH_i^{mod} is the corresponding value of the model function (Eq. (n)) and $\Delta(\Delta H_i)$ is the estimated absolute error in the measured ΔH (ITC).

7. The best fit of the model functions to the corresponding experimental curves (ΔH vs. *m*) is obtained by minimization of the corresponding χ^2. Levenberg-Marquardt algorithm is applied to select new sets of adjustable parameters *n*, $\Delta_M H^0(T_r)$, $\Delta_M G^0(T_r)$, $\Delta_M c_p^0$, and the coefficients $A'_{(T)}$ and $B'_{(T)}$ (ITC at given *T*) and by repeating steps 1. to 6. to find a minimum in χ^2. Their values at the global minimum of χ^2 are considered as the best descriptors of the experimental ITC curves.

8. Statistical analysis:

(i) The mean-square deviations (errors) of the adjustable parameters are calculated as square roots of the diagonal elements, c_{kl}, of the variance-covariance matrix, ***C***, which is defined as the inverse of the curvature matrix, β. The elements of the curvature matrix, β_{kl}, are given by the simplified relation [7,8]:

$$\beta_{kl} = \frac{\partial^2 \chi^2}{\partial B_k \partial B_l} \cong \sum_i \frac{1}{(\Delta(\Delta H_i))^2} \left(\frac{\partial \Delta H_i^{mod}}{\partial B_k} \frac{\partial \Delta H_i^{mod}}{\partial B_l} \right) \qquad (x)$$

in which B_k and B_l are the adjustable parameters (n, $\Delta_M H^0(T_r)$, $\Delta_M G^0(T_r)$, $\Delta_M c_p^0$, and the coefficients $A'_{(T)}$ and $B'_{(T)}$). The derivatives in Eq. (x) are calculated analytically.

In this work, only the global fitting of the model equation to the corresponding experimental curves at all the examined temperatures was carried out simultaneously. The advantage of this procedure over the individual fitting at a single temperature is greater confidence in the proposed model and consequently in all the adjustable parameters [9]. The main presumption concerning the global fitting was temperature independence of the aggregation number. But in our previous work it turned out that values obtained from the individual best-fit values and the global-fit value for n of the chosen system were basically the same [10].

Degree of micelle ionization was assumed to be also temperature independent for all the systems investigated. During the fitting procedure, anomalies from purely sigmoidal behavior at some titration curves were observed ([C_{10}mim]Cl at higher temperatures, [C_{12}mim]OMs at 288.15 K and at 308. 15 K, [C_{12}mim]OAc at 288.15 K and at 298. 15 K]).

All obtained thermodynamic parameters are gathered in Tables 1 and 2 in the main text and in Table S1 in Supporting Information.

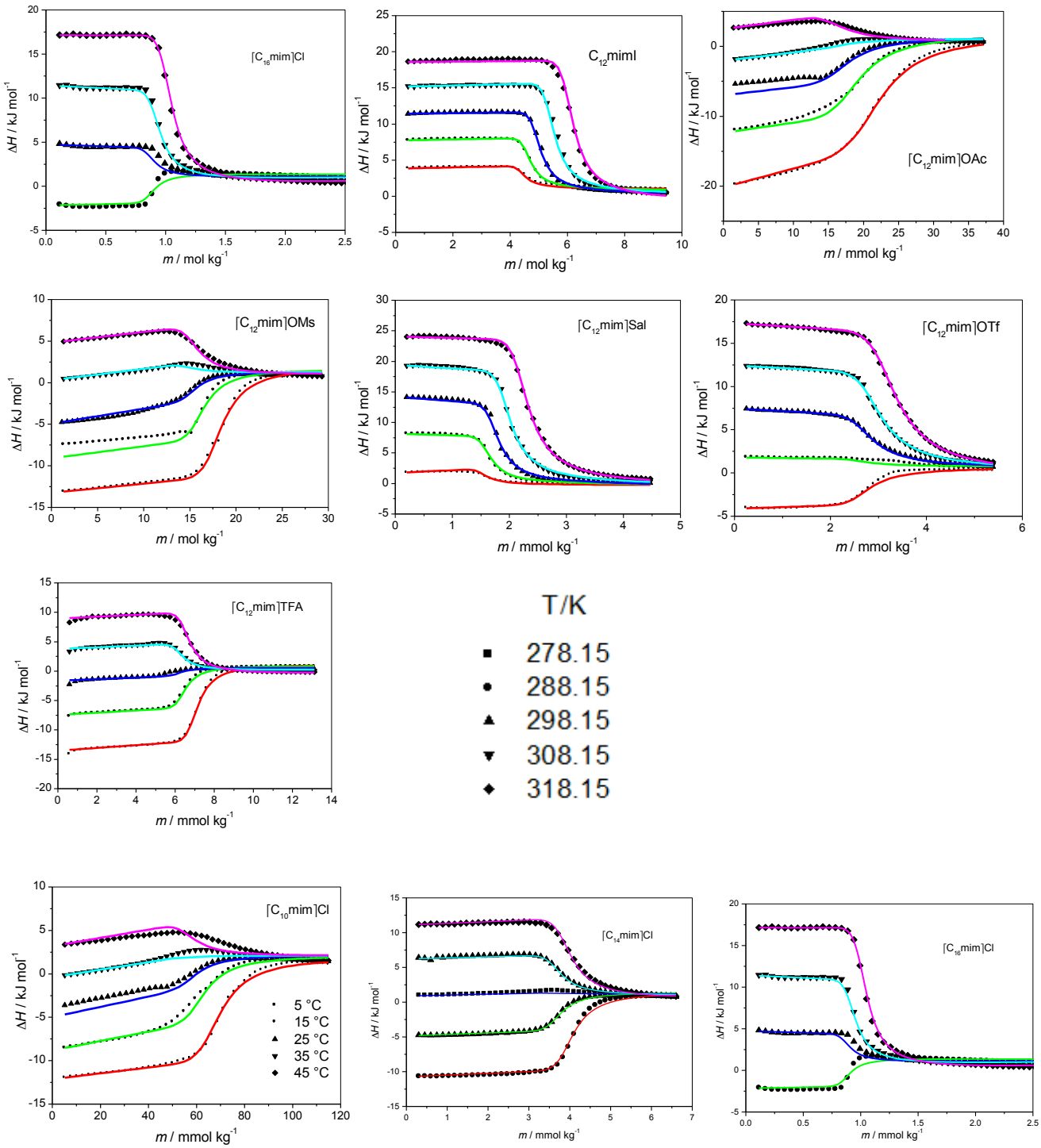

Fig. S1. Temperature dependent enthalpograms for investigated SAILs in water. Solid lines represent the global fits according to the Eqs.(n-t).

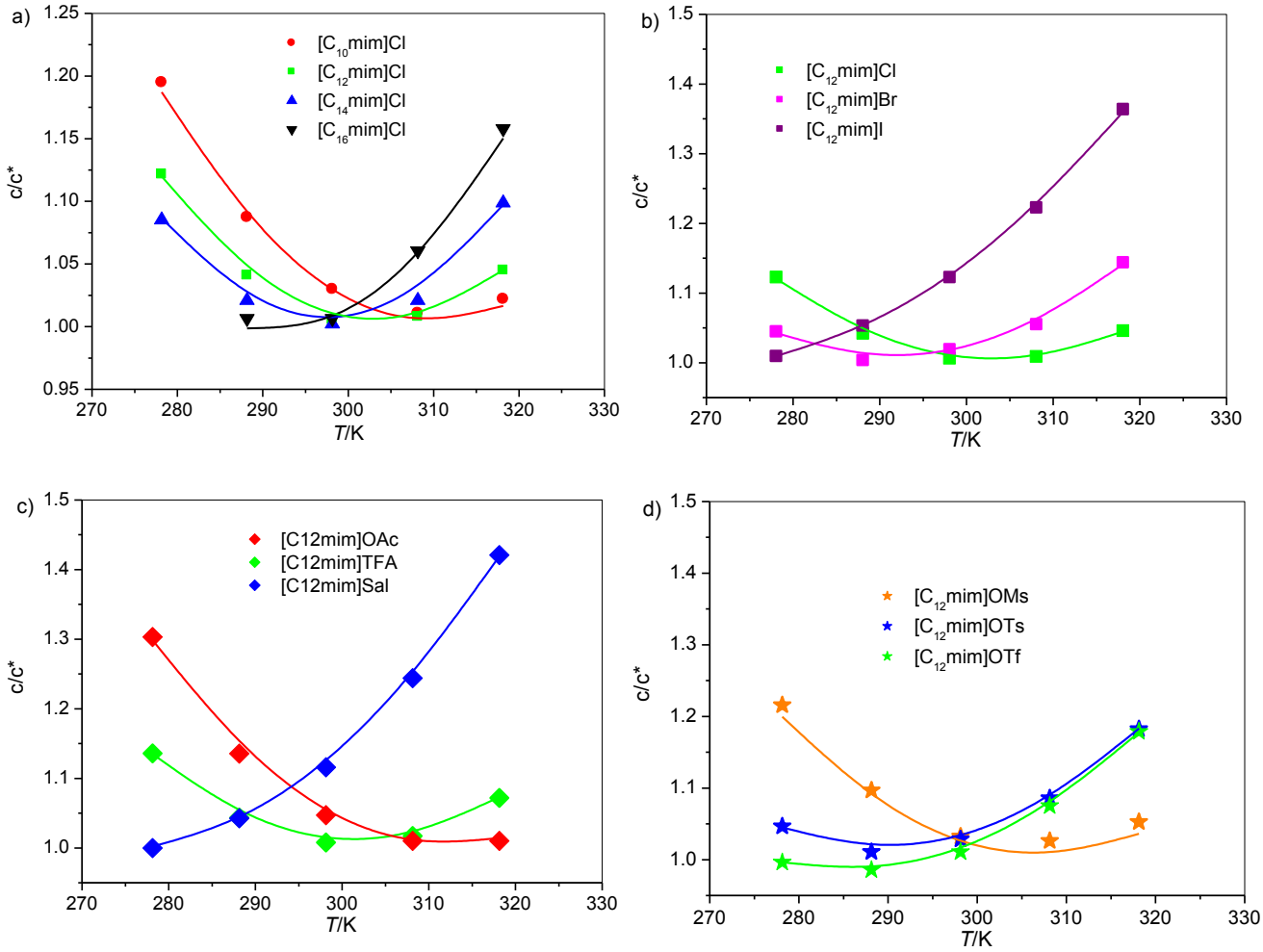

Fig. S2. Temperature dependence of cmc for investigated SAILs in water. Solid lines represent the corresponding polynomial fits, cmc=A+BT+CT^2. Coefficients are given in Table S2 in Supplementary material.

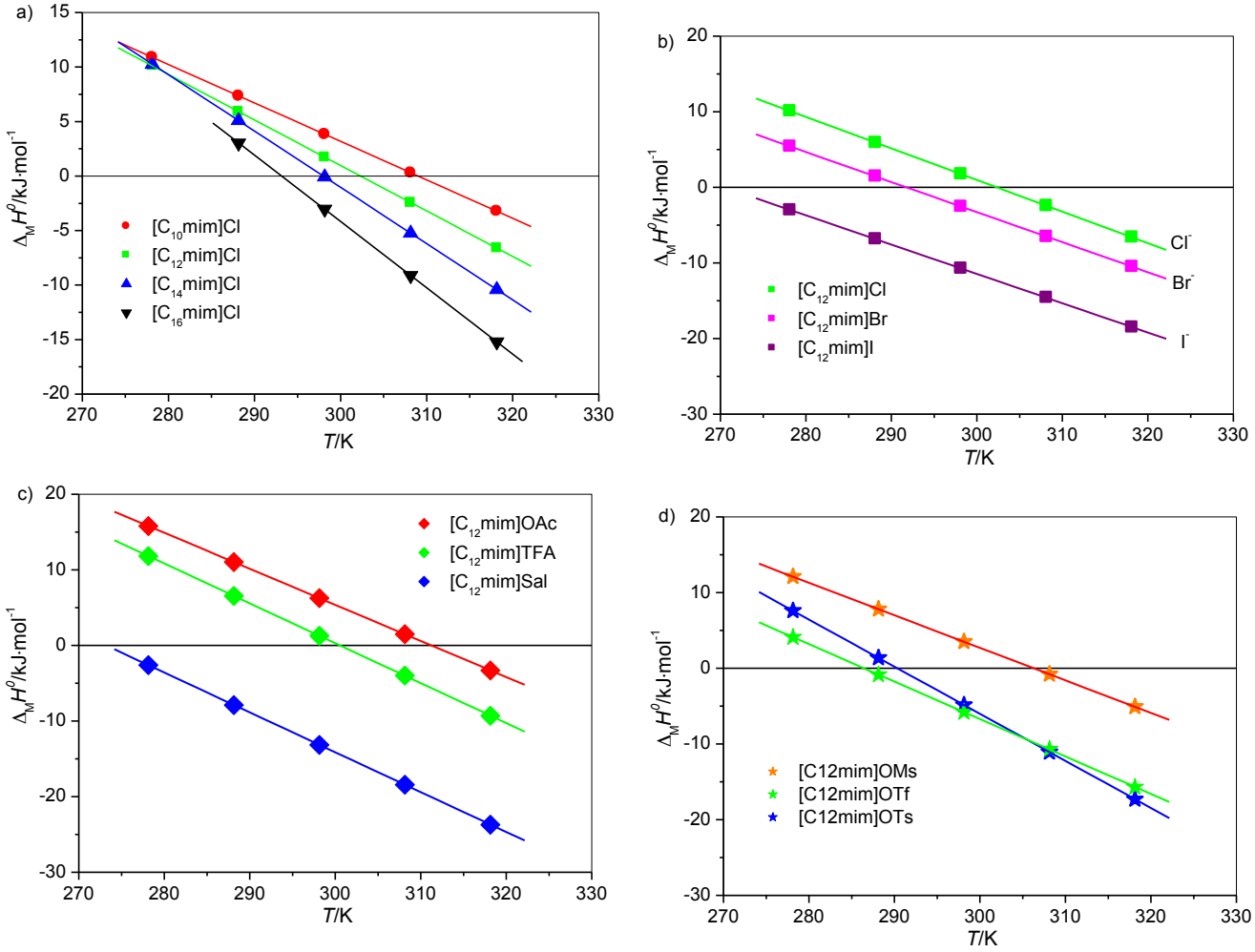

Fig. S3. Temperature dependence of the standard enthalpy of micellization, $\Delta_M H^0$, for investigated SAILs in water. Solid lines represent the corresponding linear fits.

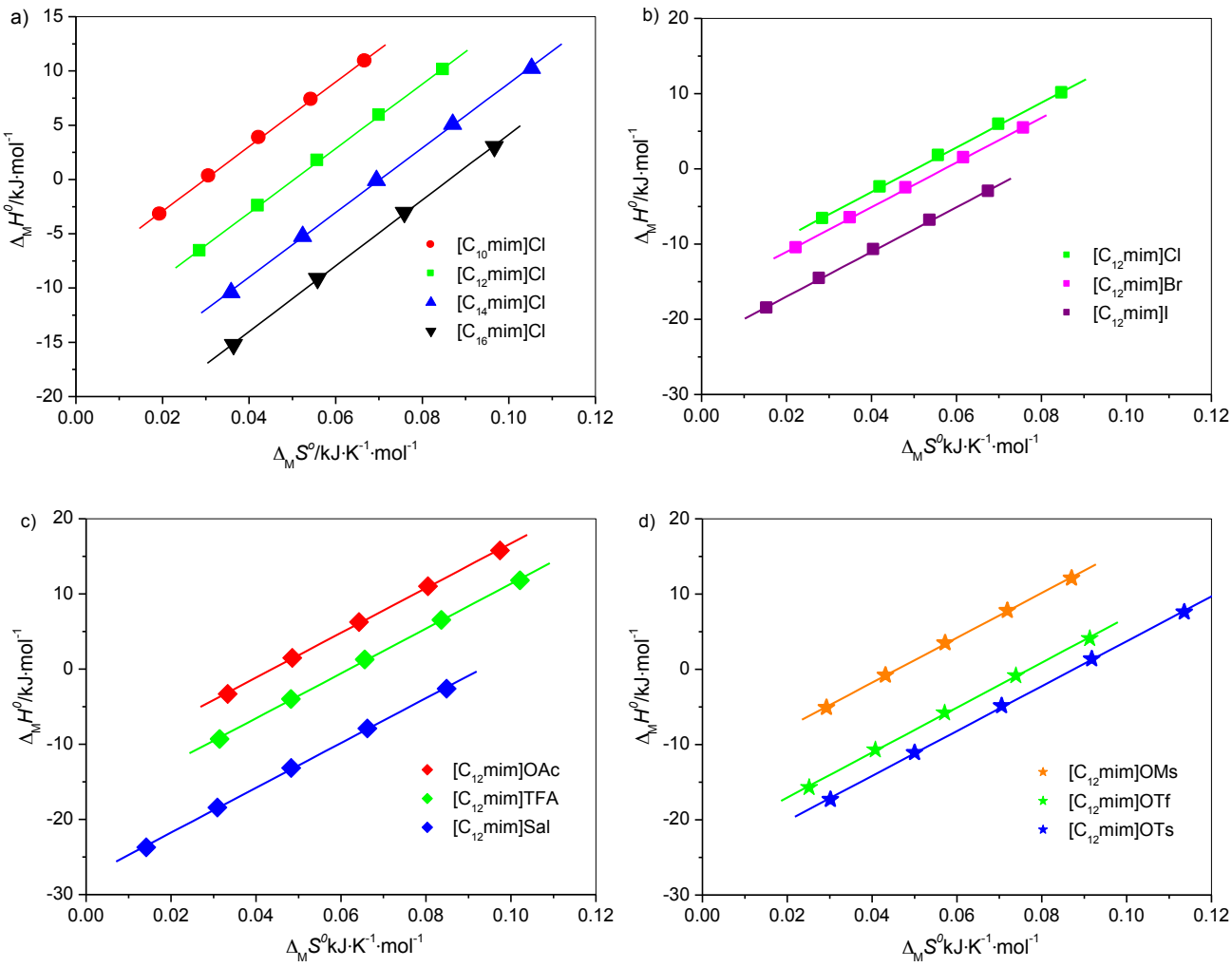

Fig. S4. Enthalpy-entropy compensation plots for the micellization process of investigated SAILs in water. Solid lines represent linear fits (Eq. (11) in main manuscript).

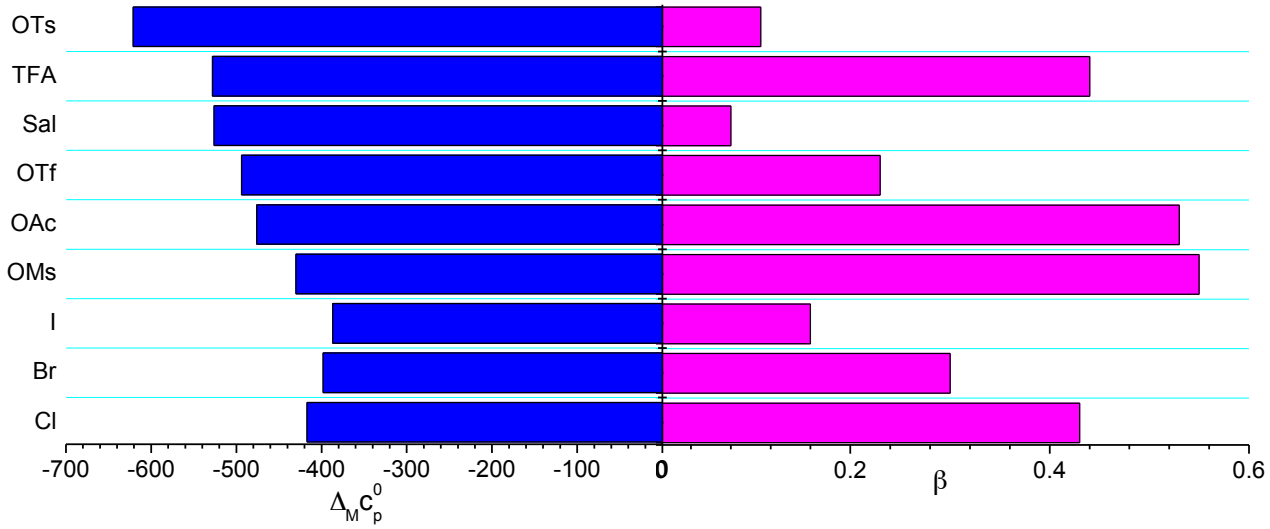

Fig. S5. Correlation between $\Delta_M c_p^0$ and β for the micellization process of investigated [C_{12}mim]X SAILs in water.

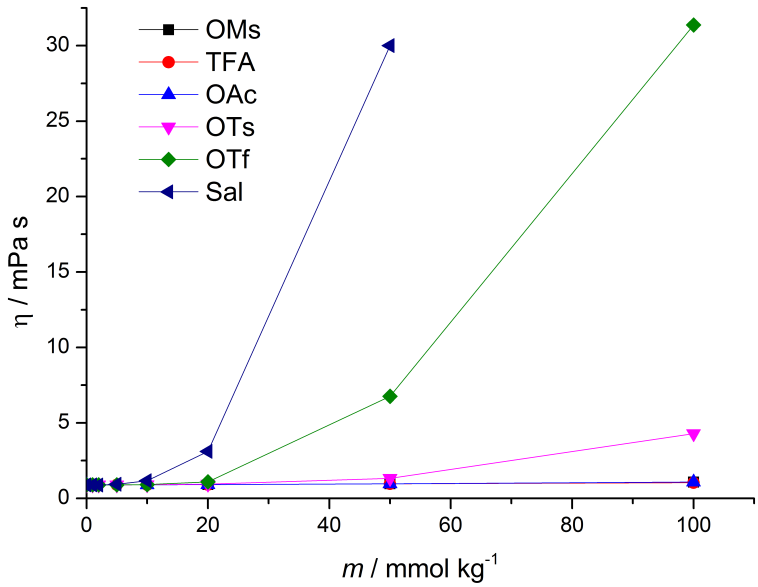

Fig. S6. Viscosities of aqueous solutions of investigated [C_{12}mim]X SAILs at 298.15 K.

Table S1: Thermodynamic parameters of micellization for investigated SAILs in water at all the investigated temperatures: critical micelle concentration, cmc, degree of micelle ionization, β, standard enthalpy, $\Delta_M H^0$, Gibbs free energy, $\Delta_M G^0$, and entropy contributions, $T\Delta_M S^0$, for micellization for investigated systems in water as obtained by the fitting procedure and comparison with literature data (where possible).[a,b]

T	cmc	β[c]	$\Delta_M H^0$	$\Delta_M G^0$	$T\Delta_M S^0$
[C$_{10}$mim]Cl					
278.15	70±2		10.89±0.09	-7.684±0.006	18.57±0.09
288.15	63±2		7.36±0.08	-8.289±0.005	15.65±0.08
298.15	60±2 58.5±1.3[d] 61.83[e]	0.54±0.02	3.83±0.09 3.5±0.2[d]	-8.771±0.006	12.61±0.09
308.15	59±2		0.31±0.12	-9.136±0.009	9.4±0.1
318.15	59±2		-3.2±0.2	-9.39±0.01	6.2±0.2
[C$_{12}$mim]Cl					
278.15	17.0±0.9		10.1 ± 0.1	-13.493 ± 0.008	23.6± 0.1
288.15	15.8±0.8		5.91± 0.07	-14.267 ± 0.007	20.18± 0.08
298.15	15.2±0.8 14.53[c] 14.23[e]	0.43±0.01	1.74± 0.06	-14.896± 0.006	16.64± 0.06
308.15	15.3±0.8		-2.43± 0.07	-15.385± 0.007	12.96± 0.07
318.15	15.8±0.8		-6.6± 0.1	-15.738± 0.008	9.1± 0.1
[C$_{12}$mim]Br					
278.15	11.0±0.5		5.4± 0.1	-15.65± 0.01	21.1± 0.1
288.15	10.5±0.5		1.45± 0.08	-16.34± 0.01	17.79± 0.08
298.15	10.7±0.5 10.29[c] 9.07[f] 10.24[g] 9.68±0.05[h]	0.30±0.01	-2.53± 0.06 -3.51±0.01[h]	-16.88± 0.01	14.36± 0.06
308.15	11.1±0.5		-6.51± 0.08	-17.30± 0.01	10.80± 0.08
318.15	12.0±0.6		-10.5 ± 0.1	-17.59 ± 0.01	7.1 ± 0.1
[C$_{12}$mim]I					
278.15	4.6±0.3		-3.0± 0.1	-21.74± 0.01	18.8± 0.1
288.15	4.8±0.3		-6.85± 0.07	-22.35± 0.01	15.50± 0.07
298.15	5.2±0.3 5.19[c] 4.76[f] 4.12[g]	0.16±0.01	-10.72± 0.06	-22.82± 0.01	12.10± 0.06
308.15	5.6±0.3		-14.60± 0.07	-23.16± 0.01	8.57± 0.07
318.15	6.8±0.4		-18.5± 0.1	-23.38± 0.01	4.9± 0.1
[C$_{12}$mim]OAc					

278.15	21.8±0.4		15.8±0.1	-11.29±0.02	27.1±0.01
288.15	19.0±0.3		11.01±0.07	-12.17±0.02	23.19±0.07
298.15	17.52±0.3 17.27[c]	0.53±0.01	6.25±0.05	-12.90±0.02	19.15±0.05
308.15	16.9±0.3		1.49±0.07	-13.46±0.02	14.95±0.07
318.15	16.9±0.3		-3.3±0.1	-13.87±0.02	10.6±0.1
[C_{12}mim]OMs					
278.15	18.5±0.9		12.10±0.08	-12.10±0.01	24.20±0.08
288.15	16.7±0.9		7.80±0.07	-12.91±0.01	20.71±0.07
298.15	15.7±0.8 14.71[c] 12.50[f] 15.26[g]	0.55±0.01	3.50±0.08	-13.55±0.01	17.05±0.08
308.15	15.6±0.8		-0.8± 0.1	-14.05± 0.01	13.3± 0.1
318.15	16.0±0.8		-5.1± 0.1	-14.41± 0.01	9.3± 0.1
[C_{12}mim]OTs					
278.15	2.93±0.09		7.6± 0.1	-24.05± 0.02	31.6± 0.1
288.15	2.83±0.09		1.36± 0.07	-25.08± 0.02	26.44± 0.07
298.15	2.88±0.09 3.44[c] 2.25[f]	0.11±0.01	-4.86± 0.06	-25.89± 0.02	21.03± 0.06
308.15	3.04±0.09		-11.07± 0.07	-26.49± 0.02	15.42± 0.07
318.15	3.31±0.09		-17.3± 0.1	-29.89± 0.02	9.6-± 0.1
[C_{12}mim]OTf					
278.15	2.79±0.09		4.1± 0.1	-21.31± 0.01	25.4± 0.1
288.15	2.76±0.08		-0.84± 0.06	-22.14± 0.01	21.30± 0.06
298.15	2.83±0.08 2.71[c] 2.37[f] 2.69[g]	0.23±0.01	-5.78± 0.04	-22.79± 0.01	17.02± 0.04
308.15	3.01±0.09		-10.71± 0.06	-23.28± 0.01	12.57± 0.06
318.15	3.30±0.09		-15.7± 0.1	-23.61± 0.01	8.0± 0.1
[C_{12}mim]TFA					
278.15	7.3±0.3		11.8± 0.1	-16.61± 0.01	28.4± 0.1
288.15	6.7±0.3		6.56± 0.06	-17.54± 0.01	24.09± 0.06
298.15	6.5±0.3 6.61[c] 5.23[f] 7.20[g]	0.44±0.01	1.28± 0.05	-18.28± 0.01	19.56± 0.05
308.15	6.5±0.3		-3.99±0.06	-18.85± 0.01	14.86± 0.06
318.15	6.9±0.03		-9.3± 0.1	-19.25± 0.01	10.0± 0.1
[C_{12}mim]Sal					
278.15	1.64±0.09		-2.6±0.1	-26.22±0.03	23.6±0.1
288.15	1.71±0.09		-7.89±0.07	-26.97±0.03	19.08±0.08

298.15	1.83±0.09 1.89[c] 1.59[f]	0.08±0.01	-13.15±0.05	-27.54±0.04	14.39±0.06
308.15	2.04±0.09		-18.41±0.07	-27.94±0.04	9.52±0.08
318.15	2.33±0.09		-23.7±0.1	-28.16±0.04	4.5±0.1
[C_{14}mim]Cl					
278.15	4.1±0.2		10.25±0.08	-19.025± 0.003	29.28±0.08
288.15	3.8±0.2		5.09±0.05	-19.985± 0.002	25.07±0.05
298.15	3.7±0.2 3.40±0.07[d] 3.45[e]	0.386± 0.008	-0.08±0.04 -0.5±0.3[d]	-20.767± 0.001	20.69±0.04
308.15	3.8±0.2		-5.24±0.05	-21.375± 0.002	16.13±0.05
318.15	4.1±0.2		-10.41±0.08	-21.816± 0.004	11.41±0.08
[C_{16}mim]Cl					
288.15	0.93±0.05		3.04±0.08	-24.81±0.04	27.85±0.08
298.15	0.93±0.05 0.99[e]	0.42±0.01	-3.04±0.07	-25.67±0.04	22.63±0.08
308.15	0.98±0.05		-9.13±0.08	-26.33±0.04	17.20±0.09
318.15	1.07±0.05		-15.21±0.09	-26.79±0.05	11.6±0.1

[a]Units: cmc, mmol kg^{-1}; $\Delta_M H^0$, $\Delta_M G^0$, $T\Delta_M S^0$, kJ·mol^{-1}.

[b]The reported errors correspond to the precision of the experimental data and the fitting procedure assuming the proposed model is correct.

[c]From conductivity measurements, some values are taken from ref. [11]

[d] ref, [12]

[e]ref. [13]

[f] From surface tension measurements, some values are taken from ref. [11]

[g] From UV-Vis spectroscopy in ref. [11]

[d h]ref. [14]

Table S2. Coefficients of polynomials *cmc* =A+ B*T* + CT^{2}[a].

	A	B	$10^3 \cdot C$
[C_{10}mim]Cl	1152.27	-7.08185	11.46
[C_{12}mim]Cl	286.4849	-1.79154	2.9570
[C_{12}mim]Br	189.4947	-1.22603	2.1000
[C_{12}mim]I	59.14728	-0.40257	0.74286
[C_{12}mim]OAc	463.1606	-2.87050	4.6143
[C_{12}mim]OMs	370.868	-2.32198	3.7929
[C_{12}mim]OTs	53.95552	-0.35234	0.60714
[C_{12}mim]OTf	46.66583	-0.30675	0.53571
[C_{12}mim]TFA	147.1805	-0.93416	1.5500
[C_{12}mim]Sal	30.38843	-0.20864	0.37857
[C_{14}mim]Cl	79.62678	-0.51011	0.85714
[C_{16}mim]Cl	20.20205	-0.13172	0.22500

[a] Units: *T*/K; A/mmol kg^{-1}, B/mmol $kg^{-1}\cdot K^{-1}$; C/mmol $kg^{-1}\cdot K^{-2}$

References

[1] J. N. Phillips, The energetics of micelle formation, J. Trans Soc. 51 (1955) 561-569.

[2] R. J. Hunter, Foundations of Colloid Science, Vol. 1, Clarendon Press, Oxford, 1987.

[3] J. Lah, C. Pohar, G. Vesnaver, Calorimetric Study of the Micellization of Alkylpyridinium and Alkyltrimethylammonium Bromides in Water, J. Phys. Chem. B 104 (2000) 2522-2526.

[4] J. Lah, M. Bešter-Rogač, T.-M. Perger, G. Vesnaver, Energetics in Correlation with Structural Features: The Case of Micellization, J. Phys. Chem. B 110 (2006) 23279-23291.

[5] E. M. Woolley, T. E. Burchfield, Model for Thermodynamics of Ionic Surfactant Solutions. 2. Enthalpies, Heat Capacities, and Volumes, J. Phys. Chem. 88 (1984) 2155-2163.

[6] W. H. Press, B. P. Flannery, S. A. Teukolsky, W. T. Vetterling, Numerical Recipes, Cambridge University Press, Oxford, 1992, p 650.

[7] D. Hallen, Data treatment: Considerations when applying binding reaction data to a model**,** Pure Appl. Chem. 65 (1993) 1527-1532.

[8] S. A., Vetterling, W. T. 1992 Numerical Recipies, Cambridge University Press, Oxford, pp. 650-694.

[9] I. Drobnak, G. Vesnaver, J. Lah, J. Model-Based Thermodynamic Analysis of Reversible Unfolding Processes, J. Phys. Chem. B 114 (2010) 8713-8722.

[10] A. Kroflič, B. Šarac,M. Bešter-Rogač, Thermodynamic Characterization of CHAPS Micellization Using Isothermal Titration Calorimetry: Temperature, Salt, and pH Dependence, Langmuir 28 (2012) 10363-10371.

[11] A. Cognigni, P. Gärtner, R. Zirbs, H. Peterlik, K. Prochazka, C. Schröder, K. Bica, Surface-active ionic liquids in micellar catalysis: impact of anion selection on reaction rates in nucleophilic substitutions, Phys. Chem. Chem. Phys. 18 (2016) 13375- 13384.

[12] J. Łuczak, C. Jungnickel, M. Joskowska, J. Thöming, J. Hupka, Thermodynamics of micellization of imidazolium ionic liquids in aqueous solutions, J. Colloid. Interface Sci. 336 (2009) 111–116.

[13] P. D Galgano, O. A. El Seoud, Surface active ionic liquids: Study of the micellar properties of 1-1-alkyl]-3-methylimidazolium chlorides and comparison with structurally related surfactants, J. Colloid. Interface. Sci. 361 (2011) 186–194.

[14] F. Geng, J. Liu, L. Zheng, L. Yu, Z. Li, G. Li, C. Tung, Micelle formation of long-chain imidazolium ionic liquids in aqueous solution measured by isothermal titration microcalorimetry, J. Chem. Eng. Data. 55 (2010) 147–51.

Supporting information for: Hydration and Counterion Binding of [C_{12}MIM] Micelles

Sergej Friesen,[†] Thomas Buchecker,[‡] Alice Cognigni,[¶] Katharina Bica,[¶] and Richard Buchner[*,†]

Institut für Physikalische und Theoretische Chemie, Universität Regensburg, Regensburg, Germany, Institut für Anorganische Chemie, Universität Regensburg, Regensburg, Germany, and Institut für Angewandte Synthesechemie, Technische Universität Wien, Vienna, Austria

E-mail: richard.buchner@chemie.uni-regensburg.de

[*]To whom correspondence should be addressed
[†]Institut für Physikalische und Theoretische Chemie, Universität Regensburg, Regensburg, Germany
[‡]Institut für Anorganische Chemie, Universität Regensburg, Regensburg, Germany
[¶]Institut für Angewandte Synthesechemie, Technische Universität Wien, Vienna, Austria

Densities, dynamic viscosities and conductivities

Table S1: Densities, ρ, dynamic viscosities, η, and conductivities, κ, of aqueous [C_{12}MIM]Br solutions at 45 °C as a function of solute molality, b, and molarity, c.

b / mol·kg^{-1}	c / mol·dm^{-3}	ρ / g·cm^{-3}	η / mPa·s	κ / S·m^{-1}
0.0108	0.0106	0.99052	0.602	0.137
0.0202	0.0199	0.99072	0.617	0.184
0.0506	0.0494	0.99152	0.627	0.302
0.0772	0.0747	0.99221	0.649	0.410
0.1033	0.0992	0.99284	0.674	0.521
0.1313	0.1250	0.99354	0.736	0.632
0.1855	0.1738	0.99476	0.800	0.855
0.2147	0.1996	0.99550	0.846	0.978
0.2642	0.2421	0.99664	0.918	1.181

Table S2: Densities, ρ, dynamic viscosities, η, and conductivities, κ, of aqueous [C_{12}MIM]I solutions at 45 °C as a function of solute molality, b, and molarity, c.

b / mol·kg^{-1}	c / mol·dm^{-3}	ρ / g·cm^{-3}	η / mPa·s	κ / S·m^{-1}
0.0074	0.0073	0.99067	0.599	0.0847
0.0202	0.0199	0.99143	0.623	0.116
0.0511	0.0498	0.99306	0.648	0.191
0.0771	0.0745	0.99479	0.679	0.252
0.1038	0.0995	0.99630	0.715	0.315
0.1307	0.1242	0.99784	0.763	0.375
0.1860	0.1739	1.00088	0.931	0.481
0.2144	0.1988	1.00242	1.128	0.536
0.2507	0.2301	1.00478	1.51	0.613

Table S3: Densities, ρ, dynamic viscosities, η, and conductivities, κ, of aqueous $[C_{12}MIM]OTf$ solutions at 45 °C as a function of solute molality, b, and molarity, c.

b / mol·kg^{-1}	c / mol·dm^{-3}	ρ / g·cm^{-3}	η / mPa·s	κ / S·m^{-1}
0.0043	0.0043	0.99042	0.598	0.0362
0.0151	0.0149	0.99086	0.631	0.0569
0.0302	0.0299	0.99148	0.703	0.0794
0.0502	0.0498	0.99232	1.224	0.110
0.0749	0.0744	0.99334	3.127	0.148
0.1000	0.0995	0.99438	8.45	0.190
0.1251	0.1245	0.99546	13.4	0.233
0.1743	0.1739	0.99742	14.6	0.311
0.2540	0.2305	0.99988	13.4	0.396

Table S4: Densities, ρ, dynamic viscosities, η, and conductivities, κ, of a [C12MIM]Br solution with b = 0.1033 mol·kg^{-1} as a function of temperature T.

T / K	c / mol·dm^{-3}	ρ / g·cm^{-3}	η / mPa·s	κ / S·m^{-1}
298.15	0.0999	1.00003	1.116	0.324
308.15	0.0996	0.99683	0.894	0.415
318.15	0.0992	0.99284	0.674	0.521
328.15	0.0987	0.98793	0.601	0.639
338.15	0.0981	0.98173	0.506	0.774

Table S5: Densities, ρ, dynamic viscosities, η, and conductivities, κ, of a [C12MIM]I solution with b = 0.1038 mol·kg^{-1} as a function of temperature T.

T / K	c / mol·dm^{-3}	ρ / g·cm^{-3}	η / mPa·s	κ / S·m^{-1}
298.15	0.1003	1.00353	1.31	0.164
308.15	0.0999	1.00032	0.903	0.233
318.15	0.0995	0.99630	0.715	0.315
328.15	0.0991	0.99161	0.598	0.403
338.15	0.0986	0.98639	0.508	0.501

Table S6: Densities, ρ, dynamic viscosities, η, and conductivities, κ, of a [C12MIM]OTf solution with b = 0.0749 mol·kg^{-1} as a function of temperature T.

T / K	c / mol·dm^{-3}	ρ / g·cm^{-3}	η / mPa·s	κ / S·m^{-1}
298.15	0.0750	1.00042	48.6	0.095
308.15	0.0747	0.99728	10.59	0.120
318.15	0.0744	0.99334	3.127	0.148
328.15	0.0741	0.98870	1.355	0.181
338.15	0.0737	0.98349	0.723	0.221

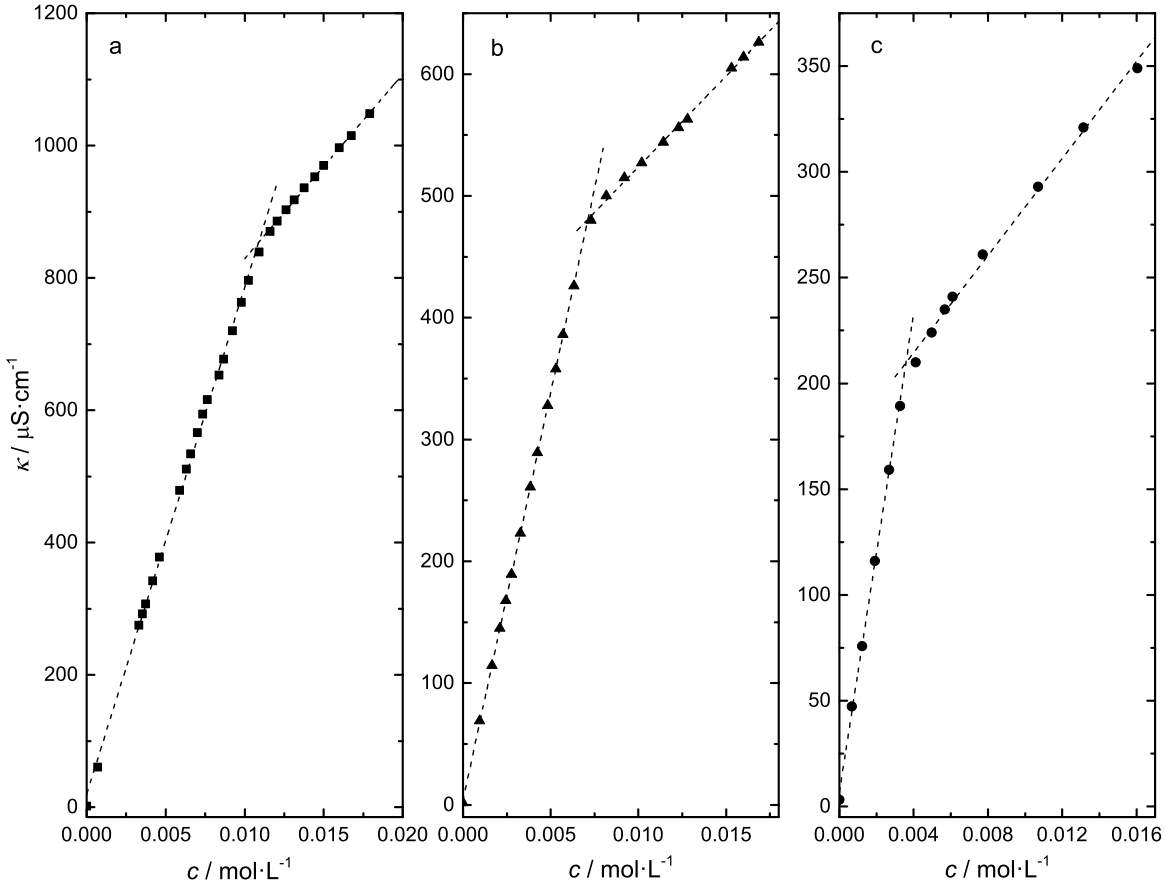

Figure S1: Conductivity, κ, *vs.* concentration, c, profiles for the determination of the critical micellar concentration, *cmc*, and the degree of counterion binding, β, for solutions of (a) [C_{12}MIM]Br, (b) [C_{12}MIM]I and (c) [C_{12}MIM]OTf in water at 45 °C (see main manuscript for details).

Correction of Raw Dielectric Spectra

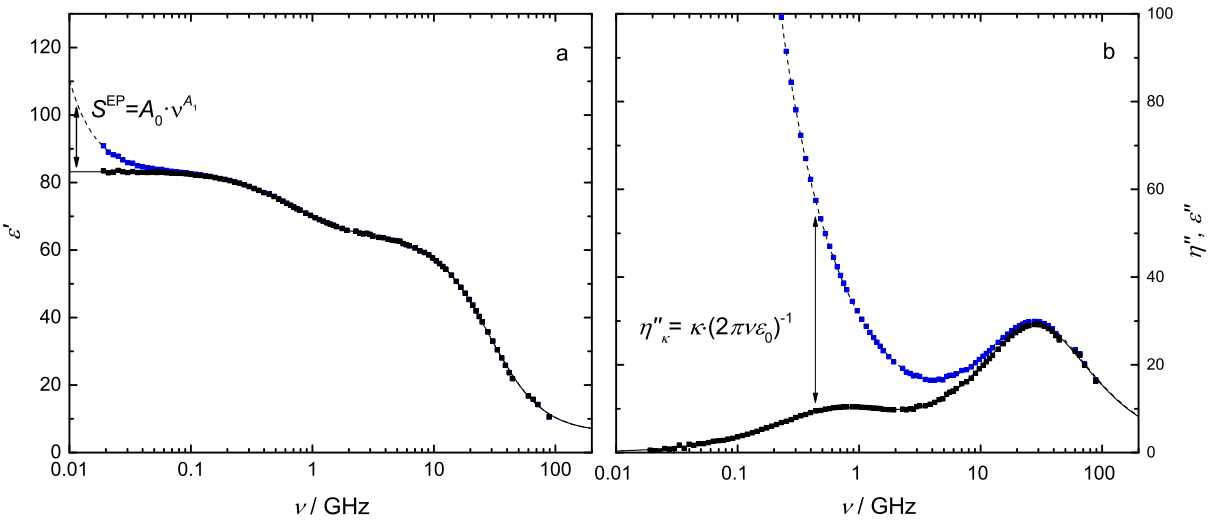

Figure S2: (a) Relative permittivity spectrum, $\varepsilon'(\nu)$, of 0.2421 mol·L^{-1} [C_{12}MIM]Br(aq) before (■) and after (■) correction for electrode polarization (EP, amplitude $S^{EP} = A_0 \times \nu^{A_1}$). (b) Spectra of the total, $\eta''(\nu)$ (■), and the dielectric, $\varepsilon''(\nu)$ (■), loss of this solution, as well as the associated contribution from dc conductivity, $\eta''_\kappa = \kappa/(2\pi\nu\varepsilon_0)$. The lines in both panels indicate the fit with the D+D+D+D model.

Relaxation Time Distribution Functions

The relaxation-time distribution functions, $P(\tau)$, of Figs. S3–S8 were obtained by fitting $N_\tau = 601$ Debye basis functions equidistantly spaced on a $\log \tau$ scale between 0.1 ps and 100,000 ps to the experimental data as described in detail in Ref. S1.

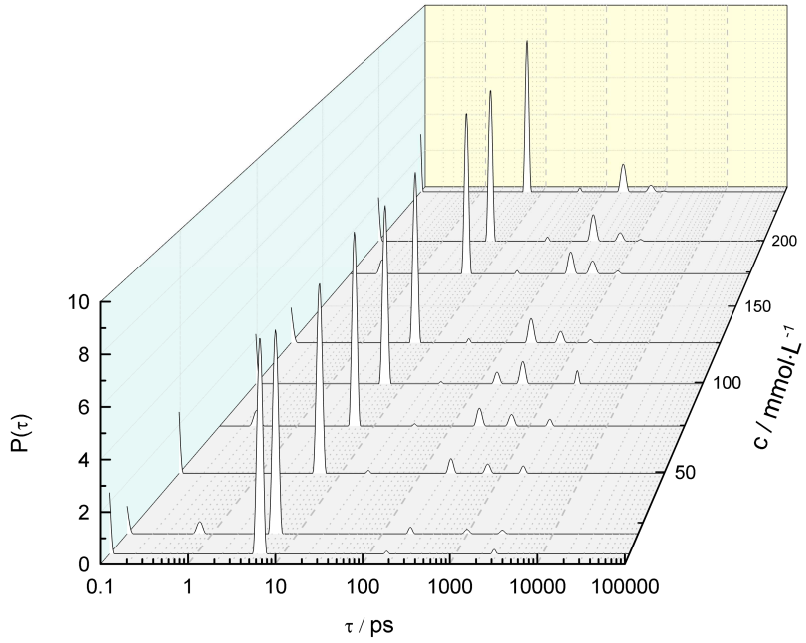

Figure S3: Zasetsky plots[S1] of the relaxation-time distribution functions, $P(\tau)$, for the dielectric spectra of aqueous [C_{12}MIM]Br solutions at 45 °C.

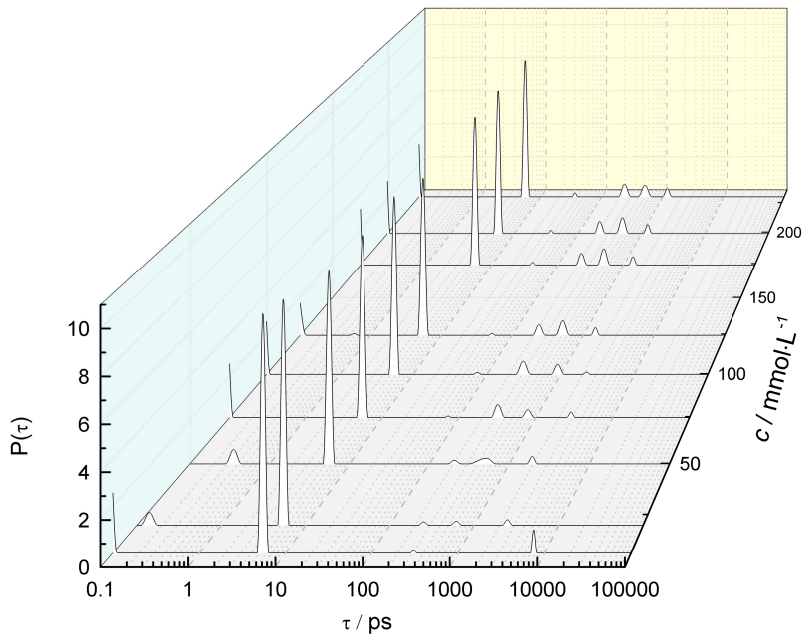

Figure S4: Zasetsky plots[S1] of the relaxation-time distribution functions, $P(\tau)$, for the dielectric spectra of aqueous [C_{12}MIM]I solutions at 45 °C.

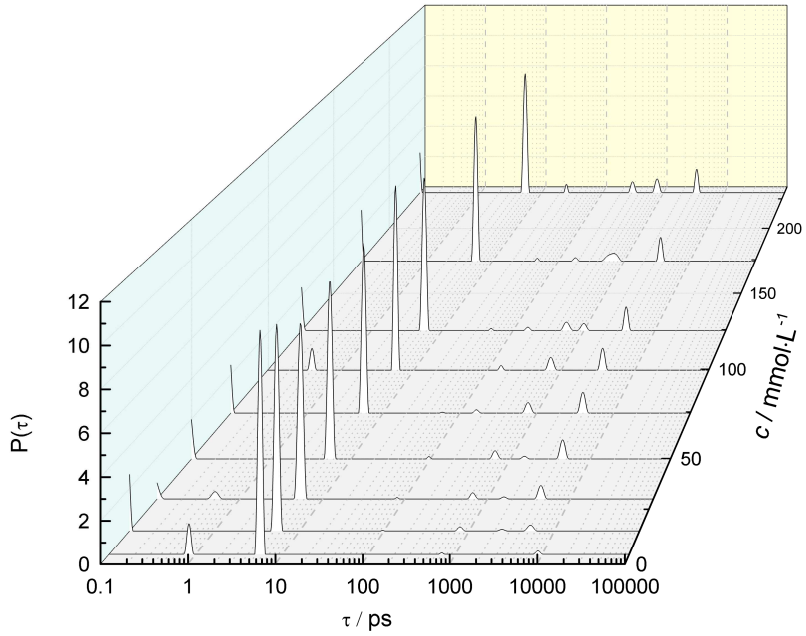

Figure S5: Zasetsky plots[S1] of the relaxation-time distribution functions, $P(\tau)$, for the dielectric spectra of aqueous [C_{12}MIM]OTf solutions at 45 °C.

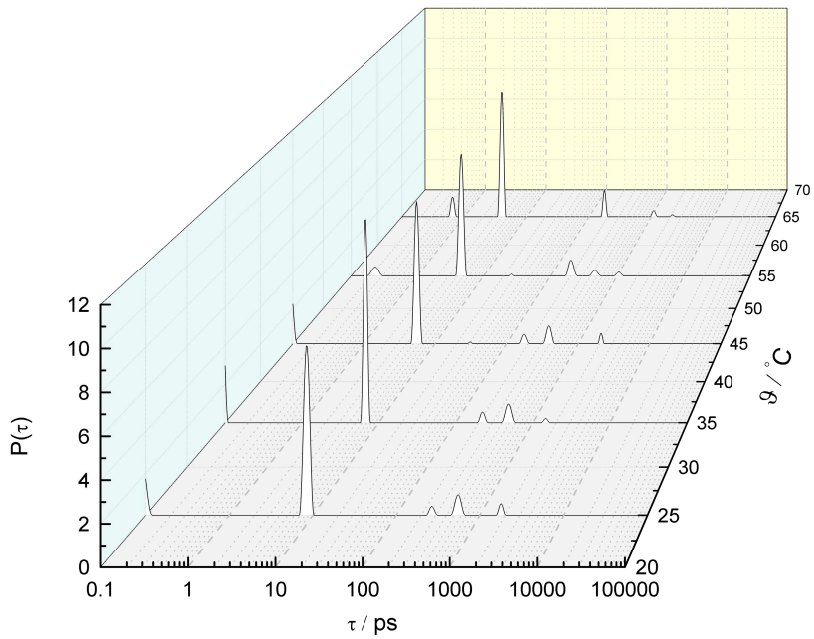

Figure S6: Zasetsky plots[S1] of the relaxation-time distribution functions, $P(\tau)$, for the dielectric spectra of 0.1033 mol/kg [C_{12}MIM]Br(aq) in the temperature range 25 - 65 °C.

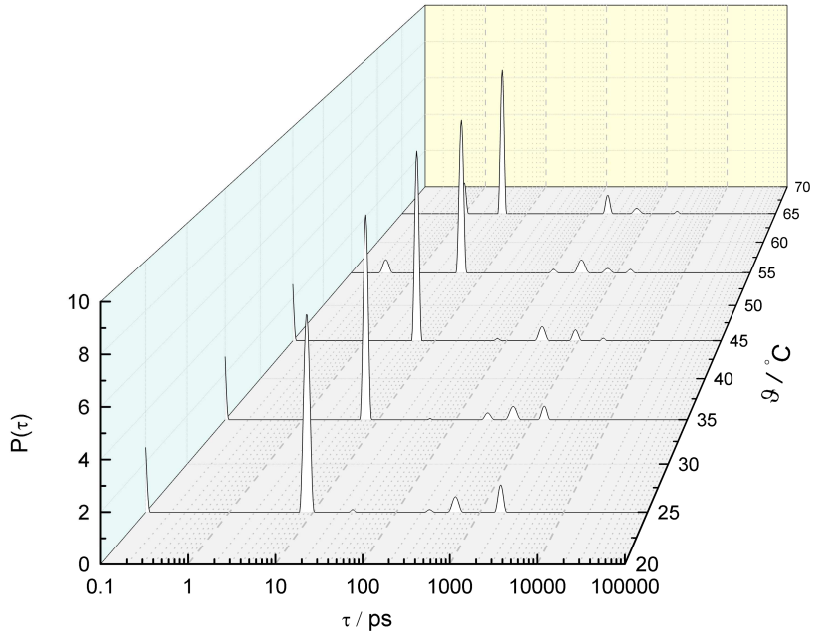

Figure S7: Zasetsky plots[S1] of the relaxation-time distribution functions, $P(\tau)$, for the dielectric spectra of 0.1033 mol/kg [C_{12}MIM]I(aq) in the temperature range 25 - 65 °C.

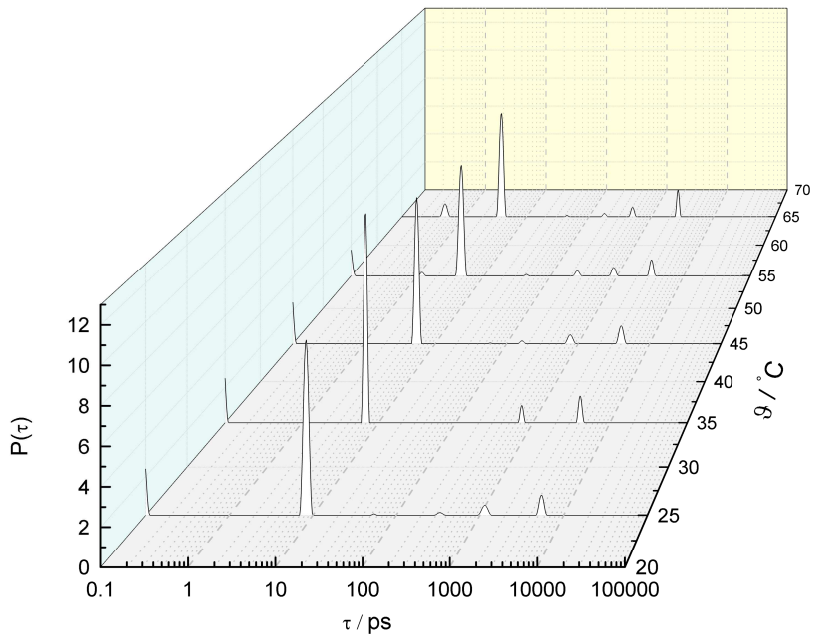

Figure S8: Zasetsky plots[S1] of the relaxation-time distribution functions, $P(\tau)$, for the dielectric spectra of 0.1033 mol/kg [C_{12}MIM]OTf(aq) in the temperature range 25 - 65 °C.

Relaxation Parameters of the D+D+D+D Model

Table S7: Parameters of the D+D+D+D model fitting the DR spectra of aqueous [C_{12}MIM]Br solutions at 45 °C and solute concentration, c: static permittivity, ε, amplitudes, S_j, and relaxation times, τ_j, of the resolved modes $j = 1 \ldots 4$, and high-frequency permittivity, ε_∞.[a]

c / M	ε	S_1	τ_1 / ns	S_2	τ_2 / ps	S_3	τ_3 / ps	S_4	τ_4 / ps	ε_∞
0.0106 [b]	72.13	0.47	2.28	0.34	171			65.91	5.39	5.41
0.0199	74.27	1.59	1.70	1.52	254	0.23	30F	65.08	5.45	5.86
0.0494	78.88	3.14	1.33	5.29	282	0.75	30F	64.05	5.42	5.66
0.0747	81.10	3.55	1.21	7.95	271	1.08	23.4	62.80	5.40	5.72
0.0992	81.94	3.13	0.985	9.64	287	1.06	80.7	62.22	5.52	5.89
0.1250	82.98	3.53	0.877	11.26	257	1.70	30F	61.07	5.35	5.43
0.1738	83.50	3.92	0.650	13.10	238	1.66	30F	59.37	5.37	5.45
0.1996	83.71	3.95	0.680	13.93	225	1.59	30F	58.53	5.43	5.70
0.2421	83.30	3.96	0.635	14.92	213	1.19	33.2	57.24	5.54	5.99

[a] Parameter values followed by "F" were fixed; [b] Data not used in further processing, see text.

Table S8: Parameters of the D+D+D+D model fitting the DR spectra of aqueous [C_{12}MIM]I solutions at 45 °C and solute concentration, c: static permittivity, ε, amplitudes, S_j, and relaxation times, τ_j, of the resolved modes $j = 1 \ldots 4$, and high-frequency permittivity, ε_∞.[a]

c / M	ε	S_1	τ_1 / ns	S_2	τ_2 / ps	S_3	τ_3 / ps	S_4	τ_4 / ps	ε_∞
0.0073 [b]	72.26	0.55	2.51	0.20	222			66.04	5.40	5.46
0.0199	74.70	1.75	2.20	1.90	385	0.22	40F	65.60	5.37	5.27
0.0498	78.33	2.79	1.66	5.20	378	0.41	40F	64.37	5.41	5.56
0.0745	79.85	2.81	1.78	7.46	370	0.56	40F	63.41	5.42	5.61
0.0995	80.75	4.68	1.09	7.28	312	0.77	34.5	62.37	5.43	5.64
0.1242	82.43	5.19	1.03	9.28	310	1.23	22.6	60.94	5.39	5.79
0.1739	83.94	6.19	1.01	11.12	309	1.31	33.6	59.28	5.47	6.05
0.1988	84.23	7.40	0.911	10.96	290	1.37	35.8	58.47	5.50	6.03
0.2301	84.12	7.57	0.901	11.57	282	1.49	41.3	57.36	5.52	6.20

[a] Parameter values followed by "F" were fixed; [b] Data not used in further processing, see text.

Table S9: Parameters of the D+D+D+D model fitting the DR spectra of aqueous [C_{12}MIM]OTf solutions at 45 °C and solute concentration, c: static permittivity, ε, amplitudes, S_j, and relaxation times, τ_j, of the resolved modes $j = 1 \ldots 4$, and high-frequency permittivity, ε_∞.[a]

c / M	ε	S_1	τ_1 / ns	S_2	τ_2 / ps	S_3	τ_3 / ps	S_4	τ_4 / ps	ε_∞
0.0043 [b]	72.51	0.85	9.05	0.18	1380			67.17	5.21	4.31
0.0149	75.21	2.58	5.16	1.41	915	0.20	89F	65.80	5.35	5.22
0.0299	78.55	5.19	4.57	2.47	814	0.46	89F	65.21	5.33	5.23
0.0498	81.59	7.63	4.39	3.58	707	0.61	79.2	64.16	5.40	5.60
0.0744	83.08	8.39	3.94	4.62	723	1.08	109	63.19	5.47	5.80
0.0995	84.19	8.64	3.83	6.15	712	1.33	115	62.12	5.47	5.95
0.1245	85.41	9.56	3.83	7.62	624	1.48	61.2	61.10	5.42	5.65
0.1739	86.65	10.17	3.63	9.52	611	1.77	81.7	59.22	5.56	5.97
0.2305	86.84	10.63	3.50	11.00	572	2.59	89F	56.83	5.56	5.78

[a] Parameter values followed by "F" were fixed; [b] Data not used in further processing, see text.

Table S10: Parameters of the D+D+D+D model fitting the DR spectra of aqueous solutions of [C_{12}MIM]Br at $m = 0.1033\,\mathrm{mol\,kg^{-1}}$ and temperature T: static permittivity, ε, amplitudes, S_j, and relaxation times, τ_j, of the resolved modes $j = 1 \ldots 4$, and high-frequency permittivity, ε_∞.[a]

T / K	ε	S_1	τ_1 / ns	S_2	τ_2 / ps	S_3	τ_3 / ps	S_4	τ_4 / ps	ε_∞
298.15	89.74	3.26	1.88	9.14	532	2.28	323	69.28	8.40	5.78
308.15	85.08	2.74	1.04	9.70	381	1.3F	150	65.70	6.67	5.65
318.15	81.94	3.13	0.985	9.64	287	1.06	80.7	62.22	5.52	5.89
328.15	78.73	3.42	0.745	9.55	214	1.22	14.8	59.02	4.45	5.51
338.15	75.10	2.92	1.28	9.43	178	0.61	12.6	56.81	3.82	5.33

[a] Parameter values followed by "F" were fixed.

Table S11: Parameters of the D+D+D+D model fitting the DR spectra of aqueous solutions of [C_{12}MIM]I at m = 0.1038 mol kg^{-1} and temperature T: static permittivity, ε, amplitudes, S_j, and relaxation times, τ_j, of the resolved modes $j = 1 \ldots 4$, and high-frequency permittivity, ε_∞.[a]

T / K	ε	S_1	τ_1 / ns	S_2	τ_2 / ps	S_3	τ_3 / ps	S_4	τ_4 / ps	ε_∞
298.15	88.88	7.96	1.74	5.72	465	0.69	32.3	68.41	8.41	6.10
308.15	84.86	6.10	1.23	6.58	389	0.49	42.7	65.73	6.71	5.96
318.15	80.75	4.68	1.09	7.28	312	0.77	34.5	62.37	5.43	5.64
328.15	78.09	3.28	1.08	8.77	270	0.94	25F	59.58	4.42	5.53
338.15	74.49	2.92	0.908	8.82	210	0.08	20F	57.17	3.85	5.51

[a] Parameter values followed by "F" were fixed.

Table S12: Parameters of the D+D+D+D model fitting the DR spectra of aqueous solutions of [C_{12}MIM]OTf at m = 0.0749 mol kg^{-1} and temperature T: static permittivity, ε, amplitudes, S_j, and relaxation times, τ_j, of the resolved modes $j = 1 \ldots 4$, and high-frequency permittivity, ε_∞.[a]

T / K	ε	S_1	τ_1 / ns	S_2	τ_2 / ps	S_3	τ_3 / ps	S_4	τ_4 / ps	ε_∞
298.15	87.96	7.15	5.29	4.59	998	0.76	147	69.85	8.28	5.62
308.15	85.38	6.97	4.88	5.18	998	0.8F	120F	67.12	6.66	5.31
318.15	83.08	8.39	3.94	4.62	723	1.08	109	63.19	5.47	5.80
328.15	79.34	7.61	2.95	4.59	527	1.08	70.5	60.84	4.46	5.23
338.15	76.34	7.30	2.42	4.56	465	1.06	77.3	57.67	3.85	5.73

[a] Parameter values followed by "F" were fixed.

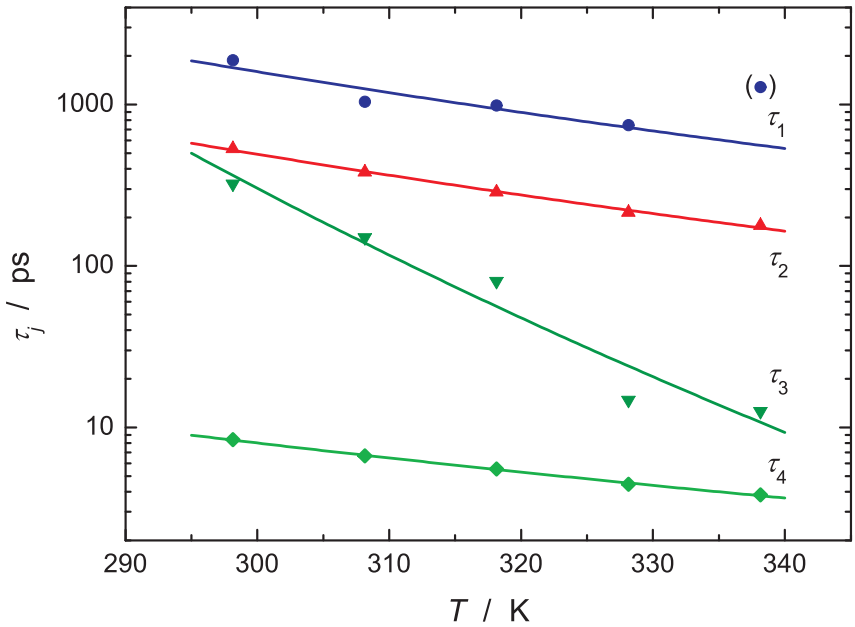

Figure S9: Relaxation times τ_1 (●), τ_2 (▲), τ_3 (▼) and τ_4 (♦) of 0.1033 mol/kg aqueous [C_{12}MIM]Br as a function of temperature, T. The solid lines show Eyring fits, eq 3 of the main paper (bracketed symbol not included in the fit).

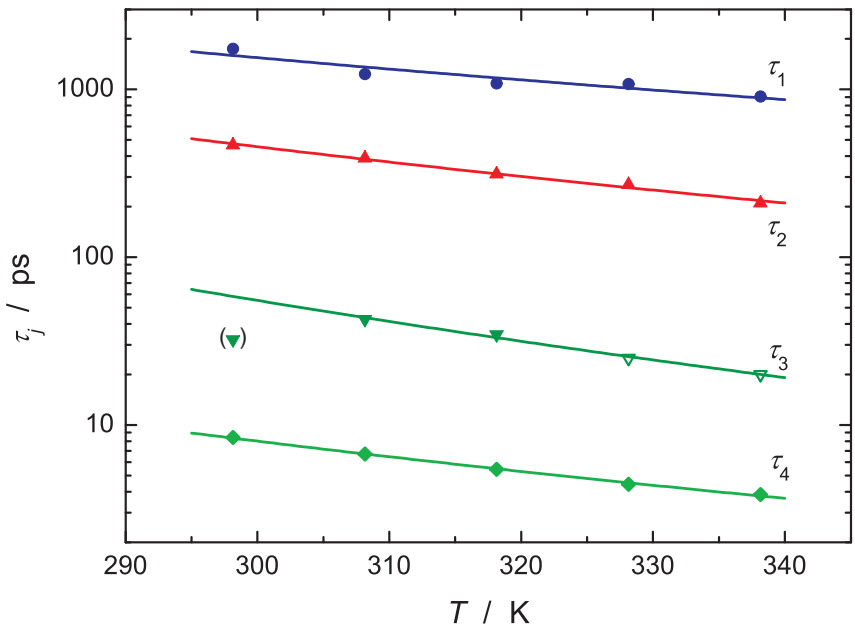

Figure S10: Relaxation times τ_1 (●), τ_2 (▲), τ_3 (▼) and τ_4 (♦) of 0.1038 mol/kg aqueous [C_{12}MIM]I as a function of temperature, T. Open symbols indicate that τ_3 was fixed in the D+D+D+D fit of the dielectric spectrum, the bracketed point was neglected in the Eyring fit. The solid lines show Eyring fits, eq 3 of the main paper, to the relaxation times.

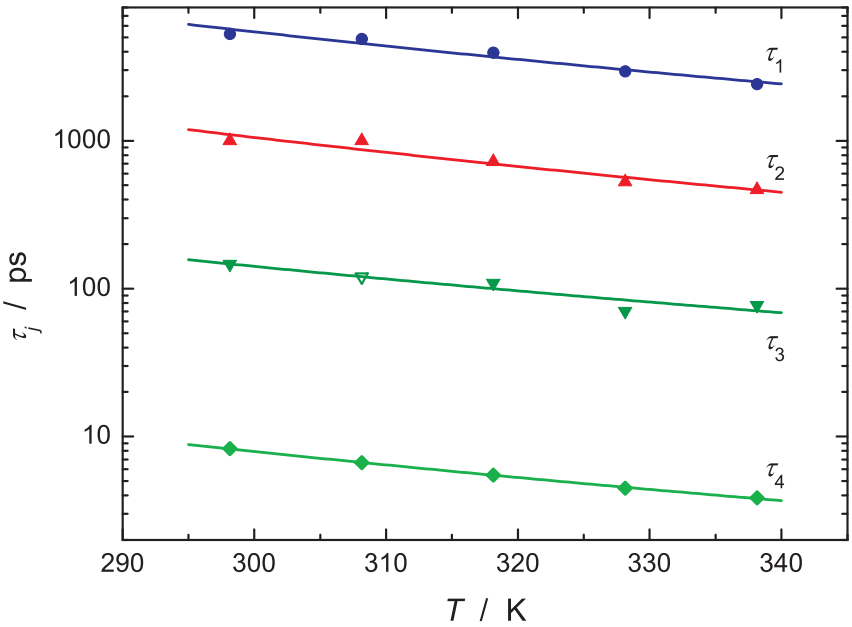

Figure S11: Relaxation times τ_1 (●), τ_2 (▲), τ_3 (▼) and τ_4 (♦) of 0.0749 mol/kg aqueous [C_{12}MIM]OTf as a function of temperature, T. Open symbol indicates that τ_3 was fixed in the D+D+D+D fit of the dielectric spectrum. The solid lines show Eyring fits, eq 3 of the main paper, to the relaxation times.

Simultaneous Fitting of the Micelle-specific Modes

For the simultaneous fitting of the solute-specific relaxation modes with the Grosse model, eqs 11-14 of the main paper, a nonlinear least-squares fitting routine was implemented using software based on MATLAB (Mathworks). In this procedure the error function

$$\chi^2_{\mathrm{G}} = \frac{1}{4m-n} \cdot \sum_{i=1}^{m} \left[\left(\frac{(S_1)_i - (S_1)_{i,calc}}{\frac{c_i}{\mathrm{mol/L^3}} \cdot (\sigma_{S_1})_i} \right)^2 + \left(\frac{(S_2)_i - (S_2)_{i,calc}}{\frac{c_i}{\mathrm{mol/L^3}} \cdot (\sigma_{S_2})_i} \right)^2 + \left(\frac{(\tau_1)_i - (\tau_1)_{i,calc}}{\frac{c_i}{\mathrm{mol/L^3}} \cdot (\sigma_{\tau_1})_i} \right)^2 + \left(\frac{(\tau_2)_i - (\tau_2)_{i,calc}}{\frac{c_i}{\mathrm{mol/L^3}} \cdot (\sigma_{\tau_2})_i} \right)^2 \right] \tag{1}$$

was minimized, where m denotes the number of the individual data points i (equal to the number of solutions of the concentration series), n is the number of fitting parameters, c_i is the IL concentration and σ a weighting parameter. The latter is defined as the deviation of

the respective relaxation parameter, S_j or τ_j (j = 1, 2), from a low-order polynomial fit. The concentration, c_i, serves as an additional weight which accounts for the condition $\phi \ll 1$ of the Grosse theory by giving larger weight to low surfactant concentrations.

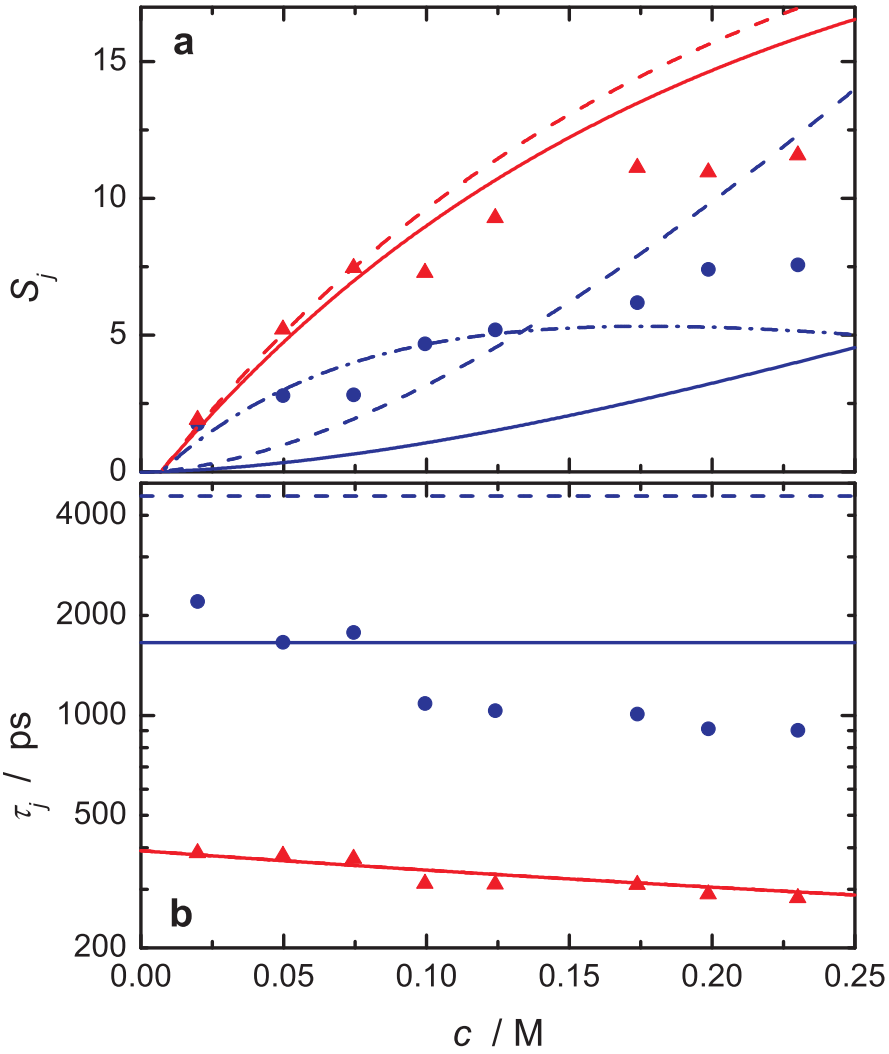

Figure S12: (a) Experimental amplitudes, S_j, and (b) relaxation times, τ_j, of the micellar relaxation processes j = 1 (●) and j = 2 (▲) of [C_{12}MIM]I at 45 °C. The correspondingly colored lines represent the fit of Grosse's model with all relaxation times and amplitudes simultaneously fitted (broken lines) and with S_1 omitted in the fit (solid lines). The dash-dotted line gives the fit of S_1 with adjusted Debye length, χ_{emp}^{-1}.

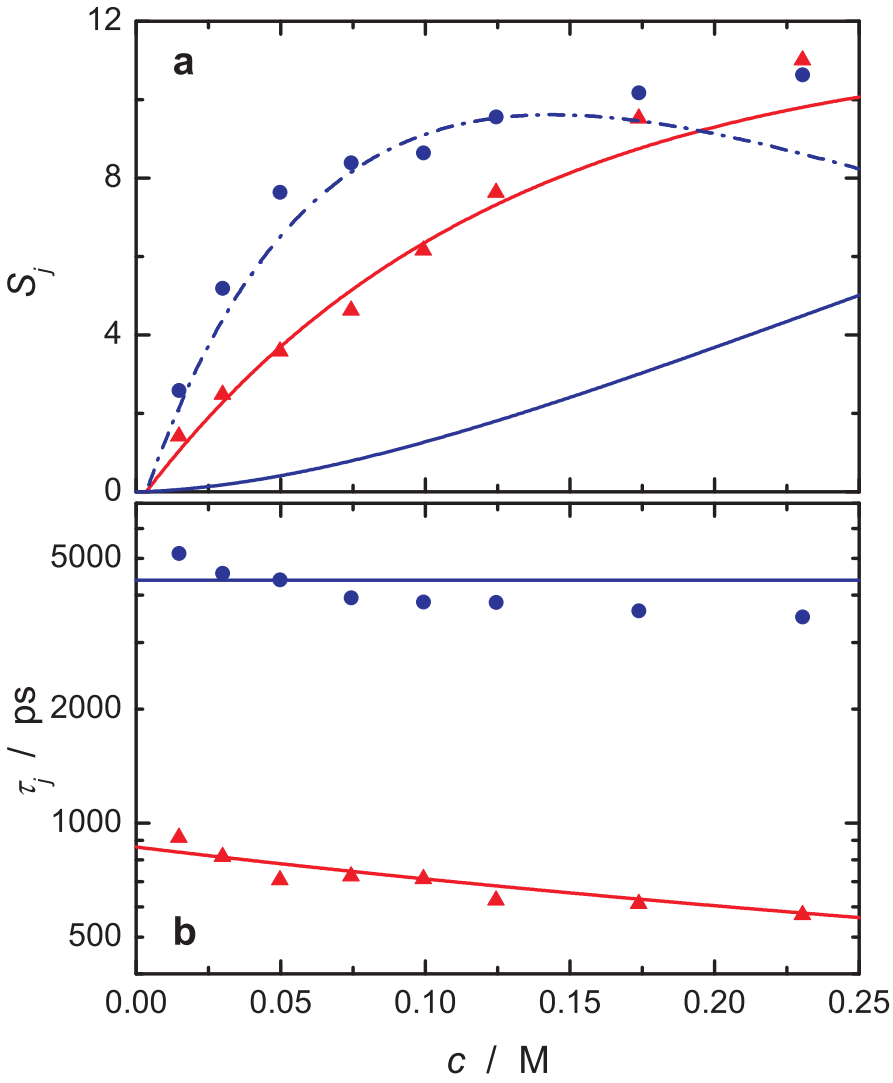

Figure S13: (a) Experimental amplitudes, S_j, and (b) relaxation times, τ_j, of the micellar relaxation processes $j = 1$ (●) and $j = 2$ (▲) of [C_{12}MIM]OTf at 45 °C. The correspondingly colored lines represent the fit of Grosse's model with S_1 omitted in the fit. The dash-dotted line gives the fit of S_1 with adjusted Debye length, χ_{emp}^{-1}.

Table S13: Intercept, a_0, and slope, a_1, of the empirical equation $\chi_{\mathrm{emp}}^{-1} = a_0 + a_1 \times c$ for the effective Debye length of the investigated surfactants at 45 °C.

	a_0 / 10^{-9} m	a_1 / 10^{-12} m^4 mol^{-1}
[C_{12}MIM]Br	0.947	2.01
[C_{12}MIM]I	0.950	2.94
[C_{12}MIM]OTf	0.703	2.48

Micelle Volume Fraction from DRS

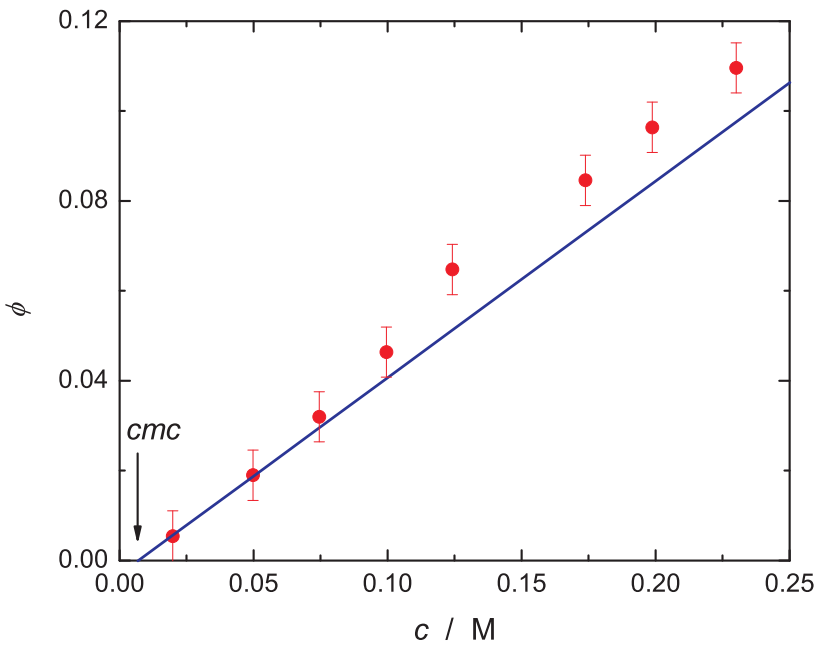

Figure S14: Effective volume fraction, ϕ, of [C_{12}MIM]I micelles in aqueous solution calculated from the Grosse radius, R_G (solid line), and from the bulk water amplitude, S_b (●).

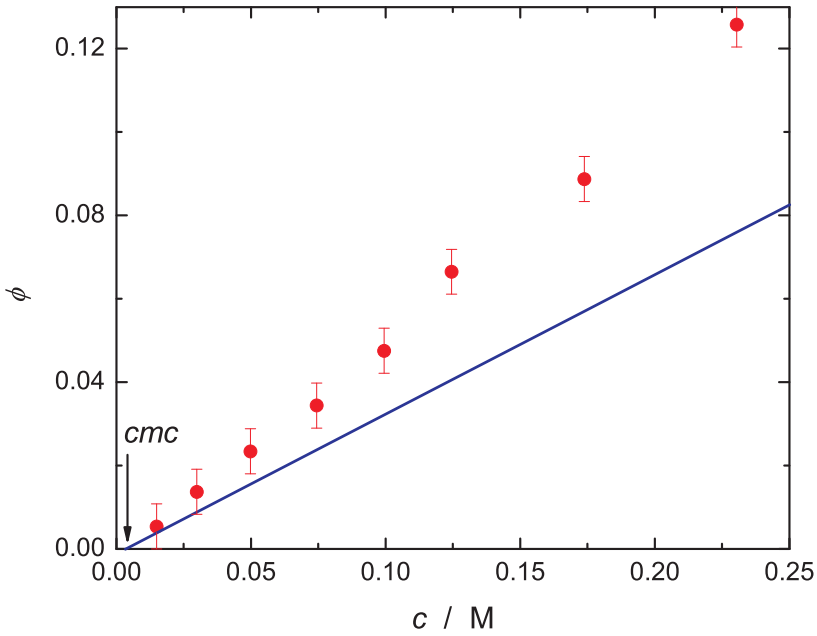

Figure S15: Effective volume fraction, ϕ, of $[C_{12}MIM]OTf$ micelles in aqueous solution calculated from the Grosse radius, R_G (solid line), and from the bulk water amplitude, S_b (●).

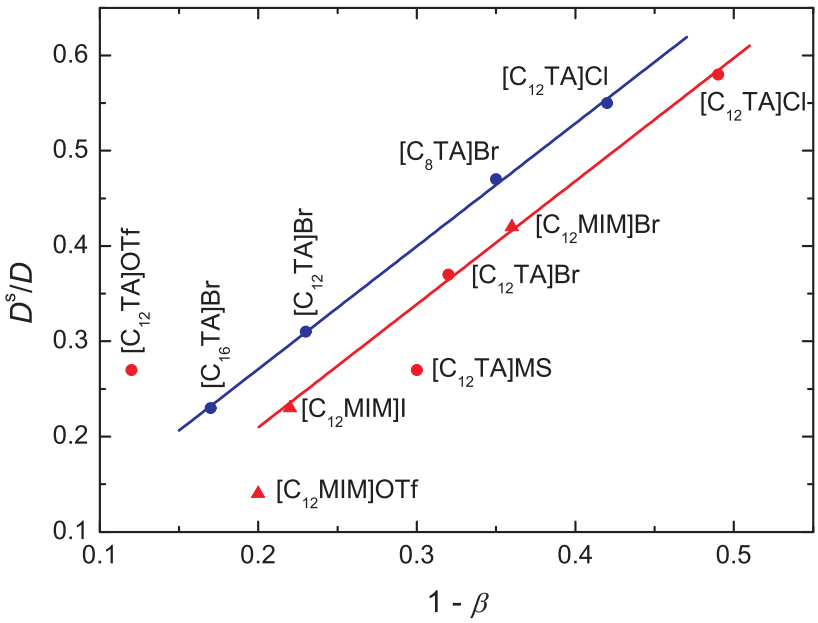

Figure S16: Relative surface diffusion coefficient of condensed counterions, D^S/D, as a function of the degree of counterion dissociation, $1-\beta$, for $[C_nTA]X$ (●)[S2,S3] and $[C_{12}MIM]X$ (▲, this work) surfactants at 25 (blue; $[C_{16}TA]Br$: 28 °C) and 45 °C (red). The lines are a guide to the eye.

References

(S1) Zasetsky, A. Y.; Buchner, R. Quasi-linear least squares and computer code for numerical evaluation of relaxation time distribution from broadband dielectric spectra. *J. Phys.: Condens. Matter* **2011**, *23*, 025903.

(S2) Buchner, R.; Baar, C.; Fernandez, P.; Schrödle, S.; Kunz, W. Dielectric spectroscopy of micelle hydration and dynamics in aqueous ionic surfactant solutions. *J. Mol. Liq.* **2005**, *118*, 179–187.

(S3) Lima, F. S.; Chaimovich, H.; Cuccovia, I. M.; Buchner, R. Dielectric Relaxation Spectroscopy Shows a Sparingly Hydrated Interface and Low Counterion Mobility in Triflate Micelles. *Langmuir* **2013**, *29*, 10037–10046.

Appendix B

Supporting information:

Application of surface-active ionic liquids in transition metal catalysis

Supporting information

Surface-active ionic liquids in catalysis: Impact of structure and concentration on the aerobic oxidation of alcohols in water

Alice Cognigni,[a] Sebastian Kampichler,[a] Katharina Bica*,[a]

[a]Institute of Applied Synthetic Chemistry, Vienna University of Technology, Getreidemarkt 9/163, 1060 Vienna, Austria.

Figure S1: Pre-catalyst decomposition under reaction conditions with $[C_{12}mim]Cl$ and $[C_{12}m_2im]Cl$ at 5 and 50 mM concentration

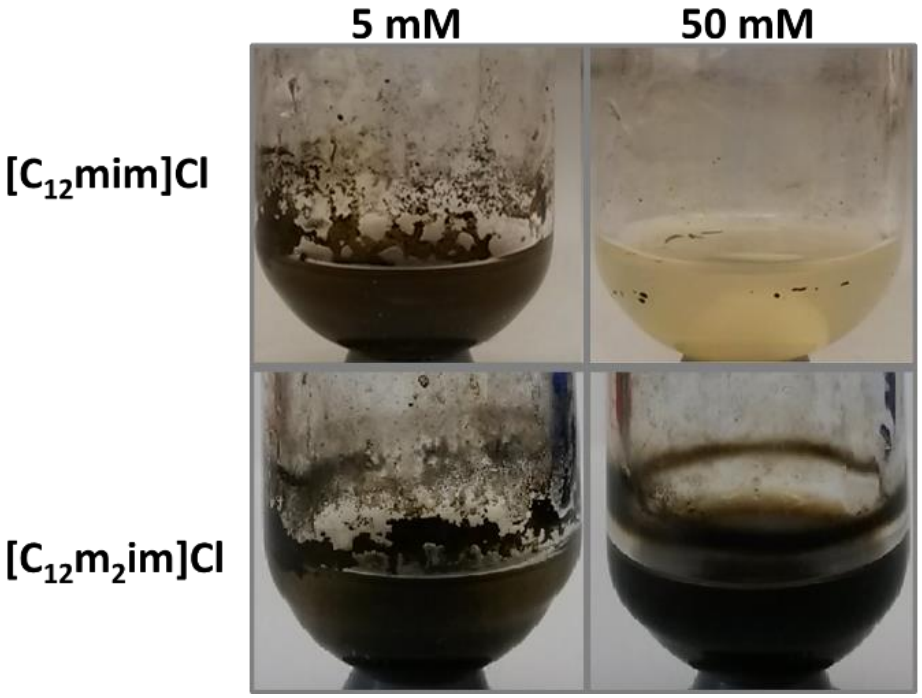

Table S1: Optimization reaction parameters using 30 bar of air as oxidizing agent

Table S1: Optimization of reaction parameters using 30 bar of air as oxidizing agent

Entry[a]	**Temp [°C]**	**Time [h]**	**$Pd(OAc)_2$ [mol%]**	**K_2CO_3 [mol%]**	**Yield [%]**[b]
1	100	18	5	25	21
2	100	18	5	50	41
3	75	12	5	50	< 8
4	125	24	5	50	46
5	100	6	2	50	26
6	100	18	2.5[c]	50	30

[a]Reactions were performed in an autoclave using 2 mmol of octanol in 10 ml of a solution of $[C_{12}mim]Cl$ 5 mM. Work-up included addition of an excess of HCl, extraction with EtOAc, and analysis through GC. [b] GC yield. [c]$[Pd(allyl)Cl]_2$ used as catalyst.

Electronic supporting information

Surface-active ionic liquids for Palladium-catalysed cross coupling in water: Effect of ionic liquid concentration on the catalytically active species

Meltem Taskin,[a] Alice Cognigni,[a] Ronald Zirbs,[b] Erik Reimhult[b] and Katharina Bica[a,*]

[a] Institute of Applied Synthetic Chemistry, Vienna University of Technology, Getreidemarkt 9/163, 1060 Vienna (Austria), Fax: +43 1 58801 16360; Tel: +43 1 58801 163601. E-mail: katharina.bica@tuwien.ac.at or katharina.schroeder@tuwien.ac.at .

[b] Group for Biologically Inspired Materials, Institute of Nanobiotechnology (DNBT), University of Natural Resources and Life Sciences, Muthgasse 11, 1190 Vienna, Austria.

1. Table S1: Critical micelle concentrations for all involved ionic liquids 2

2. Figure S1: Concentration dependence of the Heck reaction of ethyl acrylate 9 and iodobenzene 10 in aqueous solution of ionic liquids [C_{12}mim]Cl 1 using DBU as base..... 3

3. Figure S2: Copy of ^{13}C NMR spectroscopy showing the formation of a Pd-carbene at 177 ppm..... 4

1. Table S1: Critical micelle concentrations for all involved ionic liquids

	CMC [mM][a]	
Ionic Liquid	**Conductivity[b]**	**Surface tension[c]**
1	14.53 [1]	13.25 [1]
2	13.75 [2]	10.33 [2]
3	2.69 [3]	2.31 [3]
4	4.32	3.24
5	5.52	4.33
6	5.69	5.07
7	5.04	4.91
8	4.17	5.61

[a] Solutions were prepared with doubly-distilled Millipore Milli-Q water. Samples were equilibrated at 25 °C with a HAAKE K15 thermostat before measurements. [b] Conductivity measurement were performed on a Mettler Toledo SevenExcellence system. InLAB® 741-ISM electrode (cell constant k = 0.105). The conductimeter was calibrated with a standard KCl solution and measurements were performed in duplicate; [c] Surface tension was determined with the Du Noüy ring method on a Krüss tensiometer at RT. Each measurement was repeated 5 times.

[1] A. Cognigni, P. Gaertner, R. Zirbs, H. Peterlik, K. Prochazka, C. Schröder and K. Bica, *Phys. Chem. Chem. Phys.*, 2016, **18**, 13375–13384.

[2] A. Cognigni, S. Kampichler and K. Bica, *J. Colloid Interface Sci.*, 2017, **492**, 136–145.

[3] X.-f. Liu, L.-l. Dong and Y. Fang, *J. Surfactants Deterg.*, 2011, **14**, 203–210.

2. **Figure S1: Concentration dependence of the Heck reaction of ethyl acrylate 9 and iodobenzene 10 in aqueous solution of ionic liquids [C_{12}mim]Cl 1 using DBU as base.**

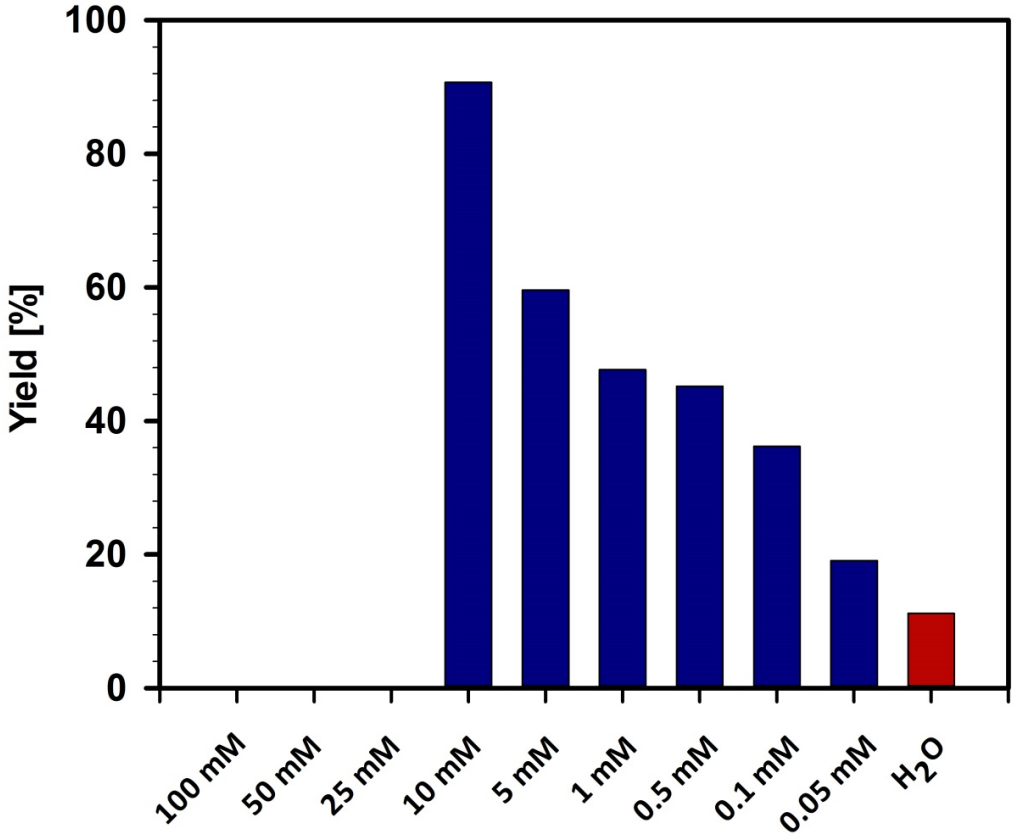

3. **Figure S2: Copy of ^{13}C NMR spectroscopy showing the formation of a Pd-carbene at 177 ppm.**

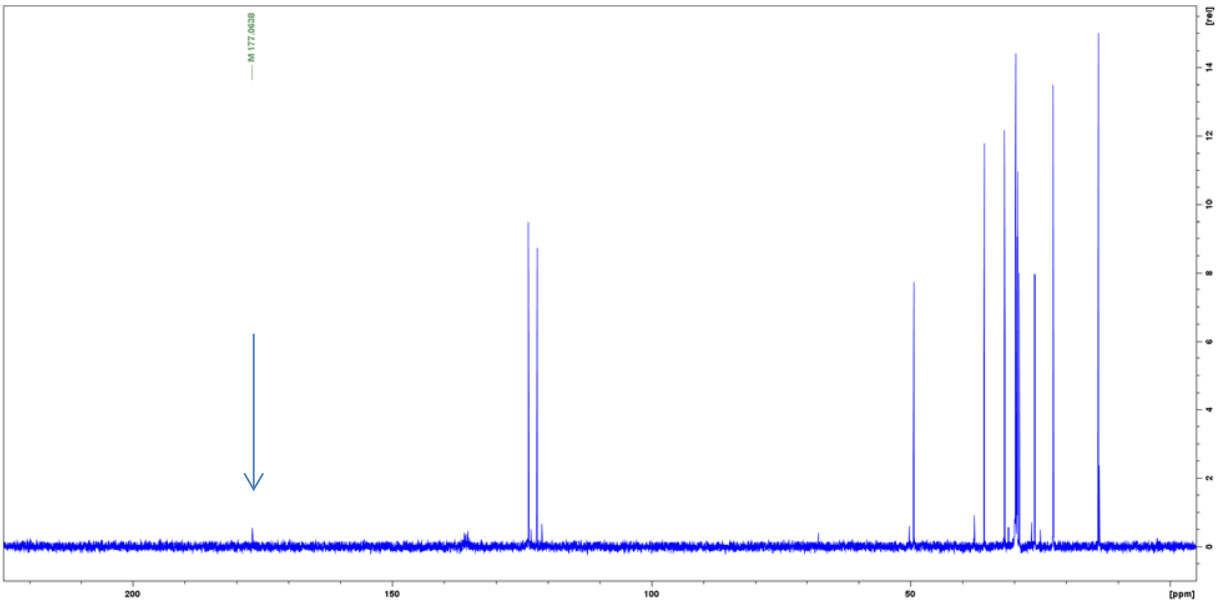

Conditions: 2 mL [C_{12}mimCl] **2** solution (50 mM) in D_2O, 0.02 mmol $Pd_2allyl_2Cl_2$ and 0.02 mmol K_2CO_3; 30 min at 80 °C under air.

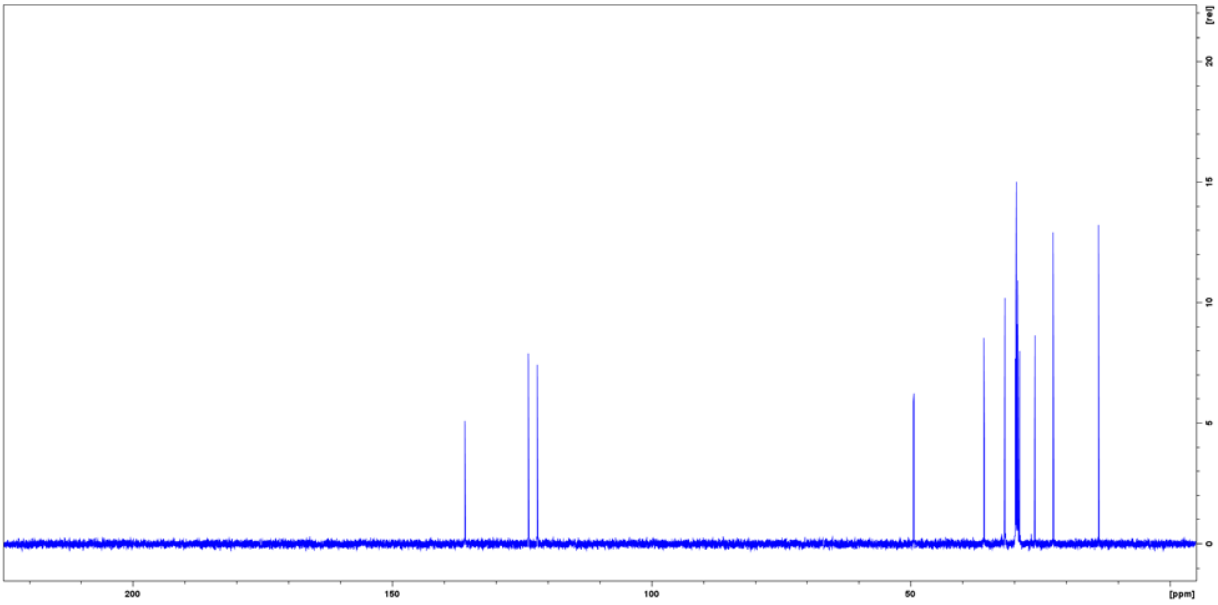

Conditions: [C_{12}mimCl] **2** solution (50 mM) in D_2O

Appendix C

Supporting information:

Surface-active ionic liquids for sustainable energy production

Supplementary information: Surface-active ionic liquids in catalytic water splitting

Alice Cognigni,[a] Christian Schröder,[b] Herwig Peterlik,[c] Alexander R. M. Müllner,[c] Ronald Zirbs[d], and Katharina Bica*[a]

Contents

1 Reaction profiles **2**

2 Reaction kinetics **4**
2.1 Rationalization 4
2.2 Turn over frequency of the autocatalyzed reaction 4
2.3 Turn over frequency of the first order reaction 4
2.4 Mean reaction time 5

3 SAXS measurements **6**

[a] *Institute of Applied Synthetic Chemistry, Vienna University of Technology, Getreidemarkt 9/163, 1060 Vienna (Austria), Fax: +43 1 58801 16360; Tel: +43 1 58801 163601. E-mail: katharina.bica@tuwien.ac.at or katharina.schroeder@tuwien.ac.at*

[b] *Institute of Computational Biological Chemistry, Faculty of Chemistry, University of Vienna, Währingerstrasse 17, 1090 Vienna, Austria*

[c] *Faculty of Physics, University of Vienna, Boltzmanngasse 5, 1090 Vienna, Austria.*

[d] *Institute for Biologically inspired materials, Department of Nanobiotechnology, University of Natural Resources and Life Sciences, Vienna, Muthgasse 11-II, A-1190 Vienna, Austria.*

1 Reaction profiles

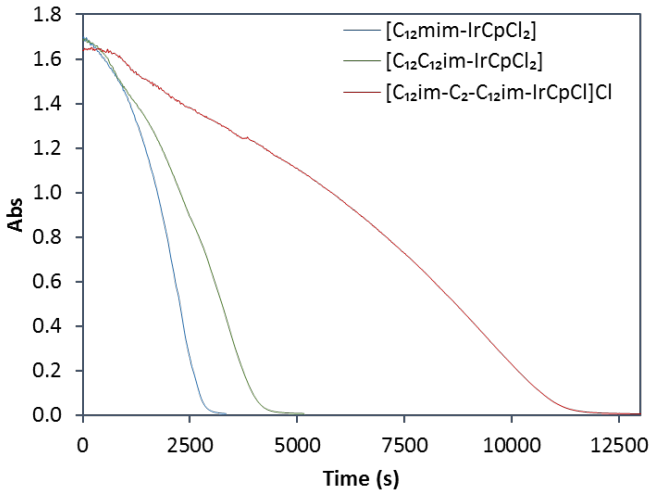

Figure 1 Representative kinetic profiles for the three new catalysts at concentration of $2\,\mu\mathrm{M}$ and CAN $3\,\mathrm{mM}$ in HNO_3 $0.1\,\mathrm{M}$

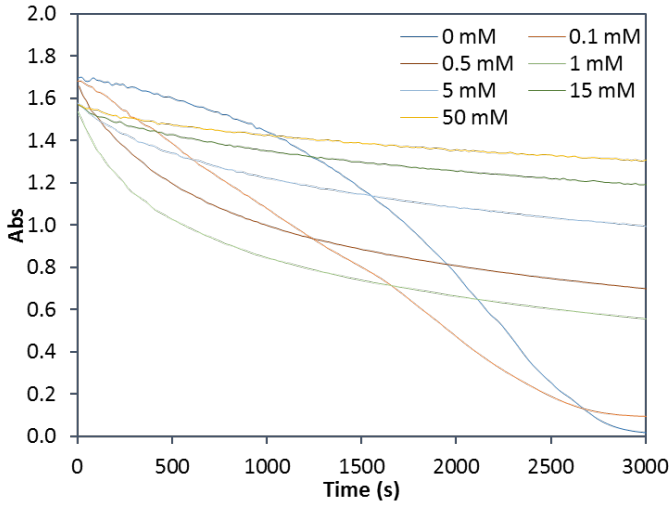

Figure 2 Reaction profiles for catalyst **2** $2\,\mu\mathrm{M}$ and CAN $3\,\mathrm{mM}$ with different concentrations of additional $[C_{12}mim]Cl$ in HNO_3 $0.1\,\mathrm{M}$

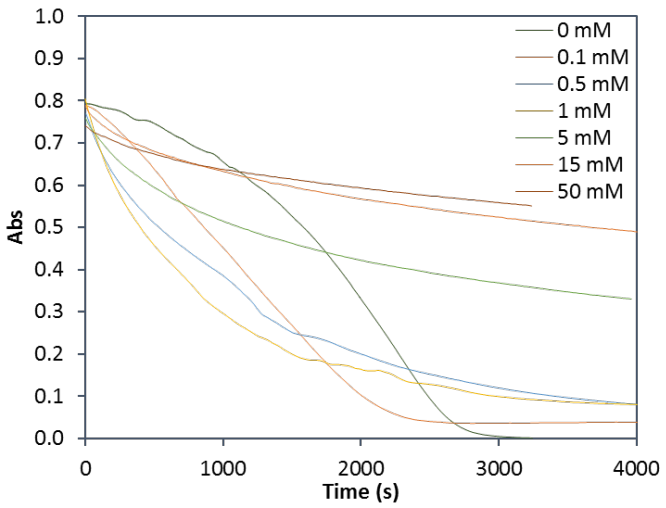

Figure 3 Reaction profiles for catalyst **2** $2\,\mu\mathrm{M}$ and CAN $1.5\,\mathrm{mM}$ with different concentrations of additional [C_{12}mim]Cl in HNO_3 $0.1\,\mathrm{M}$

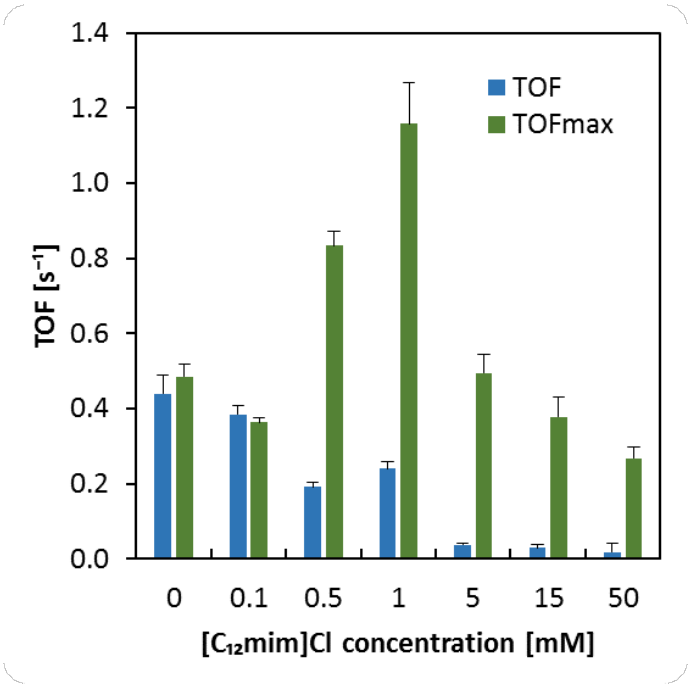

Figure 4 $TOF_{\langle t \rangle}$ and $TOF_{\max}$ for catalyst **2** $2\,\mu\mathrm{M}$ and CAN $1.5\,\mathrm{mM}$ with different concentrations of additional [C_{12}mim]Cl in HNO_3 $0.1\,\mathrm{M}$

2 Reaction kinetics

Assuming that the depletion of the Ce^{4+} can be described by

$$[Ce^{4+}](t) = a_1 e^{-k_1 t} + \frac{a_2}{(1-b_2)+b_2 e^{k_2 t}} \tag{1}$$

with the initial absorbance $a_0 = a_1 + a_2$. The first part on the right hand side is a first order reaction. The second part stems from an autocatalyzed reaction. a_1 and a_2 are the relative importance of the two processes. If, for example, a_1 is almost a_0, then the overall reaction follows first order, if a_2 is almost a_0 the reaction is determined by the autocatalyzed process. k_1 and k_2 are the corresponding rate constants in Hz. The parameter b_2 describes the position of the turn point of the logistic function.

Eq. (1) can be reformulated

$$a_1 e^{-k_1 t} + \frac{a_2}{(1-b_2)+b_2 e^{k_2 t}} = a_1 e^{-k_1 t} + \frac{\tilde{a}_2}{1+e^{k_2(t-t_0)}} \tag{2}$$

using $\tilde{a}_2 = a_2/(1-b_2)$ and $t_0 = \ln\Big((1-b_2)/b_2\Big)$. Here, t_0 corresponds to the time when half of the second process had taken place.

2.1 Rationalization

A first order reaction can be described by

$$-\frac{d[Ce^{4+}]}{dt} = k_1[Ce^{4+}]. \tag{3}$$

Solving this differential equation yields the first part of Eq. (1).

In principle, the differential equation of the pure autocatalytic part looks like

$$-\frac{d[Ce^{4+}]}{dt} = k'[Ce^{4+}] + k''[Ce^{4+}]\Big([Ce^{4+}]_0 - [Ce^{4+}]\Big) \tag{4}$$

resulting in

$$[Ce^{4+}](t) = \frac{[Ce^{4+}]_0([Ce^{4+}]_0 \cdot k'' + k')}{k' e^{([Ce^{4+}]_0 k'' + k')t} + [Ce^{4+}]_0 k''} \tag{5}$$

Substituing $k_2 = [Ce^{4+}]_0 k'' + k'$ and $k' = k_2 \cdot b_2$ one yields

$$[Ce^{4+}](t) = \frac{[Ce^{4+}]_0}{1-b_2+b_2 e^{k_2 t}} \tag{6}$$

which is similar to the logistic function of Eq. (1).

2.2 Turn over frequency of the autocatalyzed reaction

The time-dependent concentration of the product, $[Ce^3](t)$, should be $[Ce^{4+}]_0 - [Ce^{4+}](t)$. Consequently, the rate $r(t)$ of Ce^{3+}-production is

$$r(t) = \frac{d[Ce^{3+}]}{dt} \simeq \frac{[Ce^{4+}]_0}{a_0} \cdot \frac{a_2 \cdot k_2 \cdot b_2 e^{k_2 t}}{(1-b_2+b_2 e^{k_2 t})^2} \tag{7}$$

neglecting the first order reaction. The maximum rate r is reached at

$$t_{max} = \frac{\ln(1-b_2) - \ln(b_2)}{k_2} \tag{8}$$

As a result, the maximum turn-over-frequency

$$TOF = \frac{r(t_{max})}{[cat]} = \frac{a_2 \cdot k_2 \cdot [Ce^{4+}]_0}{4(1-b_2) \cdot a_0 \cdot [cat]} \tag{9}$$

2.3 Turn over frequency of the first order reaction

In the rare case, that the depletion of $[Ce^{4+}]$ follows a first order reaction without the autocatalyzed process, i.e. $a_1 \simeq a_0$ and

$$r(t) = \frac{d[Ce^{3+}]}{dt} \simeq \frac{[Ce^{4+}]_0}{a_0} a_1 \cdot k_1 \cdot e^{-k_1 t}, \tag{10}$$

the turn-over-frequency has its maximum value at $t = 0$:

$$TOF = \frac{[Ce^{4+}]_0 \cdot a_1 \cdot k_1}{[cat] \cdot a_0} \tag{11}$$

The last value can also be gained from a Taylor-series expansion of the [Ce^{3+}](t)

$$
\begin{aligned}
[Ce^{3+}] &= [Ce^{4+}]_0(1-\frac{a_1}{a_0}e^{-k_1 t}) && (12)\\
&= [Ce^{4+}]_0(1-e^{-k_1 t}) && (13)\\
&\simeq [Ce^{4+}]_0\left(1-(1-k_1 t+\ldots)\right) && (14)\\
&\simeq [Ce^{4+}]_0 \cdot k_1 \cdot t && (15)
\end{aligned}
$$

since $a_1 = a_0$ is the initial assumption of this rare case. The slope of Eq. (15) is $[Ce^{4+}]_0 \cdot k_1$ which has to be divided by [cat] to get the turn-over-frequency.

2.4 Mean reaction time

Since the maximum TOF might not be appropriate to characterize the efficiency of a catalyst in a chemical reaction as the time spent at the maximum TOF level does not enter the efficiency considerations. A lower maximum TOF level mantained over a longer period of time may result in a faster reaction overall.

As alternative property to characterize the promotion of the chemical reaction due to the catalyst or reaction conditions, the average reaction time

$$\langle t\rangle = \int_0^\infty \frac{[Ce^{4+}](t)}{[Ce^{4+}](0)}dt \tag{16}$$

Here, $[Ce^{4+}](t)$ is the time-dependant concentration of Ce^{4+} and $[Ce^{4+}](0)$ its inital value. Integrating eq. (1) yields

$$\langle t\rangle = \frac{1}{a_1+a_2}\left[a_2\frac{\ln(b_2(e^{k_2 t}-1)+1)-k_2 t}{(b_2-1)k_2} - \frac{a_1 e^{-k_1 t}}{k_1}\right]_0^\infty \tag{17}$$

For longer times t the first part of the right hand side can be simplified to $a_2 \ln b_2/\big((b_2-1)k_2\big)$. As result, eq. (17) is

$$\langle t\rangle = \frac{\frac{a_2 \ln b_2}{(b_2-1)k_2}+\frac{a_1}{k_1}}{a_1+a_2} \tag{18}$$

The turn-over-frequency at the mean reaction time is

$$
\begin{aligned}
TOF\Big(\langle t\rangle\Big) &= \frac{[Ce^{4+}]_0}{(a_1+a_2)[cat]}\cdot && (19)\\
&\left(a_1 k_1 e^{-k_1\langle t\rangle} + \frac{a_2 b_2 k_2 e^{k_2\langle t\rangle}}{\left(1-b_2+b_2 e^{k_2\langle t\rangle}\right)^2}\right) && (20)
\end{aligned}
$$

3 SAXS measurements

h SAXS measurements were performed using a Bruker Nanostar (Bruker AXS) equipped with microfocus X-ray source (Incoatec ImS High Brilliance) with CuK_α radiation with a wavelength of 0.1542 nm, a pinhole camera and a 2D-position sensitive detector (Vantec 2000). The samples were filled into glass capillaries (1.5 mm diameter, 10 μm wall thickness, from Hilgenberg). Scattering patterns were recorded for 6 hours, azimuthally integrated and corrected for background scattering from the capillary. The integrated intensity is shown in Fig. 5 in dependence on the scattering vector $q=(4\pi/\lambda)\sin\Theta$, with 2Θ being the scattering angle (black line). The red line is a fit with a core-shell model as in ref. 25 of the paper. Additionally, a power-law term was added to describe the strong intensity increase towards low q-values. The fit results in a core radius of 0.75 nm, a shell thickness of 2.1 nm and a value of 0.035 for the scaled medium contrast γ.

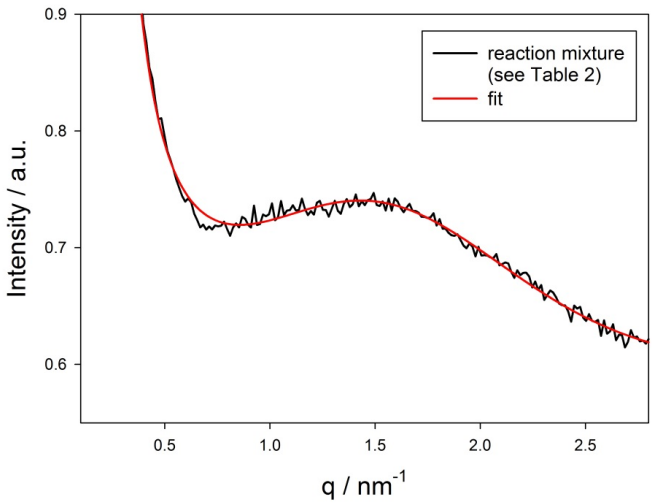

Figure 5 SAXS intensity for the reaction mixture (as described in Table 2 of the paper), black line, together with fit from the core-shell model, red line

Curriculum vitae

ALICE COGNIGNI

Education

Apr 2014 – Present

Ph.D thesis in Technical Chemistry
Vienna University of Technology (A), Institute of applied synthetic chemistry
Thesis developed under the supervision of Prof. Katharina Schröder
Title: Surface-active ionic liquids in synthesis and catalysis

Oct 2011 – Jul 2013

M.Sc Erasmus Mundus Master Course
Advanced Spectroscopy in Chemistry, final grade 1.7/1.0
University of Leipzig (D) and University of Helsinki (FI)
Thesis developed at the Institute of Technical Chemistry of Leipzig University under the supervision of Prof. Annegret Stark
Title: CO_2 activation via imidazolium-2-carboxylates
• Awarded an Erasmus Mundus Category B scholarship

Sep 2008 - Oct 2011

B.Sc in Industrial Chemistry final grade 110/110
Alma Mater Studiorum University of Bologna (I)
Thesis developed at National Council of Researches in Bologna under the supervision of Dr. Loris Giorgini and MSc. Massimo Benaglia
Title: Post-polymerization processes to obtain a library of hydrophilic and/or amphiphilic (co)polymers

Sep 2002 - Jul 2008

High School with focus on natural sciences final grade 85/100
Liceo scientifico statale "N. Copernico", Bologna (I)

Work and internship experiences

Jan 2017

Trainer at „Frauen In die Technik" event
Vienna University of Technology (A)

Jul 2016

Co-worker at the 26th EUCHEM Conference on Molten Salts and Ionic Liquids
Vienna (A)

Sep 2013 – Feb 2014

Internship at Merck KGaA
Darmstadt (D)
Division Performance materials, R & D, Dye-Sensitized Solar Cells

Sep 2012 – Dec 2012

Master studies project case study
University of Helsinky (FI)
Research conducted at the laboratory of organic chemistry under the supervision of Prof. Kristiina Wähälä
Research Area: Multi-component reactions with ionic liquids

Further academic commitment

May 2010 - Oct 2011 **University student representative**
Alma Mater Studiorum University of Bologna

Language skills

Italian	Mother tongue
English	Full professional proficiency through master degree in English
German	B2, ÖSD certificate 10/10/2014 at deutschinstitut.at, Vienna

Publications

Cognigni, Alice; Schröder, Christian; Peterlik, Herwig; Muellner, R. M. Alexander; Zirbs, Ronald; Weil, Matthias and Bica, Katharina **Surface-active ionic liquids in catalytic water splitting** submitted to *Dalton Transactions* **2017.**

Taskin, Meltem; Cognigni, Alice; Zirbs, Ronald; Reimhult, Erik and Bica, Katharina **Surface-active ionic liquids for Palladium-catalysed cross coupling in water: Effect of ionic liquid concertation on the catalytically active species** *RSC Advances* **2017**, *7*, 41144-41151.

Friesen, Sergej; Buchecker, Thomas; Cognigni, Alice; Bica, Katharina and Buchner, Richard **Hydration and Counterion Binding of [C_{12}MIM] Micelles** *Langmuir* **2017**, DOI: 10.1021/acs.langmuir.7b02201.

Šarac, Bojan; Medoš, Žiga; Cognigni, Alice; Bica, Katharina; Chen, Li-Jen; Bešter-Rogač, Marija; **Thermodynamic study for micellization of imidazolium based surface active ionic liquids in water: Effect of alkyl chain length and anions** *Colloids and Surfaces A: Physicochemical and Engineering Aspects* **2017**, DOI:10.1016/j.colsurfa.2017.01.062.

Cognigni, Alice; Kampichler, Sebastian; Bica, Katharina, **Surface-active ionic liquids in catalysis: Impact of structure and concentration on the aerobic oxidation of octanol in water** *Journal of Colloid and Interface Science* **2017**, *492*, 136-145.

Bonta, Maximilian; Anderl, Thomas; Cognigni, Alice; Hejazifar, Mahtab; Bica, Katharina; Limbeck, Andreas; **Determination of residual chloride content in ionic liquids using LA-ICP-MS**, *RSC Advances* **2016**, *6* (93), 90273-90279.

Cognigni, Alice; Gaertner, Peter; Zirbs, Ronald; Peterlik, Herwig; Prochazka, Katharina; Schroeder, Christian; Bica, Katharina; **Surface-active ionic liquids in micellar catalysis: impact of anion selection on reaction rates in nucleophilic substitutions** *Physical Chemistry Chemical Physics* **2016**, *18* (19), 13375-13384.

Oral presentations

Alice Cognigni, Ronald Zirbs, Herwig Peterlik, Christian Schroeder, Peter Gaertner and Katharina Bica **Surface-active ionic liquids in micellar catalysis**, 3rd International Symposium on Green Chemistry **2015** La Rochelle, France.

Alice Cognigni, Mahtab Hejazifar, Meltem Taskim, Ronald Zirbs, Herwig Peterlik, Christian Schröder, Peter Gaertner and Katharina Bica **Synthesis and Characterization of Surface Active Ionic Liquids**, COST CM1206 – EXIL: Exchange on Ionic Liquids Workshop, **2015**, Prag, Czech Republic.

Poster Presentations

Alice Cognigni, Ronald Zirbs, Peter Gaertner and Katharina Bica **Surface Active Ionic Liquids In Micellar Catalysis**, 8th Green Solvents conference **2016**, Kiel, Germany.

Alice Cognigni, Sebastian Kampichler, Ronald Zirbs, Peter Gaertner and Katharina Bica **Aerobic oxidation of alcohols in water-ionic liquid micellar solutions**, 26th EUCHEM Conference on Molten Salts and Ionic Liquids, **2016**, Vienna, Austria.

Alice Cognigni, Ronald Zirbs, Herwig Peterlik, Christian Schroeder, Peter Gaertner and Katharina Bica **Surface-active ionic liquids in micellar catalysis**, 3rd International Symposium on Green Chemistry **2015** La Rochelle, France.

Alice Cognigni, Anna K. Ressmann, Ronald Zirbs, Herwig Peterlik, Peter Gaertner and Katharina Bica **Micellar Catalysis In Ionic Liquids**, 25th EUCHEM Conference on Molten Salts and Ionic Liquids, **2014**, Tallin, Estonia.

Vienna 23/08/2017